AN ANALYSIS OF THE ELECTRICAL CIRCUIT OF SUBMERGED-ARC FURNACES

BY

ALISTAIR BRUCE STEWART

SUBMITTED TO THE UNIVERSITY OF CAPE TOWN IN FULFILMENT OF THE REQUIREMENTS FOR THE DEGREE OF DOCTOR OF PHILOSOPHY

FEBRUARY, 1980

-----oOo-----

D E C L A R A T I O N

I hereby certify that this whole thesis, unless specifically indicated to the contrary in the text, is my own original work

A.B. STEWART

A B S T R A C T

The measurement of the electrical variables of a submerged-arc furnace is difficult owing to errors in the measurement of electrode-to-bath voltages and the difficulty in maintaining measurement connections to the hot, harsh environment of a furnace. A system is proposed which provides an accurate, reliable measurement of the electrode-to-bath voltages so that the electrical variables of the furnace can be determined. A means for measurement of the arcing conditions under each electrode has also been developed.

The measurement system has been used in the examination of the conduction mechanisms occurring in a furnace and this has resulted in a significant improvement in the understanding of the operation. In addition, a method for determination of the lengths of the electrodes has been established.

A problem with the measurement system is that it is necessary to make connections in a hot environment and on occasions, when a furnace eruption has occurred, the measurement leads have to be replaced. As a result, an indirect technique for determination of the resistances under each electrode has been developed and used for control of the power distribution in the furnace. The technique is based on an assumption about the relationship between the reactances in the furnace and all measurements are made on the primary side of the furnace transformers where reliable connections can be made.

ACKNOWLEDGEMENTS

The author wishes to acknowledge his debt to:

PROFESSOR N.C. ENSLIN, the thesis supervisor, for his encouragement and guidance;

MR G. SOMMER for his support and enthusiasm with the project;

THE NATIONAL INSTITUTE FOR METALLURGY for their financial support of the project;

THE SOUTH AFRICAN FERROALLOY INDUSTRY, particularly SAMANCOR, for making available their furnaces for the investigation;

THE STAFF of the INSTRUMENTS DIVISION at the National Institute for Metallurgy and the STAFF OF FERROMETALS LIMITED for their assistance;

My colleages, DR I.J. BARKER and MR M.S. RENNIE for their encouragement and help;

MRS C.M. HEYNS and MRS E. REISER for assistance with the production of the thesis; and

finally to my wife KATHY, for much help and patience.

C O N T E N T S

1. INTRODUCTION

Electric arc furnaces have been used for many years as sources of energy for metallurgical operations. In the production of steel they are used primarily for the melting down of scrap iron for refinement into steel, although more recently, pig iron and prereduced iron ore are also used as ingredients. This is essentially a melting operation with visible arcs being formed between the electrodes and scrap iron and these furnaces are generally called open-arc furnaces or melting furnaces. Electric arc furnaces are also used for the reduction of ores or ore concentrates into their associated metals or alloys. Here a mixture of ore, reductant and fluxes are fed to the furnace to form a solid 'burden' with the electrodes buried so that the arcs occur beneath this material. These types of furnaces are called either submerged-arc furnaces or reduction furnaces.

The Republic of South Africa has rich reserves of chrome and manganese ores as well as cheap electricity, and over the last decade there has been a dramatic increase in the number of submerged arc furnaces, constructed for the production of ferrochromium and ferromanganese alloys. The economic benefits of reducing running costs by the employment of larger furnaces has meant that most of the furnaces that have been recently constructed have been relatively large (e.g., 48 MVA for ferrochromium and 75 MVA for ferromanganese). These large furnaces operate at much lower power factors than their smaller counterparts as a result of higher relative inductive reactances and this makes operation and control of the furnaces more difficult.

The electrical energy fed to submerged arc furnaces is dissipated as a combination of arc and resistive heating and since these are low voltage mechanisms, high currents must be used for the introduction of sufficient energy into the furnace. The high currents cause errors in the measurement of voltages between various sections of the electrical circuit, which makes it difficult to measure the electrical variables of the furnace. This increases the difficulties in the operation and control of these furnaces.

In 1973 the National Institute for Metallurgy was approached to set up a research team to study the operation of a large ferrochromium furnace (48 MVA) which was experiencing production difficulties. A minicomputer-based data acquisition system was installed on the furnace[67] and a thorough investigation into the operation of the furnace was carried out [61,62]. One aspect which was poorly understood was the measurement and control of the electrical circuit of the furnace. It was established that the furnace did not have a voltage connection to the bath so that accurate measurement of the electrical variables was not possible. Therefore, an indirect technique for calculating the resistances was developed [65] and used for control of the power distribution [5,35,66].

In 1977 the furnace was switched off for rebuilding of the lining and this provided an opportunity for installing voltage connections to the bath. A secondary measurement system was set up which, for the first time, provided accurate measurements of the electrical variables of the furnace[64]. In addition, a measurement of the arcing conditions under each electrode was provided and this enabled a better understanding of the electrical conduction mechanisms.

It was also found that the arcing measurements were closely correlated with the lengths of the electrodes and this provided an opportunity to develop models of the lengths of the electrodes.

In general, an overall improvement in the understanding of the various mechanisms which effect the operation of the electrical circuit of the furnace was achieved.

2. PROPERTIES OF SUBMERGED-ARC FURNACES

This chapter is a general description of the features and operation of submerged-arc furnaces, particularly for the production of ferrochromium and serves as an introduction to a detailed study of the electrical circuit. For a more detailed treatment of the subject, the reader is referred to comprehensive descriptions by Robiette[56] or Volkert[74].

2.1 General Description of Furnace Operation

A common type of submerged-arc furnace, used for ferrochromium production, is the three electrode circular furnace shown in Figure 2.1. In this arrangement the circular bath is fixed and three electrodes, submerged in a charge of raw materials, project into it. The charge consists of a proportioned mixture of ore, reductant and fluxes which are transported, via conveyer belts, to holding bins situated above the furnace. A combination of resistance and arc heating occurs below the electrodes and this provides the energy for the heating and reduction of the charge into molten metal. A slag is produced which is lighter than the metal and is formed in a pool above it. The ore and slag are tapped periodically from the side of the furnace near the bottom. During tapping the lowering of the molten bath causes fresh raw material to gravity feed into the reaction zone from the holding bins above the furnace.

Electrical power is fed to the electrodes through fixed busbars and flexible connections from furnace transformers situated close to the furnace. These transformers convert the high voltage power from the supply authority to a low voltage, high current form suitable for delivering power to the furnace. Control of the power circuit is achieved by either adjusting the transformer secondary voltage by means of voltage tap changers in the transformers or by varying the circuit impedance under each electrode by adjusting the vertical position of the electrodes.

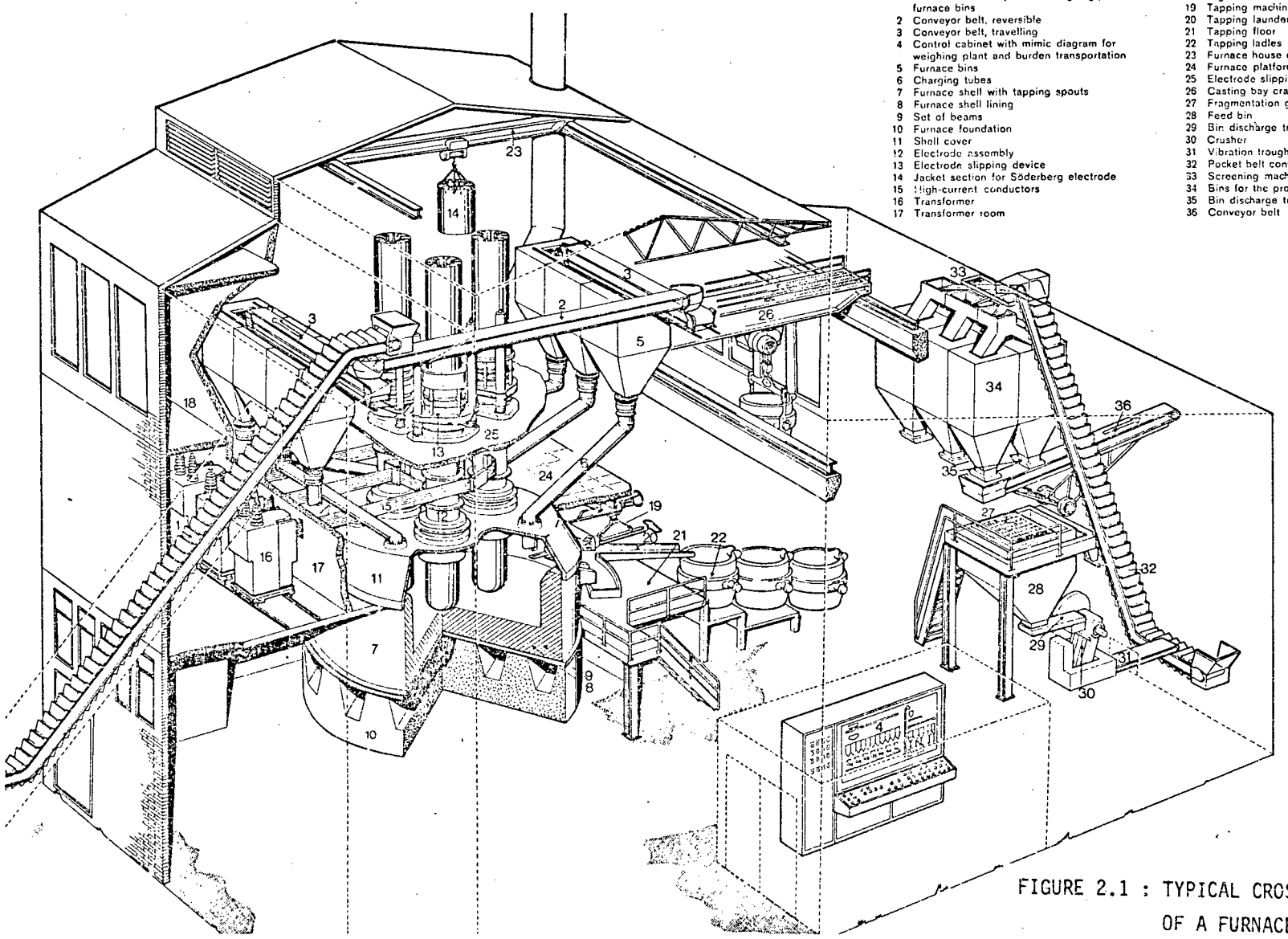

FIGURE 2.1 : TYPICAL CROSS-SECTION OF A FURNACE.
(courtesy of DEMAG.)

Careful control of the proportioning and sizing of the raw materials is a pre-requisite for good furnace operation. The reduction reaction results in the production of large volumes of gaseous products (CO and CO_2) which can cause a problem if adequate porosity of the raw material burden is not maintained. A decrease in the porosity of the burden is usually caused by the sintering of fine material and, therefore, the raw materials have to be screened to remove this fine material before being fed to the furnace. It is unfortunate that much of South Africa's ore reserves, particularly chrome ore, are found in fine form and much effort has been focused on developing methods for using these fines. A popular technique is briquetting which involves mixing the fine ore with a binder and compressing it into briquettes.

The introduction of stringent air pollution controls have forced the ferro-alloy producers to install expensive gas cleaning equipment on their furnaces. The quantity of air to be cleaned, and hence the size and cost of the gas cleaning plant, can be reduced by closing the top of the furnace so that only the gas generated by the process is cleaned. The furnace shown in Figure 2.1 is a closed-top furnace. A problem with this type of furnace is that the operator cannot observe the operation and has to rely more on instrumentation and indirect observation to assess the state of the furnace.

2.2 Furnace Equipment

2.2.1 The Knapsack connection

The connection arrangement common to virtually all circular submerged-arc furnaces, is called the Knapsack connection because of its origin at Knapsack, West Germany. A typical arrangement of this connection is shown in Figure 2.2 which has three separate single-phase transformers. On small furnaces a single three-phase transformer is used, however, the connection arrangement is essentially the same. The three secondary circuits are brought out separately from each transformer and a delta connection is made at the electrodes using flexible conductors so as to allow vertical movement of the electrodes. The reactances of the busbars are kept to a minimum by inter-

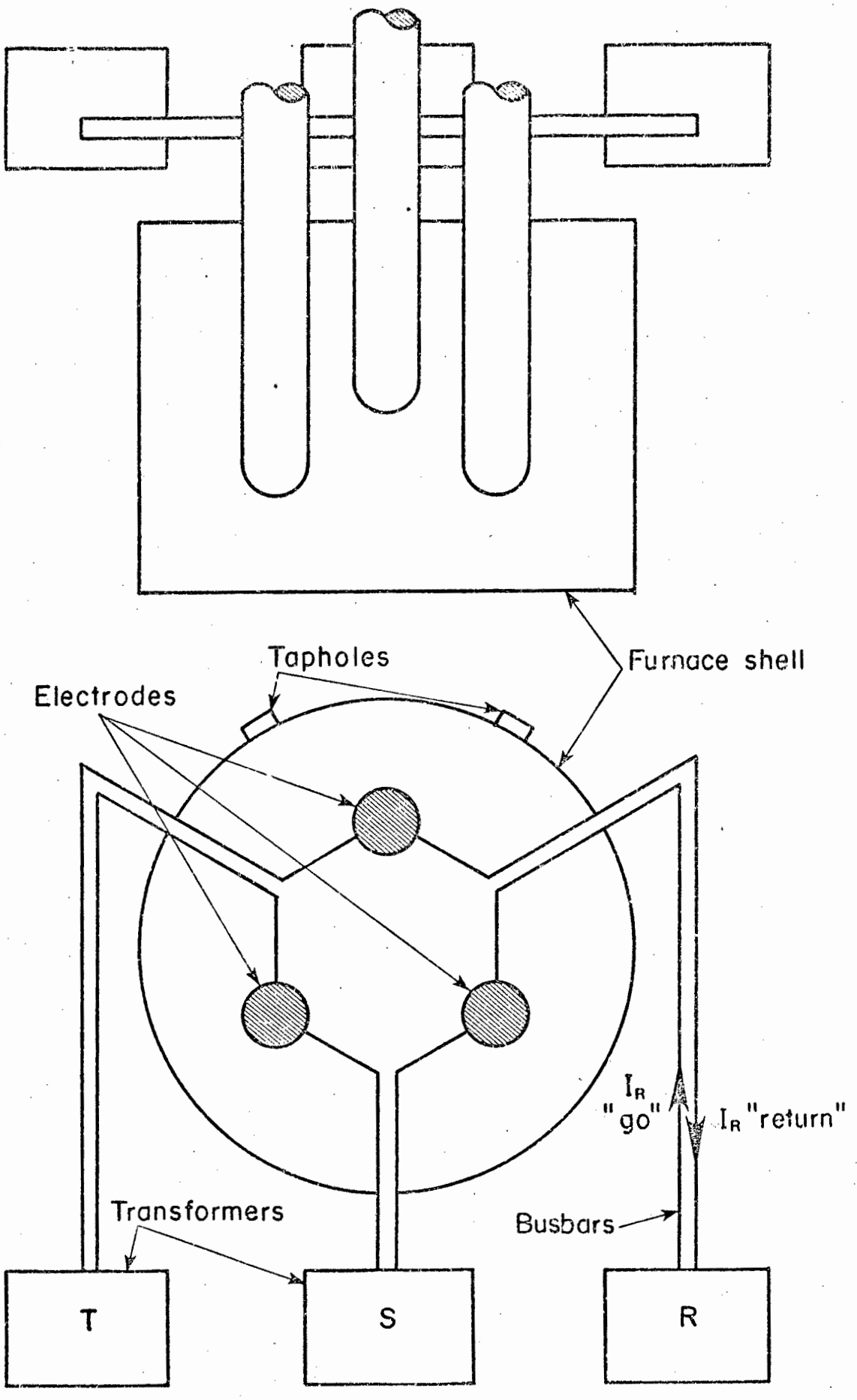

FIGURE 2.2 : LARGE SUBMERGED-ARC FURNACE SHOWING KNAPSACK CONNECTION.

leaving the 'go' and 'return' paths for each phase right up to the flexible connection point close to the electrodes. The electrodes form a star circuit carrying current down to the molten bath which is $\sqrt{3}$ times the current in the delta and transformer circuit. This is the most effective utilization of the transformer's secondary current rating. The arrangement shown in Figure 2.2 results in an asymmetry in the delta circuit owing to the longer outer busbars. In some installations where three separate single-phase transformers are used, the transformers are situated 120^{0} apart, around the furnace, in order to provide complete symmetry.

2.2.2 Primary high-voltage circuit

In view of the high-power demand for submerged-arc furnaces, practically all units have to be connected to a high-voltage electricity supply. The voltage supply to the furnace transformer is usually restricted to 33kV due to transformer design problems and the high cost of switchgear at higher voltages.

A typical example of the high-voltage circuit is shown in Figure 2.3. A dual busbar system is used to provide the facility for isolating a fault in any busbar, without having to discontinue supply to the furnace. The capacitor banks are included for power factor correction. One bank (bank A) is connected to the power system via a separate on-load circuit breaker and the other bank (bank B) is connected after the furnace breaker via an isolator switch. This avoids the necessity for an extra circuit breaker and isolator switch. However, it means that capacitor bank B can only be switched when the furnace breaker is off, whereas bank A can be switched independently. This is convenient since a certain amount of power factor correction is required for all furnace conditions with additional correction required when the power factor is low.

During normal furnace operation it is necessary to switch the load on and off quite frequently and the furnace breaker has to be capable of taking this

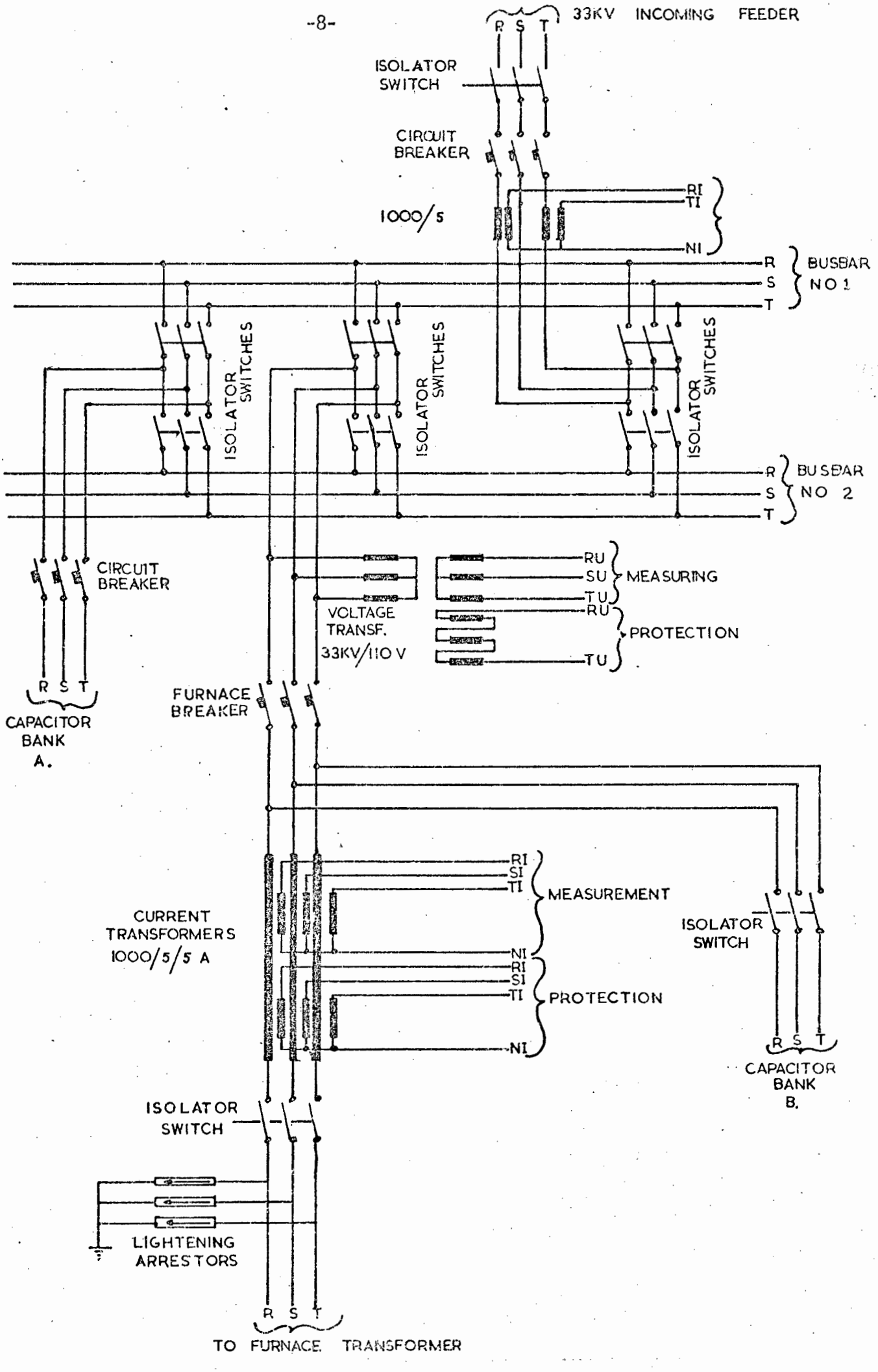

FIGURE 2.3: HIGH VOLTAGE CIRCUIT OF A LARGE SUBMERGED-ARC FURNACE

switching load as well as the short circuit current during fault conditions. In the arrangement shown in Figure 2.3 an air-blast circuit breaker is used, since this type of breaker has a high switching capability (10 000 - 15 000 operations between maintenance)[3], as well as a high breaking current capacity for short-circuit conditions.

The measurement and protection equipment for the high voltage circuit is fairly standard and uses voltage and current transformers connected as shown in Figure 2.3. The measuring equipment consists of panel meters for voltages, currents, total real power and total reactive power as well as an integrating energy meter. Chart recorders are sometimes included for the power measurements. Standard protection equipment is used for tripping the furnace if overcurrent, overvoltage, undervoltage or earth fault conditions occur.

2.2.3 The furnace transformer[26],[43]

The furnace transformer is different from standard power system transformers in that the secondary winding has to supply very high currents at low voltages. It is also necessary to be able to vary the secondary voltage, over a moderately wide range, to allow for variations in the resistance of the charge. The furnace transformer is usually fitted with on-load tap changing equipment. Off-load tap changers, although cheaper, are rarely used today as they require that the furnace be switched off for each tap change. This increases the switching load on the furnace breaker and valuable time getting power into the furnace is wasted.

On larger furnaces the furnace transformer is custom-built for the particular operation and the use of three separate single-phase transformers is quite common. The low voltage, high-current secondary winding has to be wound outside the high-voltage winding to allow for the many parallel connections that have to be made. An arrangement used by ASEA[43] is shown in Figure 2.4

where the parallel circuits connect together on alternate 'go' and 'return' vertical busbars which reduces the reactance. The windings are constructed in a core-type arrangement in accordance with modern high-voltage transformer practice, despite the fact that shell-type arrangements have inherently lower reactance owing to reduced leakage paths. The core-type windings are more robust and can be more effectively braced to withstand the forces resulting from the high currents.

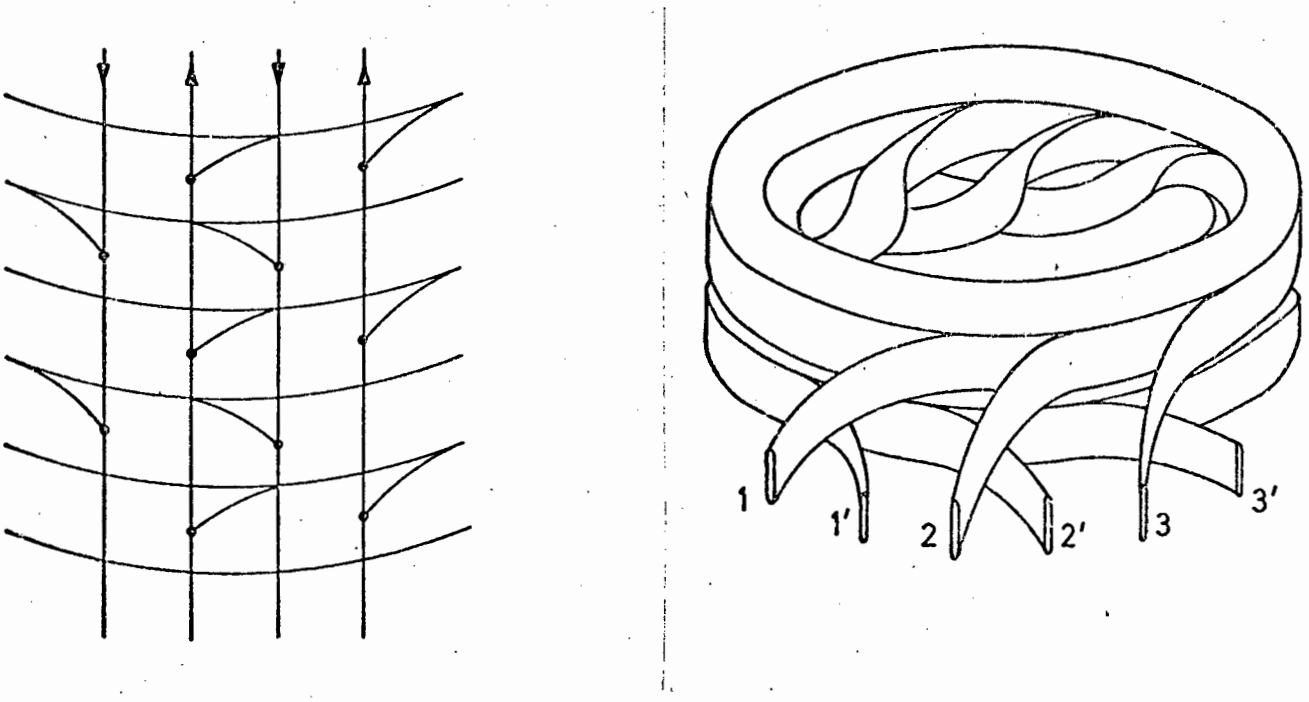

FIGURE 2.4 : ARRANGEMENT OF TRANSFORMER SECONDARY COILS (ASEA).

The tap-changing windings are included in the high voltage winding and are usually connected as an induction regulated transformer as shown in Figure 2.5(a). An alternative more expensive two-winding arrangement shown in Figure 2.5(b) is only used when a very wide secondary voltage variation is required. The tapping windings are connected to a tap-changing mechanism connected to the transformer tank. In the case of on-load tap changers, the changing contacts have to withstand the switching current which is limited by means of divertor resistors or reactors. A typical arrangement, using high-speed switches with two divertor resistors and operating on the flag-type principle, is shown in Figure 2.6. The actual on-load switch is housed in a separate oil compartment so that switching does not contaminate the transformer oil.

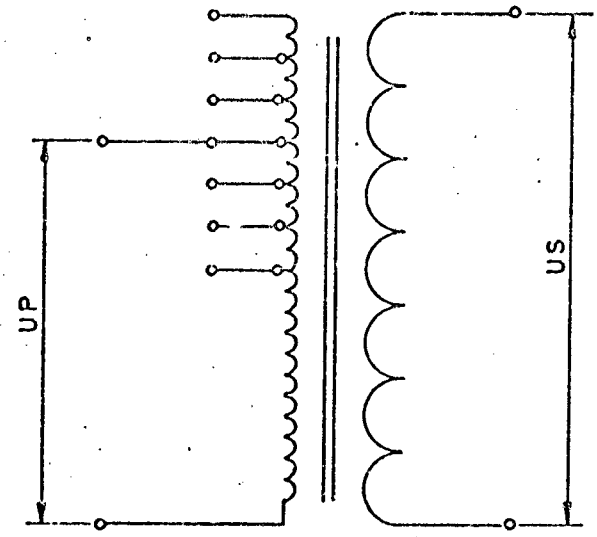

a) INDUCTION REGULATED TRANSFORMER

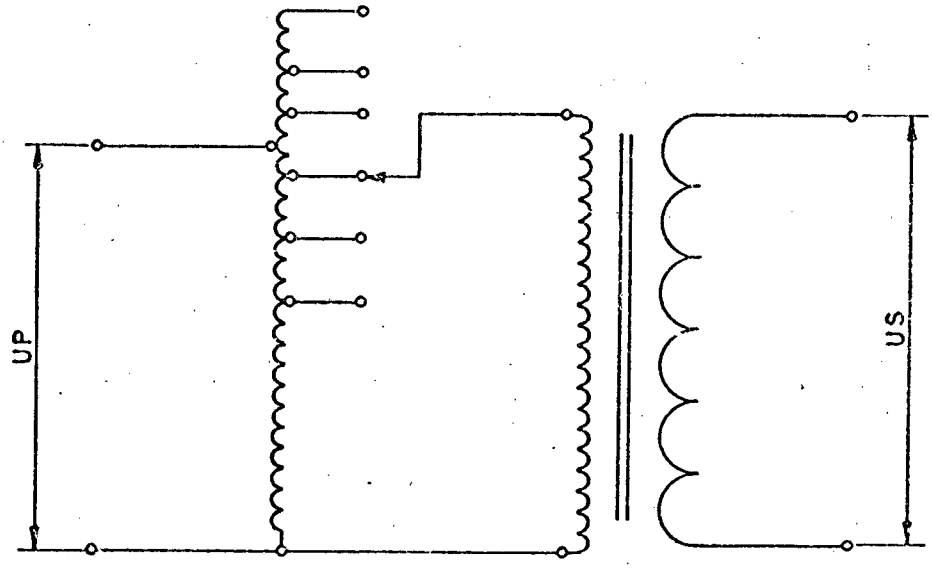

b) SEPARATE REGULATING WINDING AND FIXED RATIO TRANSFORMER

FIGURE 2.5 : FURNACE TRANSFORMER WINDING ARRANGEMENTS .

The secondary voltage adjustment range can be extended by the connection of the primary windings in delta for normal operation and the inclusion of the facility for a primary star connection during reduced load conditions. The secondary voltages for the star connection are $\sqrt{3}$ time smaller than for the delta connection.

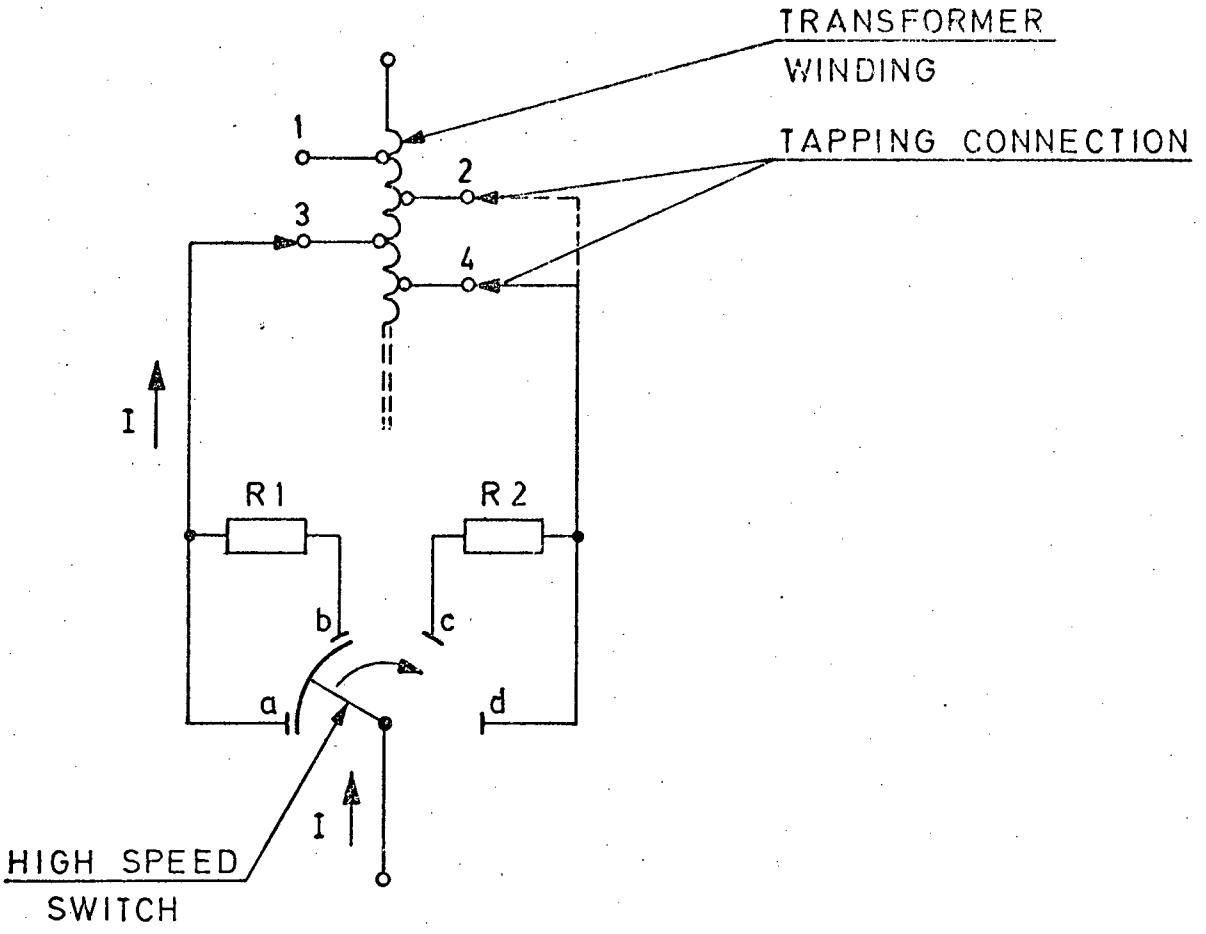

OPERATION SEQUENCE : (tap position (3) to (2))

(i) in tap position (3)

(ii) high speed switch connected to contact (a)

(iii) tap selector moved from position (4) to (2) - off load

(iv) high speed switch switched over with R_1 and R_2 limiting current generated by shorted winding

(v) high speed switch connected to contact (d).

FIGURE 2.6 : ON-LOAD TAP CHANGING WITH HIGH SPEED SWITCH AND DIVERTER RESISTORS.

2.2.4 Secondary busbars and flexibles

On large furnaces the resistance of the secondary circuit is very low (0,5 - 2 milli ohms) and the inductive voltage loss or reactance has to be made as low as possible to avoid having a low power factor operation. In the Knapsack connection the reactances of the busbars are minimized by closely interleaving the outgoing and incoming bars of the same phase and extending this interleaving as close to the electrodes as possible. Two common forms of interleaving arrangements are shown in Figure 2.7. On smaller furnaces the interleaved bus plates have been used almost exclusively, however, on larger furnaces the transposed, water-cooled bustubes are becoming more popular. The water-cooling allows for less conductor and hence cheaper construction.

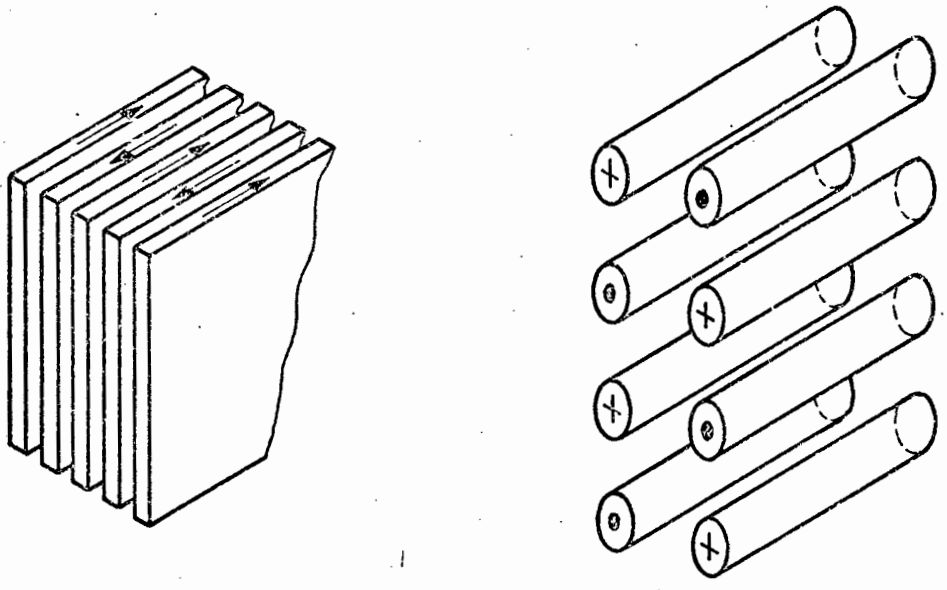

(a) interleaved bus-plates (arrow indicates current direction)

(b) transposed bus-tubes (+ go · return)

FIGURE 2.7 : COMMON INTERLEAVING ARRANGEMENTS.

The flexible cables link the busbars to the electrode column and permit vertical movement of the column (usually about 1-2 metres). They are usually made from woven copper wire for maximum flexibility. It is necessary to keep the cables as short as possible to reduce reactance. Figure 2.8(b) shows an arrangement which is used on some large furnaces to minimize the reactance of the flexibles. This is different from the more common arrangement shown in

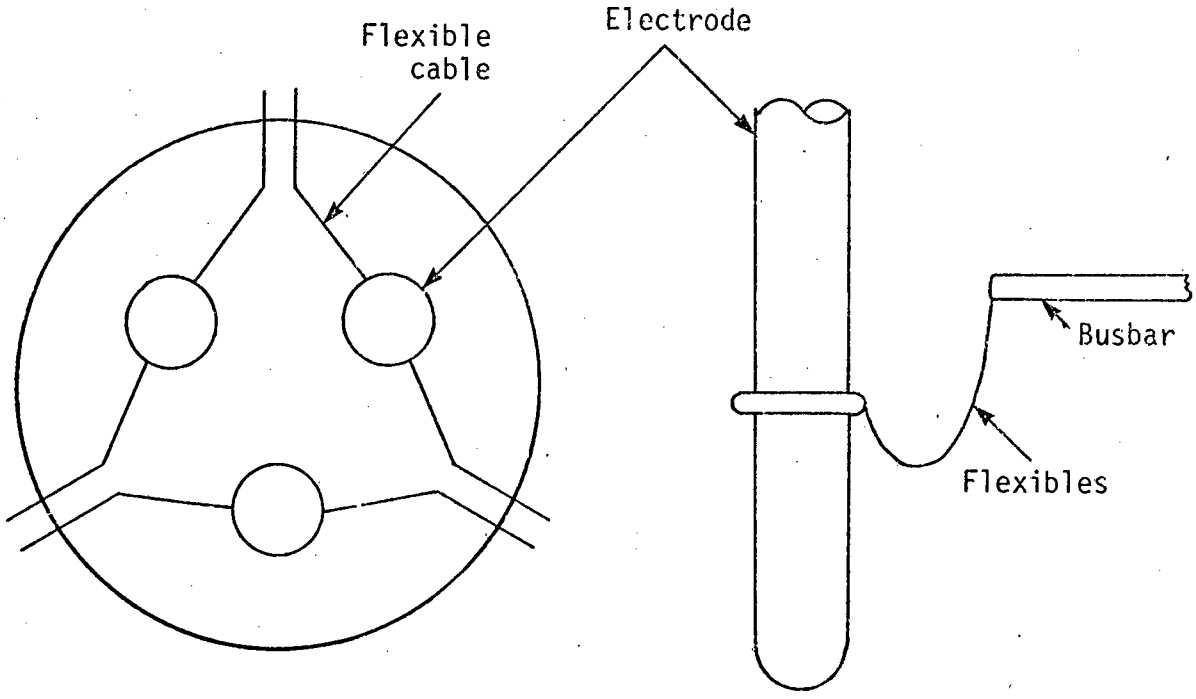

(a) Standard knapsack connection with 'long' flexibles

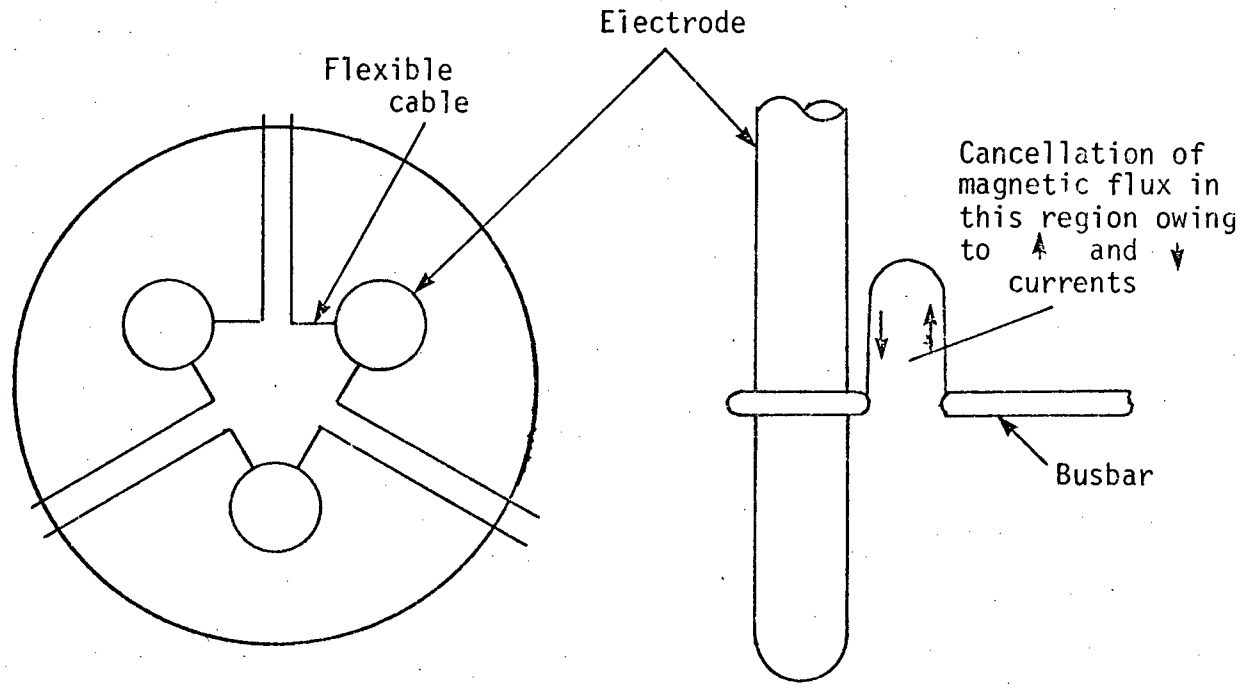

(b) Knapsack connection to reduce reactance

FIGURE 2.8 : FLEXIBLES ARRANGEMENTS FOR SUBMERGED-ARC FURNACES

Figure 2.8(a), in that the opening point of the flexibles is lower down and closer to the electrodes. This results in a lower reactance.

2.2.5 The electrode column

The electrode column consists of the supporting structure for the electrode, the electrode itself (which, together with the supporting structure may weigh as much as 20 tons) and a connection system for transferring the current from the flexibles into the electrode. The arrangement shown in Figure 2.9 is a hydraulically operated system which is common on large furnaces. On smaller furnaces motor-driven cable supports and reduction gearboxes are sometimes used. In Figure 2.9 the electrode column is supported from the upper level floor (3) by two hydraulic hoists (2) which are connected to a hoist platform (4). The electrode is held by two hydraulically operated clamping rings (5) and (6), one of which (5) is rigidly connected to the hoist platform (4). The clamp rings are connected together by a number of hydraulic actuators which, when activated, push the clamping rings apart.

During normal furnace operation the hydraulic hoists provide a means for adjusting the position of the electrode to allow for changes in the operating conditions of the furnace. The electrode tip is slowly eroded and this has to be replaced by the periodic slipping of the electrode through the clamp rings. A slip is performed by releasing the pressure in the top-clamp ring (6), applying pressure to the hydraulic actuators (7) to separate the two clamp rings, clamping (6), releasing (5) and releasing the pressure in the hydraulic actuators to allow the electrode to slip down. This results in a slip of about one to two centimetres, which is repeated until the required amount of slipping has been achieved.

Electrical current is supplied to the electrode on the floor below the supporting structure through a flexible connection plate (10). This plate is connected by water-cooled bustubes (9) to brass or copper contact shoes placed around the

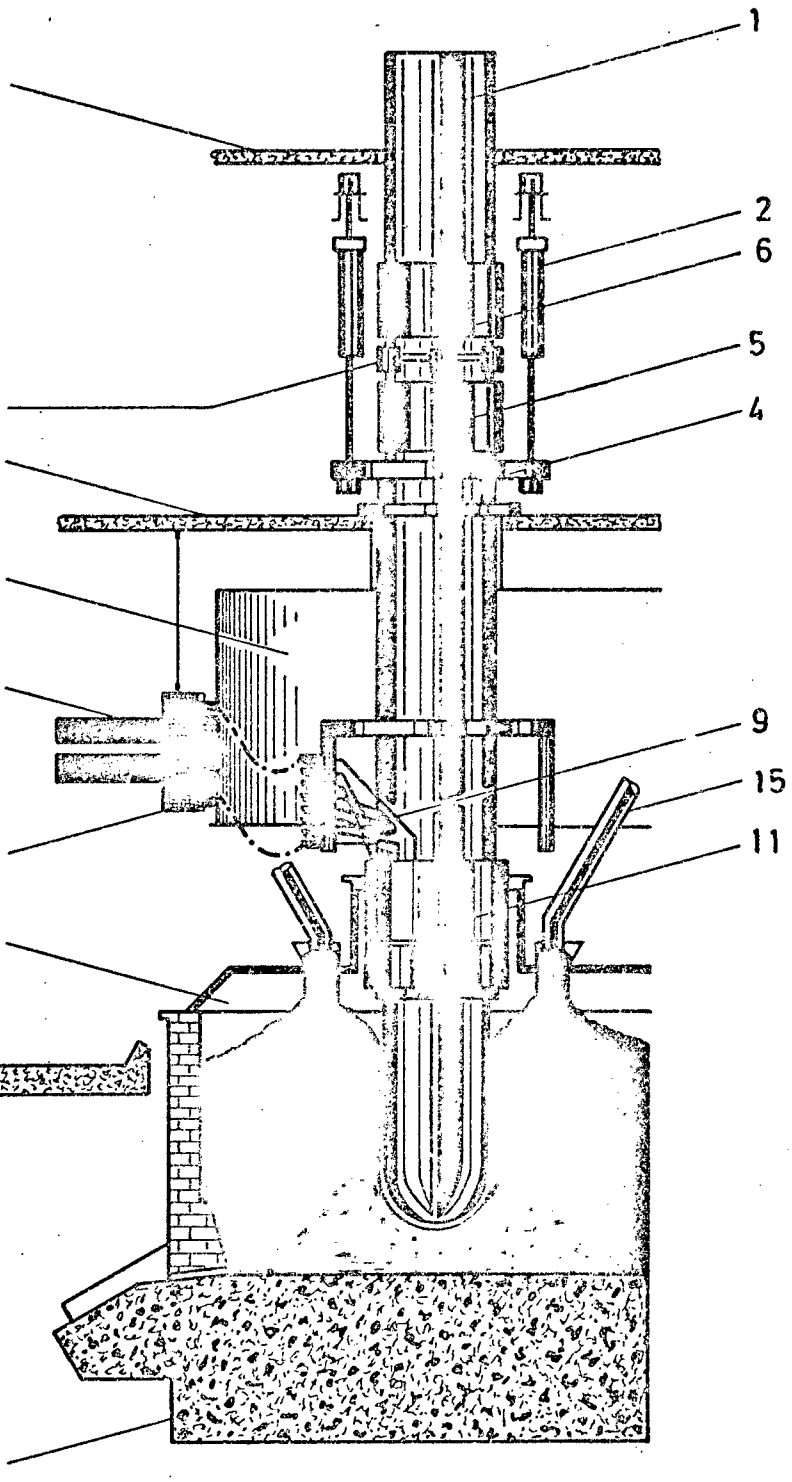

L E G E N D

1 Electrode casing
2 Hydraulic hoists
3 Upper level floor
4 Hoist platform
5 Bottom clamp ring
6 Top clamp ring
7 Hydraulic actuators
8 Middle level floor
9 Water-cooled bus tubes
10 Flexibles connecting plate
11 Housing for contact shoes
12 Busbars
13 Smoke hood
14 Furnace cover
15 Raw materials charging chute
16 Furnace body

FIGURE 2.9 : ELECTRODE AND SLIPPING MECHANISM

circumference of the electrode (11). The contact shoes are clamped onto the electrode by, either a rubber membrane activated by water pressure, or by mechanical spring pressure. The clamping pressure is maintained during slipping operations. The contact shoes are connected in segments by non-magnetic couplings to reduce eddy current problems. The contact shoe housing (11) is supported from the hoist platform (4).

2.2.6 The electrodes

The electrodes, which are made from carbon or graphite, provide the electrical link between the busbar supply and the hot furnace reaction zone. They have to be capable of carrying a high current and withstanding the very high temperatures generated by the electric arcs.

On old, small furnaces it was usual to use prebaked graphite electrodes, but with the increasing size of furnaces and larger electrodes, the maximum size of prebaked electrode available limited further increases in furnace capacity. A self-baking electrode invented by C.W. Söderberg[60],[23] provided a means for making larger electrodes, which are also cheaper than the prebaked type.

In the construction of Söderberg electrodes successive steel casings about 1-2 metres long are welded onto the electrode structure at the top of the furnace. Blocks of carbon paste are placed in the casing and these melt and bake, at the electrical contact clamping point, to form the electrode. A number of steel fins are welded onto the casing on the inside and provide strength for holding the electrode while the baked electrode is being formed. Most of the heat for baking is provided by the resistive heating from current flowing in the electrode. The maximum slipping rate of the electrode is related to the electrode size and current[50],[63]. If the electrode is slipped too fast, it may break just below the contact shoes as a result of inadequate baking (green break) and this is very detrimental to the furnace operation. The electrode

can also break further down (tip break) as a result of thermal and mechanical stresses or poor baking. If a break does occur it is necessary to replace the lost length. This involves slipping the electrode a large distance and then 'baking in' the electrode. The current is reduced to a low level and then progressively increased slowly without movement of the electrode. Depending on the length of the slip, this may take up to 12 hours and the furnace has to be run on reduced load during this period.

2.2.7 Furnace shell and lining

The lining and furnace shell of submerged-arc furnaces has to be designed for long life, since renewal involves a costly process where the complete shell and lining are replaced. This is achieved by incorporating a thick layer of carbon between the refractory lining and the charge. The carbon blocks can withstand very high temperatures and also serve as electrical conductors, so that neutral connections can be made to the molten bath. The life of a furnace lining is usually between 5 and 10 years, depending on the type of operation.

The furnace shell consists of a circular bath welded together from steel plate (usually 1 - 2 cms thick) and mounted on a circular platform about 1 - 2 metres from the ground (see Figure 2.1). On the inside of the furnace shell, the floor is covered with about ½ m of refractory brick, then a fairly thin layer of high-temperature refractory concrete which provides a smooth level surface. This surface is then covered by two layers of carbon blocks, crossed so as to cover the gaps between the blocks. The blocks, which are about 1 metre long and ½ metre square, have to be very carefully machined and aligned to minimize any gaps as gaps cause a weakness in the lining. The sides of the furnace are lined with a ½ m layer of refractory bricks and a ½ m layer of carbon bricks on the inside. Around the tapholes a special silicon carbide refractory and fire bricks are used. The roof of the furnace is water cooled and lined with a high-temperature refractory brick. During the operation of a furnace the high-temperature reaction zones under each electrode result in erosion of

the carbon lining under the electrodes. Observations of old furnace linings have revealed that in some cases this wear can be as much as 75 per cent of the carbon lining.

2.2.8 The neutral connection

The carbon lining of a furnace is electrically connected to the molten metal which acts as the neutral point for the furnace three-phase load. The measurement of the electrical potential of the neutral is provided by a copper rod imbedded in the carbon lining and connected to the side of the furnace with an insulated conductor. Unfortunately, on ferrochromium furnaces, this copper rod does not last long and until recently most large furnaces in South Africa were operated without a neutral connection.

During 1977 the lining of the ferrochromium furnace, being investigated, was rebuilt. This provided an opportunity for the installation of neutrals into the carbon lining. In order to provide a means for reducing measurement errors, it was decided to install separate neutrals under each electrode, as well as a neutral in the centre of the furnace floor (the reasons for this will be discussed later). The neutrals were constructed from stainless steel and set into the high temperature concrete layer, flush with the surface of the concrete. The area was then liberally covered with a layer of carbon paste and covered with the carbon blocks. The details of the neutral installation are given in Appendix B.

2.3 Operating Characteristics of a Furnace

The operating characteristics of a furnace have been discussed by many investigators [47,56,69], particularly the operation of open-arc furnaces. An example of these characteristics is shown in Figure 2.10. It is assumed that the furnace is balanced so that a single phase representation can be used. The characteristics are based on the assumption that the supply voltage is fixed (for a particular tap position) and the reactance is constant. The following equations, therefore, apply:

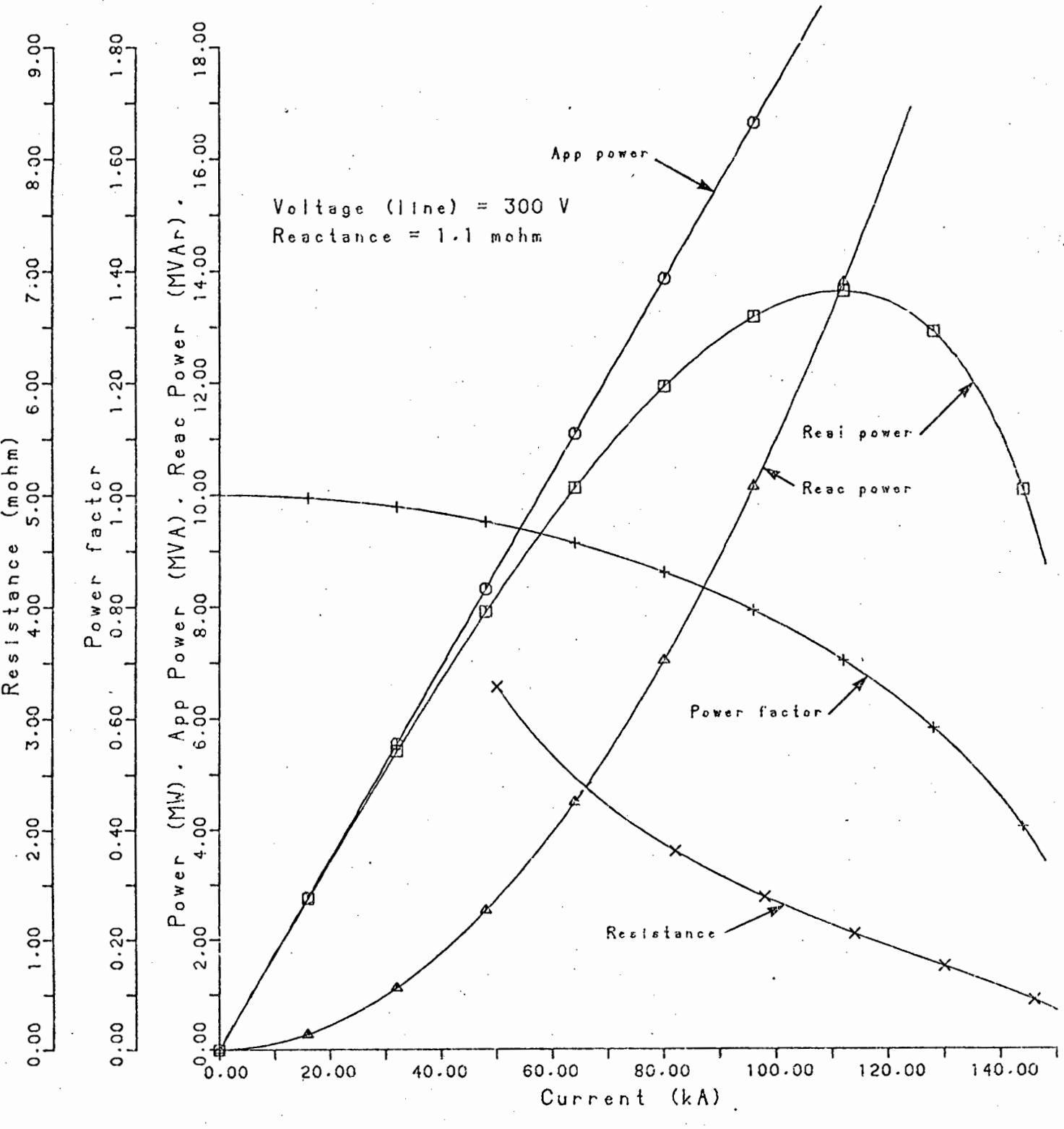

FIGURE 2.10 : OPERATING CHARACTERISTICS OF A FURNACE.

Real power per phase, $P = I.\sqrt{V^2 - (IX)^2}$ (2.1)

$= X.I.\sqrt{I_{max}^2 - I^2}$ kW (2.2)

Reactive power per phase, $Q = I^2.X$ kVAr (2.3)

Apparent power per phase, $S = V.I$ kVA (2.4)

Phase resistance, $R = \sqrt{(\frac{V}{I})^2 - X^2}$ mΩ (2.5)

where

V = transformer line to neutral voltage (volts)

I = phase current (kA)

X = phase reactance (mΩ)

The operation of submerged-arc furnaces involves trying to maintain maximum real power input to the furnace within the constraints or limits of the furnace equipment. These limits are usually, the maximum transformer MVA rating, the maximum electrode current and the maximum transformer secondary voltage. In the example shown in Figure 2.10, if it is assumed that the limits are 16 MVA for the transformer rating, 100 kA for the electrode current and 300 volts for the transformer secondary voltage, then the first limit reached on increasing electrode current will be the transformer MVA limit. If the secondary voltage is reduced, the slope of the apparent power curve will be reduced. This will allow the current to be increased until either the electrode current limit or the maximum real-power point for the particular voltage is reached.

2.4 Metallurgical Aspects

The metallurgical operation of ferrochromium furnaces is a complex problem, which is not well understood. The reduction reactions which occur in the hot region below the electrodes are dependent on many factors relating to the chemical and physical properties of the raw materials, as well as the

temperatures and material flow patterns occurring in the furnace. A major problem with studying the metallurgical operation is that virtually all observations have to be carried out indirectly, owing to the reaction zone being buried.

2.4.1 Cross-section of the interior of a furnace

The various regions in a furnace have been examined by investigators during 'digouts' of furnaces which have been taken out of operation for rebuilding. A problem with observations based on 'digouts' is that the furnace has to be allowed to cool before being excavated. This means that the conditions in the furnace may change. Nevertheless, investigations which have been carried out have revealed much about the flow of raw materials and the nature of the reaction zone beneath the electrodes.

An example of a cross-section through a pig-iron furnace is shown in Figure 2.11[2]. The region below each electrode is characterized by an area rich in coke, which forms under the electrode in the shape of a cone. The major flow of raw materials is around the electrodes with relatively inactive regions occurring away from the electrodes, next to the walls of the furnace. The molten metal forms in a well-defined open bath in the bottom of the furnace. The relatively low melting point of iron ensures that the metal remains in the molten state during normal operation of the furnace.

In another investigation of the furnace interior a Japanese team of investigators[77] studied the typical cross section of a small ferrochromium operation. Smelting operations on a 500 kVA two-phase furnace were carried out for a number of days until stable conditions had been obtained. The furnace was then switched off, quenched by a Nitrogen air blast to freeze as quickly as possible and covered with a synthetic resin, which solidified in the burden to enable it to be removed in one piece. This was then cut vertically into two pieces and one side was used for macro-observation of the furnace cross-section

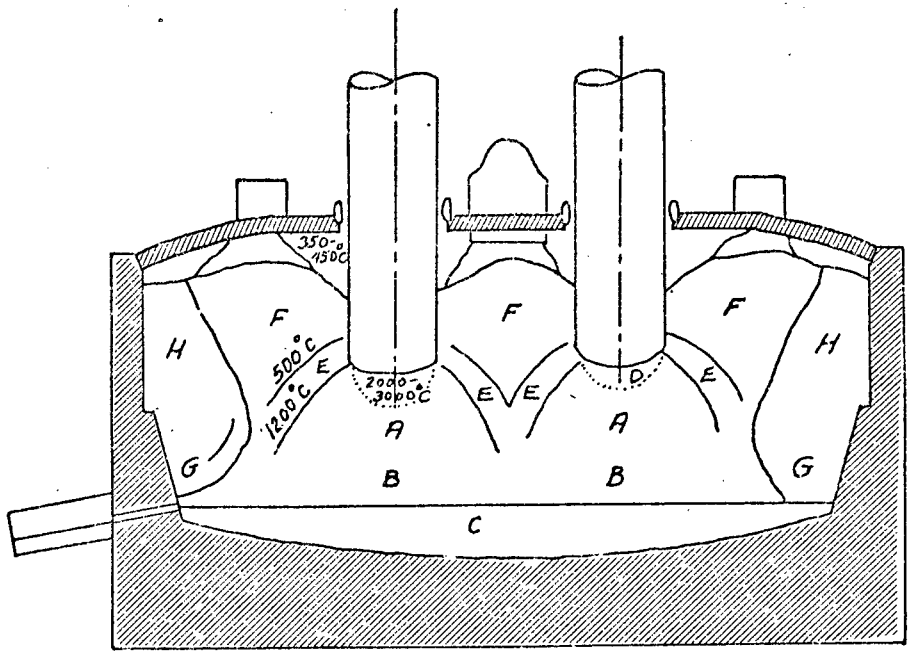

A. coke bed
B. slag bath
C. metal bath
D. highest temperature zone
E. prereduction & smelting zone
F. preheating zone
G. solidified slag
H. sponge iron

FIGURE 2.11 : METALLURGICAL STRUCTURE OF THE INTERIOR OF A PIG-IRON FURNACE.

while the other side was subjected to chemical analysis. Figure 2.12 shows the cross section observed. Alumina balls had been added to the charge 30 minutes and 1 hour before switch-off and these clearly show the material flow towards the electrodes. A small cavity was observed under each electrode, although this could have been a result of contraction of the charge. As with the pig-iron furnaces a considerable amount of coke was found in the melting and reduction area, except that in this case the coke bed did not form as a well-defined cone under the electrode. In both cases the observed cross-section suggests a current conduction path downwards from the electrode, through the slag layer and into the metal layer, with little evidence of significant inter-electrode conduction. The presence of the coke bed in the reaction zone suggests fairly stable inter-particulate conduction through the coke and slag layers, without the formation of a large arcing cavity under each electrode.

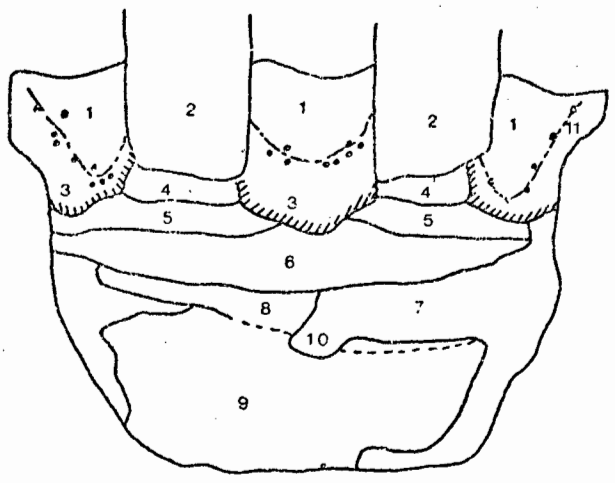

1. charge layer
2. electrode
3. coke bed
4. cavity
5. slag layer
6. layer of unmolten metal
7. layer of molten ore
8. metal pool
9. residual metal
10. tap hole
11. alumina balls

FIGURE 2.12 : CROSS-SECTION OF A 500 kVA CHARGE CHROME FURNACE.

2.4.2 Furnace resistance and 'k' factors

Many investigators have attempted to relate the furnace resistance or charge resistance to fundamental properties, the major objective being to provide a means for scaling up and designing new furnaces. In the 1920's Andreae [1] was the first to realize that for a particular type of operation, the product of electrode diameter and furnace resistance was approximately constant for various sizes of furnaces which operated satisfactorily. This can be expressed mathematically in the formulae

$$k = \Pi.R.D \qquad (2.6)$$

or

$$k = \Pi.\frac{E}{I}.D \qquad (2.7)$$

where R = resistance, D = electrode diameter, E = electrode-to bath voltage and I = electrode current. The constants for each type of operation have become known as the 'k' factors, or electrode periphery resistances. This concept can be qualitatively rationalized by a simple model discussed by Reddy[53]. Assume that current flows in a cylindrical region below the electrode which is defined by translating the electrode perimeter to the metal layer through a distance αD, then

$$R = \rho \frac{\alpha D}{\frac{\pi D^2}{4}} \qquad (2.8)$$

or $\pi RD = \rho \cdot \text{constant}$

where ρ = specific resistivity of the charge for the particular product. This is a simplified model. However, the important point is that it is based on assuming that the geometry of the reaction zone is related to the electrode diameter. Müller[48] has investigated this concept more thoroughly using water model experiments for determination of the cell constants of the reaction zone. He found that, provided the resistivity of the region could be assumed to be constant, the equation for the cell constant could be rewritten in the form of Andreae's equation for 'k' factors, and he concluded that for a particular type of process the reaction zone has a characteristic size and height/width ratio which is related to the electrode diameter.

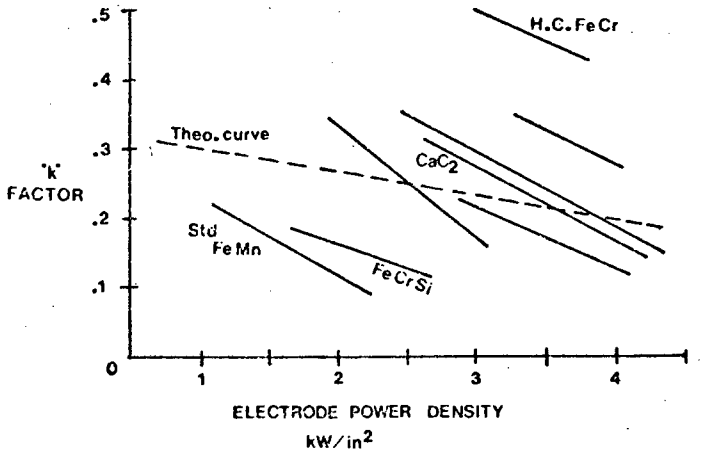

FIGURE 2.13 : PLOT OF "k" FACTORS.

In the 1950's Kelly[39], following on from Andreae's work, examined the operating characteristics of a large number of different types of furnaces. A number of interesting observations were made. The first of these was that, if the 'k' factors for each operation were plotted against the electrode power density, this resulted in a number of straight lines, as shown in Figure 2.13. Each different type of operation was characterized by a separate straight line on

the graph. Another observation was that the current density in the electrodes was proportional to the inverse square root of the electrode diameter. These two observations can be expressed mathematically as,

$$k \alpha \text{ electrode power density} \tag{2.9}$$

$$\text{electrode current density } \alpha \ D^{-\frac{1}{2}} \tag{2.10}$$

where D = electrode diameter. The area of the electrode $A = \frac{\pi D^2}{4}$

so that

$$\text{electrode current } I \alpha D^{-\frac{1}{2}} \cdot A$$

$$I \alpha D^{1,5} \tag{2.11}$$

Similarly, from equation (2.9)

$$k \alpha P.D^{-2} \tag{2.12}$$

where P is the electrode power. However, $P = I^2R$ so that

$$k \alpha I^2.R.D^{-2} \tag{2.13}$$

The combination of equations (2.11) and (2.13) gives,

$$k \alpha D^3.R.D^{-2}$$

$$k \alpha RD \tag{2.14}$$

This is equivalent to Andreae's formula (2.6). Therefore, Kelly's observations are consistent with Andreae's concept of the electrode periphery resistance.

In a subsequent investigation Persson[52], in attempting to relate Kelly's 'k' factors to large ferromanganese furnaces, found that, instead of a straight line relationship between 'k' factor and power density, the 'k' factor was inversely proportional to power density.

The equation for power density is given by

$$\text{power density, pd} = \frac{E_h^2}{R} \cdot \frac{1}{\frac{\pi D^2}{4}} \qquad (2.15)$$

where E_h = component of electrode-to-bath voltage which is in phase with the current.

The rearrangement of equation 2.15 to include Andreae's formula 2.6 gives

$$\frac{E_h}{\sqrt{D}} = \sqrt{\frac{k.pd}{4}} \qquad (2.16)$$

Persson then showed that the parameter $\frac{E_h}{\sqrt{D}}$ was a constant for a particular type of process. However, if one considers that large ferromanganese furnaces have a notoriously low power factor and that Kelly wrote his formula in the form of 2.7, where

$$k = \pi.\frac{E}{I} . D \qquad (2.17)$$

and E = electrode-to-bath voltage, then Persson's rearrangement of the formula to replace E by the in-phase component of the electrode-to-bath voltage is really an allowance for the high reactance of large furnaces, particularly ferro-manganese furnaces.

2.4.3 The significance of power density in the operation of submerged-arc furnaces

Muller has shown that Andreae's concept of electrode periphery resistance can be related to the fact that for a particular furnace operation the reaction zone beneath each electrode has fixed geometrical properties, which are dependent on the electrode diameter. If the reaction zone is represented by a parabaloid, as shown in Figure 2.14, this means that the height of the electrode above the bath h is proportional to the electrode diameter D. In a recent investigation Rennie[54,55] concluded that

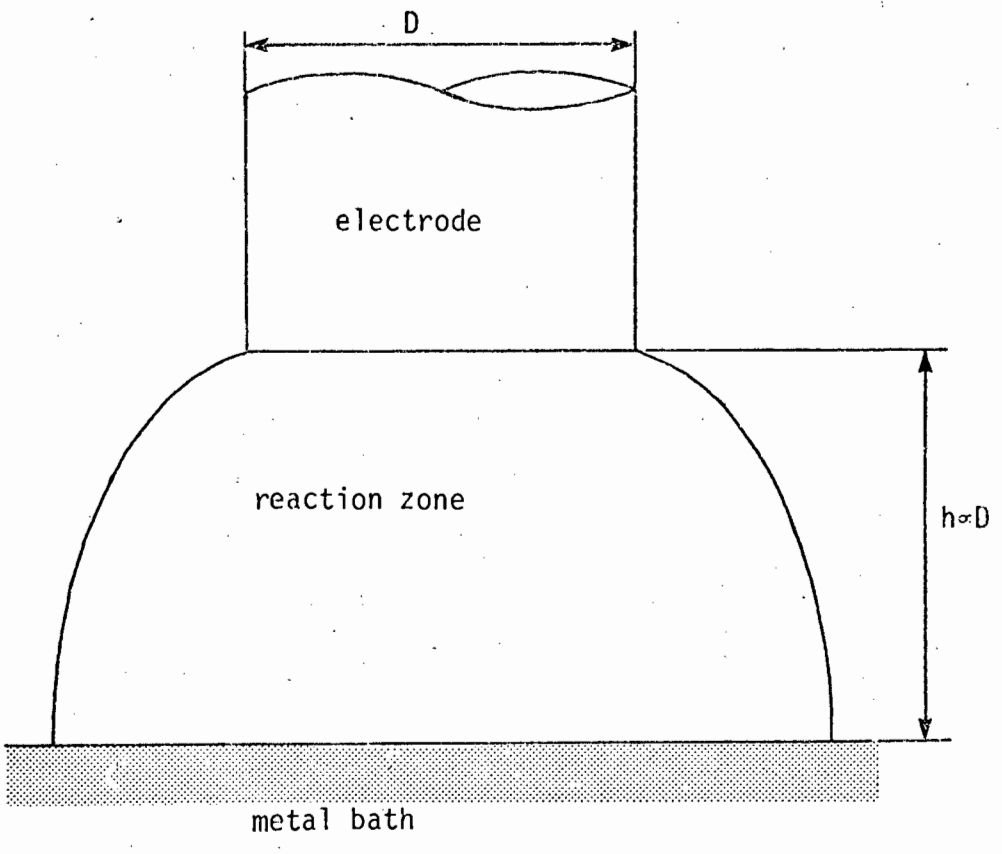

FIGURE 2.14 : REPRESENTATION OF REACTION ZONE AS PARABALOID.

the fundamental criteria, which determines the height of the electrode above the metal bath, is the power density in the reaction zone. Rennie developed a technique for measuring the height of an electrode above the metal bath in an operating furnace and found that he had to make corrections for the accumulation and draining of frozen metal below the reaction zone. It was observed that the height of the electrode above the bath remained remarkably constant at around 0,8 to 1,0 m, and this lasted for a wide range of electrode lengths and accumulations of metal. The reason for this behaviour appeared obvious in that, at a greater distance the metal would cool, solidify, and accumulate within the furnace, and that, at a shorter distance, the heat concentration was sufficient to melt any metal that had accumulated. The important parameter, which determines the position of the interface between the reaction zone and the metal (frozen or molten), is the power density sufficient to avoid freezing of the metal. This is shown in Figure 2.15.

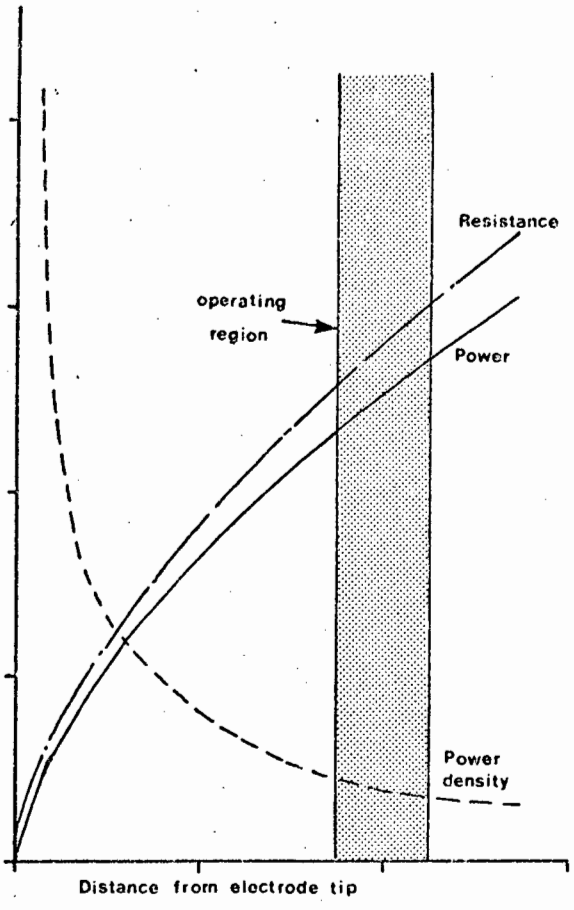

FIGURE 2.15 : TYPICAL FURNACE CHARACTERISTICS.

2.4.4 Resistivity of the furnace charge and inter-electrode conduction

The charge in a furnace is heated up as it descends in the furnace and this results in a reduction in the resistivity. At high temperatures the resistivity is sufficiently low to allow significant conduction, so that current can flow between the electrodes in a furnace. The magnitude of the inter-electrode conduction relative to the bath conduction can only be determined hypothetically, using measurements of the relationship between charge resistivity and temperature which are obtained from laboratory experiments. Various apparatus have been developed to measure resistivities[29,72,75]. These are based on measurement of the resistance between two electrodes immersed in a heated crucible containing the charge.

Urquhart[72] has used the results of laboratory measurements to predict the degree of inter-electrode conduction in a large charge-chrome furnace and concluded that up to 15 per cent of the electrode current flowed between the electrodes. However, he was only able to obtain charge resistivity measurements up to a temperature of 1500^{o}C and made incorrect assumptions about the resistivity above these temperatures. Subsequent investigations by Rennie[54]

have shown that the resistivity of the charge beneath the electrode is much lower than that assumed by Urquhart, and Rennie has concluded that only 2 per cent of the electrode current flows between the electrodes. This has a significant bearing on any modelling of the current paths in a furnace as, on this basis, the inter-electrode conduction can be ignored.

3. EQUIVALENT CIRCUIT REPRESENTATION OF ELECTRICAL CIRCUIT

In analysing the electrical circuit of a submerged-arc furnace it is usual to represent various sections of the circuit as lumped impedances, which together make up the equivalent circuit of the furnace. In this chapter the analysis will be restricted to modelling the circuit in terms of linear resistances and inductances leaving the more complicated analysis of arcing to Chapter 5.

3.1 Equivalent Star Representation

The principle load circuit of an arc furnace is a star circuit where current flows down the three electrodes to the molten bath which acts as neutral point for the three-phase circuit. This neutral point is not connected back to the furnace transformer, so the phasor sum of the three electrode currents I_1, I_2 and I_3 must add up to zero, i.e.,

$$I_1 + I_2 + I_3 = 0 \qquad (3.1)$$

In the Knapsack connection the furnace transformer secondary is connected in delta to the electrodes via the busbars and flexibles. It is usual practice to consider the delta portions of the secondary circuit together with the star circuit as a combined star representation where the delta resistances and inductances are converted to their equivalent star values. The major inductances in the circuit are generated as self and mutual inductances in the loops formed by the electrodes. The self and mutual inductances in the delta circuit are low owing to the close interleaving of the 'go' and 'return' current lines which cause cancellation of most of the magnetic flux generated by the busbars. In addition,the power source is usually assumed to be an 'infinite bus' (system with very low source impedance). This leads to the equivalent star representation as shown in Figure 3.1(a) where the electrode currents I_1 and I_3 are considered as forming current loops by returning through electrode 2. From 3.1

$$I_2 = -I_1-I_3 \qquad (3.2)$$

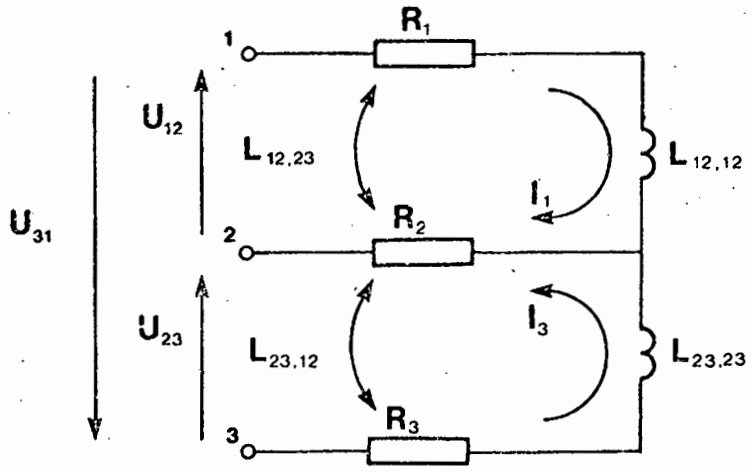

(a)

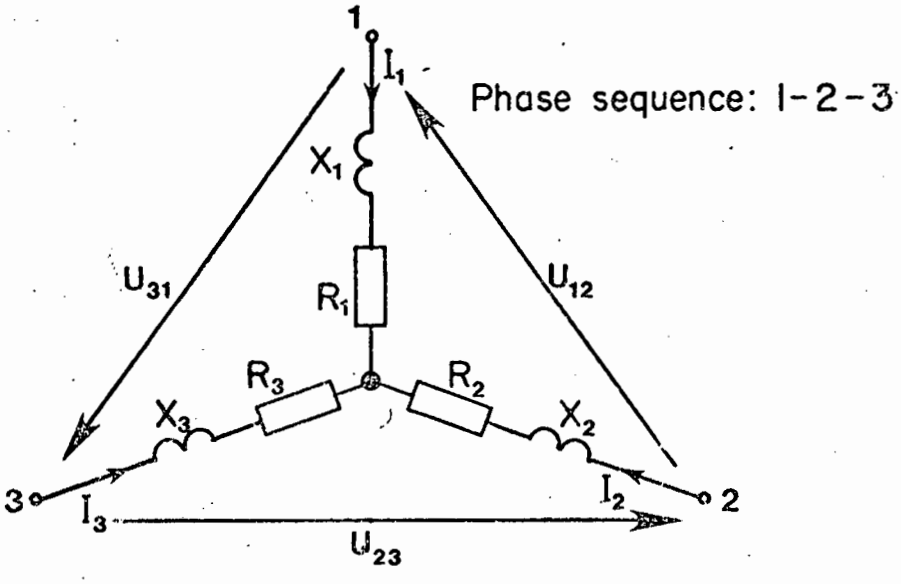

(b)

FIGURE 3.1 : EQUIVALENT STAR REPRESENTATION OF THE FURNACE CIRCUIT

The self and mutual inductances are denoted by the use of the convention where the first subscript indicates the loop in which a voltage is induced as a result of current flowing in the loop indicated by the second subscript. Thus, $jwL_{12,23}\cdot I_3$ gives the voltage induced in loop 12 as a result of current I_3 flowing in loop 23. The inductance effects in each loop can be described by a self inductance in the loop associated with current flowing in that loop and a mutual inductance associated with current flowing in the other loop, which leads to the equations:

$$\begin{aligned} U_{12} &= I_1\cdot(R_1+R_2) + I_3\cdot R_2 + jwL_{12,12}\cdot I_1 - jwL_{12,23}\cdot I_3 \\ U_{23} &= -I_1 R_2 - I_3\cdot(R_2+R_3) - jwL_{23,23}\cdot I_3 + jwL_{23,12}\cdot I_1 \end{aligned} \qquad (3.3)$$

From the Neumann double integral it can be shown that the mutual inductance associated with a voltage induced in one loop, ab, as a result of current flowing in another loop, cd, is the same as the mutual inductance associated with a voltage induced in loop cd, as a result of current flowing in the other loop, ab. Also a reversal of the flow of current results in a reversal of the sign of the induced voltage. Therefore:

$$L_{ab,cd} = -L_{ba,cd} = L_{ba,dc} = L_{dc,ba} = -L_{cd,ba} = L_{cd,ab} \qquad (3.4)$$

The use of equations 3.1 and 3.3 together with 3.4 gives

$$\begin{aligned} U_{12} &= I_1[R_1 + jw(L_{12,12}+L_{12,23})] - I_2\cdot[R_2 - jwL_{12,23}] \\ U_{23} &= I_2[R_2 - jw\,L_{23,12}] - I_3\cdot[R_3 + jw(L_{23,23} + L_{23,12})] \end{aligned} \qquad (3.5)$$

The rearrangement of 3.5 results in

$$\begin{aligned} U_{12} &= I_1\cdot(R_1+jwL_1) - I_2\cdot(R_2+jwL_2) \\ U_{23} &= I_2\cdot(R_2+jwL_2) - I_3\cdot(R_3+jwL_3) \end{aligned} \qquad (3.6)$$

and by a similar analysis

$$U_{31} = I_3(R_3+jwL_3) - I_1\cdot(R_1+jwL_1)$$

where

$$L_1 = L_{12,12} + M$$
$$L_2 = -M$$
$$L_3 = L_{23,23} + M$$
$$M = L_{23,12} = L_{12,23}$$

This leads to the 'uncoupled' equivalent circuit representation shown in Figure 3.1(b) where the star voltages U_{10}, U_{20} and U_{30} are:

$$U_{10} = I_1.(R_1+jwL_1) = I_1.(R_1+jX_1) = I_1Z_1$$
$$U_{20} = I_2.(R_2+jwL_2) = I_2.(R_2+jX_2) = I_2Z_2 \qquad (3.7)$$
$$U_{30} = I_3.(R_3+jwL_3) = I_3.(R_3+jX_3) = I_3Z_3$$

This analysis is similar to that given by Clausert [25] and Köhle [40]. The inductances L_1, L_2 and L_3 are fictitious inductances, in that inductance really only has meaning for current loops. However, they are useful in providing a simple equivalent circuit which can be analysed easily.

With reference back to the third equation in 3.6

$$U_{31} = I_3.(R_3+jwL_3) - I_1.(R_1+jwL_1)$$

L_3 can be rewritten as $L_{31,32}$, i.e., the mutual inductance associated with a voltage induced in loop 31 as a result of current I_3 flowing in loop 32.

Similarly,

$$L_1 = L_{31,21} \qquad (3.8)$$

where the 21 subscript is a result of the negative current. With the use of 3.4 equation 3.8 can be rewritten as

$$L_1 = L_{31,21} = L_{13,12}$$

By a similar analysis the rest of the mutual inductances can be derived:

$$L_1 = L_{12,13} = L_{13,12}$$
$$L_2 = L_{23,21} = L_{21,23} \qquad (3.9)$$
$$L_3 = L_{31,32} = L_{32,31}$$

3.2 Delta-Star Equivalent Circuit

In the Knapsack connection for submerged arc furnaces the secondary windings of the transformer are connected in delta together with the secondary busbars and flexibles. The delta connection is closed at the electrodes which together with the furnace bath form a star circuit. The combined delta-star equivalent circuit as shown in Figure 3.2(a), is a more exact representation of the secondary circuit than the star equivalent circuit. It is assumed that the mutual inductance effects in the delta circuit are low owing to the flux cancellation and that the mutual inductance effects in the star circuit can be combined to the uncoupled star form as shown in the previous section.

With this representation it is possible to represent the resistances and reactances of each section of the circuit separately. The transformer impedances are lumped together with the primary busbar impedances as Z_{TR}, Z_{TS}, Z_{TT}, the secondary busbars as Z_{BR}, Z_{BS}, Z_{BT}, the flexibles as Z_{FR1}, Z_{FR2}, Z_{FS2}, Z_{FS3}, Z_{FT3}, Z_{FT1} and the star load circuit as Z_1, Z_2, Z_3. The addition of the delta impedances gives:

$$Z_R = Z_{TR} + Z_{BR} + Z_{FR1} + Z_{FR2}$$
$$Z_s = Z_{TS} + Z_{BS} + Z_{FS2} + Z_{FS3} \qquad (3.10)$$
$$Z_T = Z_{TT} + Z_{BT} + Z_{FT3} + Z_{FT1}$$

as shown in Figure 3.2(b). The electrode to electrode voltages V_{12}, V_{23}, V_{31} can be determined from

$$V_{12} = V_R - I_R Z_R$$
$$V_{23} = V_S - I_S Z_S \qquad (3.11)$$
$$V_{31} = V_T - I_T Z_T$$

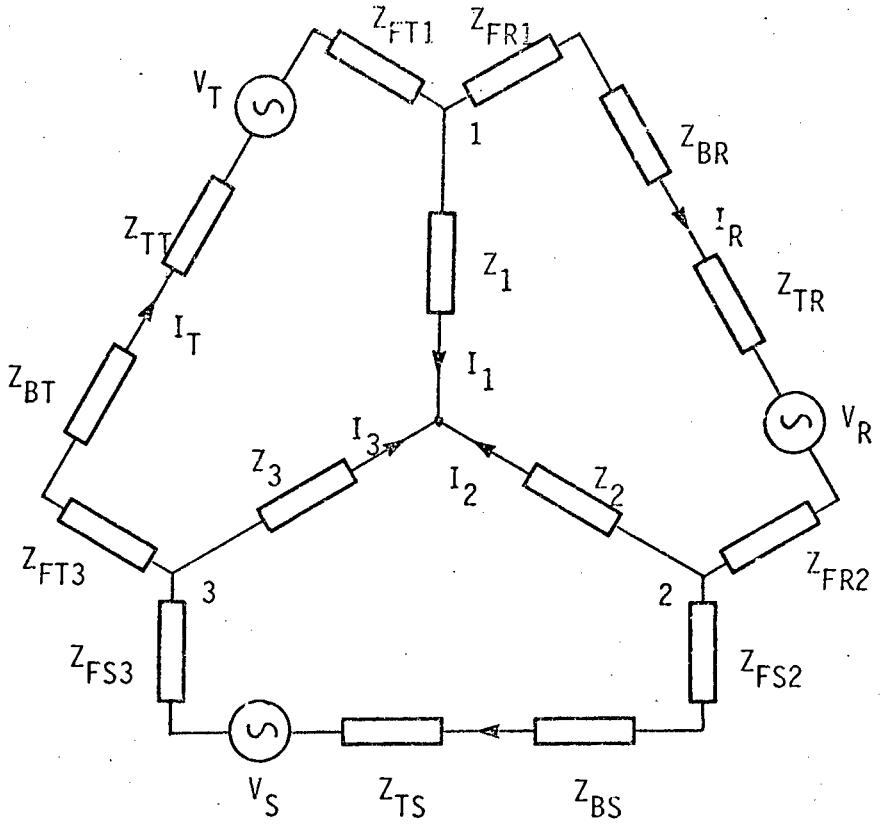

(a)

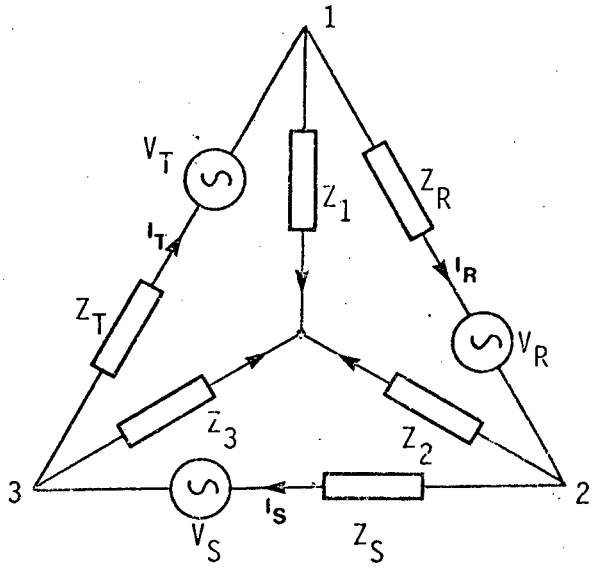

(b)

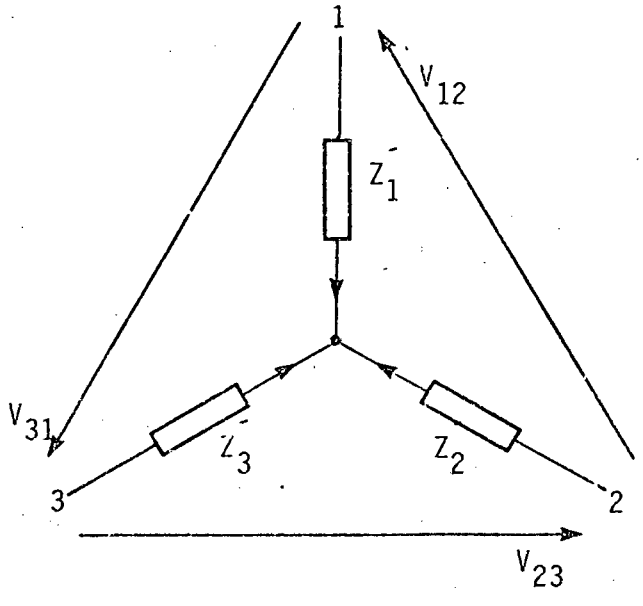

(c)

FIGURE 3.2 : DELTA-STAR EQUIVALENT CIRCUIT REPRESENTATION

and the circuit can then be analysed as the star circuit shown in Figure 3.2(c). The delta and star sections of the circuit are distinguished by using R,S and T subscripts for the delta circuit and 1,2 and 3 subscripts for the star circuit.

3.2.1 Analysis of Delta-Star Equivalent Circuit

The delta parts of the delta-star equivalent circuit have been measured on an operating furnace by measuring the line voltage power and current at the transformer secondary and also at the opening point of the flexibles simultaneously. These measurements were carried out on the 48MVA ferrochrome furnace being investigated. The measurements were taken for the R and S transformers (it being assumed that the T transformer and busbar arrangement will be the same as for the R transformer) and are summarized in Table 3.1. The results show the busbar resistances as being very small. However, the reactances are quite significant being 0,37 mΩ for the R and T busbars and 0,24 mΩ for the S busbars.

The contribution of the transformers to the delta circuit can be determined from the manufacturers test data. Typical short circuit characteristics for tap 13 are:

V = 2400 volts

I = 482 amps

P = 125352 watts

This gives a resistance of 0,533Ω and reactance of 4,95Ω . The turns ratio for tap 13 is 132,5 so referring these results to the secondary gives a resistance of 0,04 mΩ and reactance of 0,28 mΩ. There will be small changes in these values for different tap positions, however, they will be used as nominal values.

With these measurements the impedances of all parts of the delta circuit, except the flexibles have been determined. Unfortunately, there is no reliable means available to measure the impedances of the flexibles as voltage measurements

	VOLTAGE CONNECTION TO TRANSFORMER SECONDARY					VOLTAGE CONNECTION TO FLEXIBLES OPENING POINT					Busbar resistance (mΩ)	Busbar reactance (mΩ)
	Voltage (Volts)	Current (kA)	Power (MW)	Resist (mΩ)	React (mΩ)	Voltage (Volts)	Current (kA)	Power (MW)	Resist, (mΩ)	React, (mΩ)		
R BUSBAR	278	60,55	13,38	3,65	2,78	262	60,55	13,18	3,59	2,41	0,06	0,37
	277	58,79	12,77	3,69	2,92	261	58,79	12,57	3,64	2,55	0,05	0,37
	277	58,25	12,87	3,79	2,87	262	58,25	12,7	3,74	2,49	0,05	0,38
	277	58,12	13,14	3,89	2,75	262	58,12	13,01	3,85	2,34	0,04	0,41
	278	59,6	13,45	3,78	2,72	263	59,6	13,18	3,71	2,39	0,07	0,33
						A V E R A G E S					0,05	0,37
S BUSBAR	279	44,6	9,53	4,79	4,02	272	44,6	9,49	4,77	3,8	0,02	0,22
	280	44,06	9,29	4,79	4,18	272	44,06	9,26	4,77	3,92	0,02	0,26
	279	52,04	11,56	4,27	3,25	271	52,04	11,52	4,26	3,00	0,01	0,25
	276	52,71	11,05	3,98	3,41	267,5	52,71	11,02	3,96	3,17	0,02	0,24
	278	49,6	11,02	4,48	3,37	270	49,6	10,95	4,45	3,14	0,03	0,23
						A V E R A G E S					0,02	0,24

TABLE 3.1 : Measurement of busbar resistances and reactances on a 48MVA submerged-arc furnace

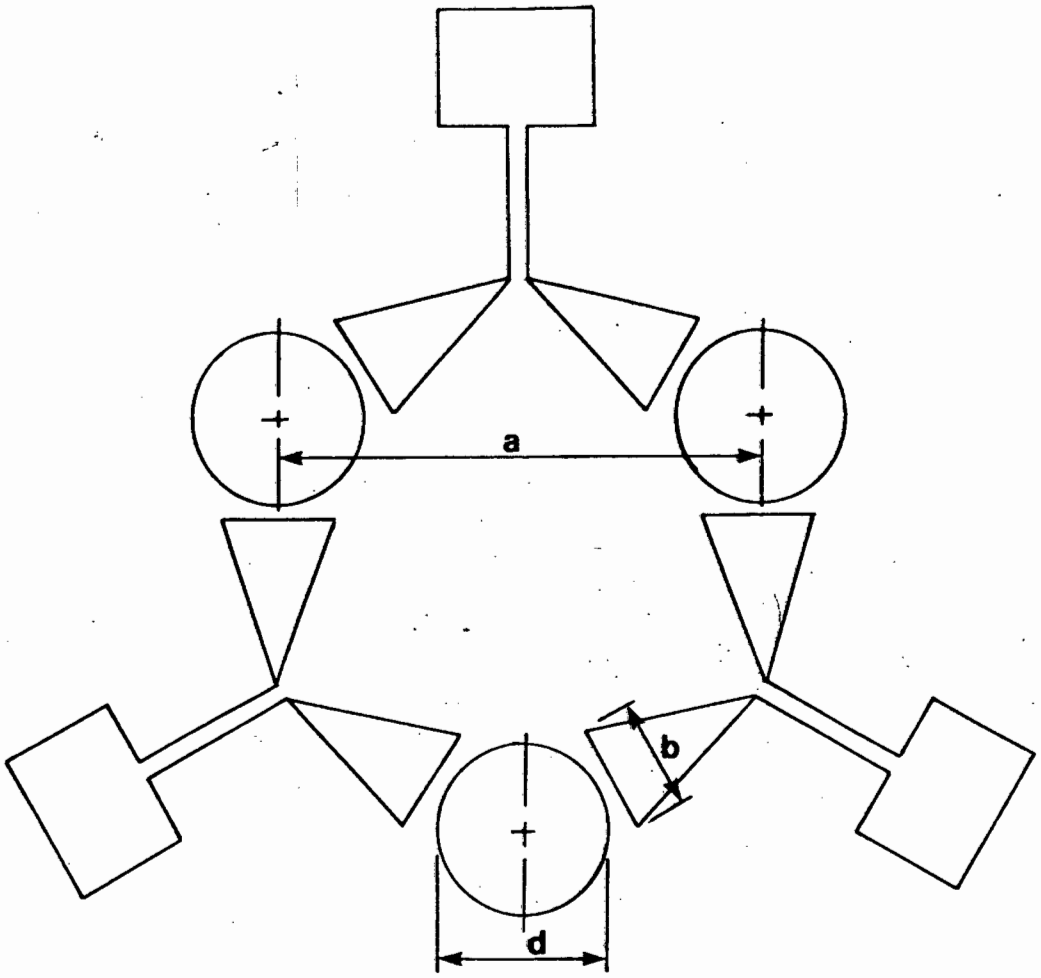

$$L = (L_D - M_D)/3$$

where L_D and M_D can be approximated by,

$$L_D = \frac{\mu_o\, h}{\pi} \ln \frac{a - d}{0{,}223\ b} \qquad \text{(self inductance)}$$

$$M_D = \frac{\mu_o\, h}{2\pi} \ln \frac{a}{d} \qquad \text{(mutual inductance)}$$

For the furnace:

$a = 3{,}7$ m

$b = 0{,}8$ m

$d = 1{,}7$ m

$h = 1{,}0$ m

$\mu_o = 4\pi \times 10^{-7}$ volt sec/amp m

$X = 2\pi fL = 0{,}11\ m\Omega$

FIGURE 3.3 : REACTANCE OF THE FLEXIBLES.

cannot be made without forming large measurement loops which would introduce errors. A calculation technique for determining the reactances of the flexibles has been derived by Ström[68] and is shown in Figure 3.3. The substitution of approximate values for the furnace gives a flexible reactance X_f = 0,12 mΩ. The resistance of the flexibles and bustubes is 0,1 mΩ.

The substitution of the above values into the star-delta equivalent circuit gives the equivalent circuit shown in Figure 3.4. If the imbalance for the S phase is ignored, the delta values must be divided by 3 to convert them to equivalent star values. This results in approximate star resistances of 0,1 mΩ and reactances of 0,28 mΩ. Typical star circuit operating values for the furnace are resistances of 1,2 mΩ and reactances of 1,1 mΩ at a secondary line voltage of 300 volts. The subtraction of the transformed delta impedances then gives 'true' star values of R = 1,1 mΩ and X = 0,82 mΩ. This means that the delta circuit contributes approximately 25 per cent of the equivalent star circuit reactance and 10 per cent of the resistance.

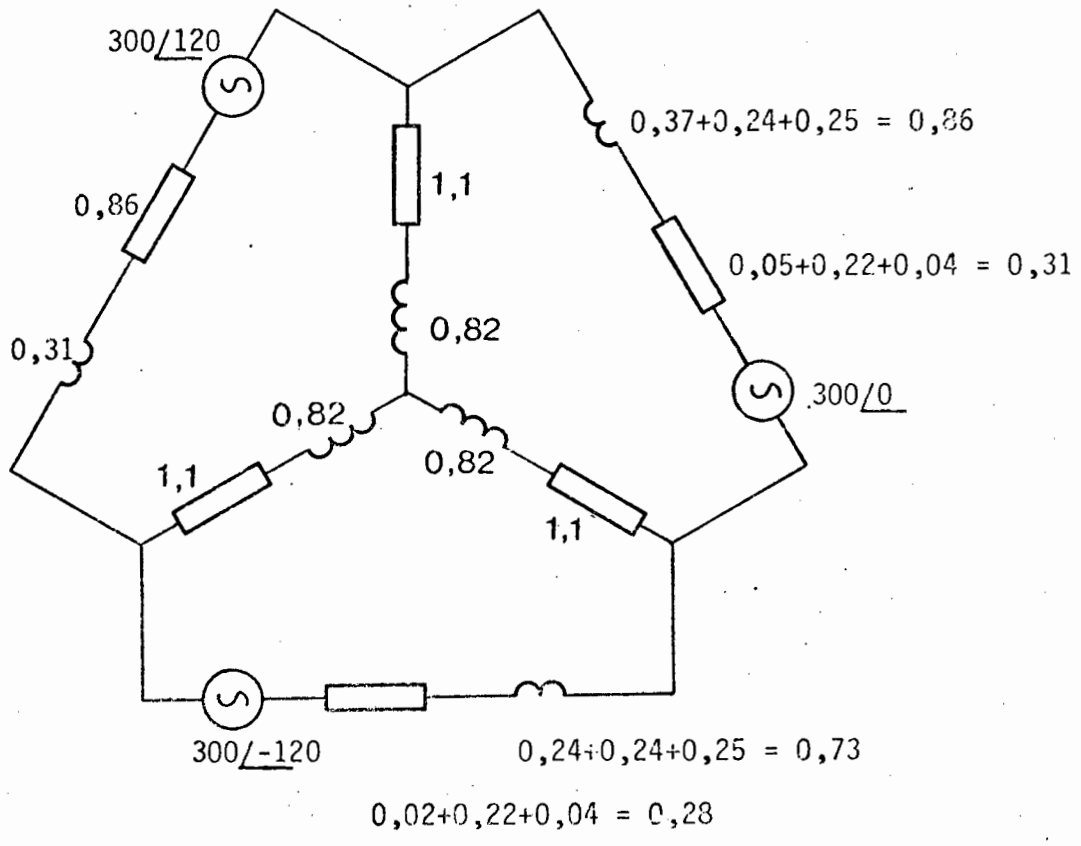

FIGURE 3.4 : RESISTANCES AND REACTANCES IN DELTA-STAR CIRCUIT OF A FURNACE.

4. FURNACE OPERATION AND PROBLEMS

A major factor in controlling the operation of a submerged-arc furnace is the correct utilization of the energy provided by the electrical power source. In order to achieve this, it is necessary to have an accurate measurement of the resistances and reactances of the furnace circuit, as well as a knowledge of how the various parameters of the electrical circuit interact and affect each other. This chapter deals with the problems associated with measuring and controlling the electrical circuit and the effect of reactance on the interactions between various elements of the circuit.

4.1 Measurement of the Secondary Electrical Circuit

The measurement of the secondary electrical circuit of a submerged-arc furnace is necessary for controlling the distribution of power between the three electrodes. This is particularly important during unbalanced conditions, especially if there is a significant amount of reactance in the circuit relative to resistance as is the case on large furnaces. The effect of unbalanced conditions on the operation of a furnace will be discussed later on in this chapter.

4.1.1 Standard measuring system

The standard secondary voltage and neutral connection arrangement for a large submerged-arc furnace is shown in Figure 4.1. The transformer secondary line-line voltage measuring leads are connected onto the secondary busbars close to the transformers and connected via twisted-pair cables to the furnace control room. Electrode-to-bath voltages are measured between one side of each transformer secondary voltage and the bath neutral which consists of a copper rod imbedded in the carbon lining. This rod is positioned in the coldest part of the lining at a point furthest away from the tapholes.

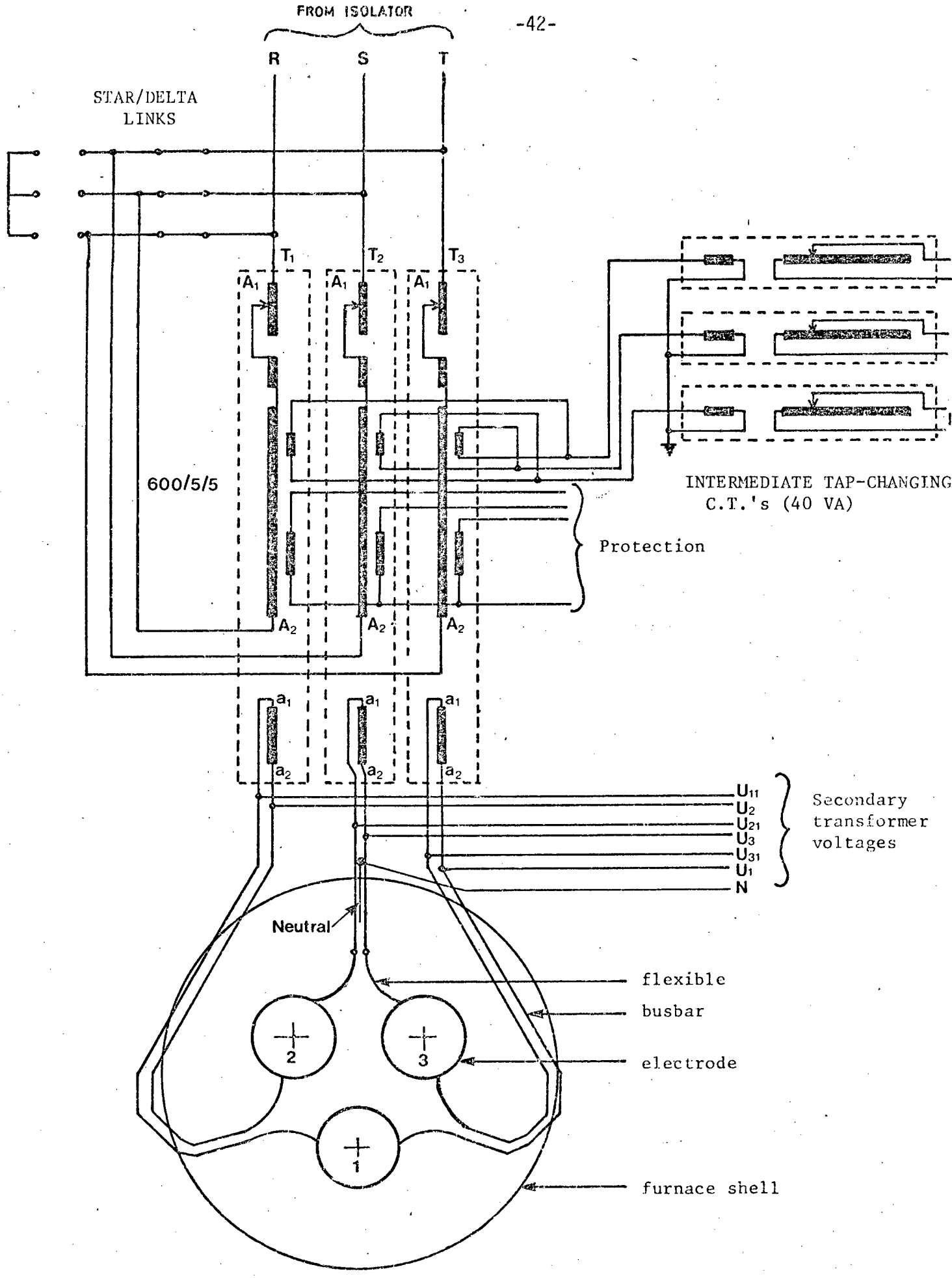

FIGURE 4.1 : FURNACE TRANSFORMER AND FURNACE SHOWING STANDARD VOLTAGE AND CURRENT CONNECTIONS.

The measurement of secondary current is obtained from primary current measurements based on the assumption of primary-secondary current/turns balance in the transformers. This is accepted as a reasonably accurate measurement which is certainly more accurate than the voltage measurement. Compensation for transformer tap changing is achieved by using an intermediate tap changing current transformer as shown in Figure 4.1. This intermediate current transformer is also wired in a delta-star arrangement so that, by addition, the currents at the secondary of the intermediate current transformers are directly proportional to electrode (star) currents.

4.1.2 Errors in measuring electrode-to-bath voltages

The measurements of electrode-to-bath voltages in a submerged-arc furnace are affected by induced voltage errors in the measuring leads as a result of the high currents flowing in the secondary circuit. The following example illustrates the magnitude of the induced voltages (for single-phase operation).

Consider the measurement of electrode-to-bath voltage as shown in Figure 4.2(a) which can be approximated to that shown in Figure 4.2(b). The alternating current I will induce a voltage in the measuring leads EBCN as a result of the electromagnetic flux passing through area A. The measured voltage V_{EN}' will differ from the actual voltage V_{EN} by an induced error voltage given by[13].

$$V_2 - V_1 = \mu b f \log_e \left(1+\frac{a}{r}\right).I \qquad (4.1)$$

where μ = magnetic permeability of the medium, f = alternating current frequency.

In a typical furnace

$I = 100$ kA

$\frac{a}{r} = 2$

$b = 3$ m

$f = 50$ Hz

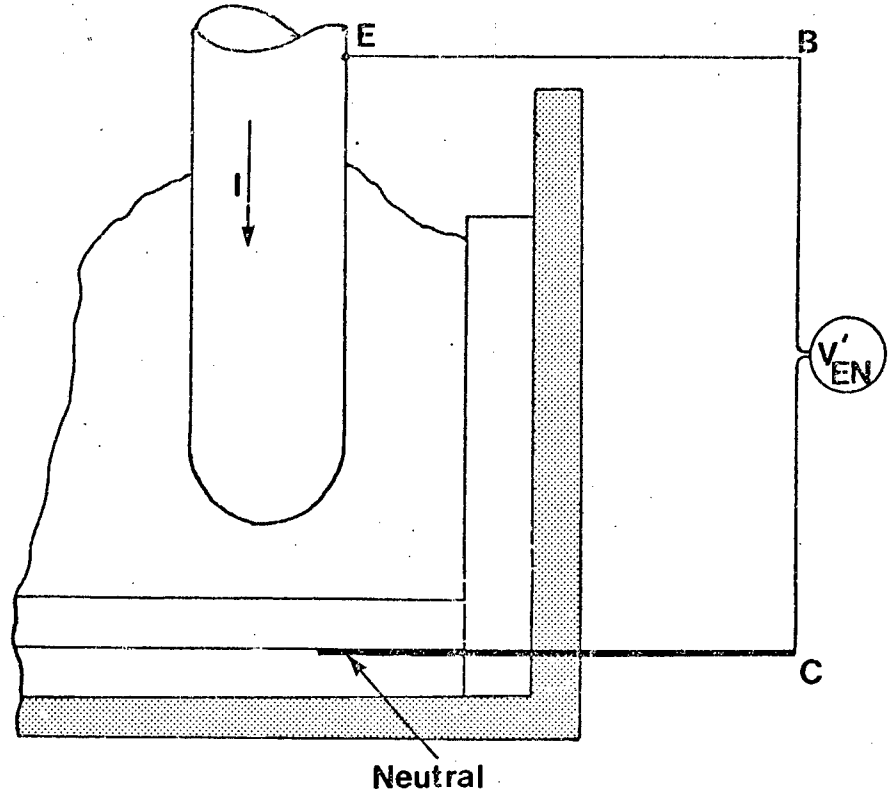

(a)

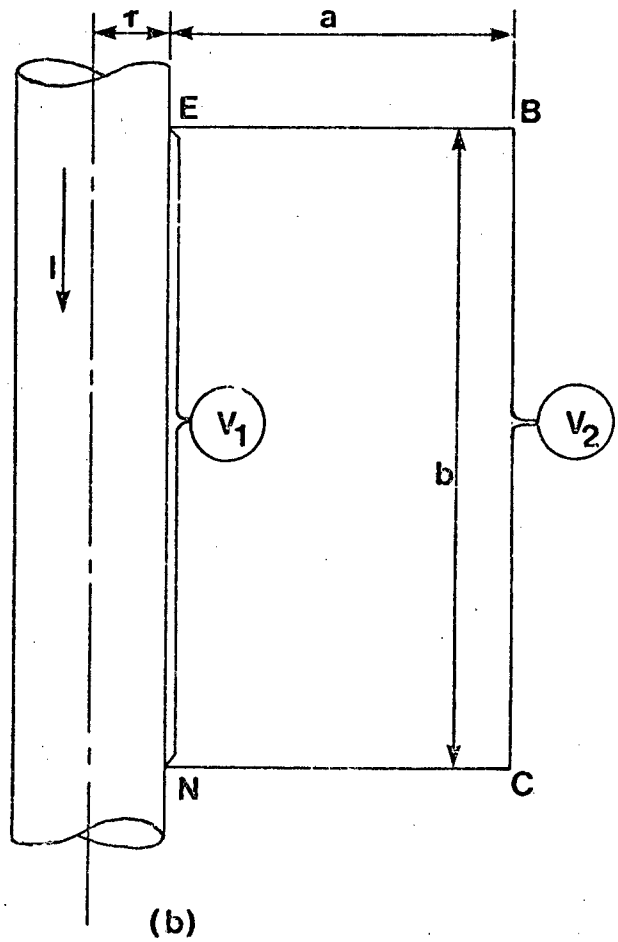

(b)

FIGURE 4.2 : ELECTRODE TO BATH VOLTAGE MEASUREMENT AND EQUIVALENT REPRESENTATION.

If μ is assumed for air ($\mu_o = 4\pi.10^{-7}$ volt sec/amp metre), then induced voltage $= 4\pi.10^{-7}.3.50.\log_e(1+2).100.10^3$

$= 20,71$ volts

V_{EN} is typically 180 volts, and although the example is only an approximate model of the actual situation, it does show that errors of the order of 12% are possible.

4.1.3 Compensation of electrode-to-bath voltage measurement errors

Investigators at the Clausthal Technical University in West Germany[12,1] have developed techniques for compensating for the induced errors in electrode-to-bath voltage measurements. These are based on the relationships between the currents flowing in the secondary circuit and the measurement errors which can be described by mutual inductances between the measuring leads and the current carrying conductors.

Consider the equivalent circuit in section 3.1 as being extended by the addition of a currentless measuring lead OM as shown in Figure 4.3(a). If the loop currents I_{12}, I_{23} and I_{31} are considered separately as single-phase currents, then three different voltages e_{1M}, e_{2M} and e_{3M} will be induced in the measuring leads as a result of the three currents resulting in 9 mutual inductances as shown in Figure 4.3(b). The mutual inductance $L_{1M,12}$ can be thought of as the ratio between the voltage induced in loop 1M as a result of the current flowing in loop 12. The same applies to $L_{3M,12}$, therefore

$$L_{1M,12} - L_{3M,12} = \frac{e_{1M} - e_{3M}}{I_{12}} = \frac{e_{13}}{I_{12}} = L_{13,12} \qquad (4.2)$$

However using equation 3.9 $L_{13,12} = L_1$ (4.3)

Consider now the measurement of U_{1M} under normal conditions with currents I_1, I_2 and I_3 flowing. I_2 can be replaced by $-I_1-I_3$ as shown in Figure 4.3(c) where I_1 forms a loop 12 and I_3 forms a loop 32. Thus

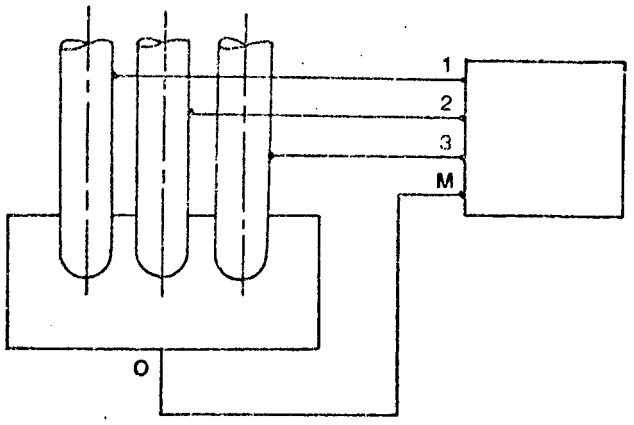

(a)

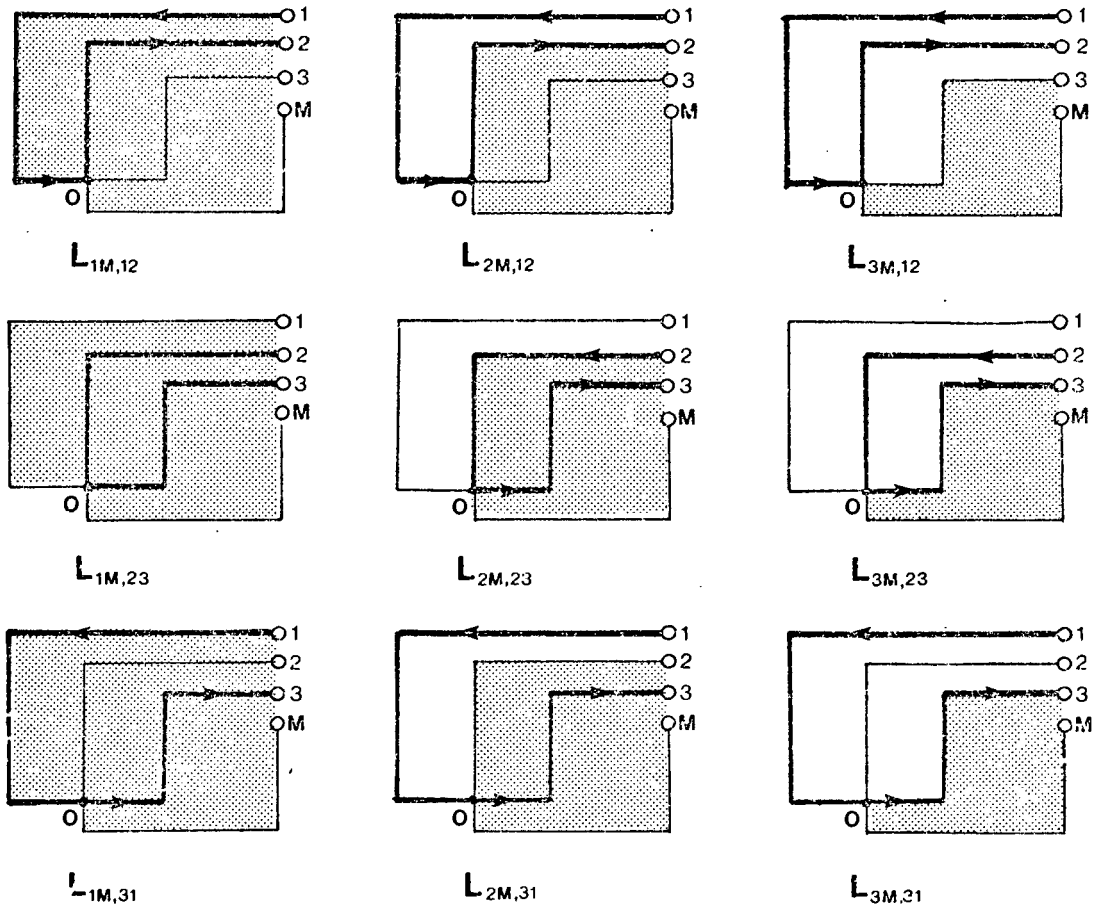

(b)

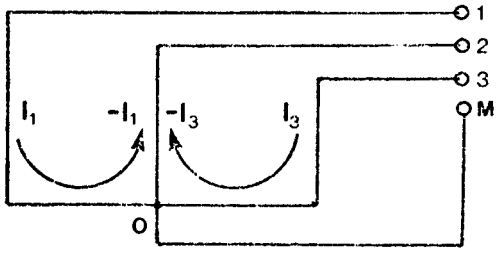

(c)

FIGURE 4.3 : MUTUAL INDUCTANCE LOOPS IN A FURNACE SECONDARY CIRCUIT

$$U_{1M} = I_1(R_1 + jw\,L_{1M,12}) - I_3\,jw\,L_{1M,23} \qquad (4.4)$$

Expanding equation 4.4 with $I_1.jw\,L_{3M,12}$ gives

$$U_{1M} = I_1[R_1 + jw(L_{1M,12}-L_{3M,12})] + I_i\,jw\,L_{3M,12} - I_3\,jw\,L_{1M,23} \qquad (4.5)$$

However, from equations 4.2 and 4.3, equation 4.5 can be rewritten as

$$U_{1M} = I_1(R_1 + jw\,L_1) + I_1\,jw\,L_{3M,12} - I_3\,jw\,L_{1M,23} \qquad (4.6)$$

$$= U_{10} + U_{0M} \qquad (4.7)$$

Similar equations can be derived for U_{2M} and U_{3M}. The conclusion that can be drawn is that the measurement of electrode-to-bath voltage, which includes a measurement lead , can be described by the addition of the correct voltage U_{10}, and an error term U_{0M}. This error voltage can be calculated from the product of two of the currents and two mutual inductances where the inductances are based on the geometry of the furnace and measuring system and, therefore constant. The mutual inductances can be measured by performing single-phase tests on each phase of the furnace and by measuring the induced voltages e_{1M}, e_{2M} and e_{3M}. On open-arc furnaces this is done fairly easily during the refining stage by merely lifting an electrode away from the molten bath until the arc in that phase is extinguished and a current loop is set up in the other two electrodes. An analogue measuring system based on this technique has been constructed and used successfully for open-arc furnace operation [15,17,20,21].

In submerged-arc furnace operation the setting-up of single-phase conditions is not as simple. The vertical movement of the electrodes is usually restricted to 1 to 2 metres, which is not enough to enable the electrode to be removed from the burden. With two electrode conduction the currents in the delta circuit are shared by the three transformer secondaries with one transformer carrying approximately double the current of the other two transformers as shown in Figure 4.4. This would mean that the error voltage in the measuring lead would be induced by three different currents which result in three mutual

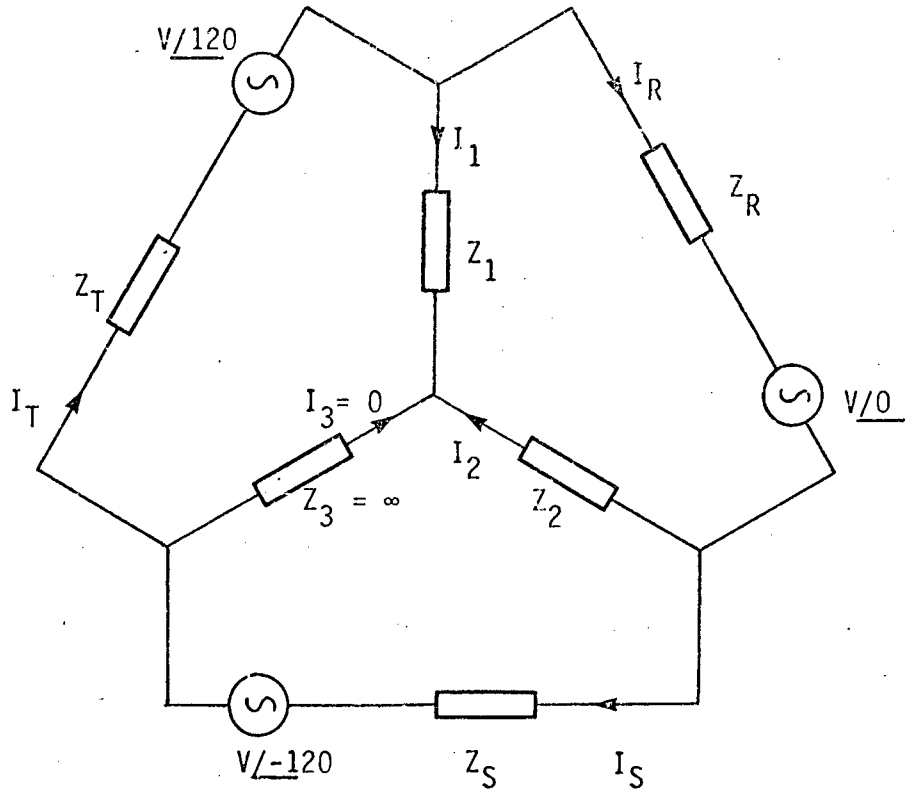

$I_3 = 0$

assume $Z_R = Z_S = Z_T = Z$

$Z_1 = Z_2 = Z'$

$$I_R = \frac{V}{Z + 3Z'}$$

$$I_S = \frac{-V}{2(Z + 3Z')} = -\tfrac{1}{2} I_R$$

$$I_1 = \frac{3V}{2(Z + 3Z')}$$

FIGURE 4.4 : DIAGRAM SHOWING EFFECT OF OPEN-CIRCUITING ONE PHASE ON THE CURRENTS IN THE DELTA CIRCUIT.

inductances having to be resolved. A further point is that the conduction region under the electrodes is not simply an open molten bath with low resistance as in open-arc operation. Single-phase operation would consequently change the conduction paths and appreciably reduce the accuracy of the measurements.

Fortunately, subsequent work by Köhle[40] has shown that a substantial amount of the induced voltage errors can be reduced by ensuring that the current carrying conductors in the furnace and the measurement leads are constructed in a symmetrical manner. Köhle developed relationships between the mutual and self-inductances of a furnace current carrying conductor system which includes a measurement lead. The resulting equations are, from Appendix A,

$$\begin{aligned} L_{3M,12} &= \tfrac{1}{2}.(L_2-L_1) + \tfrac{1}{2}(L_{1M}-L_{2M}) \\ L_{1M,23} &= \tfrac{1}{2}.(L_3-L_2) + \tfrac{1}{2}(L_{2M}-L_{3M}) \\ L_{2M,31} &= \tfrac{1}{2}.(L_1-L_3) + \tfrac{1}{2}(L_{3M}-L_{1M}) \end{aligned} \qquad (4.8)$$

where L_1, L_2 and L_3 are the self inductances of the star equivalent circuit diagram and L_{1M}, L_{2M} and L_{3M} are the self inductances of the conductor loops, which each consist of one of the secondary leads and the measurement lead. The size of the error voltage U_{0M} is determined by the magnitude of the mutual inductances $L_{3M,12}$ and $L_{1M,23}$ (equation 4.6). However, from equations 4.8 these mutual inductances can be reduced to zero if the self inductance groups L_1, L_2, L_3 and L_{1M}, L_{2M}, L_{3M} are made equal to each other.

In a submerged-arc furnace operation the geometry of the secondary circuit is fairly symmetrical as a result of the Knapsack connection, even in the case where the transformers are on one side of the furnace building (section 3.2.1). The major asymmetry is only in the reaction zone resulting from metal being tapped from one side of the furnace. It can, therefore, be assumed that L_1, L_2 and L_3 are approximately equal. The other inductances L_{1M}, L_{2M} and L_{3M} can be made approximately equal by bringing the measuring leads out from the furnace in a symmetrical manner. This mathematical result is the basis of a

compensation arrangement patented by Böckman[9]. The patent claims that the induced voltage errors in a furnace can be reduced by taking three measuring leads from the neutral under the furnace, up the side of the furnace shell, with each of the leads opposite an electrode, and then joining the three leads through equal resistors in a region of low magnetic flux above the furnace to form a 'true' neutral point. An alternative arrangement used by the author[64] is shown diagramatically in Figure 4.5 (Appendix B). Voltage connections are made on the bustubes of each electrode and brought out perpendicularly from each electrode via a flexible connection. Separate neutral connections under each electrode are brought out underneath the furnace and led up the side of the furnace adjacent to each electrode, to join the lead from the electrode and are then taken away from the furnace as twisted pair cables.

4.1.4 Reactance Assumptions

The determination of the resistances and reactances of the star circuit is dependent on accurate measurements of the electrode currents and the electrode-to-bath voltages. An alternative method of determining the resistances of the star circuit which does not require measurement of the electrode-to-bath voltages, involves making an assumption about the interrelationship between the three reactances of the star circuit. This is reasonable since the reactances of the circuit are related to the geometry of the furnace and as such are relatively constant compared to the resistances. Arcing also affects the reactances in the circuit but these changes are usually fairly small.

The analysis is based on the star circuit representation where all of the impedances in the circuit are lumped together with the load circuit. The measurements are made on the primary side of the furnace transformer and transformed to their equivalent secondary representation by use of the transformer turns ratio. The method for determining the resistances which follows is based on those measurements which can be easily and reliably measured on a furnace, viz., primary real power P, primary line voltages U_{12}', U_{23}', U_{31}'

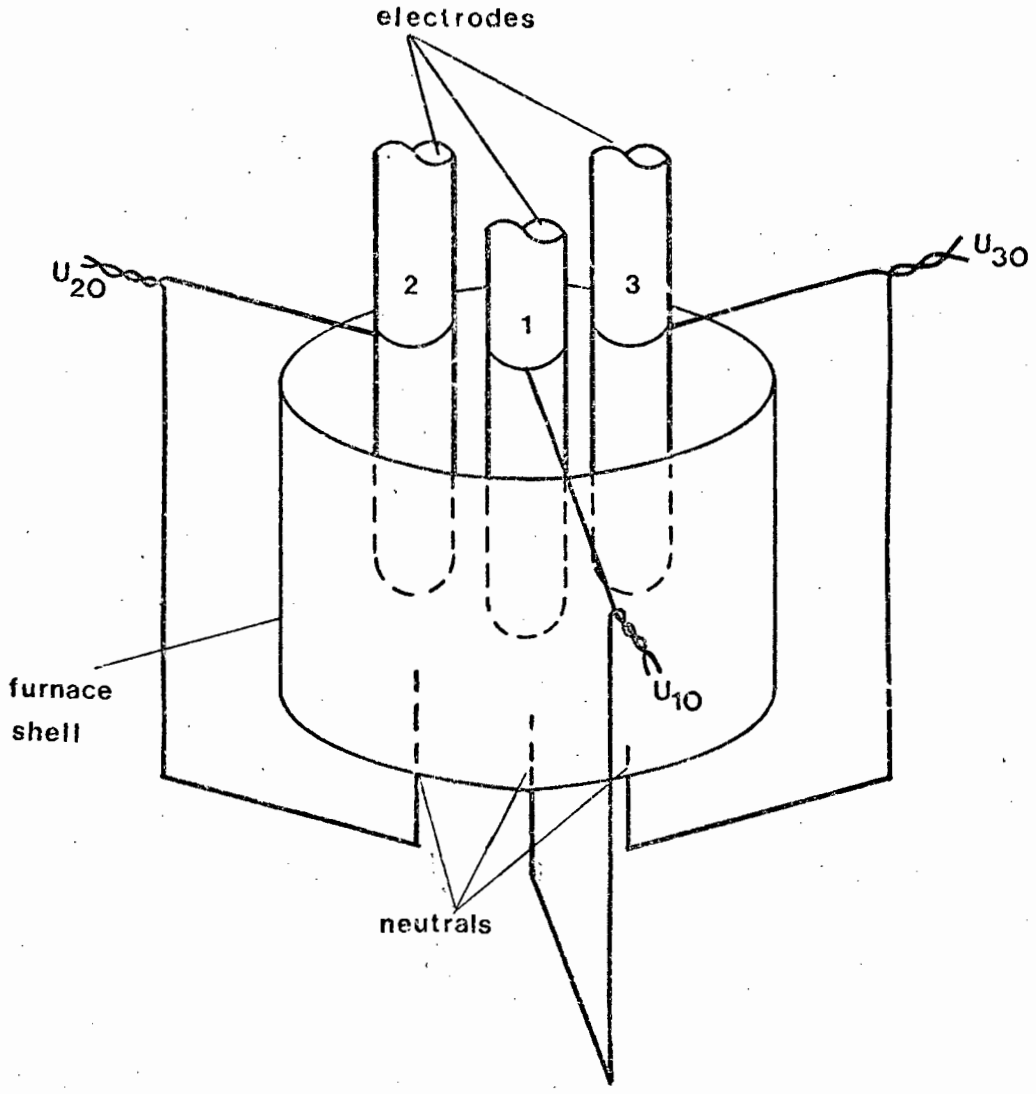

FIGURE 4.5 : SCHEMATIC REPRESENTATION OF WIRING ARRANGEMENT DEVELOPED FOR MEASUREMENT OF ELECTRODE-TO-BATH VOLTAGES.

(scalor), primary line currents I_1', I_2', I_3' (scalor) and transformer tap position, k. Assume that the transformation from primary to secondary can be described by f(k). The secondary voltages and currents are then given by:

$$\begin{aligned} I_1 &= f(k).I_1' \\ I_2 &= f(k).I_2' \\ I_3 &= f(k).I_3' \end{aligned} \tag{4.9}$$

and

$$\begin{aligned} U_{12} &= U_{12}'/f(k) \\ U_{23} &= U_{23}'/f(k) \\ U_{31} &= U_{31}'/f(k) \end{aligned} \tag{4.10}$$

The secondary circuit is shown in Figure 4.6(a). Applying Kirchoff's loop law:

$$\begin{aligned} I_1.Z_1 - I_2.Z_2 &= U_{12} \\ I_2.Z_2 - I_3.Z_3 &= U_{23} \\ I_3.Z_3 - I_1.Z_1 &= U_{31} \end{aligned} \tag{4.11}$$

The last equation in 4.11 is not independent of the other three since:

$$I_1 + I_2 + I_3 = 0 \tag{4.12}$$

and $$U_{12} + U_{23} + U_{31} = 0 \tag{4.13}$$

From 4.12 and 4.13 the voltage and current phasors form closed triangles and the angles between the currents θ_1, θ_2, θ_3 and the voltages ϕ_1, ϕ_2, ϕ_3 as shown in Figure 4.6(b) can be determined by using the cosine rule. If U_{12} is arbitrarily assumed to be on the real axis as shown in the phasor diagram in Figure 4.6(c), then the currents and voltages will be uniquely defined on the phasor diagram if the angle β between U_{12} and I_1 can be determined.

From the two wattmeter method of power measurement

$$P = U_{12}.I_1 . \cos \beta + U_{23}.I_3.\cos[\pi - (\theta_2+\phi_3+\beta)] \tag{4.14}$$

$$P = U_{12}.I_1 . \cos \beta - U_{23}.I_3.\cos (\theta_2+\phi_3+\beta) \tag{4.15}$$

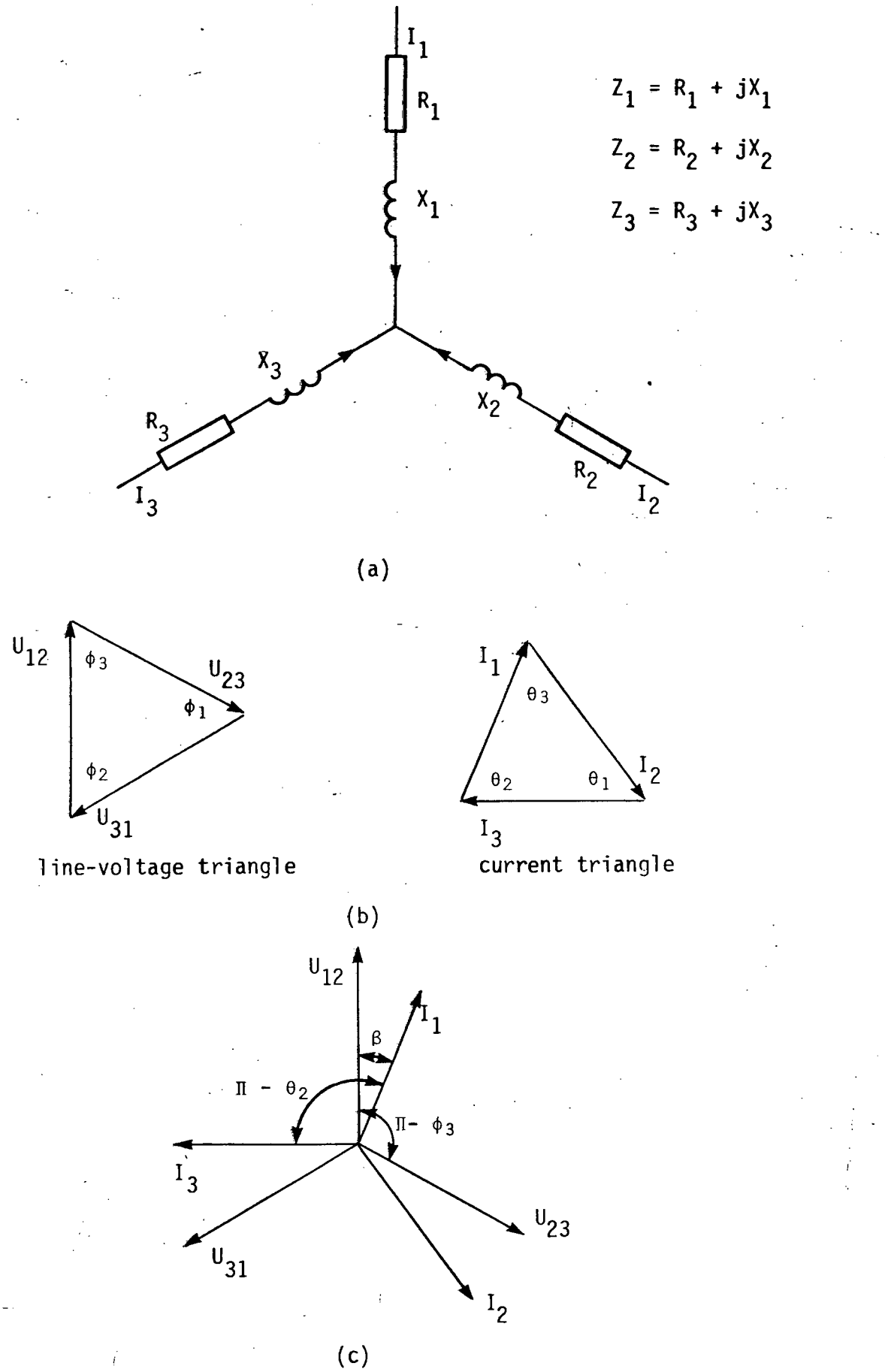

FIGURE 4.6 : EQUAL REACTANCE ASSUMPTION CIRCUIT AND PHASOR DIAGRAMS.

Equation 4.15 can be solved for β. The expansion of the first equations in 4.11 into real and imaginary components gives:

$$\begin{aligned} I_1.R_1.\sin\beta + I_1X_1\cos\beta + I_2R_2\sin(\theta_3+\beta) + I_2.X_2.\cos(\theta_3+\beta) &= 0 \\ I_1.R_1\cos\beta - I_1X_1\sin\beta + I_2.R_2.\cos(\theta_3+\beta) - I_2.X_2.\sin(\theta_3+\beta) &= U_{12} \end{aligned} \qquad (4.16)$$

When R_1 has been removed

$$-I_1X_1 - I_2R_2\sin\theta_3 - I_2.X_2.\cos\theta_3 = U_{12}\sin\beta \qquad (4.17)$$

Similarly the expansion of the second equation in 4.11 into real and imaginary terms and the removal of R_3 gives

$$I_3X_3 - I_2R_2\sin\theta_1 + I_2.X_2\cos\theta_1 = U_{23}\sin(\beta-\phi_3-\theta_2) \qquad (4.18)$$

The combination of equations 4.17 and 4.18 to remove R_2 gives

$$I_1X_1\sin\theta_1 + I_2X_2\sin\theta_2 + I_3X_3\sin\theta_3 = U_{23}\sin\theta_3.\sin(\beta-\phi_3-\theta_2) - U_{12}\sin\theta_1\sin\beta \qquad (4.19)$$

There are three unknowns X_1, X_2, X_3 in equation 4.19 and if some assumption is made about the interrelationship between these reactances the equation can be solved. If a linear relationship is assumed then

$$\begin{aligned} X_1 &= aX \\ X_2 &= bX \\ X_3 &= cX \end{aligned} \qquad (4.20)$$

and equation 4.19 can be solved as

$$X = \frac{U_{23}.\sin\theta_3.\sin(\beta-\phi_3-\theta_2) - U_{12}\sin\theta_1\sin\beta}{aI_1\sin\theta_1 + bI_2\sin\theta_2 + cI_3\sin\theta_3} \qquad (4.21)$$

With X determined R_2 can be calculated from 4.17

$$R_2 = -\left(\frac{U_{12}\sin\beta + I_1aX + I_2bX\cos\theta_3}{I_2\sin\theta_3}\right) \qquad (4.22)$$

$$R_1 = -\frac{I_1 aX\cos\beta + I_2 R_2 \sin(\theta_3 + \beta) + I_2 bX\cos(\theta_3 + \beta)}{I_1 \sin\beta} \quad (4.23)$$

Finally from a power balance

$$I_1^2 R_1 + I_2^2 R_2 + I_3^2 R_3 = P \quad (4.24)$$

and

$$R_3 = \frac{P - I_1^2 R_1 - I_2^2 R_2}{I_3^2} \quad (4.25)$$

4.2 The Reactance Problem

The economic benefits of reducing running costs by the employment of larger furnaces has resulted in a proliferation of the larger types with the older, smaller furnaces being phased out of operation. With increasing size furnace, the ratio between the reactance and the resistance of the furnace increases, resulting in a low power factor. This is shown in Table 4.1 where the resistances and reactances of two sizes of furnace are compared. It is generally assumed that the low power factor can be corrected by the inclusion of capacitors across the high voltage section of the circuit and apart from the added capital cost of the capacitors and larger transformers, the problem can be solved. However, this is not correct, since a high relative reactance in the circuit also has a significant effect on its operation and control.

	9 MVA furn.	48 MVA furn.
Resistance	2.4 mΩ	1,2 mΩ
Reactance	0,5 mΩ	1,1 mΩ
Power factor	0,98	0,74

TABLE 4.1 Comparison of typical resistances and reactances for two different sizes of submerged-arc furnaces producing similar products

4.2.1 Interaction effects between Electrodes

Interaction effects between electrodes result from the "3-wire" nature of the power circuit where changes in one phase cause a shift in the position of the neutral and effect the other two phases. In a "4-wire" system the neutral is held by the driving circuit and changes in one phase will only affect that phase and the neutral current. Langman[42] has discussed one of the properties of the "3-wire" three phase circuit where changes in the resistance in one phase have an appreciable effect on the power and current in the previous phase in the sequence of phase rotation, whereas the following phase is hardly affected. This property is not affected by the reactance in the circuit, but is included here as an interaction effect. It results from the neutral shifting in a direction which has a marked effect on the phase to neutral voltage of the previous phase and not the following phase as shown in Table 4.2. The resistance in phase 1 has been increased from a balanced condition at 1,1 mΩ to 2 mΩ resulting in large changes in the current, line to neutral voltage and power in the previous phase - phase 3, whereas the changes in phase 2 are relatively small.

The interaction between phases is also affected by the relative amount of reactance in the circuit. A description of this effect is given in a paper by the author and Barker[7]. Here the power imbalance on a large furnace resulting from a current imbalance, is plotted against varying circuit reactance. The aim was to show that a current imbalance on a small furnace where the power factor is close to unity results in a much smaller power imbalance than that resulting from a comparable current imbalance on a large furnace where the power factor is much lower. The analysis given in reference [7] gives a rather exaggerated result since the effect of reactance on the power imbalance of only one size of furnace is considered. This has now been modified to include the effects of changes in furnace size.

Table 4.3 gives a summary of the typical operating conditions of seven submerged arc furnaces producing charge chrome. The data for furnaces 1,2 and 6 are

	UNITS	BALANCED CIRCUIT			RESISTANCE IN PHASE 1 INCREASED		
		1	2	3	1	2	3
RESISTANCE	mΩ	1,1	1,1	1,1	2,0	1,1	1,1
REACTANCE	mΩ	1,2	1,2	1,2	1,2	1,2	1,2
POWER	MW	12,45	12,45	12,45	13,86	13,04	9,45
CURRENT	kA	106,4	106,4	106,4	83,24	108,9	92,7
VOLTAGE	V	173,2	173,2	173,2	194,1	177,2	150,9

TABLE 4.2 : Effect of a resistance change in one phase on powers, currents and voltages in a three-phase circuit

RANSFORMER ATING MVA)	ELECTRODE DIAMETER (m)	ELECTRODE CURRENT (kA)	80% ELECTRODE CURRENT (kA)	RESISTANCE (mΩ)	REACTANCE (mΩ)	LINE VOLTAGE (Volts)	REAL POWER (MW)	REACTIVE POWER (MVAr)	APPARENT POWER (MVA)	POWER FACTOR
9	0,85	34,2	27,4	2,4	0,5	145	8,41	1,76	8,6	0,98
16	1,10	50,4	40,3	1,85	0,68	172	14,09	5,17	15,01	0,94
19	1,20	57,4	45,9	1,7	0,75	184	16,77	7,41	18,33	0,91
30	1,45	76,2	61,0	1,4	0,92	222	24,49	16,03	29,27	0,84
40	1,60	88,35	70,7	1,27	1,03	251	29,81	24,12	38,35	0,78
48	1,70	96,8	77,4	1,2	1,1	273	33,66	30,9	45,69	0,74
78	2,0	123,5	98,8	1,02	1,32	357	46,58	60,37	76,26	0,61

TABLE 4.3 : Operating conditions of various size furnaces producing the same product

based on measurements taken from operating furnaces[76] and the data for the other furnaces are extrapolated from the data using formulae from Kelly[39] and Andreae[1] (Appendix C). Consider the effect of an 80% imbalance in the current in phase 2 for each furnace while the line voltages, reactances, and currents in the other two phases are kept unchanged from the balanced conditions. The results are plotted in Figure 4.7 where the relative amounts of power in each phase, expressed as a percentage of the total power in all three phases, are plotted against increasing reactance for each furnace from 0,5 mΩ to 1,31 mΩ. At small furnace sizes where the power factor is close to unity the 80% current imbalance has little effect on the percentage power imbalance. However, as the furnace size, and hence relative reactance increases, the power imbalance becomes more severe. It can also be seen that the phase consuming the least current (phase 2) is not the phase consuming the least power (phase 1). This is a situation not often appreciated by furnace operators. When one considers that the normal technique for measuring the power in each phase is very inaccurate and as a result the adjustment of electrode position is based on current control, the power distribution in the furnace under unbalanced current conditions will be quite different from that assumed by the operator.

Consider the unbalanced conditions for furnace number 6 in Table 4.3 which are summarized in Table 4.4(a). Assume that electrode 2 has had a tip break and is short which results in a high resistance and low current in that phase even with the electrode hoist position on bottom stops. Assume, as is quite possible, that this condition continues for a number of days. Electrodes 1 and 3 both maintain their normal currents so the electrode slipping rate for these electrodes is not changed from the normal rate. The operator is aware that electrode 2 is short and has increased the slipping rate on this electrode. However, it is unlikely that this increased slipping rate will be enough, since the electrode is consuming more power than the operator thinks it is. In addition an electrode on bottom stops with a high resistance will have a large arc under it which dramatically increases the electrode erosion rate. The short electrode condition will, therefore, persist and in the meantime electrode 1

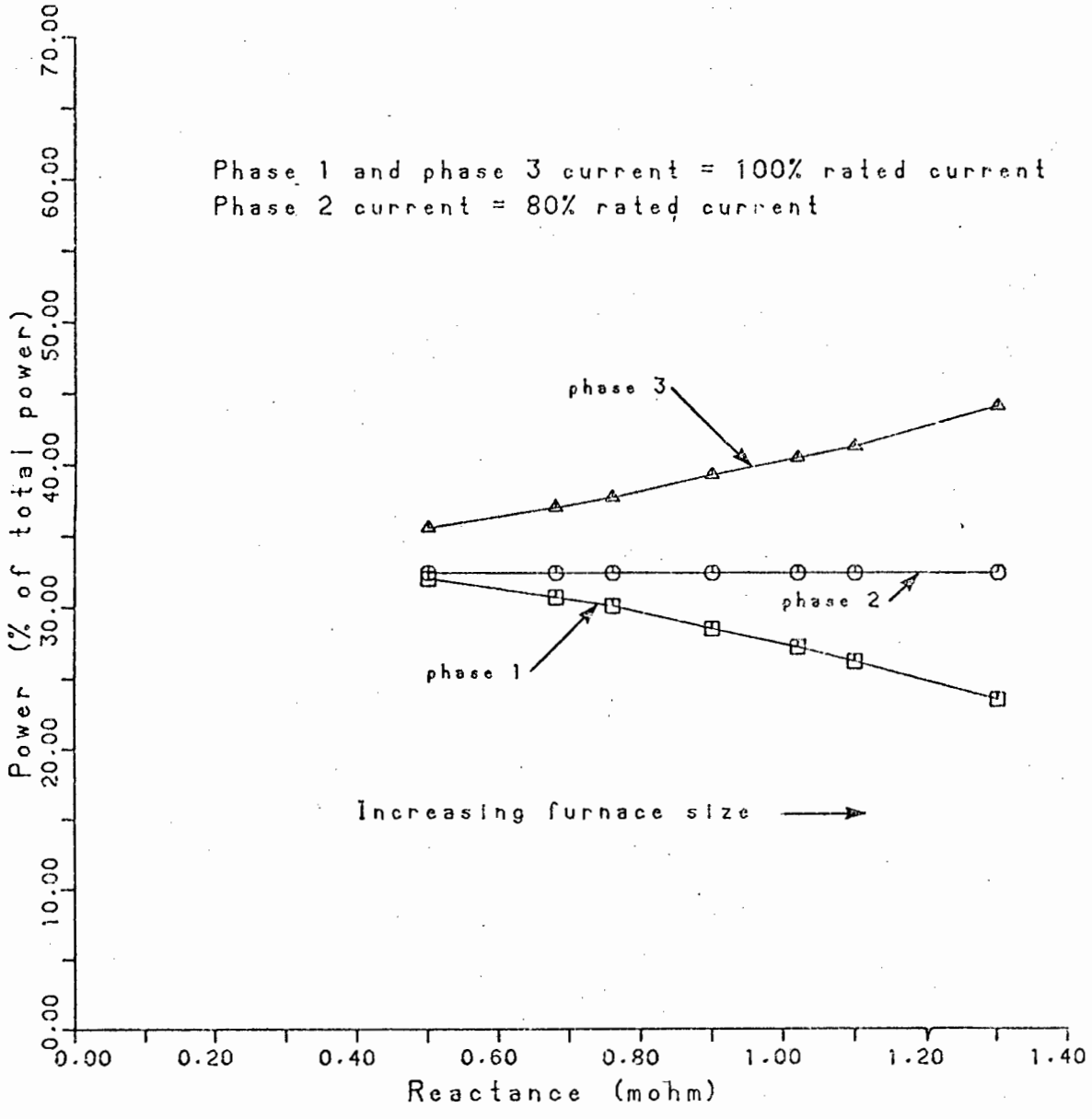

FIGURE 4.7 : EFFECT OF REACTANCE ON POWER IMBALANCE IN A FURNACE DURING UNBALANCED CURRENT CONDITIONS.

will be growing long, owing to the low power in this phase, while electrode 3 grows short. In the absence of any reliable electrode length determination (which is the normal situation) it will not be long before a very unbalanced condition results and the furnace production will drop dramatically.

(a)

	UNITS	1	2	3
Total power & line volt		33,132	275,000	
Power	MW	8,729	10,669	13,733
Current	kA	97,200	77,760	97,200
Phase voltage	volts	139,633	161,687	177,186
Resistance	mohm	,924	1,765	1,454
Reactance	mohm	1,100	1,100	1,100
Power	%	26,347	32,203	41,451

(b)

	UNITS	1	2	3
Total power & line volt		31,210	275,000	
Power	MW	10,421	8,589	12,201
Current	kA	97,200	77,760	70,000
Phase Voltage	Volts	151,411	139,701	190,548
Resistance	mohm	1,103	1,420	2,490
Reactance	mohm	1,100	1,100	1,100
Power	%	33,388	27,519	39,092

TABLE 4.4 : Unbalanced conditions in a furnace

Another furnace power imbalance situation relates to the tapping of the furnace. Tapping of the metal and slag is performed every 2 to 3 hours. It is essential for good furnace operation that most of the metal and slag accumulated are drained from the furnace. On many furnaces the tapholes are situated on one side of the furnace as shown in Figure 2.2 close to electrode 1. During tapping it is important that the power in electrode 1 is high to ensure an easy flow of metal. However, if the situation shown in Table 4.4 has

occurred, the power in phase 1 is low. This will seriously affect the tapping conditions in the furnace. Assuming that the current in phase two cannot be adjusted, the situation could be improved as shown in Table 4.4(b) by temporarily decreasing the current in phase 3 immediately before and during tapping.

4.2.2 The 'Dead' and 'Live' Phases

Dead and live phases are caused by imbalances in the reactances and are better known in open-arc steelmaking furnaces where they cause problems with uneven refractory erosion[18,57,70]. They also exist in submerged-arc furnaces but tend to be misinterpreted under normal operation.

In the circuit arrangement shown in Figure 2.2, the busbar connections for 'R' and 'T' transformers are longer than that for the 'S' phase and, even though the reactance in the busbars is minimized by interleaving of the 'go' and 'return' conductors, an asymmetry in reactance does occur, as discussed in section 3.2.1. An additional and usually more severe asymmetry occurs if the furnace is tapped from one side since the metal tends to flow downwards towards the taphole from the rear electrodes, so that the current path for the front electrode tends to be longer than for the other two electrodes. A third source of asymmetry in reactance results from an imbalance in the relative amounts of arcing in each phase.

When a furnace is run with equal currents in each phase, as is usually done when furnaces are operated on current control, the resistances must be unbalanced in order to compensate for the unequal reactances. If the phase rotation is 1-2-3 and electrode one has a higher reactance than the other two phases, then the power in phase two (dead phase) will be lower than the power in phase one, and phase three (live phase) will have a higher power.

This phenomenon can be demonstrated using the phasor diagrams shown in Figure 4.8 which are based on the simple star equivalent-circuit representation.

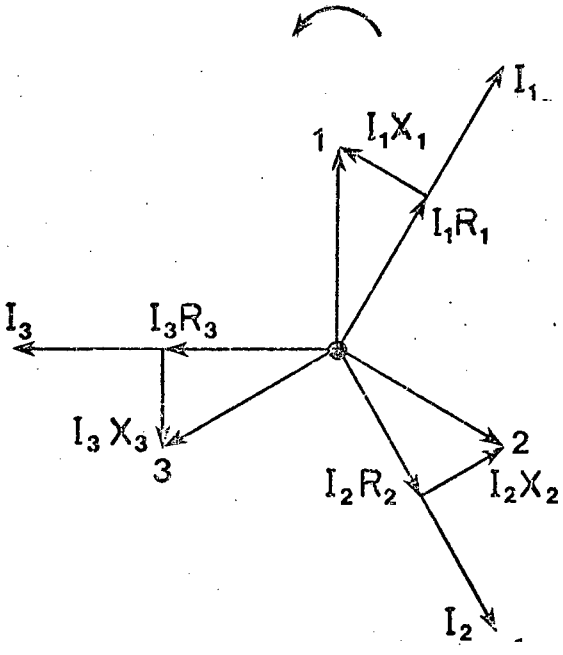

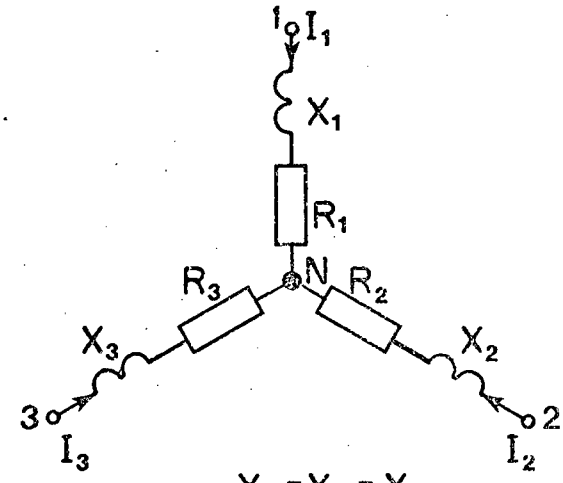

(a) Balanced furnace

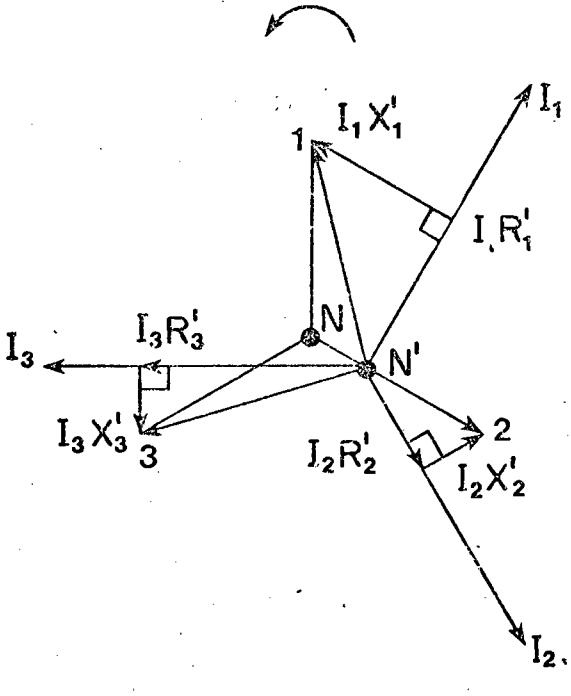

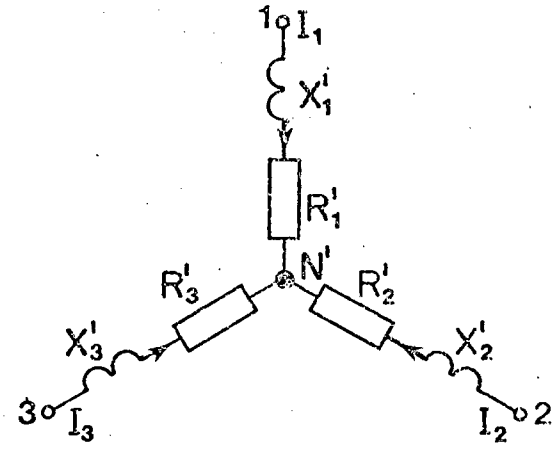

(b) Unbalanced furnace
(dead and live phases)

FIGURE 4.8 : PHASOR DIAGRAMS SHOWING "LIVE" AND "DEAD" PHASE PHENOMENON.

In Figure 4.8(a) the furnace is shown as completely balanced with the reactances equal and with resistances equal, the result being equal currents in each phase.

Consider the effect of an increase of the reactance in phase one, while the reactances in the other two phases are reduced, so that the reactances become asymmetrical. The resistances in phases two and three are adjusted so that the currents remain equal. This is shown in Figure 4.8(b) where the neutral has shifted from the centre N to N' and the resistances are unbalanced so that

$$I_1R_1' = I_1R_1 \qquad \text{(no change)}$$
$$I_2R_2' < I_2R_2 \qquad \text{(dead phase)}$$
$$I_3R_3' > I_3R_3 \qquad \text{(live phase)}$$

and since the currents are the same, $R_3' > R_1' > R_2'$. Consequently with the power in each phase, $P_3' > P_1' > P_2'$.

In a submerged-arc furnace, a problem with dead and live phases usually reveals itself as a consistent imbalance in the consumption of raw materials around each electrode as a direct result of the differing amounts of power being dissipated in the phases. The main danger with dead-and-live phases is that they contribute towards the development of gross imbalances on large furnaces in a manner similar to that discussed in the previous section. They also result in a situation where each electrode exhibits different properties from the other two electrodes. This can be a disadvantage. One effect can be seen during tapping of the furnace. In the furnace arrangement shown in Figure 2.2 one of the tapholes is closer to electrode 2 (the 'dead' phase) and the other closer to electrode 3 (the 'live' phase). On the furnace which has this configuration it has been observed that if one of the tapholes has to be used repeatedly because the other taphole is faulty, then problems with draining the furnace arise. If the taphole next to electrode 3 is being used, difficulty in draining metal from the distant 'dead' phase electrode 2 is experienced, whereas when the other taphole is used the problem is not so severe. This would suggest that there is a strong case for providing the facility for periodically changing the sequence of phase rotation on a furnace.

4.2.3 Control Sensitivity and Reactance

Another effect of reactance on the control of a submerged-arc furnace concerns the sensitivity of the control action. This is illustrated in Figure 4.9 which shows the power and resistance curves for furnace 1, 6 and 7 selected from Table 4.3. The normal operating regions for each furnace are shown as shaded areas. The 9MVA furnace operating point is on the upward sloping portion of the power curve and also on the steep portion of the resistance curve. This contrasts with the higher reactance 48 MVA furnace where the operating regions occur on the relatively flat portions of the power curves and also on the flatter regions of the resistance curves. The 78 MVA furnace operating point is past the maximum power point where increasing the current actually results in a reduction in the phase power. The control action sensitivity can be expressed as the rate of change of resistance with current and if a 10 kA band is taken around the operating point for each furnace, the resulting sensitivities are:

9 MVA furnace = 0,075 mΩ/kA

48 MVA furnace = 0,025 mΩ/kA

78 MVA furnace = 0,02 mΩ/kA

The reduction in the sensitivity of resistance to current means that larger current changes have to be made to compensate for resistance disturbances.

4.3 Electrodes and the Measurement of Electrode Length [34,41,45]

In a submerged arc furnace operation the electrodes are buried in the charge and the vertical movement of the electrodes is usually insufficient to allow them to be withdrawn for the electrode tip to be observed. This means that the measurement of the length of the electrodes is very difficult and usually involves a lengthy procedure where the raw material feed to the furnace is stopped and the burden is "burnt down" so that the electrode tips can be observed and their positions measured. During this period the furnace roof is exposed to higher than normal temperatures and the load on the

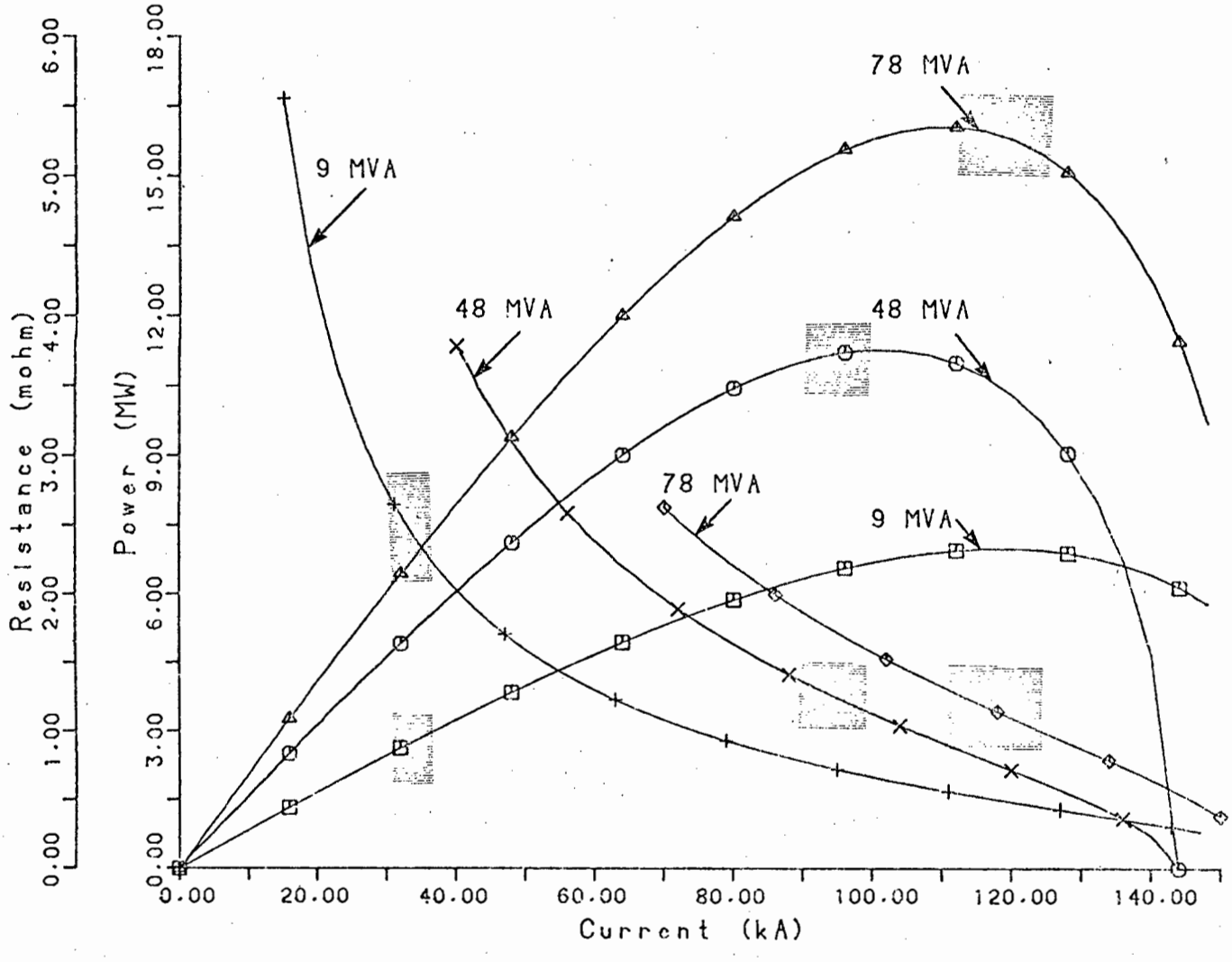

FIGURE 4.9 : CHARACTERISTIC CURVES OF VARIOUS SIZES OF FURNACES.

furnace has to be reduced. This is obviously an undesirable situation and many alternative methods for determining electrode lengths, mostly unsuccessful, have been tried out. In view of the problems associated with measuring the length of the electrodes it is difficult to understand why furnace designers do not allow more vertical movement of the electrodes so that they can be raised out of the furnace burden for measurement. The argument is usually made that the flexibles have to be kept short to minimize reactance. However, there are flexibles arrangements which allow a large vertical movement as well as keeping reactance effects to a minimum, (Figure 2.7(b)). This would add to the initial cost of the furnace but it is felt that this is justified.

The most common technique for monitoring the length of the electrodes involves measuring the electrodes periodically by the method outlined above. During the period between measurements of electrode length, the lengths are determined from measurements of the slipping rate and predictions of the electrode erosion rates. The accuracy of this method depends on the accuracy of the erosion rate predictions which are based on power measurements. Before an accurate measurement of the power per electrode was available the normal practice for determining the power distribution, involved taking the total power delivered to the furnace and dividing this by a proportion based on the relative quantity of raw materials used up around each electrode. The historical erosion rate of each electrode was also taken into account. This method worked moderately well during normal operation.

When the equal reactance assumption measurement technique was developed and used in modelling the erosion rate, this improved the accuracy of the models. However, it was not until accurate electrode-to-bath voltage and arcing measurements were available that a more reliable erosion model was obtained.[55] This erosion model has now been replaced by an electrode length model based on reactance and arcing directly which will be discussed more fully in Chapter 8.

Another electrode length determination method which is currently being investigated[8] involves measuring the "weight" of the electrode by measuring the hydraulic pressure in the electrode hoists. The problem here is that the electrode can "stick" to the burden and also the build up of gases in the reaction zone can exert an appreciable upward pressure on the electrode. However, encouraging results have been observed by perturbing the electrode (moving it up and down) and then looking at the hydraulic pressure.

4.4 Control of the Secondary Electrical Circuit

The various problems which have been discussed in this chapter have a detrimental effect on the control of the secondary electrical circuit. Using the standard measuring arrangement the errors in the measurement of the electrode-to-bath voltages results in inaccurate power and resistance measurements so that control of the electrodes from resistance or power is unsatisfactory. This has resulted in a widespread use of current measurements for the control of the electrodes. However, referring back to Figure 4.7 it was shown that particularly for large furnaces there is no simple relationship between the currents in a furnace and the associated powers and resistances in each phase. The use of current control on a large furnace is particularly bad during unbalanced current conditions since the extent of the power and resistance imbalances are not obvious from the conventional instrumentation.

The result is that these conditions often go unnoticed until the problems start to appear. Also, the problems that do occur, such as difficulties in tapping, broken electrodes, and high rates of electrode erosion, are often attributed to metallurgical factors and the operator is unaware that the source of the troubles is actually the behaviour of the electrical circuit and the control of the electrodes.

As discussed in section 4.1.3 various techniques have been developed for reducing the errors in the measurement of the parameters of the electrical circuit. However, these methods suffer from the disadvantage that they involve connecting measuring leads to the furnace in a harsh, hot environment. The neutral connections to the carbon lining are particularly difficult to maintain since the temperature of the carbon lining is high (900 - 1400^{o}C) and the connections have to last the life of the furnace lining (5 to 10 years).

As a result of these problems the reactance assumption measuring technique (section 4.1.4) has been selected as the most reliable means for measuring the resistances in the furnace. An electrode controller, which uses this technique has been developed for submerged arc furnace operation [5,65,66]. As the controller is a resistance controller it avoids the interaction problems and the accuracy of the reactance assumption has been shown to be satisfactory based on comparisons with the authors direct measuring system. A prototype controller has been operating very successfully on a furnace [35] for over 2 years and additional units are currently being manufactured for other furnaces.

5. ARCING

Arcing occurs when electricity is conducted through a gaseous medium which has become ionized by an electric field. In electric arc furnaces it occurs in the region between the electrodes and the molten bath and constitutes a major energy source for the metallurgical operation being performed. The arc cannot be represented as a linear circuit element and the non-linear approximate representations which are generally used do not fully account for all the properties of the arc, especially under widely varying conditions. In submerged-arc furnace operation, the arc is difficult to analyse since it occurs in a region which is buried and cannot be observed, so that its properties have to be deduced from indirect measurements. The power generated by an arc is less than the power generated by a comparable resistor and it is usually preferable to avoid arcing wherever possible, except in conditions where the very high temperatures of the arc can be beneficial to the metallurgical operation.

5.1 Occurrence of Arcing in Arc-Furnace Operation

The arc is particularly dominant in open-arc furnace operation where it provides the energy for the melting down and subsequent refining of metal scrap. Two distinctly different types of arcing conditions can be observed during open-arc furnace operation. During the melting-down phase, when the electrodes are boring down through the cold metal scrap, the arcs are noisy and unstable and the voltage and current waveforms are extremely distorted. This contrasts with the other condition which takes place during the refining stage, when all the metal has been melted and arcing occurs between the electrodes and a not uniform molten bath. Here the hot conditions promote ionization of the gases and quiet, stable arcs are observed with much less distortion of the voltage and current waveforms.

In submerged-arc furnace operation the voltage and current waveforms are even less distorted than those observed during the refining stage in open-arc furnace operation and some controversy exists as to the extent of arcing in submerged

arc furnaces. In slag free operations (e.g., Ferrosilicon), the waveforms are fairly distorted and it is generally accepted that the electrical conduction does involve appreciable arcing [73]. In a ferrosilicon furnace, arcing has actually been observed, using a 'peep pipe' by Otani et al [51], who found that a large cavity exists under each electrode with a well-defined arc column occurring between the electrodes and the molten metal. In submerged-arc operations, where a slag is formed (e.g., Ferrochromium, Ferromanganese) the situation is not as well defined. The presence of a coke bed immediately below the electrodes increases the possibility of ohmic conduction rather than arcing [73]. Also digouts [2,77] have shown that no large cavity exists below the electrodes as in Ferrosilicon operation, although Yamagishi et al [77] did observe a small cavity.

The mechanism of conduction in a ferrochromium charge has been studied on a laboratory scale by Urquhart [72]. It was found that the types of conduction in the charge depended on the applied voltage and that below a certain critical voltage ohmic conduction occurred, whereas above this voltage the conduction was characterized by sporadic arcing. This arcing was also dependent on the presence of coke (the reductant) in the charge, since arcing could not be induced in charges which contained no reductant. Urquhart concluded that the resistance of the charge is the sum of many inter-particulate resistances in series and in parallel and proposed the conduction mechanism shown in Figure 5.1. This mechanism assumes that conduction occurs when two particles (one of which must be a char and the other a chromite particle) are touching and heat is generated by resistance conduction. Some reduction occurs and eventually a cavity appears and an arc strikes between the two particles. Further reduction then causes the cavity to increase in size until the arc is extinguished.

The effect of coke on arcing has also been examined on a small 68 kW two-electrode furnace at the National Institute for Metallurgy. At first conduction was set up using a slag without any coke and an unstable, noisy arc was observed. The

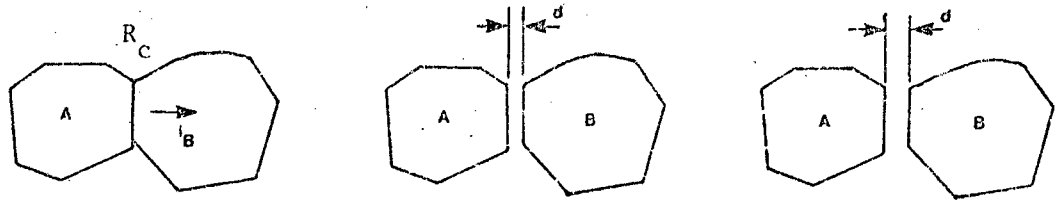

(a) time t

$C + \frac{1}{2}O_2$ CO

or C + FeO Fe + CO

(b) time t + t

arc strikes

(c) time t + 2 t

$C + \frac{1}{2}O_2$ CO

or C + FeO Fe + CO

arc extinguished

FIGURE 5.1 : THE MECHANISM OF ARCING IN THE FURNACE BURDEN.

voltage waveform was also distorted. (This is not contradictory to Urquhart's observations, since these were open-arc conditions.) On the addition of coke to the charge, a dramatic change in the arcing conditions occurred. The noise of the arc was reduced , a glowing bed formed and many small arcs occurred between the carbon pellets. The distortion in the voltage waveform was also reduced considerably.

Other investigations of the occurrence of arcing in ferrochromium charges have been carried out by Channon[24]. It was found that the onset of arcing in the charge was dependent on the current density in the electrode and that arcing occurred above a critical current density. Also, the arcing conditions were maintained even when there was no cavity between the electrode and the charge. The critical current density was found to be 12 amps/cm^2 which is significantly higher than the current density in a typical large furnace (1,7 metre diameter electrodes carrying 100 kA will have a current density of 4,5 amps/cm^2). However, if skin and proximity effects in the electrodes are considered, the current density in certain regions of the electrode can be between two and three times greater than the dc current density[10,31].

Without any strong evidence to suggest that there is any appreciable arcing in slag forming submerged-arc operations, some investigators have concluded that the

mechanism of conduction is mainly resistive[32,73]. However, as will be shown later, some arcing does occur especially during tapping of the furnace.

5.2 Arcing Theory

An arc occurs when a sufficiently high voltage is applied between two conducting bodies which are separated by a gaseous medium so that electrical conduction occurs. Very high temperatures (approximately $5000^{o}k$) occur in the gaseous region which can be regarded as a plasma. The arc is a complex non-linear phenomenon affected by many different factors (temperature of gas and electrodes, nature of gas, type of anode, type of cathode, type of conduction, current, source voltage, source impedance, arc gas and others) which are continually changing so that a rigorous analysis of the arc is virtually impossible. There are also many different types of arcs depending on the quantity of current flowing and the applied voltage. For arc furnace operation the only arc of interest is the high current arc.

The physical mechanisms occurring during arcing have been described by various investigators[28,58] who consider the arcing region between two electrodes as being distinguishable into three distinct regions, each with its own physical properties. These are illustrated in Figure 5.2 and consist of two very thin areas next to each electrode, A and C, called the anode and cathode fall regions, with a large area, B called the arc column joining these two regions. The anode and cathode fall regions have very steep voltage drops and consequently very strong electric fields, whereas the arc column has a much lower voltage gradient. In the arc column the gas becomes an extremely hot plasma.

The electrical conductivity of the arc column is an important parameter in determining the total arc volt drop. Although not linearly related to temperature, this electrical conductivity increases appreciably with temperature as shown for Argon in Figure 5.3. Generally, it can be concluded that the

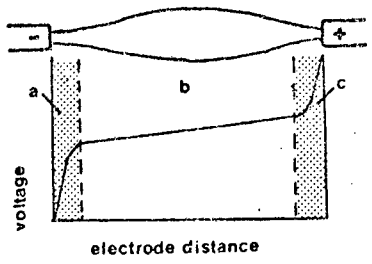

FIGURE 5.2 : ARCING REGIONS.

a= cathode fall region

b= arc column

c= anode fall region

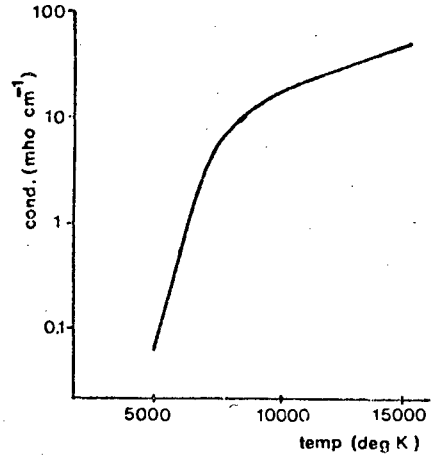

FIGURE 5.3 : RELATIONSHIP BETWEEN CONDUCTIVITY AND TEMPERATURE FOR ARGON GAS.

stability of the arc increases with increasing electrode column conductivity, so that low ionization energy gases and high gas temperatures are favourable conditions for promoting arc stability. Another factor which determines the total arc voltage drop across an arc is the volt drop across the anode and cathode fall regions. These regions can be regarded as transition areas with very high temperature gradients occurring between the relatively cold electrodes and the hot arc column. The anode and cathode volt drops are usually of the order of 10-30 volts. Under equilibrium conditions with constant arc gap, the voltage drop between two electrodes carrying an arc can be regarded as approximately constant.

In considering the arc as a circuit element the formula given by Ayrton and later modified by Nottingham,can be used[22] where

$$V_a = A + B\ell + \frac{C + D\ell}{I^n} \qquad (5.1)$$

Here Va = arc voltage drop

ℓ = arc length

I = arc current

n = variable exponent dependent on the anode material (n=1 for carbon in air) and A,B,C,D are constants.

If a high current arc is being considered equation 5.1 simplifies to

$$Va = A + B\ell \qquad (5.2)$$

or even more simply to

$$Va = B\ell \qquad (5,3)$$

if the arc is fairly long. Equations 5.2 and 5.3 show that the voltage drop across a high-current arc is independent of the current flowing. For alternating current conditions,the voltage of a high-current arc with constant arc length can be represented by a square wave (with voltage equal to Va). The zero crossings of the square wave coincide with the zero crossings of the arc current and the arc voltage has the same sign as the arc current. It is assumed that there is sufficient voltage available at the electrodes to re-ignite the arc in the opposite direction as the current changes direction. One of the major weaknesses of this model is that it ignores any dynamic characteristics of the arc.

5.2.1 Dynamic arc characteristics

With currents changing slowly enough, the voltage drop in an arc follows the static characteristic, but as the frequency of the current changes are increased, hysteresis effects become evident so that the arc voltage departs from the static characteristics by an amount dependent on the rate of the current change and the nature and condition of the arc. This is a complex

phenomenon which is difficult to model. The graphs shown in Figure 5.4 taken from Browne[22] illustrate the sort of effects that can occur. Figure 5.4(b) shows the volt-amp cyclogram for a vertical, 60 cycle, 100 amp (rms), 18 inch arc in air with the associated voltage and current waveforms shown in the inset. The voltage waveform is typical of that seen on open-arc furnaces during the melt-down stage when conditions for arcing are not particularly favourable. Clearly the hysteresis effects play a significant role during such arcing conditions. The volt-amp cyclogram for a higher current (15 000 amps) and shorter arc length (12 inches) is shown in Figure 5.4(a). At the higher currents there is less hysteresis. On this basis the dynamic characteristics of very high current arcs closely approximate the static characteristic and equations 5.2 and 5.3 can be used.

In dealing with the mathematical representation of dynamic arc behaviour Browne introduces two models, one by Mayr and the other by Cassie. Cassie's equation is the most interesting since it is suitable for representing high-current arcing conditions,and under steady state conditions it simplifies to the square wave equations 5.2 and 5.3. Under dynamic conditions Cassie's equation has the effect of delaying fast changes so that the square wave representation of the arc becomes more rounded.

5.2.2 Influence of gas injection on arcing

In addition to temperature, the ionization potential of the gas in the region between the electrodes of an arc has a significant effect on the striking voltage. Some gases also tend to remain in an ionized state longer than others thus promoting arc stability. Therefore, arcing conditions can be improved by introducing arc supporting gases (e.g., Argon, Nitrogen) into the arcing region. Maddever and Segsworth[44] have investigated this effect by feeding arc supporting gases down hollow electrodes in a laboratory furnace and they have reported steadier arcing conditions with a higher level of useful power and lower electrode consumption. Tests on an operating open-arc furnace also showed encouraging results. Enomoto[33] has shown that the presence of

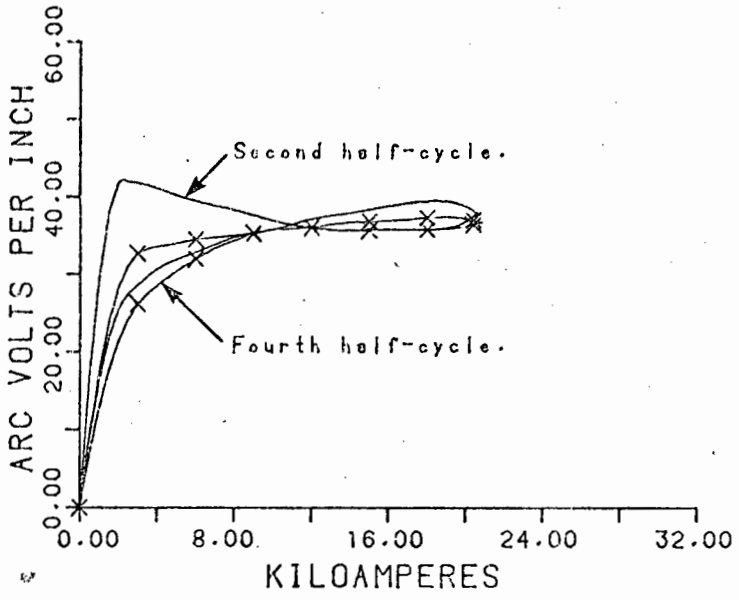

(a) Volt-amp cyclograms of vertical 60-cycle arc 12 in. long in air, 15000 amp rms.

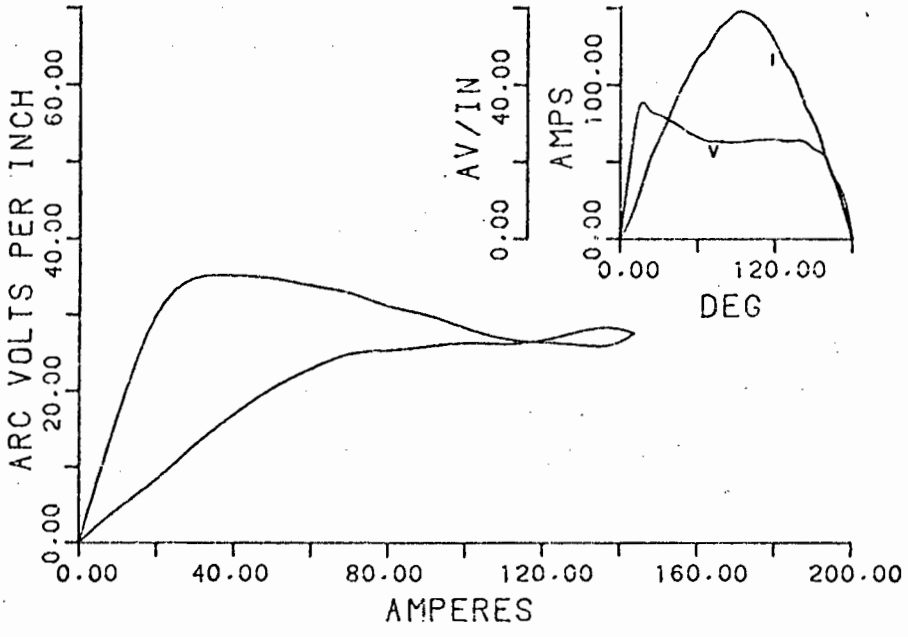

(b) Volt-amp cyclogram of vertical 60-cycle arc 18 in. long in air, 100 amp rms.

FIGURE 5.4 : ARC CYCLOGRAMS.

SiO gas, which is produced in the production of ferrosilicon, has a significant effect on improving the stability of the arc with resultant improvement in the utilization of power.

As will be shown later, the loss in efficiency of power utilization in even the so-called low arcing, slag-forming furnace operation is appreciable, so that the benefits of introducing arc supporting gases down hollow electrodes should be considered. Most of the work to date has been on open-arc furnaces where the potential benefits are more marked. There are, however, some indications that improvements in arcing conditions in submerged arc operation will be small, since the arcing conditions are stable to start with and the presence of CO gas, which is produced by the reduction process, will tend to mask the effect of adding arc supporting gases.

5.3 Laboratory Investigations of High-Current Arcs

In open-arc furnaces the arc plays a dominant role in the operation since virtually all the energy for melting and subsequent refining is provided from the arcs. Such factors as the efficiency of melting, electrode consumption, refractory erosion and voltage flicker are all directly related to the arcing process and it is for these reasons that the British Steel Corporation has set up an arc laboratory at Swinden to study high current arcs in conditions closely related to those of operating furnaces.

Bowman et al[11] have described the equipment available which consists of a high current chamber lined with refractory and resting on a water calorimeter in which arcs with currents up to 10 kA can be struck from a carbon electrode onto a steel block. The chamber is fitted with observation ports and sophisticated photographic equipment to enable high-speed photography of the arc under controlled conditions. The power for the arc is provided by a 3MVA 3-phase on-load tap changing transformer where one secondary phase powers the arcing chamber and the other two phases are loaded by a ballast resistance. For short periods currents of up to 25 kA can be obtained.

Investigations carried out on arcs at this laboratory have been published in numerous publications[11,36,37,46]. A large amount of the work is specifically related to open-arc furnace operation and only the results relating to submerged arc furnace operation will be summarized here.

Photographic studies of high current (6 kA) a.c. arcs showed a marked difference in the arc pattern between the half cycle when the carbon electrode is the cathode (cathode half cycle) and the half cycle when the carbon electrode is the anode. During the cathode half cycle the arc was characterized by a rigid plasma jet emanating from the electrode towards the steel, and although the cathode spot tended to wander around the electrode surface at moderate speeds (10-100 ms^{-1}) the plasma jet maintained its rigidity. In contrast the anode half cycle was less stable and highly mobile so that the high-speed camera could not resolve its motion. The instability of the anode half cycle is also shown in Figure 5.5 taken from Bowman et al[11] which shows voltage and current waveforms for 'cold', 'warm' and 'hot' arcing conditions. Once again the reduction in distortion of the current waveforms with increasing temperature is clearly evident. The investigators also observed a hysteresis effect in the expansion and contraction of the arc column and in the size of the cathode spot during a half cycle of current. This would be related to the hysteresis effects shown in the cyclograms in Figure 5.4.

In investigating the velocity of the plasma jet Jordan et al[37] found that the mean pressures generated at the carbon electrode and steel surfaces were 0,8 atm and 0,2 atms respectively for a 10 kA arc. At higher currents these pressures would increase appreciably. Nevertheless, even at 0,2 atm, the pressure was sufficient to cause large depressions in the molten steel, a phenomenon which has been observed in large open-arc furnaces as well. This suggests that a cavity will be generated between the electrodes and the molten charge in submerged arc furnaces by the forces holding the charge away from the electrodes. The cavity would only be generated when a current is flowing, so would not be observed after a 'digout'. This conclusion depends on whether the arc occurs

as a single-current plasma jet as is observed in open-arc furnace operation or as many diffuse arcs occurring in the coke bed as is suggested by Urquhart[72,73]. However, in the absence of direct observation, what actually does occur is open to speculation. The most likely situation is a combination of the two mechanisms.

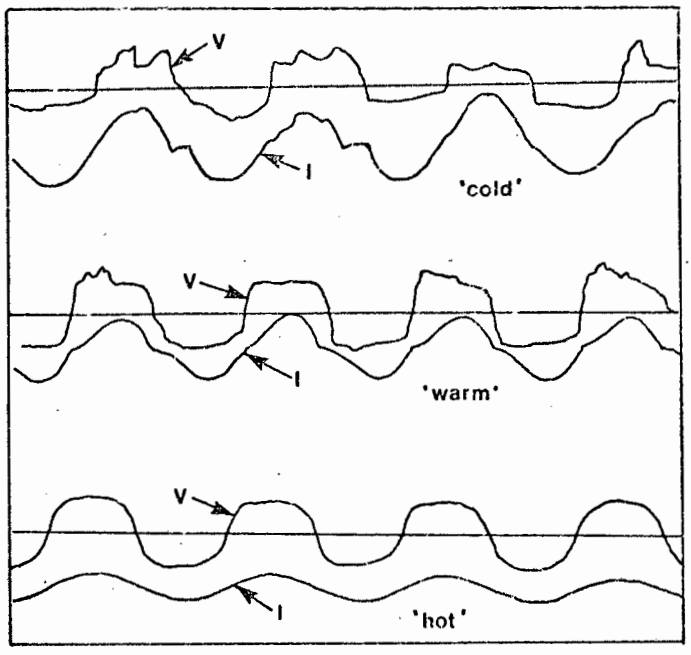

FIGURE 5.5 : OSCILLOSCOPE TRACES FOR ARCS IN DIFFERENT TEMPERATURE ENVIRONMENTS.

5.4 Single-phase Circuit with Arcing

Virtually all the operations of submerged-arc furnaces use three-phase circuit power. However, as an introduction to the effects of arcing on the electrical circuit, a single-phase circuit consisting of a resistance, a reactance and an arc powered by a purely sinusoidal voltage source, as shown in Figure 5.6, will be considered. The full mathematical analysis of this circuit is given in Appendix D and only the results will be considered here.

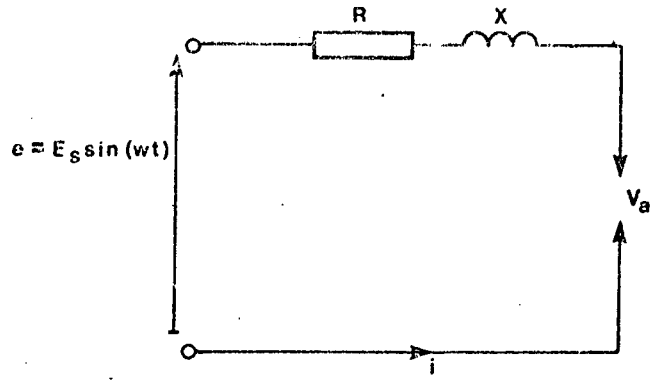

FIGURE 5.6 : EQUIVALENT CIRCUIT OF SINGLE-PHASE CIRCUIT WITH ARCING.

The effect of arcing on the current waveform is shown in Figure 5.7 which gives the voltage, current and arc voltage waveform for a circuit with fairly high arcing of 70 volts and source volts = 141,4 volts (200 volts pk). The distortion of the current waveform is fairly low despite the high-arc voltage. The reactance in the circuit has a beneficial effect of causing a lag between the current and voltage waveforms so that when the arc voltage (which is in phase with the current) changes direction, there is already a voltage available to restrike the arc immediately. If the arc voltage is too high or there is insufficient voltage available to restrike the arc and the current remains at zero for a while. This phenomenon which is called extinction operation results in excessive distortion of both the current and voltage waveforms. In the operation of large submerged-arc furnaces the arc voltages usually encountered are relatively low and there is a large amount of reactance present in the circuit so that extinction operation does not usually occur.

In analysing the single-phase circuit it is useful to determine the total circuit resistance and reactance, which are based on measurements of real power, (P) voltage (V_{rms}) and current (I_{rms}) using the standard equations:

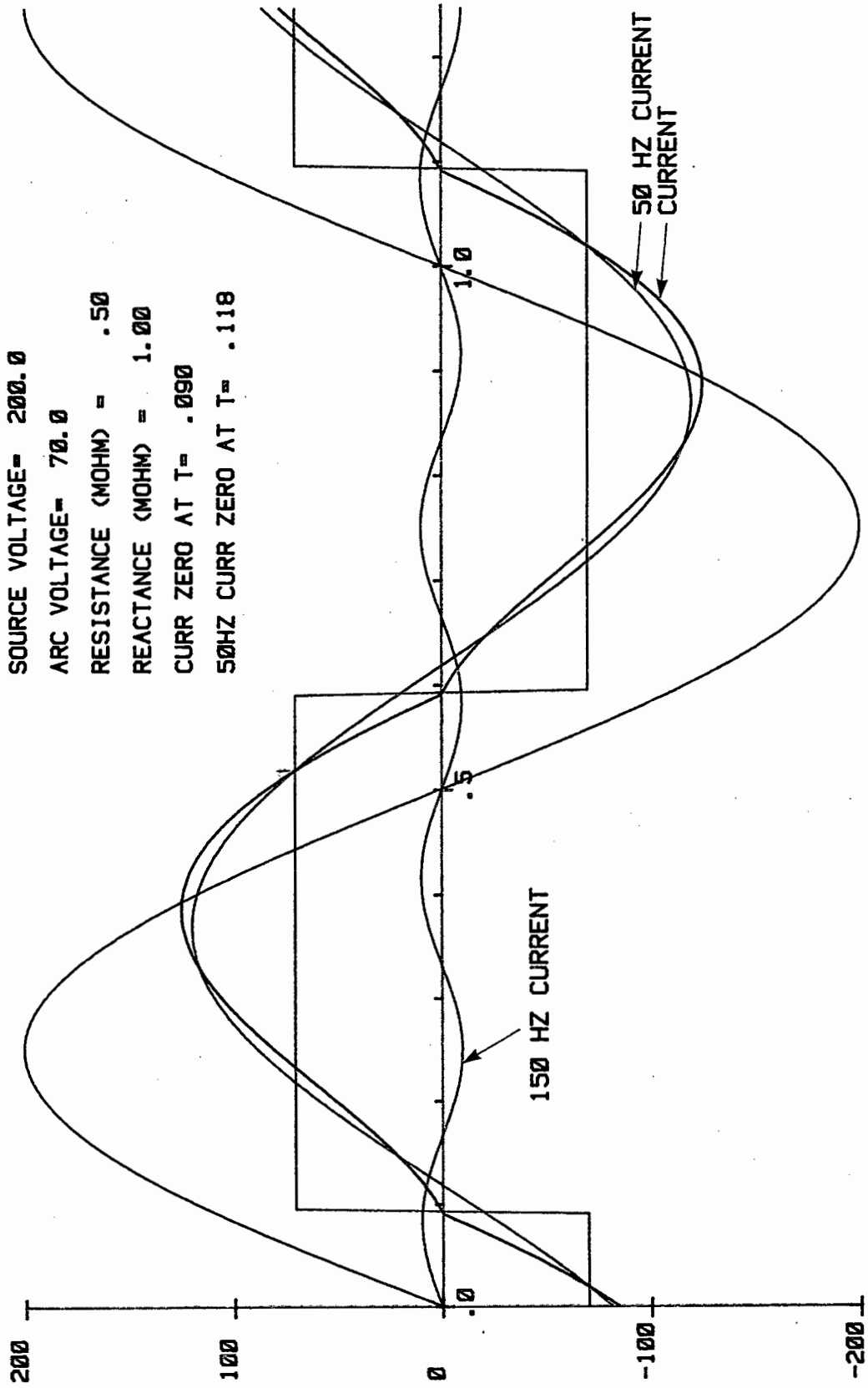

FIGURE 5.7 : VOLTAGE CURRENT & ARCING WAVEFORMS FOR SINGLE PHASE CIRCUIT

$$R = \frac{P}{I^2} \qquad (5.4)$$

$$X = \sqrt{\left(\frac{V}{I}\right)^2 - R^2} \qquad (5.5)$$

The variation of these two variables with arc voltage is shown in Figure 5.8. As expected, both the resistance and reactance increase with increasing arc voltage. However, the same changes occur if only the fundamental frequency components are used for the calculations. This effect cannot be shown graphically as the curves coincide, however, the results given in Table 5.1 show that there are only minor differences in the reactances and resistances when derived from rms computation using the total waveforms or just the fundamental frequency (50Hz) waveforms. This is contradictory to Bretthauer and Farschtschi's statement[16].

"If one is to disregard all the harmonic frequencies of the voltage, current and power, then the reactance remains constant for each value of arc voltage; this is the reactance of the basic frequency which is given by the geometry of the high current paths, namely X = wL".

Arc voltage (volts)	Source voltage (volts)	Real power (MW)		Current (kA)		Resistance (mΩ)		Reactance (mΩ)	
		RMS	50Hz	RMS	50Hz	RMS	50Hz	RMS	50Hz
0	141,42	0,80	0,80	126,5	126,5	0,50	0,50	1,0	1,0
20	141,42	0,9084	0,9085	118,0	118,0	0,652	0,653	1,005	1,005
40	141,42	0,9545	0,9544	106,9	106,8	0,835	0,836	1,026	1,026
60	141,42	0,9276	0,9277	93,0	92,8	1,071	1,077	1,078	1,078

$R = 0{,}5\ m\Omega$

$X = 1{,}0\ m\Omega$

$E_s = 200$ volts (pk)

TABLE 5.1 : Comparison of 'RMS' and '50Hz' electrical parameters for various arc voltages computed using single-phase circuit with arcing equations

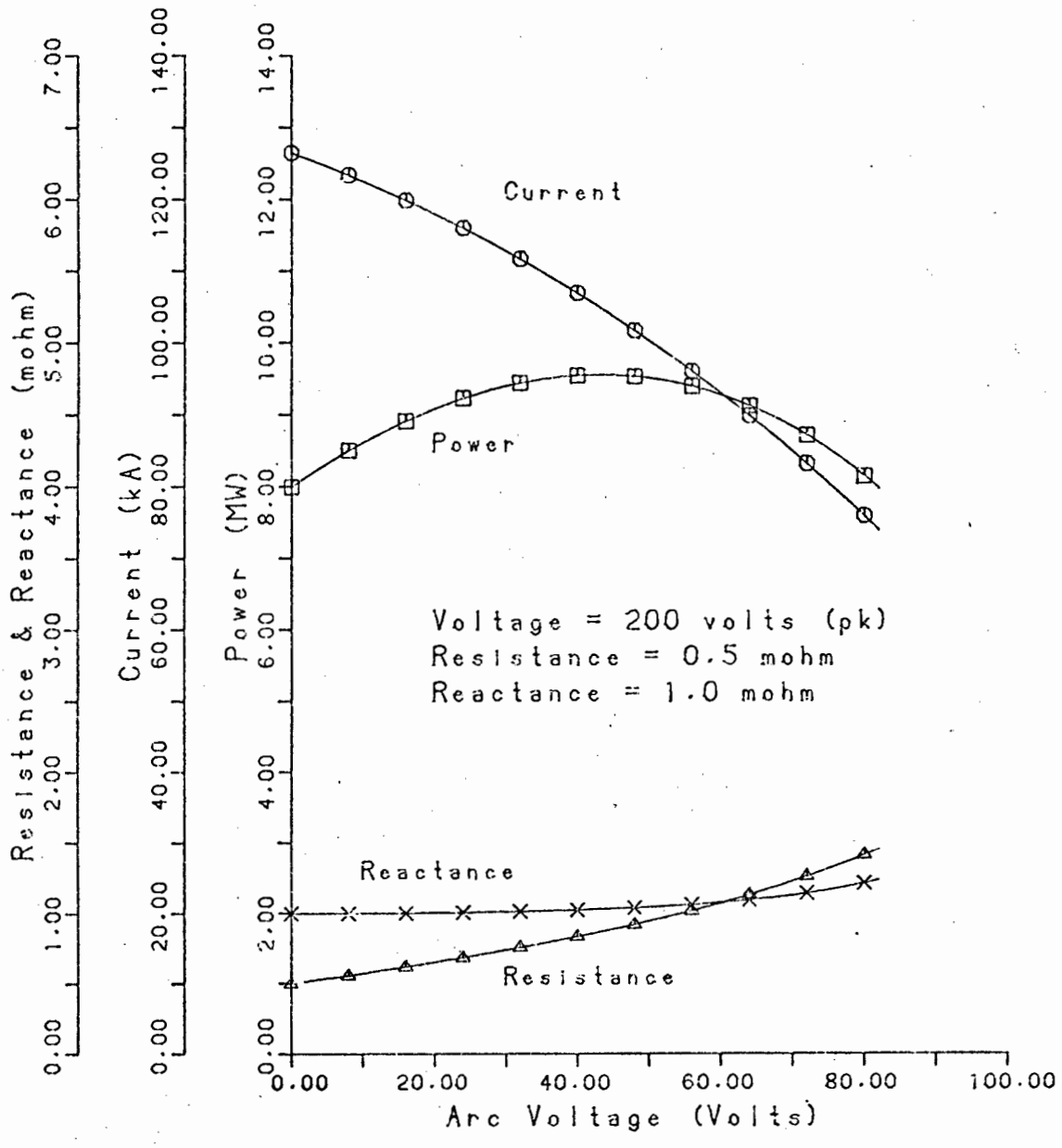

FIGURE 5.8 : VARIATION OF ELECTRICAL VARIABLES WITH ARCING (SINGLE PHASE).

The error in this statement can be seen by examining Figure 5.7 which shows that the 50 Hz current waveform (green curve) is out of phase with the arc voltage waveform, (blue curve). Therefore, there is an in-phase and out-of-phase component of arc power even at the fundamental frequency.

The reactive nature of the arc has the effect of reducing the efficiency of power utilization in the circuit. This is the major detrimental effect of arcing since the rating of the power circuit has to be increased to make up for the lost real power. The extent of the reduced power efficiency is shown in Figure 5.9 for single-phase operation which compares the furnace operating curves of three different loads for constant source voltage and reactance. The best power utilization is for the case where there is no arcing, and the worst occurs for the hypothetical case of no resistance and pure arcing.

Figure 5.9 : Comparison of operating curves for pure resistance operation and for arcing (single phase)

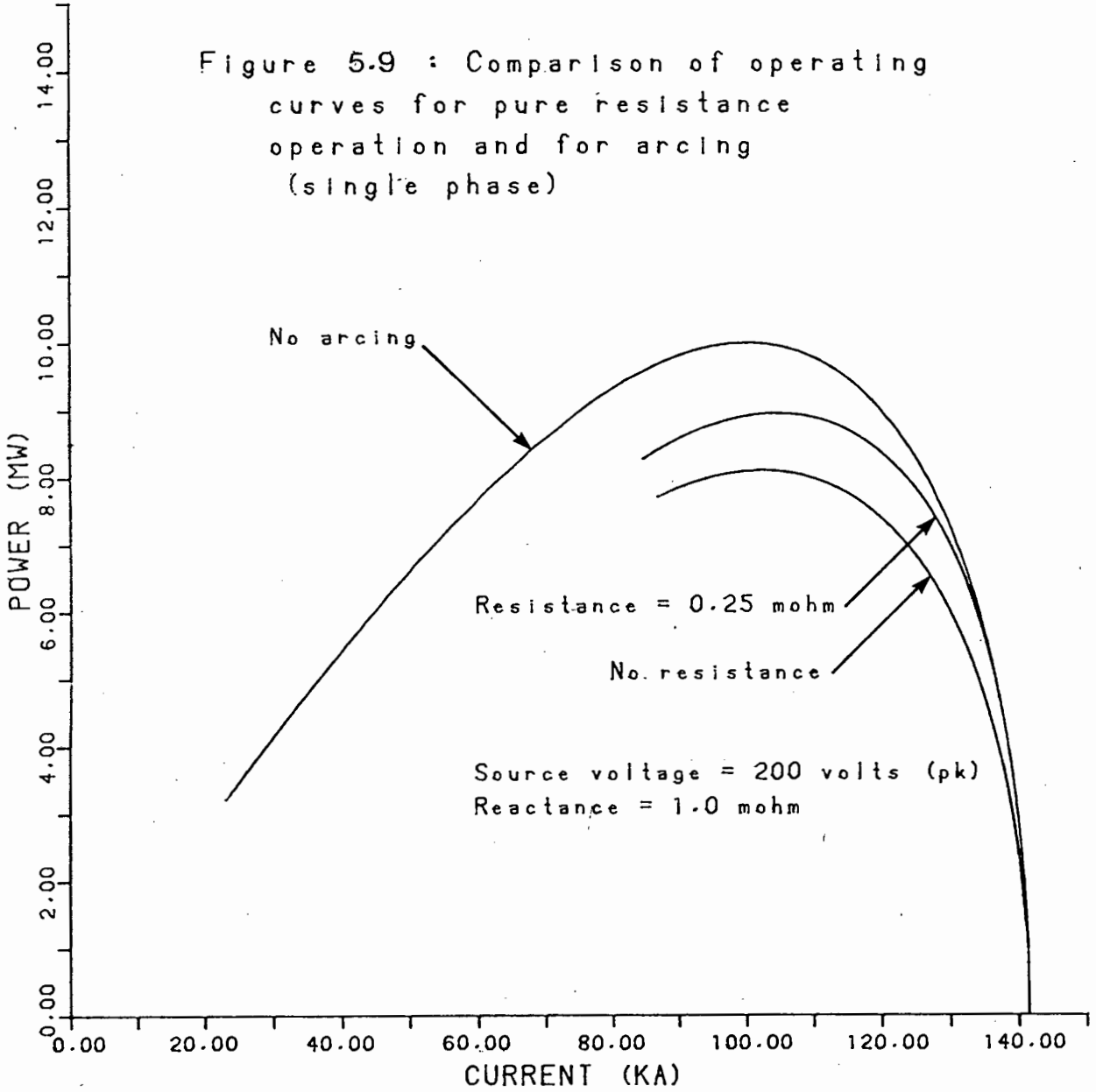

5.5 Equivalent Circuit of an Arc

5.5.1 Kasper and Jahn's equivalent circuit

The resistive and reactive nature of the arc suggests that it can be represented in a linear circuit as a combination of resistances and reactances. Kasper and Jahn[38] have proposed representing the arc as a parallel combination of a resistance and a reactance as shown in Figure 5.10. The arc reactance X_{NL} is related to the circuit reactance X_L by the equation

$$X_{NL} = \frac{\sigma}{1-\sigma} X_L \qquad (5.6)$$

where σ is a constant describing the type of arcing. For single phase operation with the arc represented by a square wave $\sigma = 8/\pi^2 = 0{,}81$ and $X_{NL} = 4{,}28\ X_L$. When there is no arcing $\sigma = 1$ and $X_{NL} = \infty$ so that the circuit becomes the same as a standard single-phase circuit without arcing.

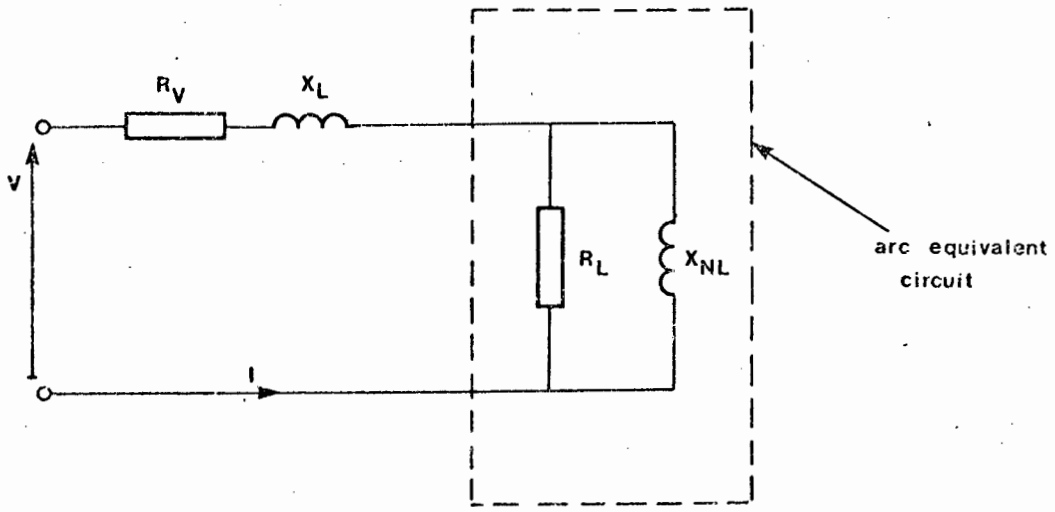

FIGURE 5.10 : KASPER AND JAHN'S EQUIVALENT CIRCUIT FOR ARCING.

The validity of Kasper and Jahn's equivalent circuit is shown in Figure 5.11 which gives the power circle diagram plots (P-Q plots) for various values of arc reactance X_{NL}. (The equations for these curves are given in Appendix E.)

The lower curve corresponds to the single-phase case with square wave arcing where $\sigma = 0{,}81$ and $X_{NL} = 4{,}28\ X_L$, and this curve coincides identically with the P-Q curve derived from the single-phase arcing equations given in Appendix D (circled portion of curve). The other curves are included to illustrate the progression towards the no-arcing curve which has the highest real-power maximum.

Figure 5.11 : Curves showing P-Q plots for various reactances using Kasper and Jahn's arc model.

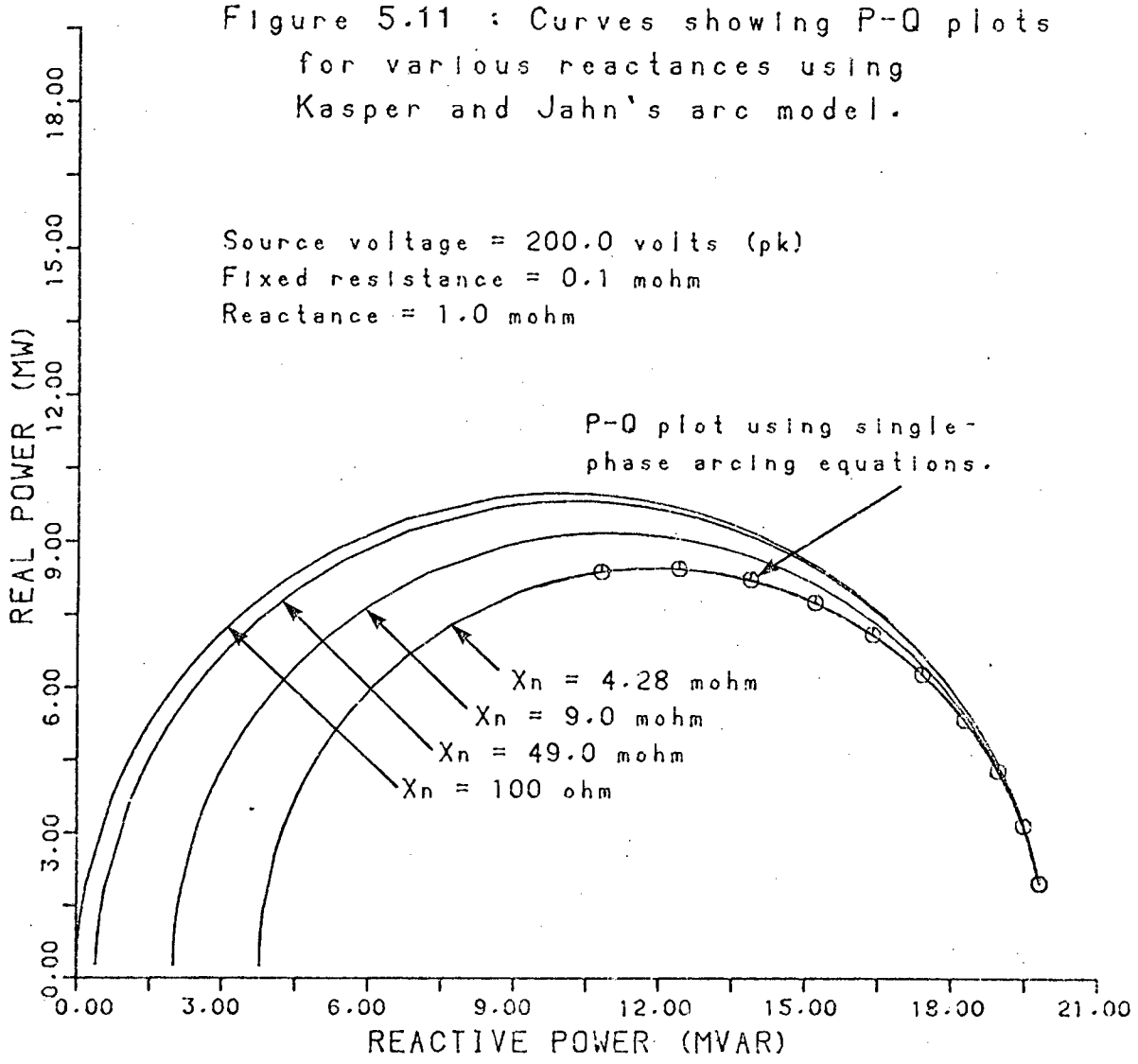

5.5.2 Barker's equation

In a paper submitted to Elektrowärme Int. (but not yet published), Barker[6] has described a simple equation which can be used to describe the operating characteristics of a furnace when arcing is present. The equation is of the form

$$P = k \times I_{rms} \sqrt{I_{max}^2 - I_{rms}^2} \qquad (5.7)$$

This is the same as the power-operating characteristic given in section 2.3 except that a constant k has been introduced. The constant is the same as Kasper and Jahn's σ and for single-phase operation it varies between 0,81 and 1,0 depending on the amount of arcing in the circuit. In three-phase operation the lower limit is 0,91. The validity of the equation can be proved for the case where the single-phase circuit consists of a reactance and an arc without any resistance (Appendix F). It is also necessary to assume that I_{rms} is the value of the current which is in phase with the arc voltage. If the true rms current is used, the resulting PQ operating characteristic is different from the true characteristic as shown in Figure 5.12. However, the region where the two curves agree corresponds with normal furnace operating conditions

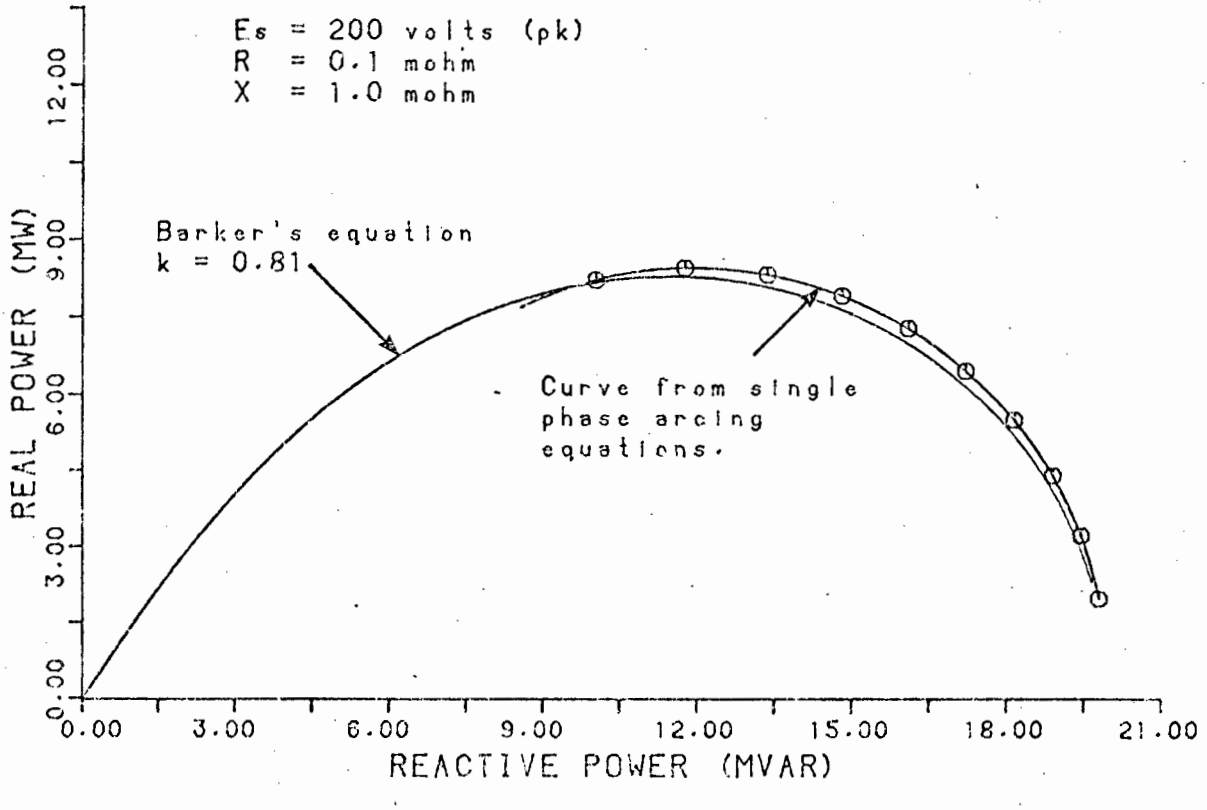

FIGURE 5.12 : P-Q PLOT FOR BARKER'S EQUATION AND SINGLE-PHASE ARCING EQUATIONS.

Barker's equation can be used to determine the extent of arcing in the operation of a submerged-arc furnace. The rearrangement of equation 5.7 gives:

$$\frac{P^2}{I_{rms}^2} = k^2 X_L^2 (I_{max}^2 - I_{rms}^2) \qquad (5.8)$$

$$I_{max} = \frac{V}{X_L}$$

so that

$$\frac{P^2}{I_{rms}^2} = -k^2 . X_L^2 . I_{rms}^2 + k^2 V^2$$

Barker plotted $\frac{P^2}{I_{rms}^2}$ against I_{rms}^2 for a large number of readings from an operating furnace producing ferrochromium (48 MVA furnace) and found that $k = 0{,}95$. This is about half way between the complete arcing and no arcing conditions and does indicate that an appreciable amount of arcing does occur.

5.6 Three-phase Circuit with Arcing

As with the single-phase circuit the details of the derivation of the mathematical equations for the three-phase circuit are given in Appendix G. The equivalent circuit considered is shown in Figure 5.13. It is essentially the same as the three-phase equivalent star circuit considered in Chapter 3 with the inclusion of an arc voltage in each phase. The inclusion of these three non-linear elements increases the complexity of the mathematics considerably and only the case where $R_1=R_2=R_3$ and $L_1=L_2=L_3$ will be considered here. This is reasonable since one is really only interested in looking at the effects of changing arc voltages while keeping other variables constant. Of particular interest are the interaction effects between the phases in terms of the powers, resistances and reactances.

Ignoring interaction effects, the equivalent circuits developed for the single-phase circuit are also applicable to the three-phase circuit if each phase is considered separately as a single-phase circuit. An important difference,

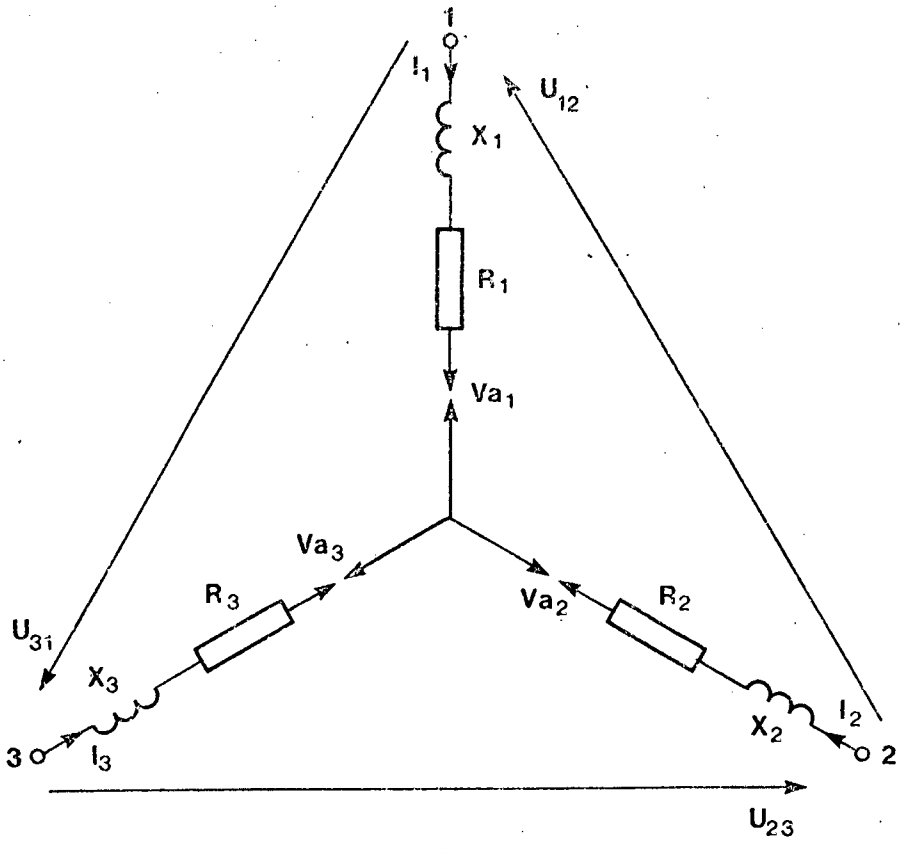

FIGURE 5.13 : EQUIVALENT CIRCUIT OF THREE-PHASE CIRCUIT WITH ARCING.

however, is that the reduction in power efficiency as a result of arcing is less in a three-phase circuit than in a single-phase circuit. This is shown in Figure 5.14 which compares the power operating characteristics for three-phase and single-phase operation, all other factors being equal. This result is caused by the interaction between the arc voltages at the neutral point and is discussed more fully in Appendix H.

Considering Kasper and Jahn's equivalent circuit and Barker's equation, the value of k or σ for three-phase arcing conditions equals $9/\pi^2$ which equals 0,9112. The power circle diagrams comparing these representations with the characteristic calculated from the arcing equations (assuming equal arc voltages in each phase) are shown in Figure 5.15. The agreement between the curves is good and Barker's equation is valid over a wider operating range than for single-phase operation.

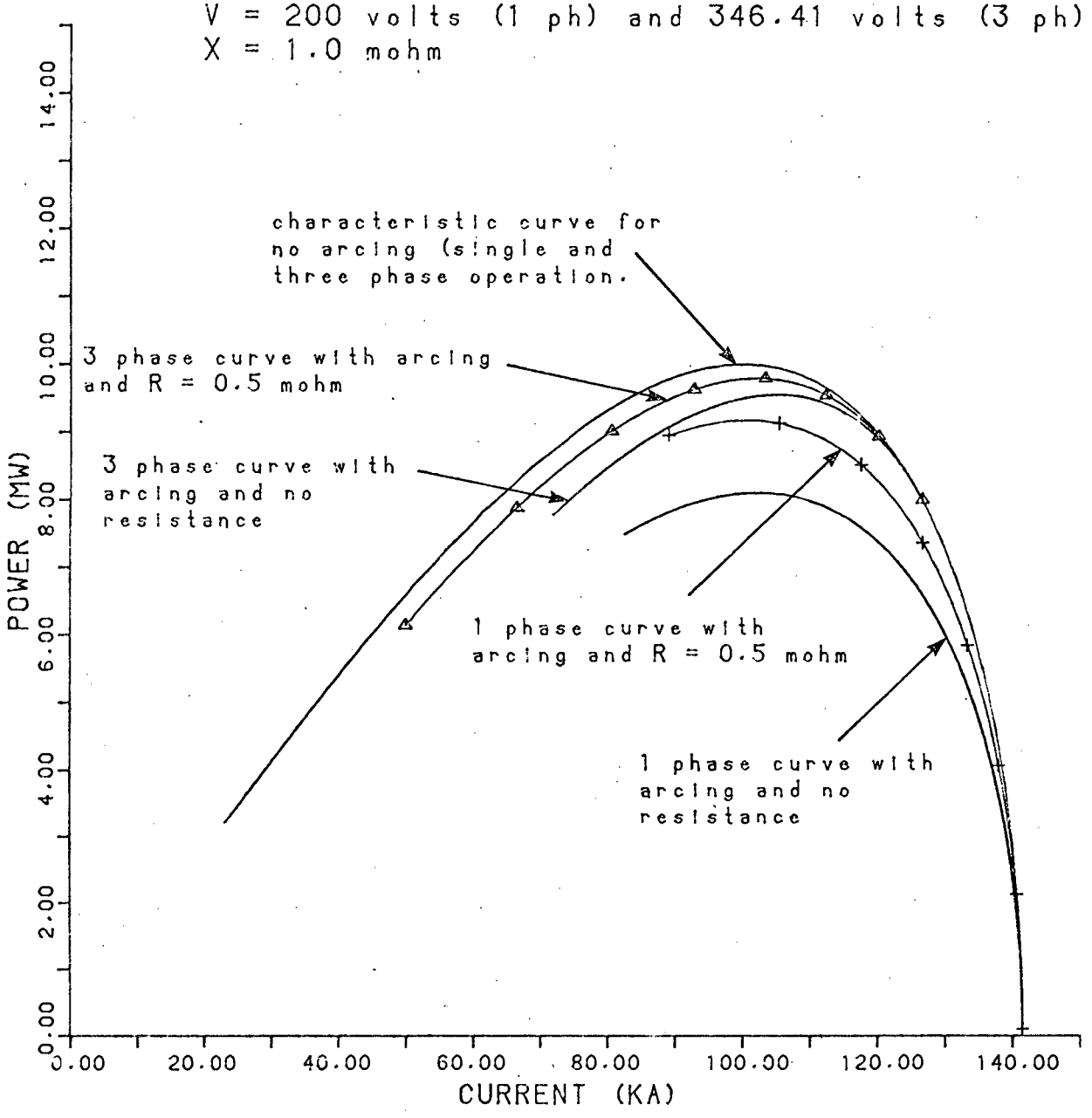

FIGURE 5.14 : POWER EFFICIENCY FOR THREE-PHASE AND SINGLE-PHASE OPERATION.

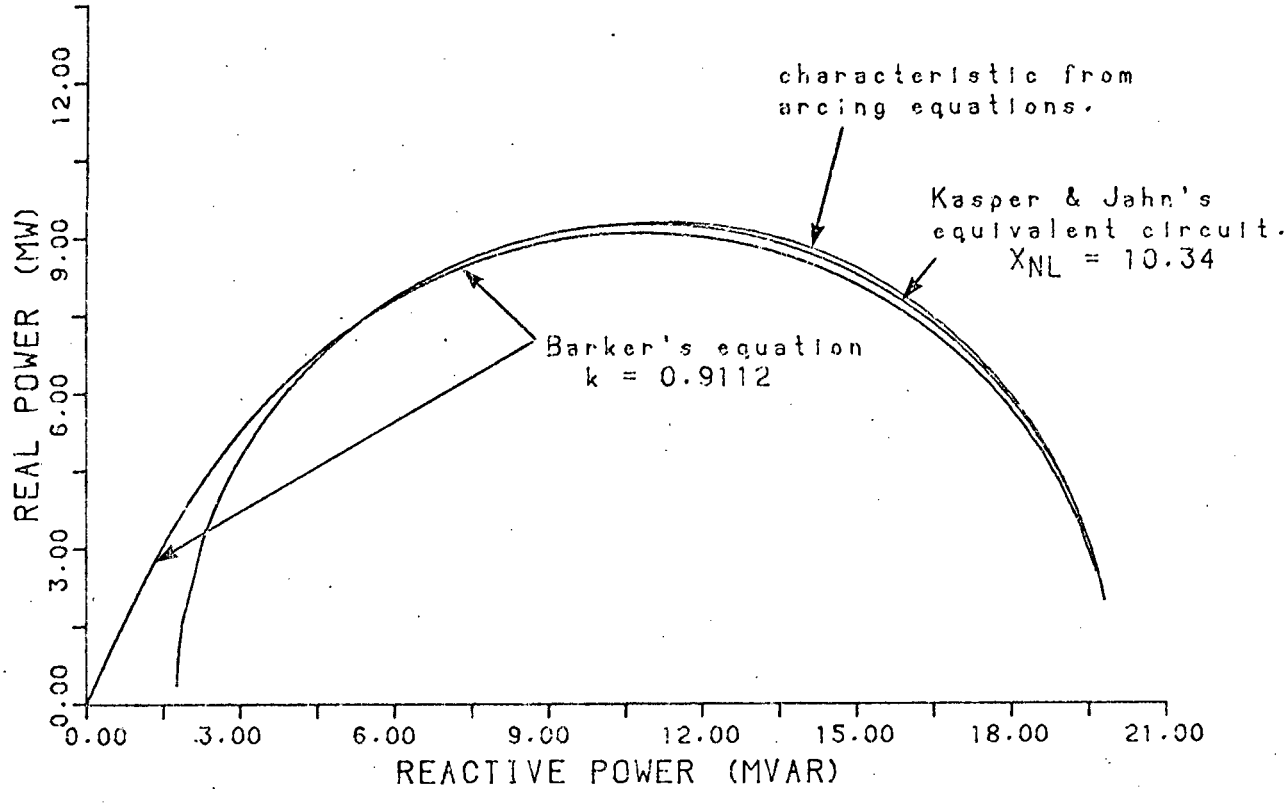

FIGURE 5.15 : COMPARISON OF P-Q PLOTS FOR THREE-PHASE OPERATION.

5.6.1 Interaction effects in three-phase circuit with arcing

The floating neutral connection of the furnace secondary power circuit results in a situation where arcing in one phase of the circuit has a marked effect on the currents and voltages and hence arcs of the other two phases. This interactive nature of the circuit is complex since the results of a change in the arcing in one phase of the circuit varies with the state of the whole circuit.

The effect of a change in arcing in one phase of the circuit on the three-phase powers is shown in Figures 5.16 and 5.17. In Figure 5.16 the arc voltages in the other two phases are zero and in Figure 5.17 the arc voltages in the other two phases are fixed at 50 volts. In each case the powers are plotted for three values of fixed reactance 0,5 mΩ, 1,0 mΩ and 1,5 mΩ. The arc voltage changes are for phase one and in all cases there is a marked

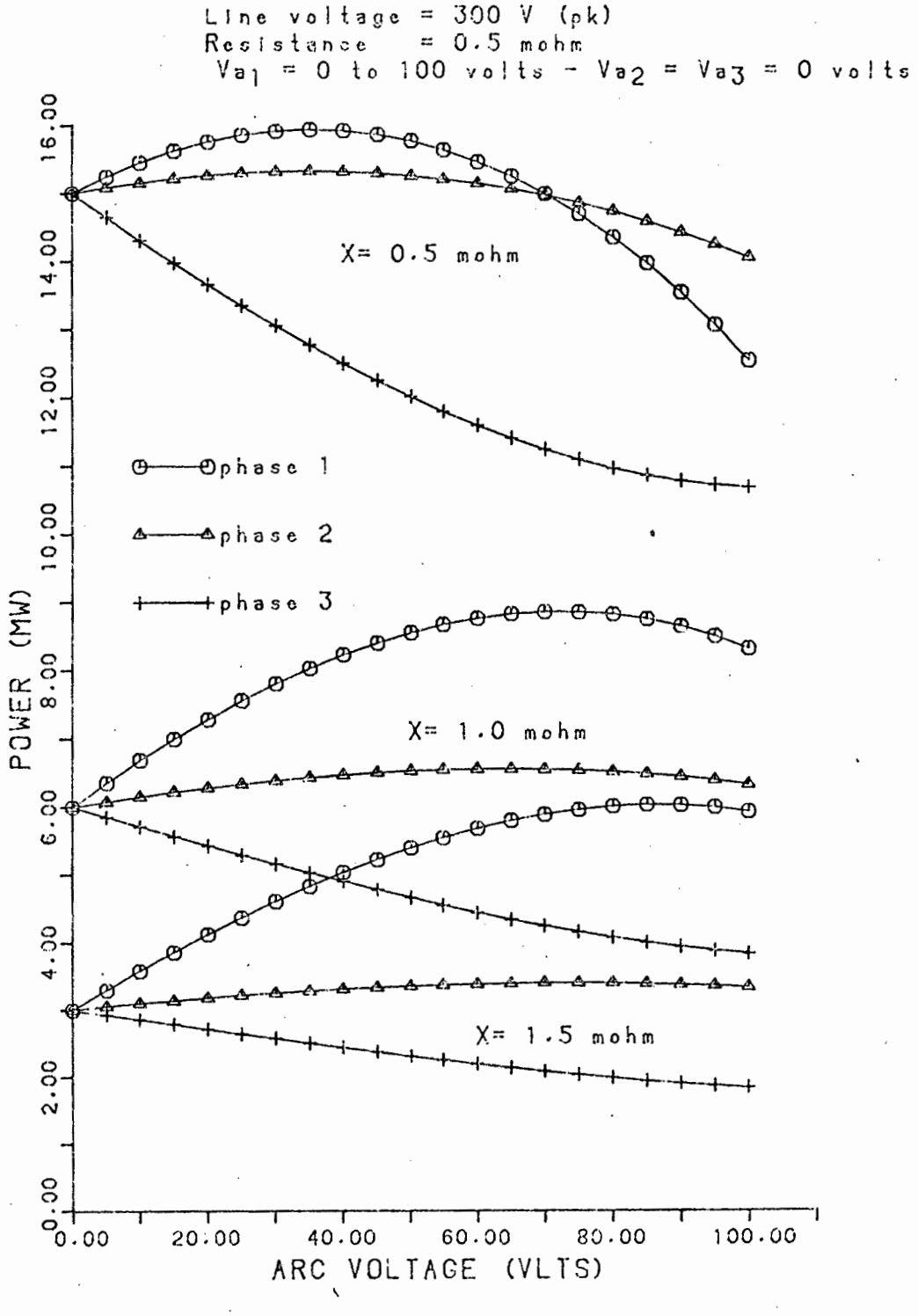

FIGURE 5.16 : VARIATION OF PHASE-POWERS WITH ARCING IN PHASE 1

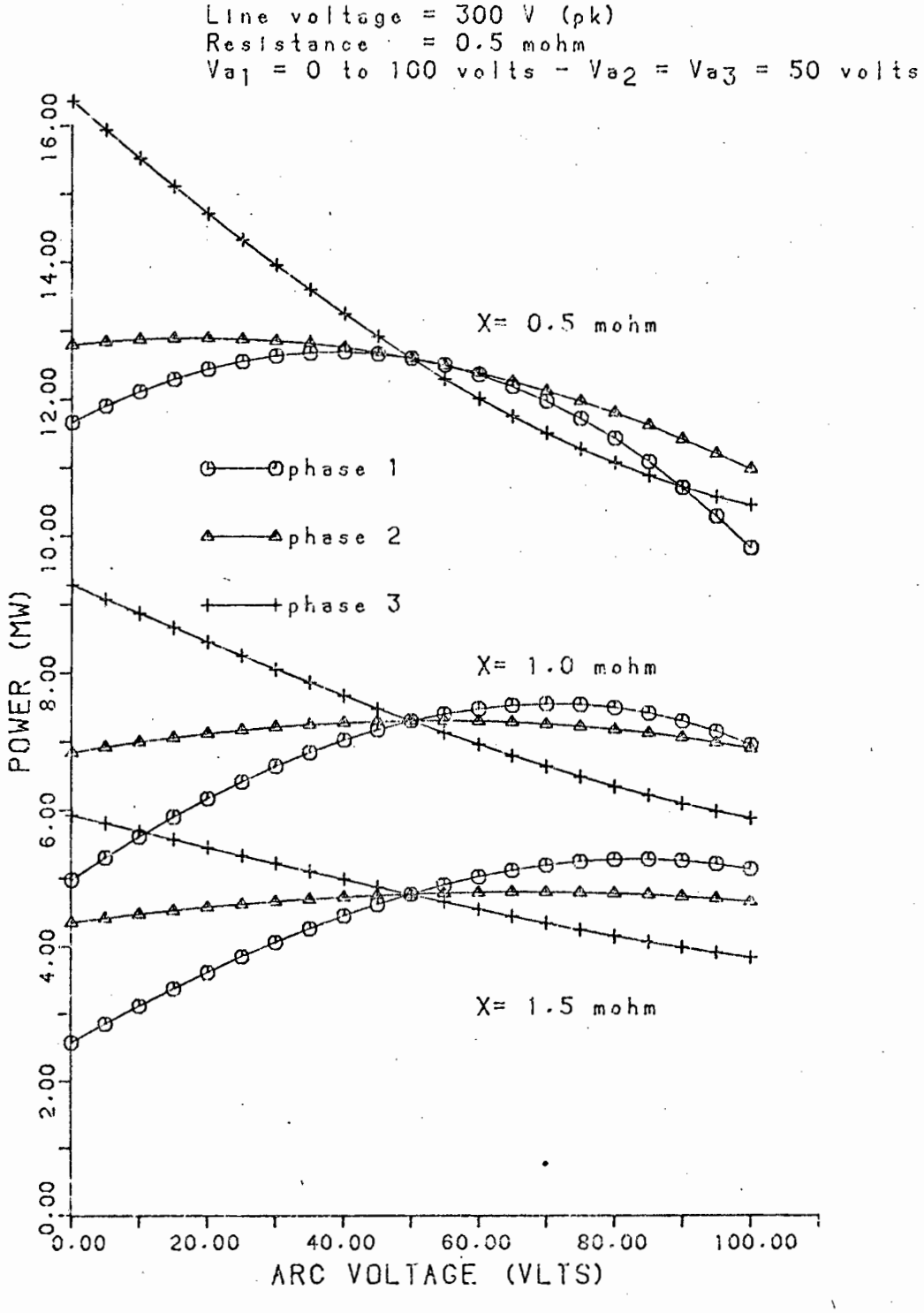

FIGURE 5.17 : VARIATION OF PHASE-POWERS WITH ARCING IN PHASE 1 (ARCING IN OTHER PHASES FIXED AT 50 VOLTS).

effect on the power in that phase. Considering the other two phases, the major effect is on phase three, the previous phase in the sequence of phase rotation, with relatively minor changes in phase two. This is similar to the results of resistance disturbances in one phase when there is an appreciable amount of reactance in the circuit. Considering the effect of reactance on the arcing curves there is a gradual, but small trend towards less separation in the phase powers as reactance is increased.

Turning now to the results of arcing disturbances in one phase on the phase resistances and reactances, there is, surprisingly, very little interaction as shown in Figure 5.18. The only significant changes are in the phase with the arc voltage change. The differences between rms and 50 Hz measurements are also only significant for the resistance and reactance in phase one and are shown in Figure 5.18 as a slight separation in the curves at high arc voltages.

5.6.2 Examination of waveforms for three-phase circuit with arcing

The non-linear nature of the arc introduces harmonics into the voltage and current waveforms. The arc itself can be represented as a sum of the fundamental sinusoidal voltage and harmonic voltages which cause harmonics to be generated in the arcing current. The distorted arcing current causes additional harmonic voltages to be generated across the linear resistances and reactances in the circuit. In the case of the single-phase circuit, all harmonic voltages must add up to zero since the circuit is driven by a purely sinusoidal source voltage. In the three-phase circuit this also applies to the delta voltages which are purely sinusoidal, however, harmonics can occur in the line to neutral voltages.

The current waveforms for a three-phase circuit with arcing are shown in Figure 5.19 together with the delta voltage waveforms and arc voltages. The associated line to neutral voltage waveforms are shown in Figure 5.20. It can be seen that the current waveforms are relatively undistorted, whereas the

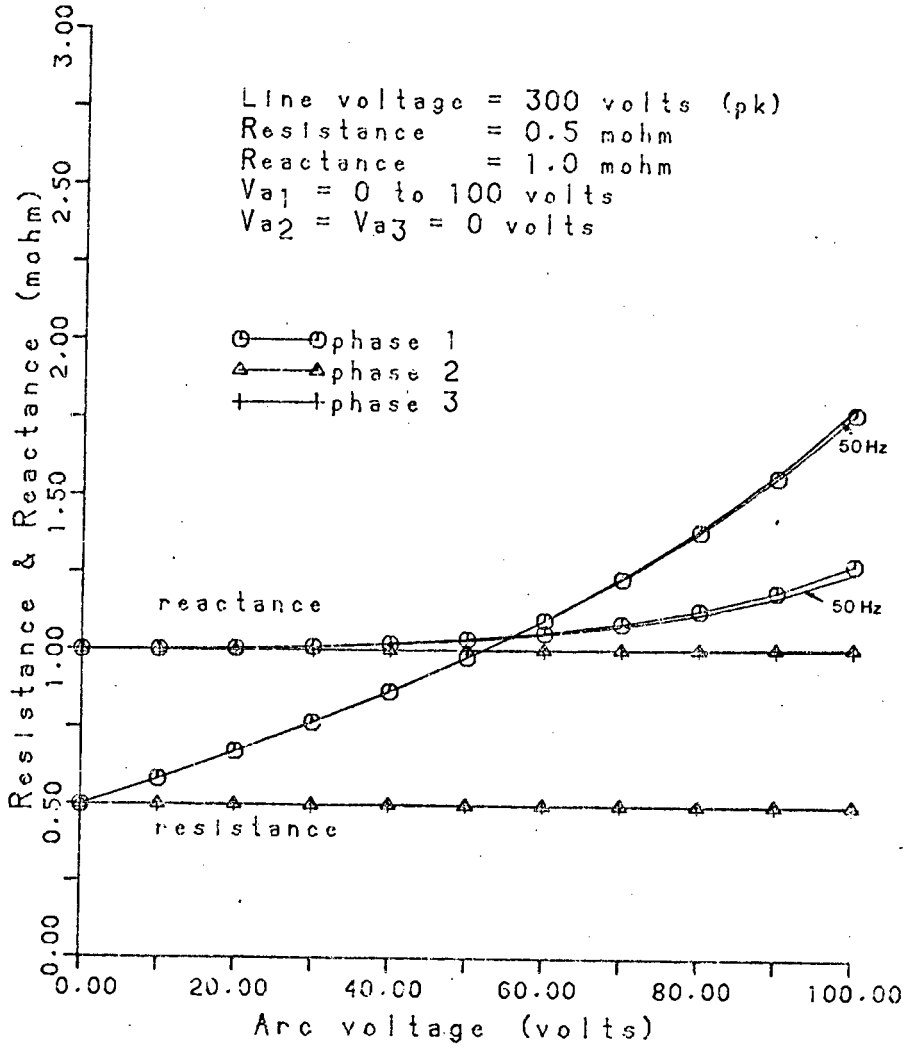

FIGURE 5.18 : VARIATION OF RESISTANCES AND REACTANCES WITH ARCING IN PHASE 1 (NO ARCING IN OTHER PHASES).

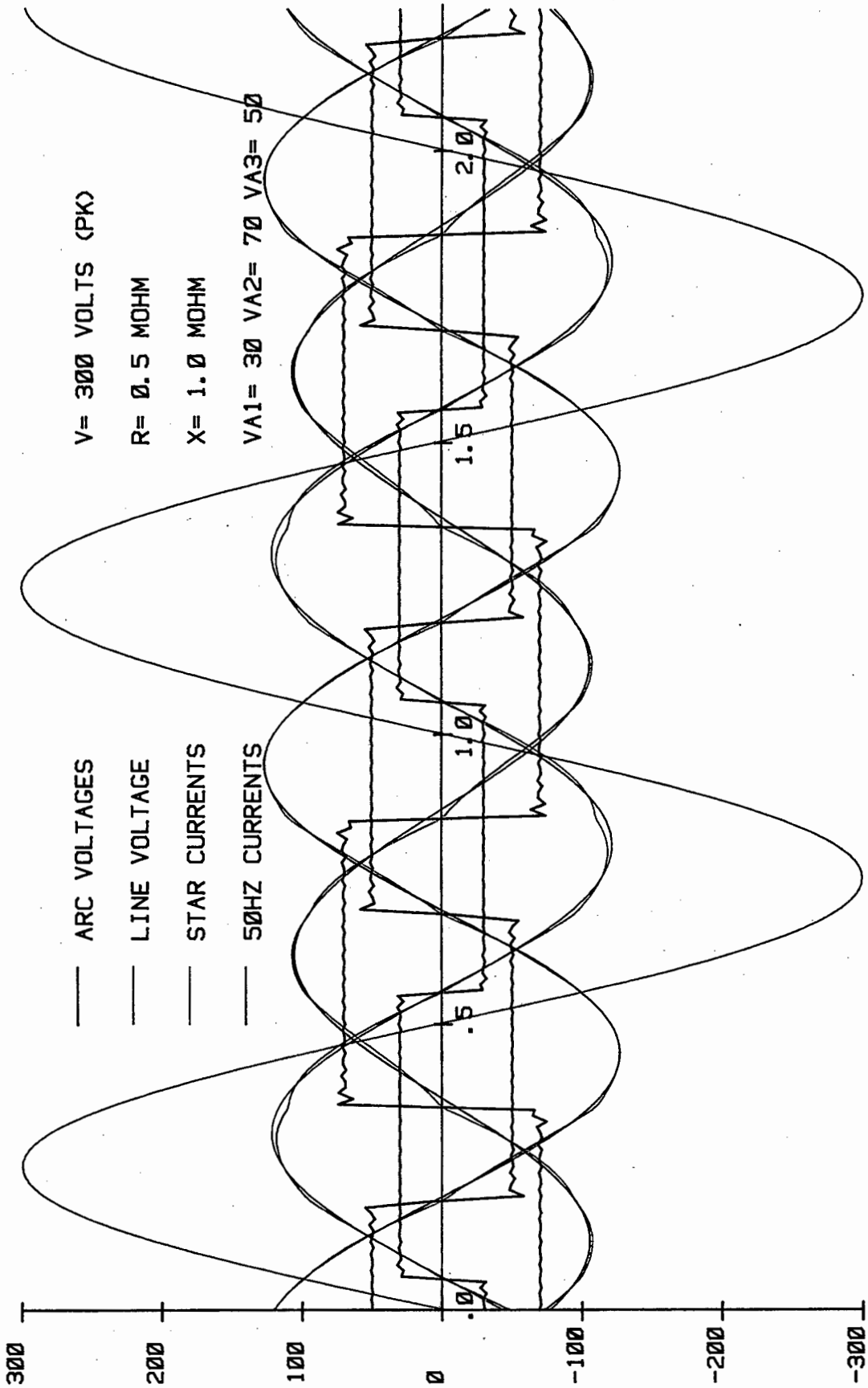

FIGURE 5.19 : THREE-PHASE ARCING WAVEFORMS

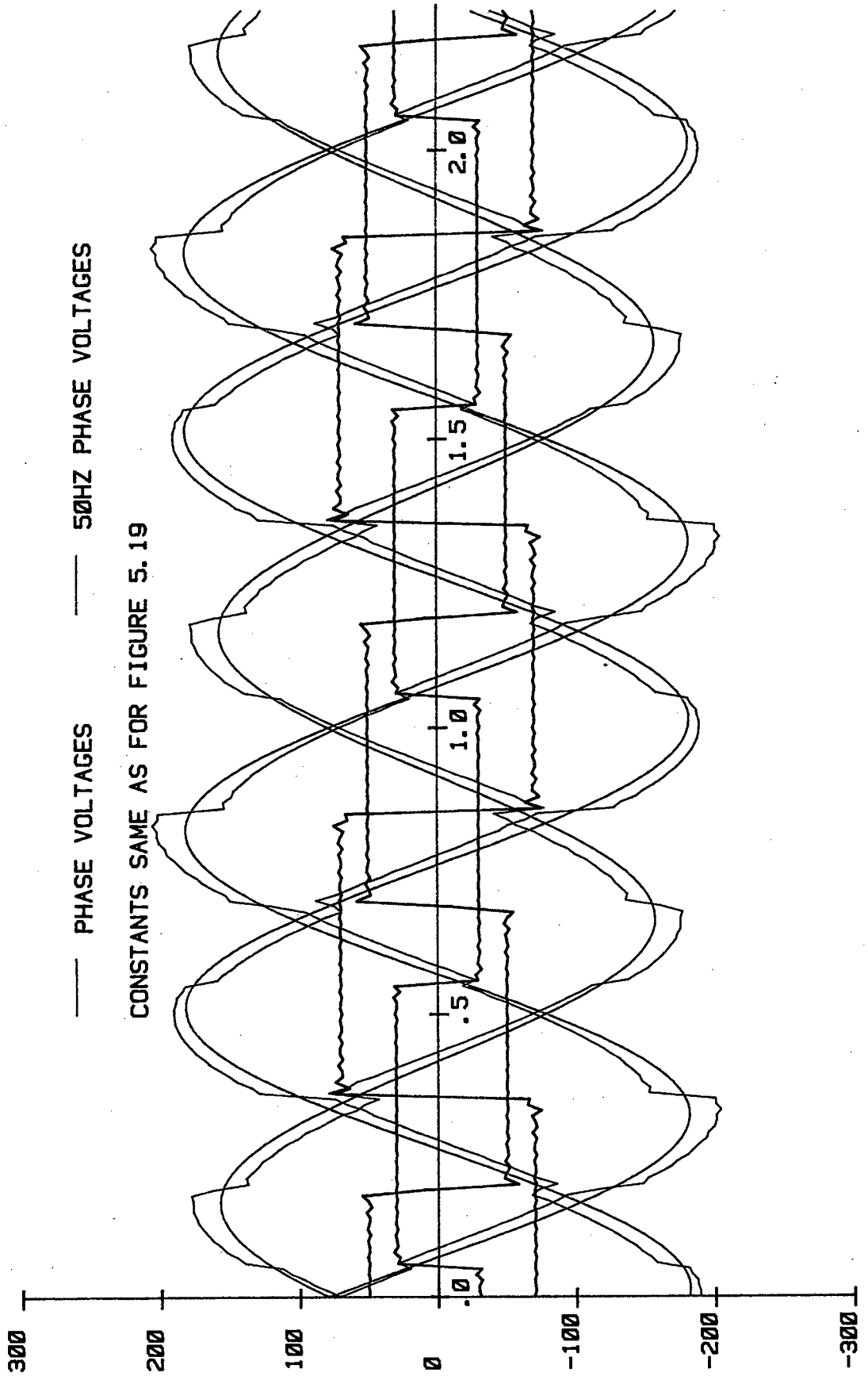

FIGURE 5.20 : THREE-PHASE ARCING WAVEFORMS

distortion in the arc voltages is more marked. This effect is also observed on oscilloscope traces taken from operating furnaces. However, the voltage waveforms are usually not as 'spiky' as shown in Figure 5.20. This is where the representation of the arc as a square wave breaks down since in actual practice the dynamic properties of the arc result in a more rounded waveform which would reduce the 'spiky' nature of the electrode-to-bath voltage waveform. The use of Cassie's equation to model the arcing gives a waveform which is a better representation, however, this will not be considered here.

5.6.3 Fourier analysis of arcing waveforms for three-phase circuit operation

The introduction of harmonics into the voltage and current waveforms as a result of arcing can be used as a means for measuring the extent of arcing in each phase of an operating furnace.[59] This measurement has been carried out on a large ferrochromium furnace and the results are discussed in the next chapter. However, there is a considerable amount of interaction between the phases which needs to be considered theoretically as a basis for analysing the experimental results. Of particular interest is the effect of changing the arc voltage in one phase, on the harmonics measured in all three phases.

The harmonic measurements on the furnace consisted of measuring the average harmonic content in the electrode-to-bath voltage waveforms and the primary current waveforms (which give pseudo secondary current waveforms). These two sets of measurements can be simulated using the three-phase arcing equations developed in Appendix G. The harmonic averages are obtained by assuming perfect full-wave rectification and computing the combined average of all frequency terms in the waveform except for the fundamental. In the computation of the harmonic average of the electrode-to-bath voltages it is not accurate to consider the total line-to-neutral voltages of Figure 5.13.

Voltage measurements are made at the electrodes which means that some impedance in each phase of the star equivalent circuit occurs before the measurement point. The electrode voltage measurements are connected at the changeover from delta to star connection so that the results of section 3.2.1 can be used to determine the split in the impedances. This means assuming that 10 per cent of the resistance and 25 per cent of the reactance occurs before the measuring point for each phase.

The degree of interaction between harmonic measurements in each phase can be seen from the graphs in Figure 5.21 and 5.22. These graphs show the change in harmonic average measurements in each phase resulting from increasing the arcing conditions in phase one. There is no arcing in the other two phases. Figure 5.21 gives the harmonic average measurements for the electrode-to-bath voltage waveforms (harmonic voltages) and Figure 5.22 gives the harmonic average measurements for the electrode current waveforms (harmonic currents). Ideally the harmonic average measurements for phases 2 and 3 should be zero which would mean that there is no interaction between the phases. However, the harmonic averages for these phases are appreciable in both the voltage and current waveform measurements. This creates a problem if these measurements are used to determine the level of arcing in each phase. The voltage measurements are better than the current measurements, since the slope of the phase 2 and 3 curve is 40 per cent of the slope of the phase 1 curve for the voltage waveforms and 50 per cent for the current waveforms.

In Figures 5.21 and 5.22 the arcing in phases 2 and 3 is set to zero. This does not give a full picture of the degree of interaction between the phases. During normal furnace operation arcing occurs in all three phases and one is interested in examining the effects of changing the arcing conditions in one phase while maintaining constant arcing conditions in the other two phases. This is shown in Figures 5.23 and 5.24 where the arcing conditions in phases 2 and 3 have been fixed at 50 volts. Here the degree of interaction in the harmonic voltage measurements is much better than for the harmonic current measurements. The phases 2 and 3 curves should be horizontal and the phase 1 curve should be a

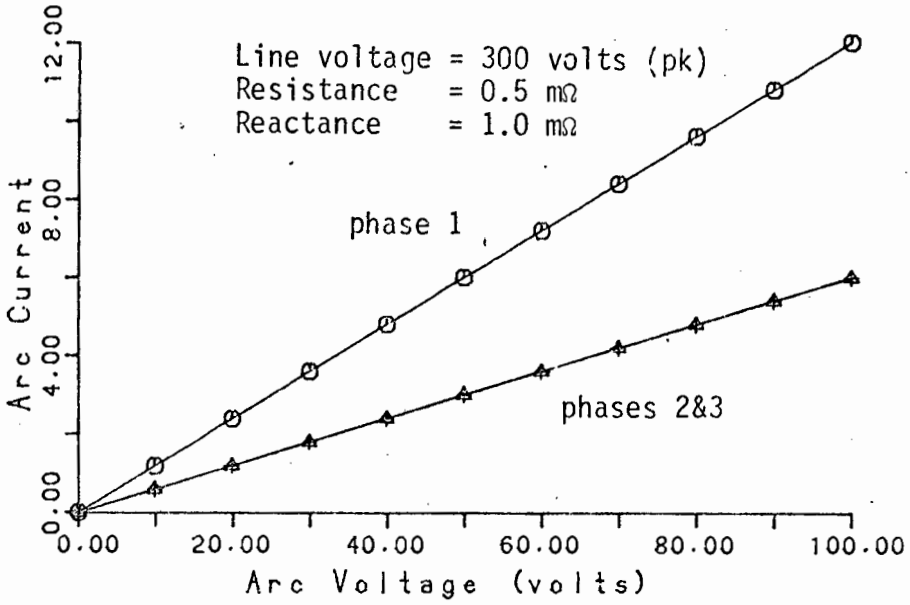

FIGURE 5.21 : VARIATION OF HARMONICS IN CURRENT WAVEFORM WITH ARCING IN PHASE 1 (ARCING IN OTHER PHASES = 0)

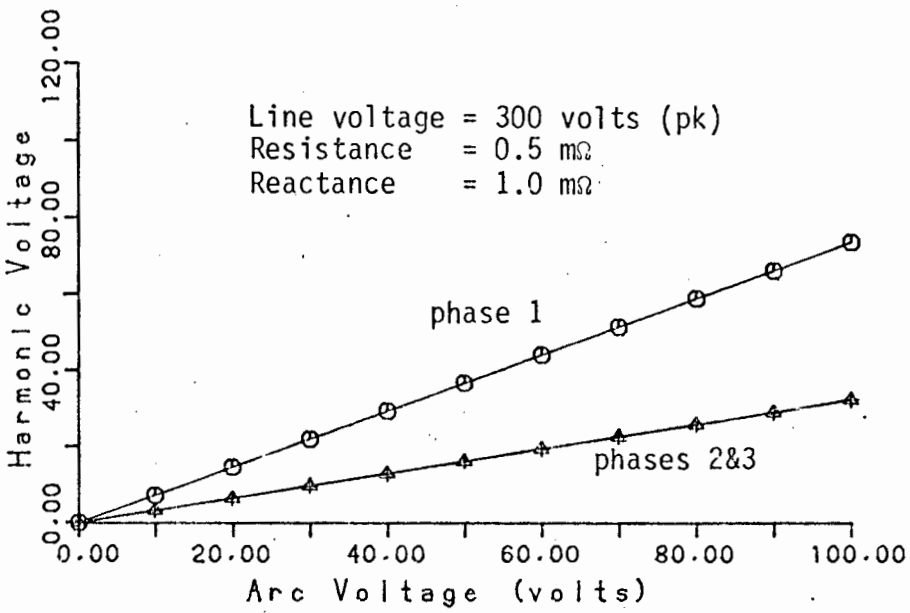

FIGURE 5.22 : VARIATION OF HARMONICS IN VOLTAGE WAVEFORM WITH ARCING IN PHASE 1 (ARCING IN OTHER PHASES = 0).

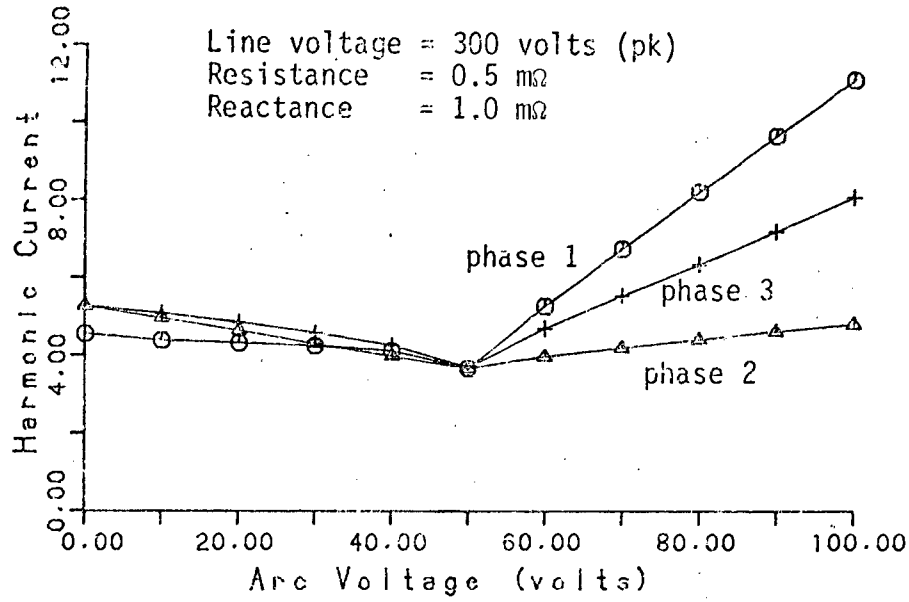

FIGURE 5.23 : VARIATION OF HARMONICS IN CURRENT WAVEFORM WITH ARCING IN PHASE 1 (ARCING IN OTHER PHASES = 50 VOLTS).

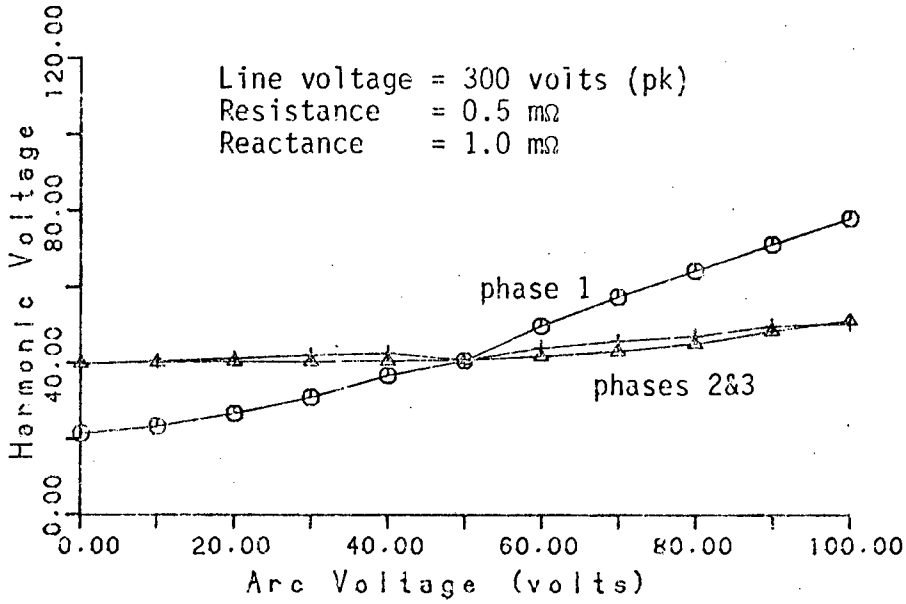

FIGURE 5.24 : VARIATION OF HARMONICS IN VOLTAGE WAVEFORM WITH ARCING IN PHASE 1 (ARCING IN OTHER PHASES = 50 VOLTS).

positive sloping line starting at the origen. In this respect the interaction in the harmonic current measurements is particularly bad for arc voltages below 50 volts. Therefore, harmonic voltage measurements provide the best possible means for determining the arcing conditions under each electrode. However, it is important that voltage measurements are made as close to the arcs as is possible. Figure 5.25 shows the harmonic voltage measurements which would be obtained from taking voltage measurements at the transformer secondary leads. The increase in interaction is clearly evident.

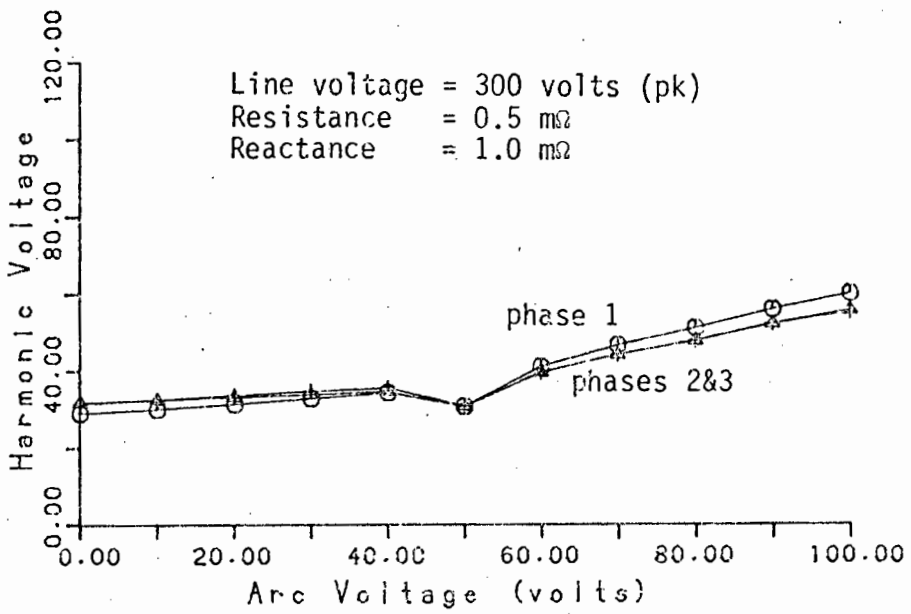

FIGURE 5.25 : VARIATION OF HARMONICS IN TRANSFORMER SECONDARY PHASE VOLTAGES WITH ARCING IN PHASE 1 (ARCING IN OTHER PHASES = 50 VOLTS).

6. EXAMINATION OF THE EFFECT OF FURNACE GEOMETRY ON REACTANCE USING FURNACE MODELS

On large furnaces the inductances (or reactances) of the secondary electrical circuit have a major effect on the operation of the furnace. Thus an examination of the relationships between the geometry of the current carrying conductor loops and the associated mutual and self inductances can provide useful information on ways to reduce the inductances or alternatively to use the inductances as a means for measuring important properties of a furnace.

The effect of furnace geometry on the inductances has been investigated using scaled-down models of a furnace, powered from a three-phase source, where measurements of changes in the circuit reactances were related to changes in the geometry of the models. Before continuing to discuss these models it is necessary to derive the lumped parameter equivalent circuit for the models. The equivalent circuits discussed in Chapter 3 are not directly applicable here as measurements for the modelling work were taken in the delta circuit. Therefore, the equivalent circuit must be established for the delta circuit rather than the star circuit as in Chapter 3.

6.1 Delta Equivalent Circuit of Three-phase Furnace

The furnace secondary circuit can be considered as being made up from three loops R, S and T formed between each transformer secondary winding and the associated two electrodes which are connected via the flexibles and bus-bars to the transformer winding as shown in Figure 6.1(a). The equivalent circuit is shown in Figure 6.1(b) where the resistances are divided into lumped delta and star resistances and all the inductances are referred to the three loops R, S and T. Each loop has a self inductance and two mutual inductances resulting from currents in the other two loops. As before, the inductances are represented by subscripts where the first subscript refers to the loop in which a voltage is induced as a result of current flowing in the loop referred to by the second subscript. On this basis the following equations can be written:

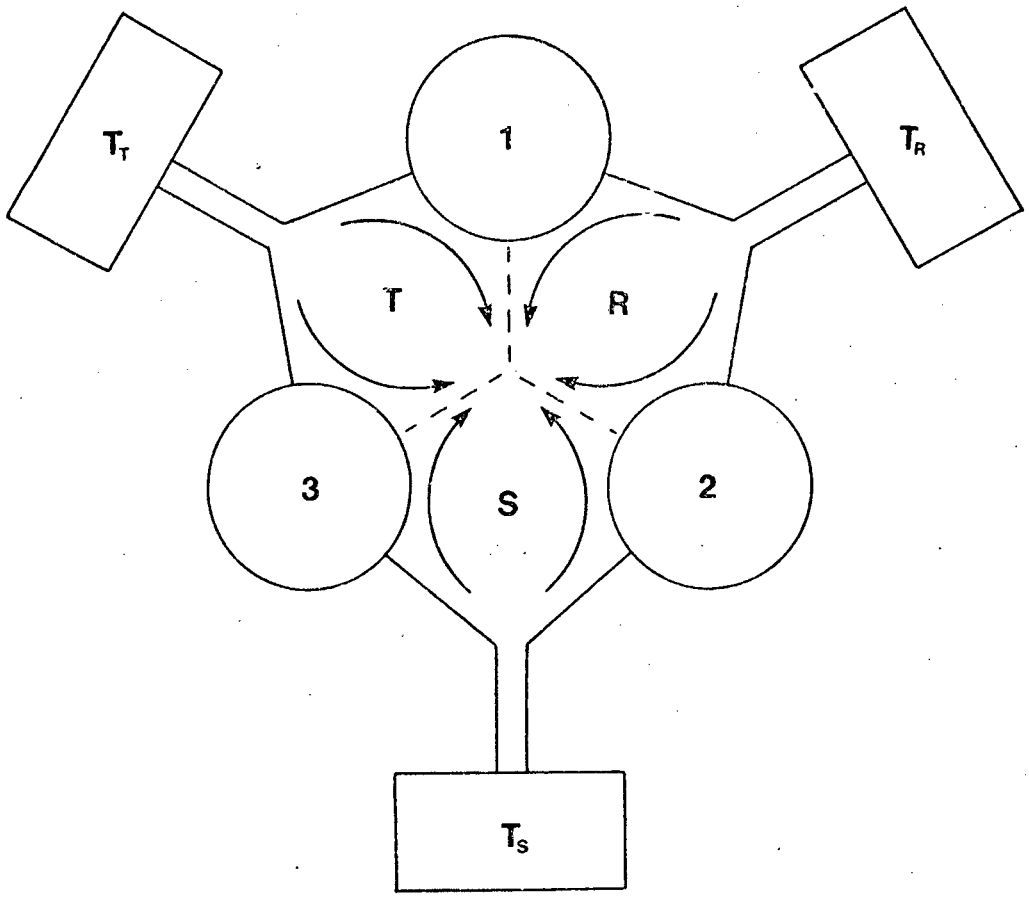

(a)

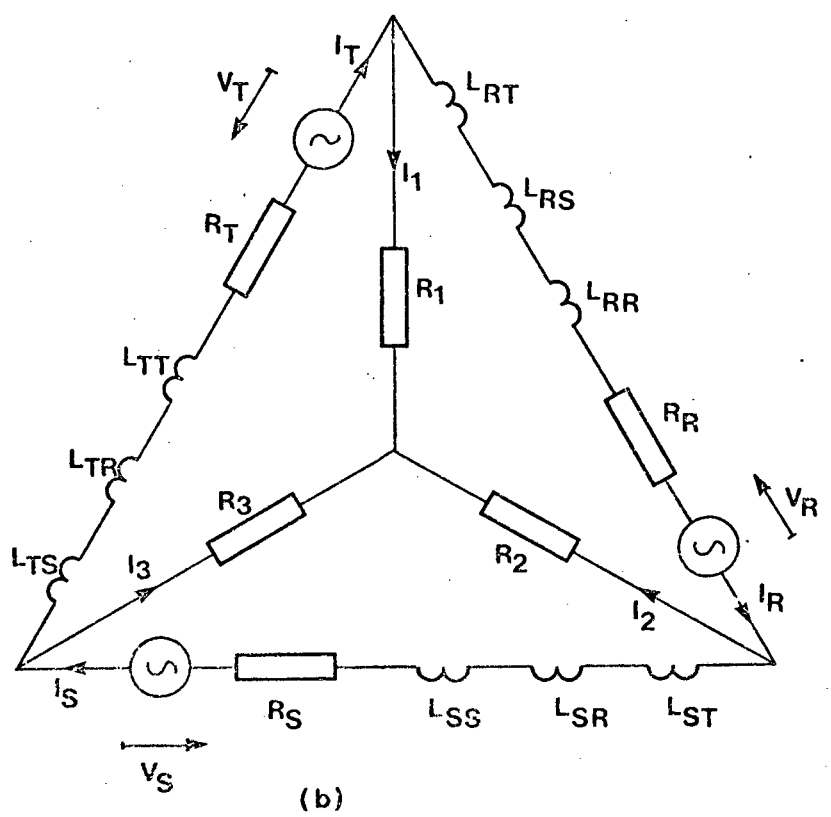

(b)

FIGURE 6.1 : DELTA EQUIVALENT OF CIRCUIT OF A FURNACE

$$V_R = jwL_{RR}.I_R + jwL_{RS}.I_S + jwL_{RT}.I_T + I_R R_R - I_1 R_1 + I_2 R_2$$

$$V_S = jwL_{SS}.I_S + jwL_{ST}.I_T + jwL_{SR}.I_R + I_S R_S - I_2 R_2 + I_3 R_3 \qquad (6.1)$$

$$V_T = jwL_{TT}.I_T + jwL_{TR}.I_R + jwL_{TS}.I_S + I_T R_T - I_3 R_3 + I_1 R_1$$

Again from equation 3.4

$$L_{RS} = L_{SR}$$
$$L_{ST} = L_{TS} \qquad (6.2)$$
$$L_{TR} = L_{RT}$$

If the inductance terms are converted to reactances and all the resistances are converted to equivalent star resistances R_R', R_S' and R_T', then,

$$V_R = I_R(R_R' + j\,X_{RR}) + j(I_S.X_{RS} + I_T.X_{TR})$$
$$V_S = I_S(R_S' + j\,X_{SS}) + j(I_T.X_{ST} + I_R\,X_{RS}) \qquad (6.3)$$
$$V_T = I_T(R_T' + j\,X_{TT}) + j(I_R.X_{TR} + I_S.X_{ST})$$

Thus, the inductance effects in the circuit are described by three self inductances and three mutual inductances.

6.2 Power System for Models

The models were driven from a power system, arranged so that it resembled the power system on a large furnace. Three single-phase stepdown transformers were arranged in a triangle and connected to the models in a Knapsack-type connection where the 'go' and 'return' current conductors for each transformer secondary were placed adjacent to each other until they were close to the model connection point as shown in Figure 6.2. The three transformers were driven from a 380 Hz 3-phase motor-alternator power source driven by a d.c. motor whose speed was controlled by a Ward-Leonard speed controller. The alternator voltage was adjusted by varying the d.c. excitation

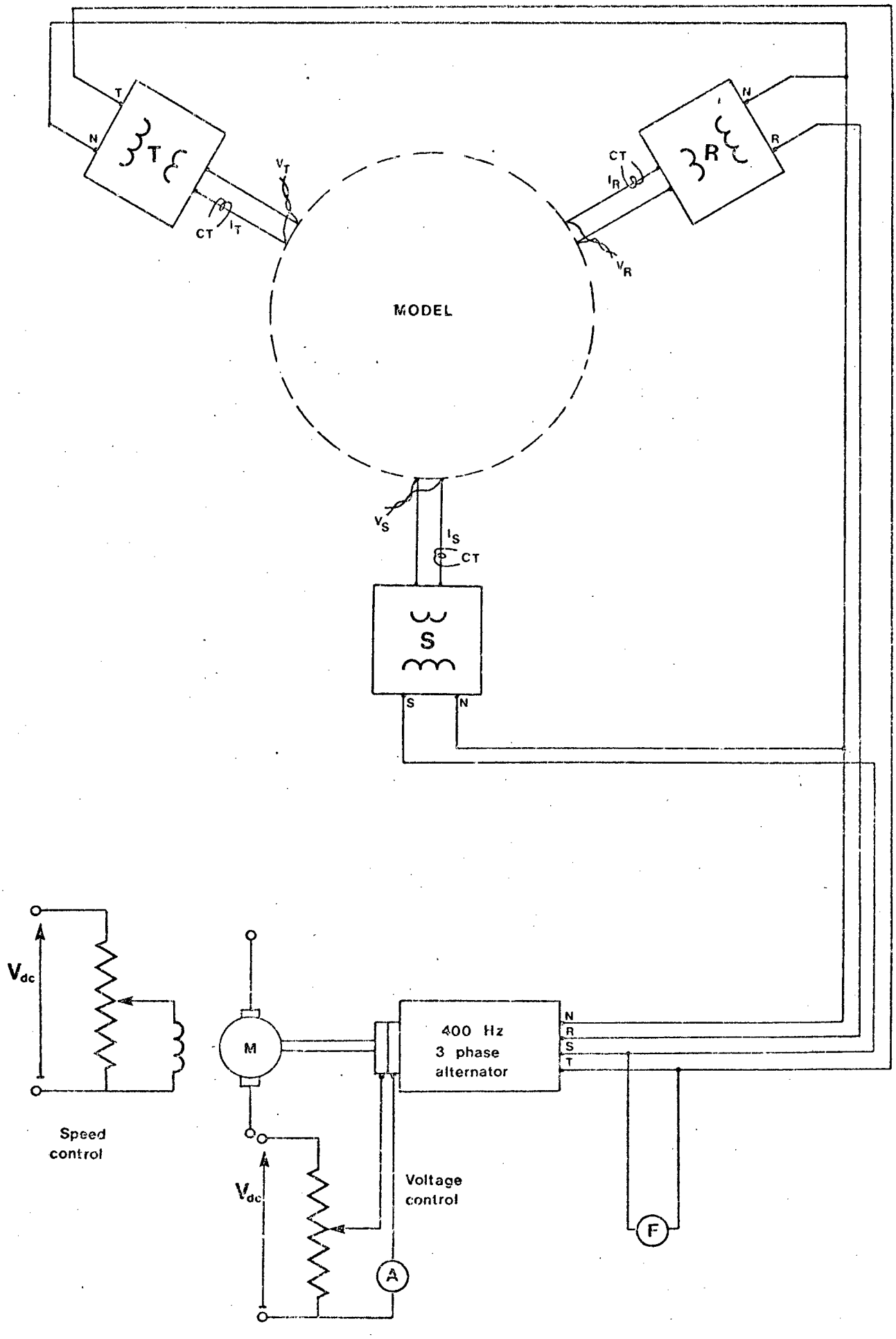

FIGURE 6.2 : POWER SYSTEM FOR MODELS

using a potentiometer. The high frequency of 380 Hz was used to increase the reactive effects in the circuit over a normal 50 Hz supply.

6.3 Model Construction

The first model constructed consisted of three separate coils constructed from aluminium strip and arranged in a triangle as shown in Figure 6.3. This was then modified to the arrangement shown in Figure 6.4, where the downward connection of each coil was combined with the downward connection of the adjacent coil to form an 'equivalent electrode' with a star connected load. Finally a scaled-down model of an actual furnace was constructed with circular electrodes bolted onto a baseplate and aluminium busbars as shown in Figure 6.5. The electrode structure was placed in a shell consisting of a circular bath constructed from steel sheeting to simulate the furnace bath.

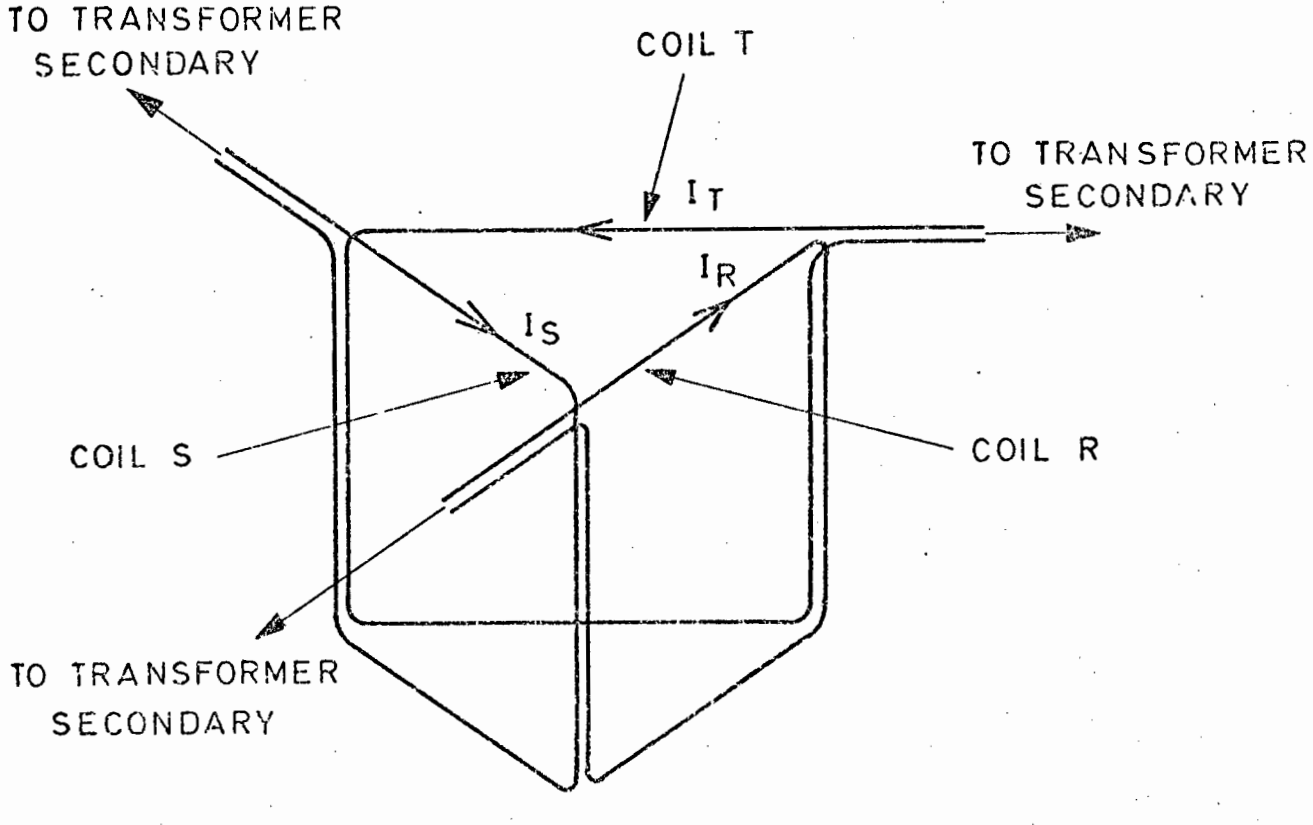

FIGURE 6.3 : CONSTRUCTION OF FIRST MODEL

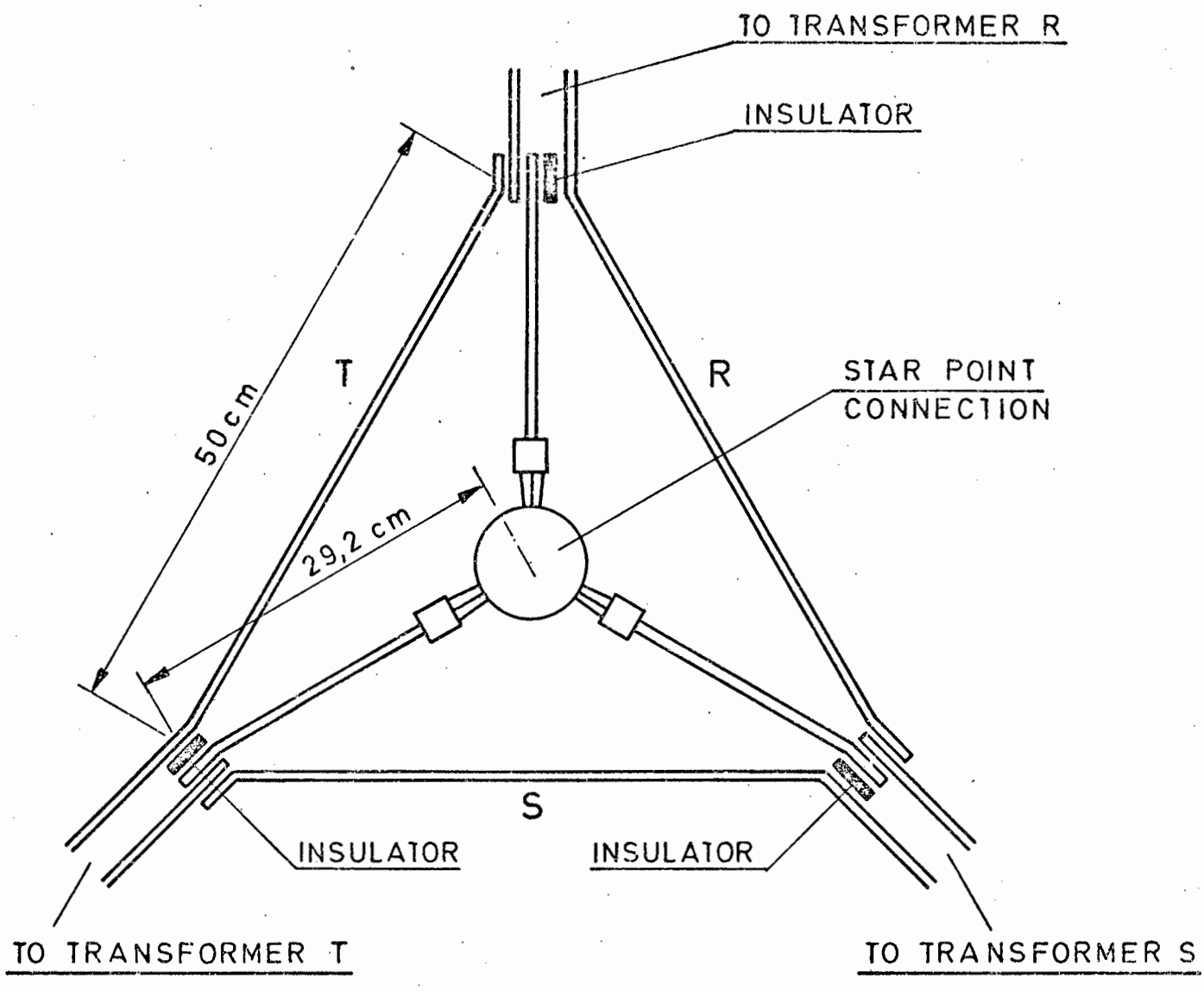

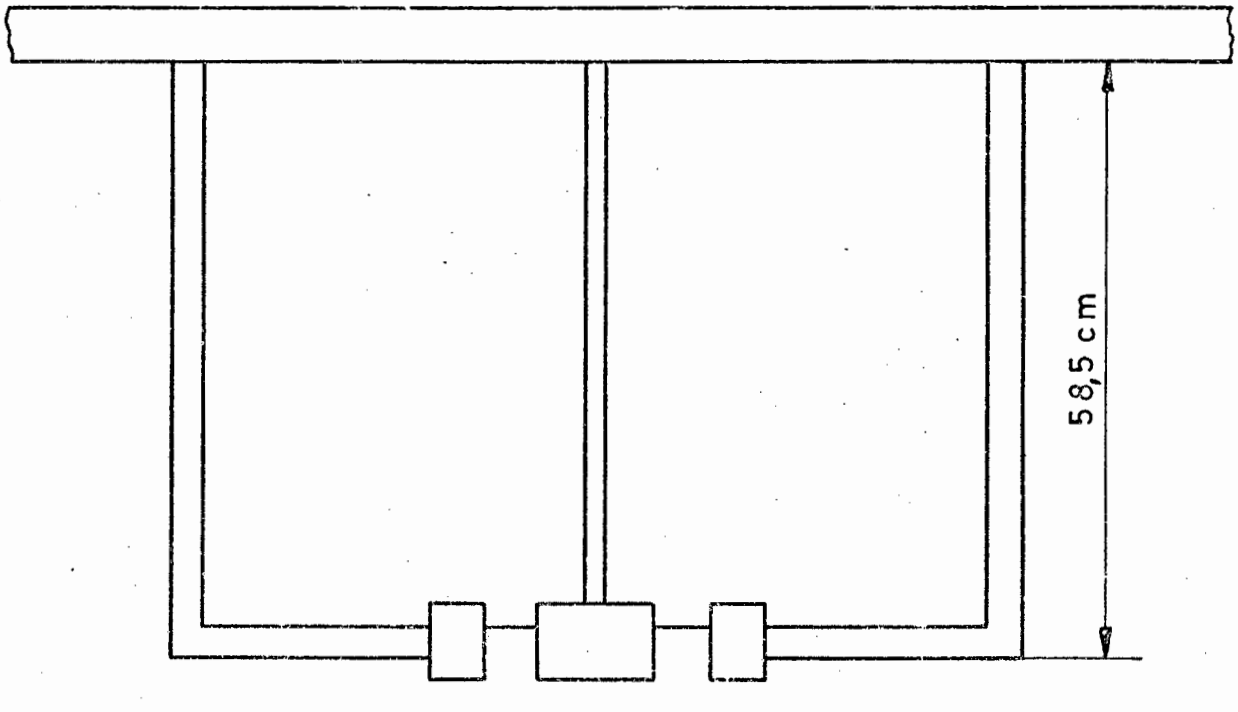

FIGURE 6.4 : CONSTRUCTION OF SECOND MODEL.

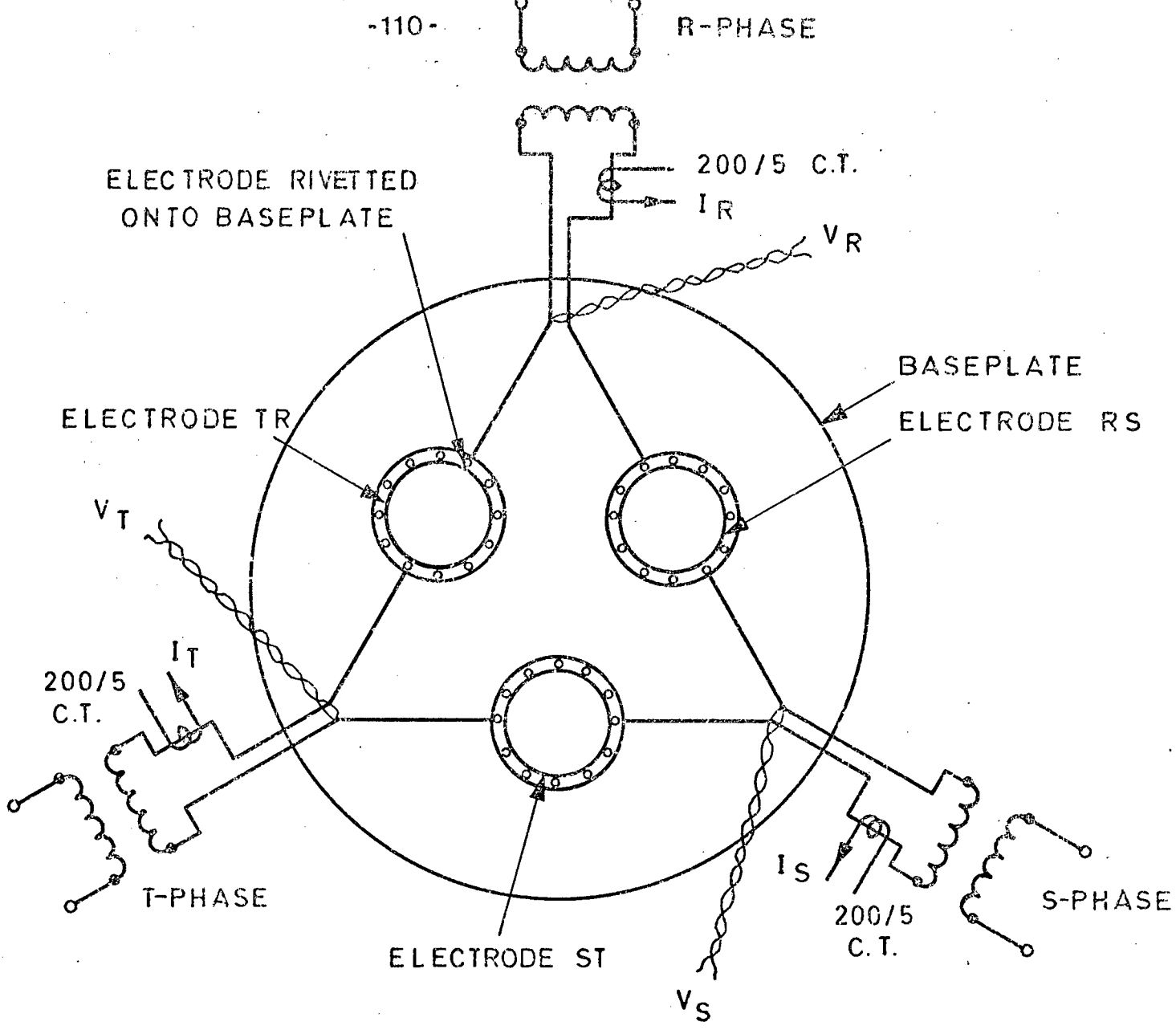

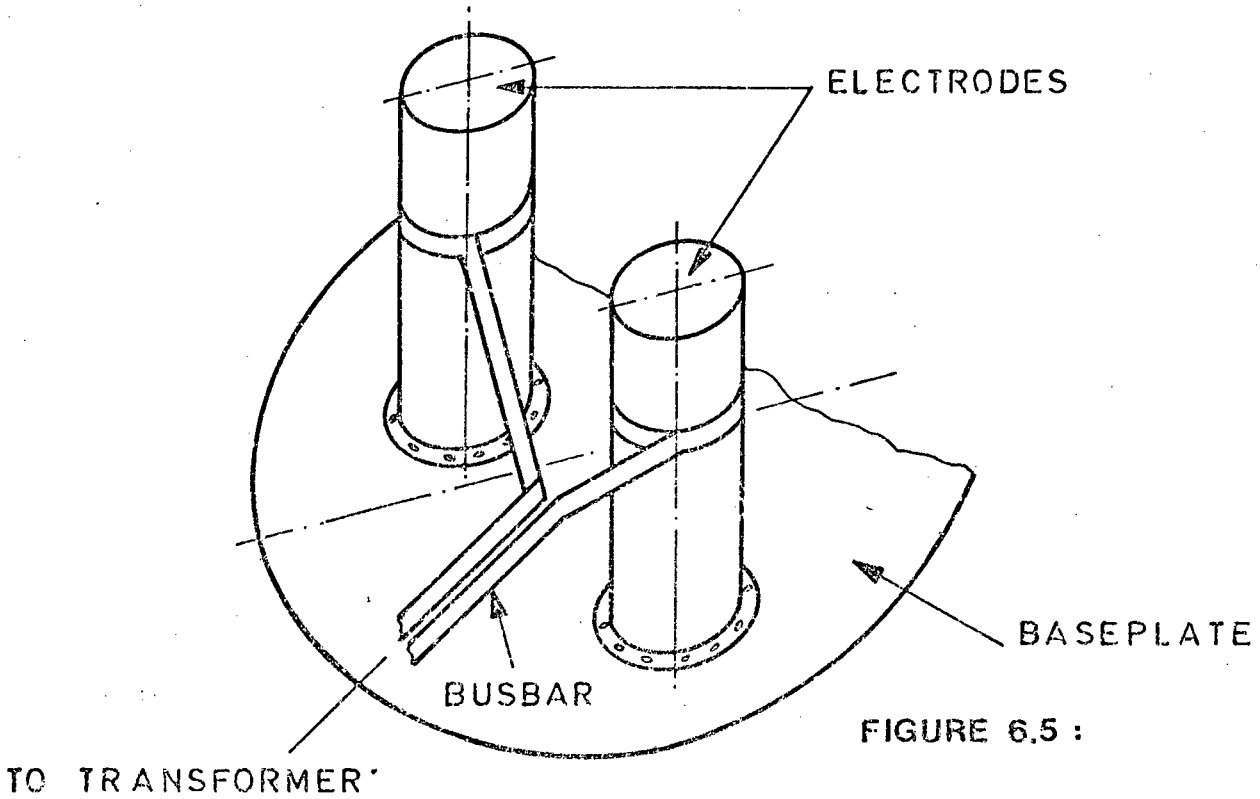

FIGURE 6.5 :

CONSTRUCTION OF THIRD MODEL

Each model was connected to the power system as shown in Figure 6.2. Current transformers in each transformer secondary current loop provided delta current measurements and voltage connections were made at each secondary opening point in the Knapsack connection with a twisted lead. This ensured that the measurements of the voltages were free from error due to current induced voltages.

The self and mutual inductances for each loop were measured by applying a single phase load to each loop in turn and measuring the induced voltages in the other two (open circuited) loops, together with the voltage and current in the loop being loaded. Difficulty was experienced in obtaining a balanced load as a result of the transformers being virtually short circuited. Therefore, the circuit was particularly sensitive to the short circuit impedances of each transformer. This was solved by adding inductors in the primary of two of the transformers so that the short circuit characteristics for each transformer were matched.

6.4 Measuring System

An a.c. measuring bridge, connected as shown in Figure 6.6, was used to measure the reactances and resistances for each phase. This is a null balance technique where the secondary voltage for each phase is balanced against the summation of two slide wire voltages, one of which is in phase with the secondary current and the other is in quadrature with the secondary current. At the balance point, one slide wire will directly indicate resistance units while the other slide wire (quadrature component) indicates reactance units. A detector, used for determining the balance point, is tuned to the system fundamental frequency so that harmonics are ignored. In the measuring arrangement used, a voltage which was in-phase with the current was generated by connecting the current transformer secondary to a resistive burden. The voltage across this resistance was connected to a resistor and slide wire to give the in-phase component voltage. The quadrature component was generated by transforming the voltage from the current transformer to a higher voltage which was

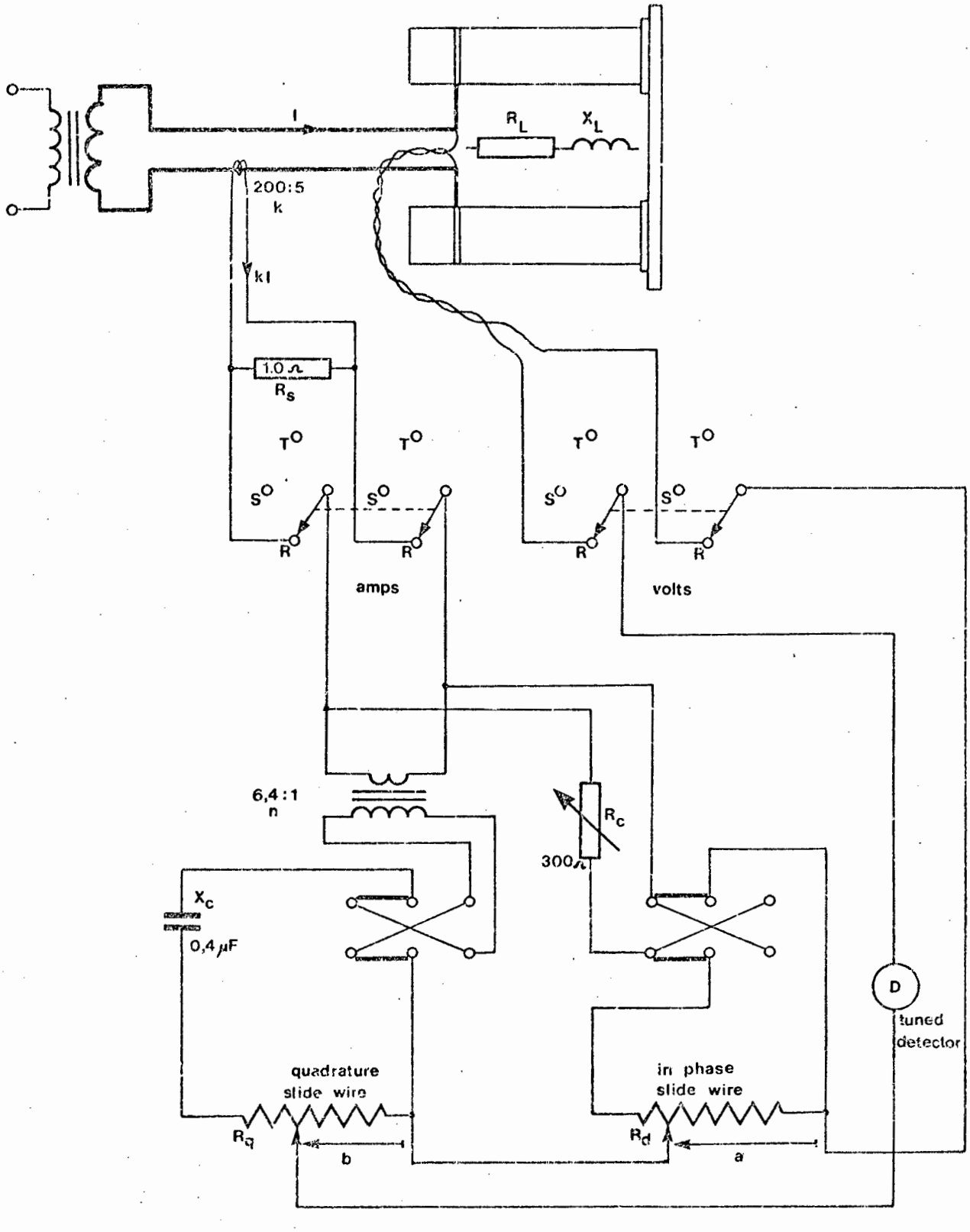

FIGURE 6.6 : MEASURING SYSTEM FOR MODELS

then connected to a large capacitive reactance in series with a slide wire to give a 90^{o} phase shift. Change over switches in each circuit allowed full four quadrant operation. At balance the circuit resistances and reactances are given by the following equations:

$$R_L = k \frac{R_s . R_d}{R_d + R_c} . a \qquad (6.4)$$

$$X_L = n\, k \frac{R_s . R_q}{X_c} . b \qquad (6.5)$$

where K = current transformer ratio (40)

R_s = current transformer burden resistance (1Ω)

$R_d = R_q$ = resistance of slide wires (29Ω)

R_c = in-phase resistor (300Ω)

X_c = capacitive reactance (C = 0,4 μF)

n = quadrature component transformer ratio (6,4)

6.5 Results using First Model

The construction of the first model is shown in Figure 6.3 with each transformer secondary connected to a separate coil, with the three coils forming a triangle. The measurements involved setting up a balanced load of approximately 80 amps in each phase and then passing current through each phase (loop) in turn, while the other two phases were open circuited. The following measurements were taken:

(i) Measurement of resistance and reactance for each phase with all three coils carrying full current (RR - SS - TT);

(ii) Measurement of coil resistance and self and mutual reactances for all three coils with each coil being energised in turn, with the other two coils open circuited,

(RR-SR-TR), (SS-TS-RS), (TT-RT-ST);

(iii) Coil R was modified as shown in Figure 6.7 to show the effect of reducing loop length and the whole sequence of measurements was repeated.

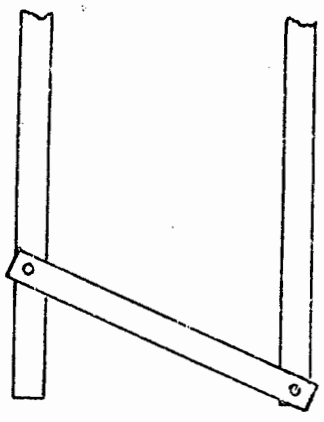

FIGURE 6.7 :
MODIFICATIONS TO COIL R

The results of these measurements are summarised in Table 6.1.

With balanced three-phase currents and symmetrical connection, the three currents in equation 6.3 can be rewritten as:

$$\begin{aligned} I_R &= I \\ I_S &= (-0{,}5 - j\ 0{,}866)\ I. \\ I_T &= (-0{,}5 + j\ 0{,}866)\ I. \end{aligned} \qquad (6.6)$$

and $$X_{SR} = X_{TR} \qquad (6.7)$$

so that the first equation in 3.3 becomes

$$V_R = I[R_R + jX_{RR} + j\ (\ -0{,}5-j\ 0{,}866)X_{RS} + j(-0{,}5+j\ 0{,}866)\ X_{TR}] \qquad (6.8)$$

$$= I[R_R + j\ (X_{RR} - X_{RS})] \qquad (6.9)$$

From Table 4.1

$$\begin{aligned} R_R &= 351 \\ X_{RR} &= 690 \\ X_{RS} &= 136 \end{aligned} \qquad (6.10)$$

		RR	SS	TT	RR	SR	TR	SS	TS	RS	TT	RT	ST
Symmetrical coil arrangement	RL	299	418	455	351	000	000	415	000	000	480* 603	000	000
	XL	825	818	806	690	-125	-114	687	-110	-136	686	-132	-136
Coil R connected unsymmetrically	RL	201	474	411	306	000	000	396	000	000	441	000	000
	XL	711	802	798	603	-93	-122	686	-126	-100	688	-118	-136
		Coils R,S,T carrying current			Coils S & T open			Coils T & R open			Coils R & S open		

* Change in resistance as a result of tightening the joints

$kI_a = kI_b = kI_c$ = 2 amps f = 380 Hz

TABLE 6.1 : MEASUREMENT ON FIRST MODEL

which gives

$$V_R = I(351 + j\ 826) \qquad (6.11)$$

with balanced three-phase load the measurements were:

$$\begin{aligned} R_R &= 295 \\ X_{RR} &= 825 \end{aligned} \qquad (6.12)$$

which yields

$$V_R = I(295 + j\ 825) \qquad (6.13)$$

There was a large variation in the resistances in the model as a result of oxidation of the aluminium joints. This explains the differences in the resistances. However, the reactances agree closely and it can be concluded that the delta reactance for each phase, measured with all three coils carrying equal currents and the coils arranged symmetrically, is equal to the sum of the mutual and self-inductances of one of the coils considered alone. This result is independent of the magnitude of the currents.

The agreement between the mutual inductances (which should all be equal for the symmetrical connection) is not close due to the disturbance of the configuration by the open circuiting of the coils in each instance. This resulted in the alteration of their relative positions.

$$\left.\begin{aligned} RS &= -136 \\ SR &= -125 \\ ST &= -136 \\ TS &= -110 \\ RT &= -132 \\ TR &= -114 \end{aligned}\right\} = 125 \qquad \left.\begin{aligned} RR &= 690 \\ SS &= 687 \\ TT &= 686 \end{aligned}\right\} = 687$$

The mutual magnetic coupling between the coils is expressed as the ratio between the mutual and self inductances, so that:

$$\text{mutual coupling} = \frac{125}{687} = 18\%$$

This coupling is relatively low owing to the coil sides being adjacent but independent to one another with a spacing of one conductor diameter.

With the assymmetrical arrangement of coil RR the major changes in self and mutual inductances relate to the coil RR, viz.:

X_{RR} 690 → 603 = 87

X_{RS} -136 → -100 = -36

X_{SR} -125 → -93 = -32

compared to

X_{SS} 687 → 686 = 1

X_{ST} -136 → -136 = 0

X_{TS} -110 → -126 = -16

These results show a relationship between the loop length of a coil and the associated self and mutual inductances. However, they are not conclusive owing to the variation in the results.

6.6 Results using the Second Model

In the first model the variability in the self and mutual inductances was attributed to the loose mechanical connection of the coils. This was rectified in the second model shown in Figure 6.4 where single conductors were used as common connections for the downward sections of the coils, and these were connected together to form a star connection.

Once again measurements were taken with balanced currents and a symmetrical configuration and then repeated with an asymmetrical arrangement. The results are summarised in Table 6.2. The asymmetrical arrangement was obtained by shortening the downward conductor common to coils T and R by 11 cms.

		RR	SS	TT	RR	SR	TR	SS	TS	RS	TT	RT	ST
Symmetrical coil arrangement	RL	368	492* 495	374	291	-85	-73	302	-97	-79	277	-68	-82
	XL	984	969* 970	955	689	-279	-278	688	-276	-277	688	-277	-279
Coil R connected unsymetrically	RL	579	516	459	387	-85	-116	305	-89	-70	372	-147	-77
	XL	972	971	875	657	-278	-245	688	-277	-279	656	-246	-279
		kI_R=1,92 kI_S=2,04 kI_T=2,00			kI_R=1,92 kI_S=kI_T=Ø			kI_R=Ø kI_S=2,04 kI_T=Ø			kI_R=kI_S=Ø kI_T = 2,00		
		Coils R,S & T energised			Coils S & T open			Coils T & R open			Coils R & S open		

f = 384 Hz

* Joints tightened

TABLE 6.2 : MEASUREMENT ON SECOND MODEL

The self and mutual inductances in Table 6.2 are far more consistent than in the first model. This is a result of the more rigid interconnection of the coils and is reflected in the increase in the mutual coupling between the coils which is given by:

$$\text{mutual coupling} = \frac{278}{689} = 40 \text{ per cent}$$

The self and mutual inductances for each coil are:

Coil RR = 689 + 278 = 967 (compare with 984)

Coil SS = 688 + 277 = 965 (compare with 969)

Coil TT = 688 + 278 = 966 (compare with 955)

The differences for coils RR and TT can be attributed to the low current in coil RR. With the asymmetrical connection, the change in dimension for coils RR and TT effects the self-inductances of RR and TT and the mutual inductances between these two coils.

X_{RR} 689 → 657 = 32

X_{TT} 688 → 656 = 32

X_{RT} -277 → -246 = -31

X_{TR} -278 → -245 = -33

as compared to

X_{SS} 688 → 688 = Ø

X_{TS} -276 → -277 = -1

X_{RS} -278 → -278 = Ø

Considering the path lengths for the self and mutual inductances, the self inductance loop length is given by:

$$\text{loop length} = 50 + (2 \times 58{,}5) + 29{,}2 + 29{,}2$$

$$= 225{,}4 \text{ cms}$$

With a self inductance of 688 units this corresponds to

$$\frac{688}{225{,}4} = 3{,}5 \text{ units/cm}$$

The common path length for the mutual inductances is given by mutual path length

$$= 58,5 + 29,2$$

$$= 87,7 \text{ cms}$$

With a mutual inductance of 278 units this corresponds to

$$\frac{278}{87,7} = 3,17 \text{ units/cm}$$

In the asymmetrical arrangement the path lengths for the self and mutual effects was reduced by 11 cms. If a linear relationship between inductance and length is assumed the corresponding predicted reductions in self and mutual inductances would be

self inductance = 3,05 x 11

= 33,5 units (compare with 32 units)

mutual inductance = 3,17 x 11

= 34,9 units (compare with 33 units).

From this it can be deduced that:

(i) the self inductances are linearly related to the circumference of the associated coils,

(ii) the mutual inductances are linearly related to the length which is common to the two mutually interacting coils.

6.7 Results using the Third Model

In the second model a linear relationship between the self and mutual inductances and the associated path lengths was established. However, this was for a model where the equivalent electrode diameter was 3 cms with a separation of 50 cms. On actual furnaces the electrode diameter is proportionately much larger and so the third model shown in Figure 6.5 was constructed as a direct scale down from an actual furnace. The electrodes were constructed from

aluminium sheeting curved to make circular pipes which were bolted to an aluminium baseplate. A clamping arrangement on the electrodes made it possible to progressively shorten the electrodes and measure the resulting changes in the self and mutual inductances.

These results are summarised in Table 6.3 and the associated changes in self and mutual inductances with electrode lengths are shown plotted in Figure 6.8. The readings taken with all three phases energised simultaneously, do not correlate as well as in the previous tests owing to the asymmetrical resistance configuration (particularly the baseplate) and the asymmetry of the three currents. The self inductance decreased from 689 to 331 and the mutual coupling was reduced from 40 to 15 per cent, as a result of the increase in electrode diameter and the configuration of the baseplate which allowed a spread-out current path. The variation of self inductance with electrode length is linear over the measured range, while the corresponding mutual inductance vatiation, though non-linear, is much more sensitive to the common path shared within an electrode and is therefore more sensitive to changes in electrode length.

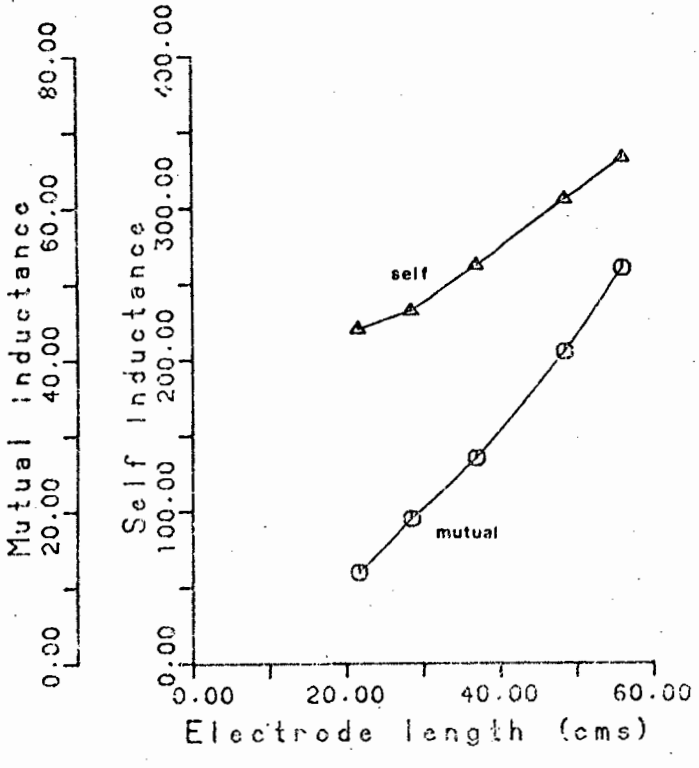

FIGURE 6.8 :

PLOT OF SELF AND MUTUAL INDUCTANCE AGAINST ELECTRODE LENGTH

	RR	SS	TT	RR	SR	TR	SS	TS	RS	TT	RT	ST	Electrode height
RL	1090	1034* 1058	829	905	-040	-086	1040	-549	-127	986	-149	-584	56 cms
XL	357	313* 308	464	331	-052	-053	333	-057	-051	332	-047	-059	
			RL	402	-029	-063							48,5 cms
			XL	305	-041	-042							
			RL	275	-005	000							37 cms
			XL	262	-027	-027							
			RL	342	-008	000							28,5 cms
			XL	232	-019	-019							
			RL	286* 617	-049	-024	330	000	-015				21,6 cms
			XL	223* 227	-013	-012	220	-012	-012				

f = 380 Hz kI_R = 1,98A; kI_S = 2,04; kI_T = 1,97A

* Joints tightened

TABLE 6.3 : MEASUREMENT ON THIRD MODEL

If these results are related to a large furnace with an electrode diameter of 1,7 metres and the same proportions as in the model are used, this would correspond to an electrode separation of 3,75 metres and the electrode length of 56 cms would correspond to 4,0 metre electrodes. Consider the reduction in star reactance for a one metre reduction in the lengths of the electrodes. This corresponds to an electrode length of 42 cms on the model. If a balanced load is assumed, the delta reactances, which at an electrode length of 42 cms corresponds to 280 + 033 = 313 units and at 56 cms corresponds to 331 + 053 = 384 units. With a balanced circuit the star reactances will be $\frac{1}{3}$ of the delta reactances (star-delta transformation) which corresponds to a reduction from 128 units to 104 units, i.e. 19 per cent for a 25 per cent reduction in electrode length. On the actual furnace which was used for scaling the model it has been established that the variation in reactance per metre of electrode is approximately 0,13 mΩ/m with a four-metre electrode and a star reactance of 1,2 mΩ. This corresponds to a 13,5 per cent reduction in the reactance for a 25 per cent reduction in the electrode length. These are approximate figures, but do serve to illustrate that the results from the model can be related to an actual furnace.

6.8 Conclusions

The model experiments serve to illustrate that the lengths of the electrodes in a furnace are related to the star reactances for each electrode. In particular, the mutual reactances associated with the furnace, were it made up of three coils arranged in a triangle, are particularly sensitive to electrode lengths. Unfortunately the direct measurement of self and mutual reactances on an actual furnace would be very impractical. However, if accurate measurements of the electrode-to-bath voltages are available, the associated reactances derived from these measurements (together with electrode currents) should yield values which can be related to electrode length. Variations in the height of the molten bath and in the length of the arcs under each electrode would affect the reactances. However, it should be possible to compensate for this.

On the other hand in the absence of accurate electrode-to-bath voltage measurements the star reactances could be assumed to be linearly related to the electrode lengths. This would yield a derivation of the powers under each electrode (reactance assumptions).

7. ELECTRICAL MEASUREMENTS ON A 48 MVA FERROCHROME FURNACE

A study of the measurement of the electrical variables of a 48 MVA closed-top submerged arc furnace producing high-carbon ferrochromium, has been carried out over a period of 5 years starting in 1974. At the beginning of the investigation the electrical measurement leads on the furnace were connected in the standard arrangement described in Section 4.1.1. The voltage measurement leads were connected to the furnace transformer secondary terminals and a neutral was provided by a copper electrode imbedded in the lining, at the side of the furnace, away from the tapholes. It was found that phase power and resistance measurements based on this connection arrangement were distorted and control of the power distribution had to be based on current control.

In April 1977 the furnace was switched off for a rebuild and this provided an opportunity to install neutrals into the furnace lining. A neutral connection was made to the carbon blocks under each electrode and also in the centre of the furnace as described in Appendix B. The measurement of electrode-to-bath voltages was achieved by connecting measurement leads to each electrode and to the neutrals under each electrode. The aim was to generate a small measuring loop so as to minimize induced voltages in the measurement leads. This arrangement provided an accurate direct measurement of the electrical circuit which provided reliable measurements of the resistances and reactances of the star equivalent circuit. These measurements have been used successfully in analysing various aspects of the operation of the furnace. After approximately six months of operation, the neutral connection under electrode 1 was lost and the connections were rearranged so that all measurements of line to neutral voltages were made with respect to the central neutral point.

7.1 Measuring Equipment

The furnace is equipped with a minicomputer-based data acquisition [67] system which provides a means for continuously monitoring all the measurements available from the furnace, including those from the electrical circuit. A summary of the variables measured or derived, which are relevant to this investiga-

tion, are shown in Tables 7.1 and 7.2. The measurements on the primary side of the furnace transformers, and also the secondary measurements using the standard voltage connection arrangement, were made with rectify and average electrical transducers. A special system was developed later for the measurement of the secondary electrical variables once the neutrals had been installed. This included rms measurements and fundamental frequency (50 Hz) measurements of real powers, currents and phase voltages, and harmonic measurements of the voltages and currents. The arcing measurements included arc factors, which were derived from the ratios between the harmonic voltages, and phase voltages. The measurement system is described in detail in Appendices I and J.

All signals from the furnace are sampled every 6 seconds by the computer, which also performs the calculation of the derived variables and the averaging of all the variables to give two minute, shift (8-hourly) and daily averages. The data are presented in two minute, shift and daily reports. The computer also has the facility for the selection of up to 62 of the variables and the storage of the two-minute averages of these variables on a magnetic disc for up to one week. Every week the data file containing these variables is copied onto magnetic tape and stored away so that the operating history of the furnace over a number of years is available for subsequent analysis. This has proved to be a very useful tool, as models developed to describe various conditions in the furnace can be 'played back' on historical data to test their validity. It has also provided a means for comparing the various electrical measurement systems over a period of time.

7.2 Accuracy of Measuring System

It is not possible to quantitatively establish the absolute accuracy of the developed measuring system since there is no proven accurate measurement available for comparison. The theoretical analysis of the voltage measurement errors given in Section 4.1 showed that the errors are likely to be comparatively small. Also, the voltage measurement leads for each phase form loops which are perpendicular to the electrode currents, so that the induced

VARIABLE NAME	UNITS	SYMBOL	TRANSDUCER OR DERIVATION EQUATION
Primary real power	MW	P	Camille Bauer
Primary reactive power	MVAr	Q	"
Primary voltage R	kV	V_R	"
" " S	kV	V_S	"
" " T	kV	V_T	"
Primary currents 1	Amps	I_1'	"
" " 2	Amps	I_2'	"
" " 3	Amps	I_3'	"
Transformer tap position	-	k	Acromag
Derived secondary current 1	kA	I_1	$f(k)*I_1'$
" " " 2	kA	I_2	$f(k)*I_2'$
" " " 3	kA	I_3	$f(k)*I_3'$
Furnace resistance	mΩ	R	$P*1000/(I_1^2+I_2^2+I_3^2)$
Furnace reactance	mΩ	X	$Q*1000/(I_1^2+I_2^2+I_3^2)$
Electrode hoist position 1	m	h_1	Acromag
2	m	h_2	"
3	m	h_3	"
Secondary real power 1	MW	P_1	Camille Bauer
2	MW	P_2	"
3	MW	P3	"
Electrode current 1	kA	I_1	Camille Bauer
2	kA	I_2	"
3	kA	I_3	"
Electrode-to-bath voltage 1	Vlts	V_{1N}	"
2	Vlts	V_{2N}	"
3	Vlts	V_{3N}	"
Phase resistance 1	mΩ	R_1	P_1*1000/I_1^2
2	mΩ	R_2	P_2*1000/I_2^2
3	mΩ	R_3	P_3*1000/I_3^2
Phase reactance 1	mΩ	X_1	$SQRT[(V1N/I_1)^2-R_1^2]$
2	mΩ	X_2	$SQRT[(V_{2N}/I_2)^2-R_2^2]$
3	mΩ	X_3	$SQRT[(V_{3N}/I_3)^2-R_3^2]$

TABLE 7.1 : Summary of electrical variables

VARIABLE NAME	UNITS	SYMBOL	TRANSDUCER OR DERIVATION EQUATION
Real power 1 (rms & 50Hz)	MW	P_1	New measuring system
" " 2 "	MW	P_2	
" " 3 "	MW	P_3	
Electrode current 1 (rms & 50Hz)	kA	I_1	
2	kA	I_2	
3	kA	I_3	
Electrode-to-bath voltage 1 (rms & 50Hz)	Volts	V_{1N}	
2	Volts	V_{2N}	
3	Volts	V_{3N}	
Phase resistance 1 (rms & 50Hz)	mΩ	R_1	P_1*1000/I_1^2
2	mΩ	R_2	P_2*1000/I_2^2
3	mΩ	R_3	P_3*1000/I_3^2
Phase reactance 1 (rms & 50Hz)	mΩ	X_1	$SQRT\ [(V_{1N}/I_1)^2-R_1^2]$
2	mΩ	X_2	$SQRT[(V_{2N}/I_2)^2-R_2^2]$
3	mΩ	X_3	$SQRT[(V_{3N}/I_3)^2-R_3^2]$
Harmonic voltage 1	-	AV_1	New measuring system
2	-	AV_2	
3	-	AV_3	
Harmonic current 1	-	AI_1	
2	-	AI_2	
3	-	AI_3	
Arc factor 1	-	AF_1	AV_1/V_{1N}
2	-	AF_2	AV_2/V_{2N}
3	-	AF_3	AV_3/V_{3N}

TABLE 7.2 : Summary of secondary electrical measurements added after furnace rebuild

voltage errors in each phase will be largely determined by the electrode currents in that phase. The induced voltages will, therefore, be 90^{o} out of phase with the electrode currents so that any errors will be 'reactance errors' and the resistance and real-power measurements will be accurate.

Some furnace operating characteristics can be used to qualitatively establish the validity of the measurement system. One of these is the measurement of the relative amounts of raw materials consumed under each electrode. The developed system has shown a good correlation between power in a phase and raw material throughput for that phase, whereas the old system sometimes indicated widely conflicting relationships between the phase powers and the throughput of raw materials. Another factor which can be considered is the accuracy of the modelling of the electrode erosion using phase power measurements. This method for predicting electrode length was not used for the old system owing to its unreliability, yet with the new system a good erosion model has been developed which is based on real-power measurements with corrections being made for variations in the arcing conditions[54]. This model does, however, still suffer from the disadvantage that electrode tip breaks and variations in the quality of the electrode paste cannot be accounted for.

7.3 Comparisons between Measuring Arrangements

Since the installation of the neutrals under the furnace various situations have occurred in the operation which have enabled comparisons to be made between different measurement arrangements. The standard measurement system, used prior to the rebuild of the furnace, has been simulated by the use of the neutral connection in the centre of the furnace and the transformer secondary voltage connections. This is not a true representation of the standard measurement system, since, in the original arrangement, a bath connection was provided by a copper electrode which was imbedded in the side of the furnace lining. Therefore, the standard arrangement is more asymmetrical than the simulated connection where a centrally placed neutral was used. The comparison between the standard system and the new system was carried out after

the loss of the neutral connection under electrode 1 and the central neutral was used for all measurements. This resulted in a situation where the measurements from the standard arrangement were more accurate than was expected. However, when the new leads were removed from the central neutral connection, the accuracy of the measurement for the standard arrangement was reduced substantially. This could only have been a result of some interaction between the two measurement arrangements. However, it is difficult to deduce how this could occur. Other measurement systems which will be compared are the equal reactance assumption and a floating neutral measurement. The floating neutral connection was achieved by the removal of the lead to the central neutral.

For simplicity the various arrangements which are compared will be denoted as follows:

SYSTEM A: Standard measurement arrangement (with new system leads also connected to central neutral)

SYSTEM B: Equal reactance assumption

SYSTEM C: New measurement arrangement (using central neutral)

SYSTEM D: Standard measurement arrangement (new system leads removed)

SYSTEM E: Standard measurement with floating neutral connection (no connection to furnace bath)

These arrangements have been compared by taking spot readings (2-minute averages) which represent various typical conditions occurring during the operation of the furnace. The normal condition in the furnace is a balanced state with the currents in each electrode set at 100 kA, with moderate arcing conditions and the electrode lengths set so that the electrode hoist positions are not close to their upper or lower limits. This state can be disturbed if an electrode becomes short, as a result of a tip break or incorrect slipping, and the electrode cannot be lowered far enough into the furnace as a result of the limits of travel of the hoist position. The electrode then runs on 'bottom stops' with reduced current as a result of higher arcing and resistance

conditions under it. This affects the other two phases and the furnace power distribution becomes unbalanced. Another factor which affects the electrical operation is the tendency of the metal to freeze in regions away from the electrodes. This causes the formation of separate molten baths under each electrode, which can change in height independently from the other electrode baths, resulting in changes in the current flow paths. These baths also increase the live and dead phase effect, since the back two electrode baths (electrodes 2 and 3) drain into the bath next to the tapholes (electrode 1). Therefore they are situated higher up in the furnace thus effectively increasing the current path and hence reactance for phase 1.

Some results from the various measurement arrangements are summarised in Tables 7.3 and 7.4. In each case the real powers and reactances from each system are compared, and the common measurements of currents, harmonic voltages and hoist positions are included on the right hand side of the table. In Table 7.3 the measurements available with the new system are given for various days in March 1979. In each case the power measurements from systems A and B are compared with those of system C (the new measurement system) on a percentage basis. The results in Table 7.4 are from a period when the new system leads were burnt away after a furnace eruption and only transformer secondary voltage measurements were available. As discussed earlier, System D is a better representation of the standard system than system A, since there seems to have been some interaction between the systems. In the absence of the new system the equal reactance assumption measurement results have been used for comparison.

7.3.1 Equal reactance assumption

The relationship between the equal reactance assumption and the new system measurements can be shown by comparing systems B and C in Table 7.3, where five sets of readings, representing various typical furnace conditions, are given. The first measurement on the 17th March represents a typical balanced furnace with moderate arcing conditions and intermediate hoist

NUMBER DATE & TIME	MEAS. TYPE	REAL POWERS (MW)				RELATIVE POWERS (%)			REACTANCES (mΩ)						
		1	2	3	TOTAL	1	2	3	1	2	3		1	2	3
1 17/3 10:44	A	11,25	9,44	11,48	37,17	103,9	93,5	102,1	0,95	0,87	0,75	CURRENT (kA)	100,4	100,0	99,9
	B	12,34 (12,34)	12,32 (11,74)	12,43 (13,01)	37,09	98,8 (98,9)	105,8 (100,8)	95,9 (100,4)	1,04 (1,108)	1,04 (1,007)	1,04 (1,007)	HARMONIC VOLTAGE	21,5	62,6	52,9
	C	12,23	11,41	12,7	36,34	100,0	100,0	100,0	0,62	0,56	0,53	HOIST POSITION (m)	0,46	0,32	0,12
2 13/3 10:1	A	10,39	12,25	9,33	31,97	101,9	98,1	100,4	0,83	0,88	0,79	CURRENT (kA)	89,1	98,7	102,8
	B	11,31	14,21	10,95	36,47	97,3	99,8	103,3	1,01	1,01	1,01	HARMONIC VOLTAGE	68,4	79,7	28,0
	C	11,42	13,99	10,41	35,82	100,0	100,0	100,0	0,56	0,53	0,57	HOIST POSITION (m)	0,0	0,02	0,29
3 18/3 1:0	A	12,82	6,68	11,52	31,02	106,0	89,4	100,6	0,94	0,81	0,75	CURRENT (kA)	101,3	85,2	63,7
	B	12,91	8,80	12,24	33,95	97,5	107,5	97,7	1,06	1,06	1,06	HARMONIC VOLTAGE	70,4	86,6	34,0
	C	13,03	8,05	12,33	33,41	100,0	100,0	100,0	0,63	0,61	0,53	HOIST POSITION (m)	0,69	0,37	0,0
4 19/3 9:28	A	14,04	7,59	9,12	30,75	106,8	90,7	98,7	0,59	1,18	1,01	CURRENT (kA)	104,7	88,4	66,8
	B	13,02 (13,0)	8,6 (9,21)	12,33 (11,7)	33,95	89,7 (89,7)	93,1 (99,8)	120,8 (114,8)	1,04 (0,94)	1,04 (1,13)	1,04 (1,13)	HARMONIC VOLTAGE	85,7	121,0	154,0
	C	14,25	9,07	10,02	33,34	100,0	100,0	100,0	0,31	0,96	0,68	HOIST POSITION (m)	0,39	0,53	0,0
5 27/3 6:1	A	10,53	12,58	8,26	31,37	101,9	99,9	97,8	0,96	0,80	1,19	CURRENT (kA)	79,8	104,2	86,5
	B	13,35 (12,08)	12,31 (13,38)	9,74 (9,94)	35,4	114,5 (103,6)	86,6 (94,2)	102,2 (104,2)	1,11 (1,09)	1,11 (1,0)	1,11 (1,29)	HARMONIC VOLTAGE	148,1	97,7	185,8
	C	11,45	13,95	9,36	34,76	100,0	100,0	100,0	0,54	0,47	0,99	HOIST POSITION (m)	0,0	0,38	0,2

TABLE 7.3 : Comparison of electrical measurement systems

positions. With balanced currents the 'live' and 'dead' phase effect with low power in phase 2 and high power in phase 3 can be seen from System C. The equal reactance assumption measurements (System B) indicate fairly balanced conditions in the furnace. However, if it is assumed that the reactance in phase 1 is 10 per cent higher than for the other two phases, when carrying out the reactance assumption, then the power measurements for the two systems agree very closely as is shown in brackets.

The second and third sets of readings in Table 7.3 show typical unbalanced furnace conditions where one of the electrodes is on bottom stops (0.0m) and the currents are not balanced. In both cases the arcing conditions are fairly low. The differences in power measurements between systems B and C are not particularly high except for the high phase 2 power measurement of 107.5 per cent on the 18th March. However, the assumption of a higher reactance in phase 1 would improve the agreement of the measurements. These two sets of measurements contrast with the last two sets on the 19th and 27th March, where there are large differences in the power measurements between systems B and C. These last two sets of readings are typical of conditions in the furnace when the arcing under one or more electrodes has increased dramatically. This results in large changes in the phase reactances so that the equal reactance assumption is no longer valid. The accuracy of the assumption is improved if the relative amounts of reactance in each phase are adjusted according to the harmonic voltages, as is illustrated in brackets for the last set of readings in Table 7.3. However, the application of the corrections for arcing to the 4th set of readings does not improve the agreement significantly, particularly for phase 1. This is a result of the high reactance in phase 2 despite the relatively low arcing conditions in this phase and can only be attributed to a change in the bath conditions.

7.3.2 Standard measurement system

The standard measurement system is compared with the new system in Table 7.3 where both systems use the same neutral point under the furnace. In the comparison of the real power measurements for systems A and C the differences are not excessive, even for the high arcing conditions of readings 4 and 5, except for a fairly consistent low power measurement for phase 2. This is confusing since one would expect system A to be more inaccurate than indicated by the results of Table 7.3. However, a comparison between systems D and B in Table 7.4 shows much larger differences in the power measurements. The only difference between systems A and D is that the new system leads have been removed for system D. All the measurements in Table 7.4 are for moderate arcing conditions (the absolute values of the harmonic voltages are higher than for Table 7.3 as a result of the transformer secondary voltages being higher than the electrode-to-bath voltages used for harmonic measurement in Table 7.3). This means that the equal reactance assumption readings can be assumed to be accurate. The readings in Table 7.4 give the results for various furnace conditions, from a balanced furnace to low-current conditions in each of the phases. The differences in the power measurements between system D and B are large especially for phase 1 where the errors are of the order of 20 per cent. However, the differences are fairly consistent, so that the possibility for applying correction factors to system D does exist.

7.3.3 Standard measurement system with neutral floating

The measurement of the electrical circuit with the standard system and a floating neutral is included in Table 7.4 as a simulation of the case where the neutral in the furnace has been burnt away. The comparison of systems E and B for the first 4 readings shows that the differences in power measurements are moderately high but not excessive. These measurements are for fairly balanced conditions. In the unbalanced conditions shown in the last set of readings, the power differences between systems E and B are high. However, under these conditions it is difficult to say which measurement

NUMBER DATE & TIME	MEAS. TYPE	REAL POWERS (MW)				RELATIVE POWERS (%)			REACTANCES (mΩ)						
		1	2	3	TOTAL	1	2	3	1	2	3		1	2	3
1 30/7 21:43	D	8,59	11,65	10,88	31,12	83,3	110,8	105,7	0,99	0,93	1,19	CURRENT (kA)	99,88	99,87	99,86
	E	10,38	10,1	10,43	30,91	101,3	96,7	102	1,01	1,05	1,01	HARMONIC VOLTAGE	113,9	167,2	112,4
	B	11,99	12,22	11,97	36,18	100,0	100,0	100,0	1,17	1,17	1,17	HOIST POSITION (m)	0,66	0,53	0,44
2 24/7 2:11	D	8,27	12,76	9,7	30,73	81,2	109,1	109,6	1,03	0,83	1,14	CURRENT (kA)	90,0	101,6	99,9
	E	9,58	11,19	9,78	30,55	94,6	96,2	111,2	1,03	0,92	1,0	HARMONIC VOLTAGE	92,3	105,3	52,5
	B	11,74	13,49	10,2	35,43	100,0	100,0	100,0	1,13	1,13	1,13	HOIST POSITION (m)	0,02	0,47	0,82
3 12/7 9:41	D	8,0	11,72	13,71	33,43	77,2	107,9	112,3	0,93	0,83	1,09	CURRENT (kA)	100,5	90,3	99,5
	E	11,01	10,05	12,3	33,36	106,5	92,7	100,9	0,92	1,09	0,83	HARMONIC VOLTAGE	73,7	145,9	89,6
	B	11,82	12,39	13,93	38,14	100,0	100,0	100,0	1,10	1,10	1,10	HOIST POSITION (m)	0,57	0,01	0,04
4 29/7 7:15	D	10,8	9,13	9,97	29,9	92,0	106,7	103,8	0,98	0,91	1,09	CURRENT (kA)	99,6	102	88,0
	E	11,23	9,54	8,98	29,75	96,2	112,0	93,9	0,82	1,0	1,11	HARMONIC VOLTAGE	69,8	126,9	42,8
	B	13,52	9,86	11,07	34,45	100,0	100,0	100,0	1,13	1,13	1,13	HOIST POSITION (m)	0,54	0,90	0,05
5 22/7 17:59	D	5,6	15,05	3,51	24,16	89,8	100,5	118,6	1,43	0,81	1,0	CURRENT (kA)	43,9	97,8	91,1
	E	5,0	12,68	6,19	23,87	81,1	85,8	211,8	1,8	0,59	1,15	HARMONIC VOLTAGE	66,3	95,7	36,3
	B	6,81	16,34	3,23	26,38	100,0	100,0	100,0	1,00	1,10	1,10	HOIST POSITION (m)	0,07	0,43	0,08

TABLE 7.4 : Comparison of electrical measurement systems

system is the most accurate. This last set of measurements also shows the effect of reactance on the power distribution where an imbalance in the currents results in an excessively distorted power distribution in the furnace.

7.3.4 Conclusions

It can be assumed that the new measurement system gives reliable results which are much better than those obtained from the standard arrangement, particularly for real power measurements. The equal reactance assumption measurements are also fairly reliable except under highly unbalanced arcing conditions in each phase. These are unusual conditions, but should be accounted for since it is at these times that accurate measurements of the conditions in the furnace are essential. The control of the power circuit based on a reactance assumption has distinct advantages with regard to reliability as it is not based on a neutral connection. It is suggested that the best arrangement is to use the assumed reactance method for power control, but to back this up with an accurate direct measurement system so that the abnormalities occurring in the furnace can be detected and accounted for. All new versions of the power controller will include the facility for adjusting the ratio between the assumed reactances in each phase so as to be able to adjust the controller to take into account reactance imbalances.

7.4 Comparison of Measurements with Neutrals brought away from the Furnace via two different Routes

After the furnace rebuild there was a delay in installing the conduit through the concrete floor as described in Appendix B, so that, initially, the neutral leads were taken via the most direct route to the furnace control room. Once the conduits had been installed the extra leads provided an opportunity to compare the measurement of the electrode-to-bath voltages using the two different connection routes for each electrode.

In the one case leads were taken from the neutral connections up the side of the furnace to join the leads connected to the electrodes (route N) whereas in

the other case the neutral leads were taken directly to the furnace control room (route N') as shown in Figure 7.1. A comparison between the two arrangements was made by alternatively switching each neutral connection to the measurement system. The effect of the switching on the various electrical variables for phase 3 is shown in Figure 7.2, which is taken from a chart recorder trace. The neutral connection was alternatively connected to N' and then to N while the trace was being recorded. The major changes during switching are in the electrode voltage and the reactance, with none of the other variables showing any significant change.

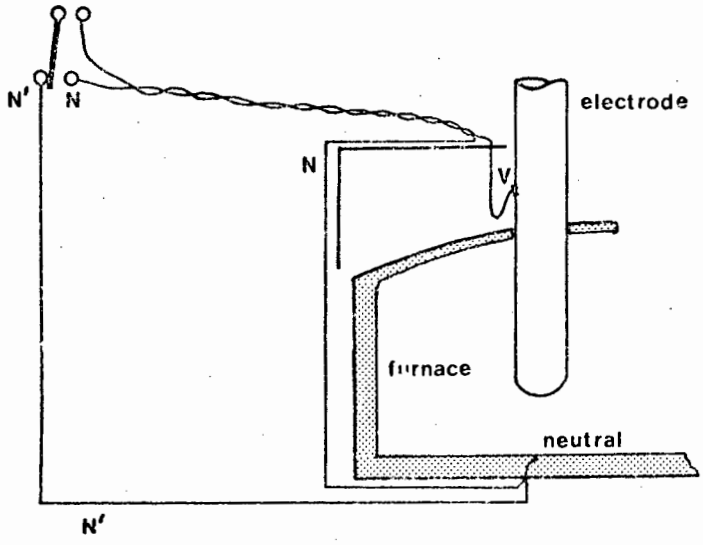

FIGURE 7.1 :

NEUTRAL SWITCHING ROUTES

This switching arrangement was automated using the computer so that at each six second scan the computer measured the electrical variables and then switched the neutral connections so that on the next six-second scan the other neutral connection electrical variables were measured. The two-minute averages of both sets of data were stored on disc for a week and analysed later. It was found that there were consistent differences between the phase resistances and reactances calculated from the two arrangements and that these differences were constant during variations in the voltage and current conditions in the furnace. The results for a week of data are shown in Table 7.5. The differences are relative to the neutral position N' so that a negative reactance difference means that the reactances measured for neutral route N are less than those for neutral route N'. In all cases the standard deviations of the differences are very low, despite fairly large changes in

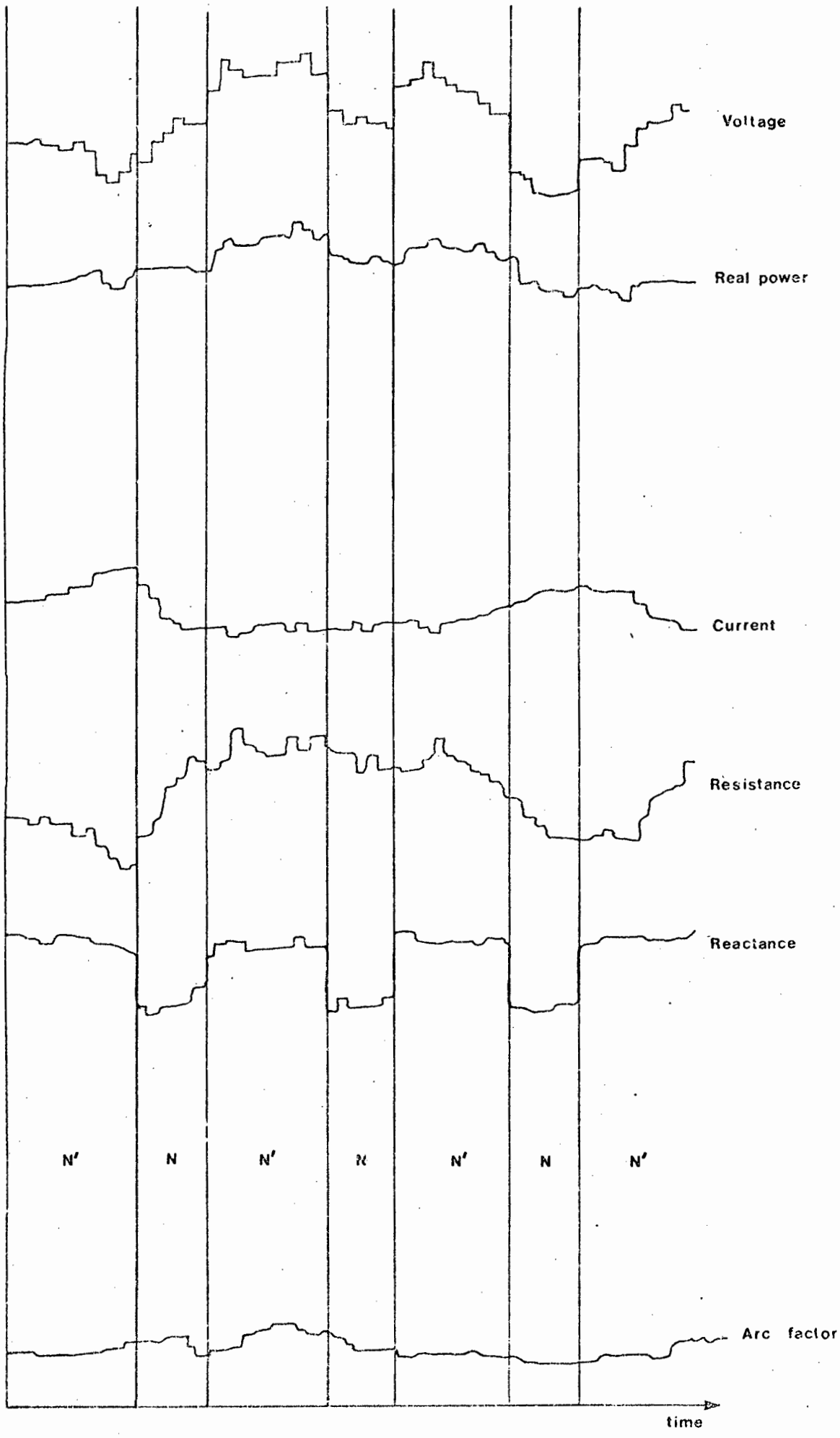

FIGURE 7.2 : CHART RECORDER TRACE OF ELECTRICAL VARIABLES DURING SWITCHING OF NEUTRALS (Phase 3)

Phase	Mean resistance mΩ	Stand.dev. of resist.	Mean resistance difference	Stand.dev. of resist. difference	Mean reactance mΩ	Stand dev. of react.	Mean reactance difference	Standard dev. of react.diff.
1	1,399	0,187	-0,065	0,002	0,662	0,035	-0,175	0,005
2	1,101	0,195	+0,034	0,008	0,854	0,061	-0,158	0,007
3	1,557	0,33	-0,043	0,003	0,660	0,022	-0,077	0,007

TABLE 7.5 : Comparison of resistances and reactances during neutral switching period

resistance. The mean resistance differences are much less than the mean reactance differences.

The differences in the reactances for the two loops can be attributed to induced voltages in the electrode voltage measurement leads which become common mode voltages (and hence are ignored by the measurement) for the case where the neutrals are brought up the side of the furnace (route N). The lower reactance difference for phase 3 is a result of the way in which the electrode voltage leads were taken to the control room. The leads for electrodes 1 and 2 were brought to a connection box close to electrode 3 and then taken with the leads from electrode 3 to the control room. This resulted in a much larger measurement loop for electrodes 1 and 2 than for electrode 3. The loops were equal in size for the N neutral route, since the connections from each electrode were taken away as twisted pairs (including the neutral).

Another interesting result that can be seen from Table 7.5 is the phenomenon of 'live' and 'dead' phases. The results were taken over a period of moderately balanced operation and over the week the means of the three electrode currents were approximately equal, yet the mean resistances in each phase were quite different. The phase with the lowest resistance or power is phase 2 (the 'dead' phase) and the phase with the highest resistance or power is phase 3 (the 'live' phase).

7.5 Comparison of '50Hz' and RMS Measurements

It has been shown in Chapter 5 that arcing affects the reactance in a circuit even if only the fundamental frequencies of voltage, current and power are considered. This is contrary to the conclusions made by Bretthauer and Farschtschi[16]. After the rebuilding of the furnace transducers for the measurement of 50 Hz real power, current and voltage were included as well as rms transducers, so that these two techniques could be compared. The 50 Hz transducers were calibrated using an rms instrument and a low distortion 50 Hz supply so that the two sets of transducers would give the same outputs

for purely sinusoidal voltages and currents. Subsequent operation on the furnace showed that the two measurement systems gave the same results even under high arcing conditions.

A typical plot of reactance derived from 50 Hz and rms measurements is shown in Figure 7.3 for a period of 24 hours. The measurement of arc harmonics is included to show the change in arcing conditions during the period. The 50 Hz reactance trace is displaced downwards from the rms trace by 1 cm so as to allow comparison of the traces. The close correlation between the two sets of readings is clearly evident. The periodic peaks in the reactances and arcing curves are a result of tapping of the furnace every 3 - 4 hours. The reactance changes are fairly large and can be attributed to changes in the arcing conditions and the heights of the metal baths. This can be seen in the period between 14h00 and 18h00 hours. The furnace has been tapped at about 14h30 and there is a dramatic increase in the reactance and the level of arcing as metal is drained from the furnace and cold charge is introduced into the reaction zone below the electrode. After the tap, the reaction zone heats up again, the level of arcing is reduced, and the reactance drops as metal builds up in the furnace.

7.6 Spectral Analysis of Voltage and Current Waveforms

The harmonic filters, which have been installed on the furnace for the measurement of the harmonic content of the voltage and current waveforms, provide a composite measurement of the level of the harmonics without providing a measurement of which harmonic frequencies are dominant. A more detailed analysis of the waveforms has been carried out over a short period of time using a spectrum analyser. The analyser used provides a display in the frequency domain of the harmonics present in the waveform.

Typical traces of the voltage and current waveforms from the furnace are shown in Plates 1 and 2 and the voltage waveform is significantly more distorted than the current waveform. This is also shown in frequency domain plots in

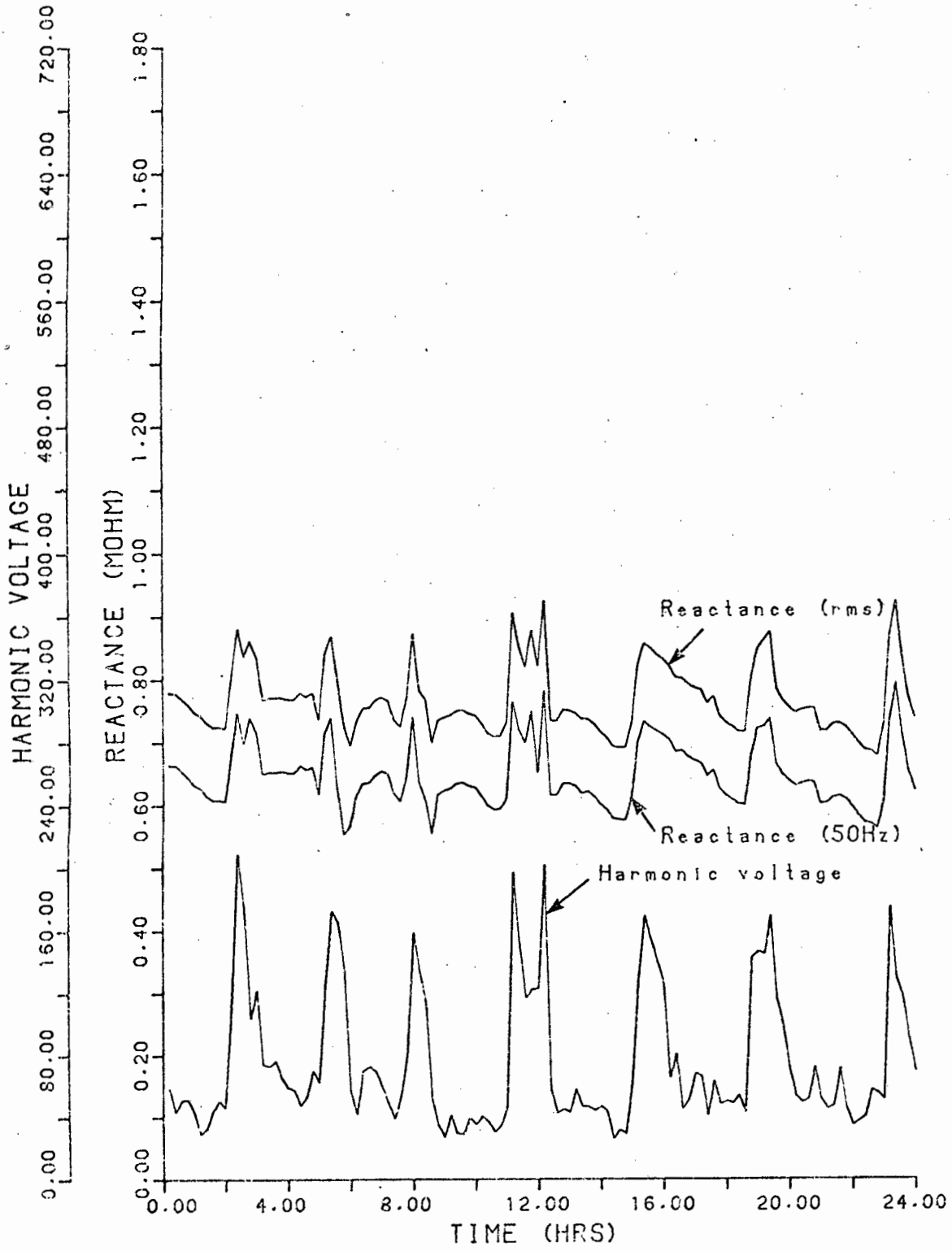

FIGURE 7.3 : COMPARISON BETWEEN REACTANCE MEASUREMENTS FOR RMS AND 50Hz MEASUREMENTS.

plates 3 and 4 (the frequency domain plots and the waveforms are not directly comparable as they were taken at different times).

In the frequency domain plots the 50 Hz peak is on the left of the plates with harmonic frequency peaks to the right in 50 Hz increments. The vertical axis is in decibels so as to accentuate the harmonics. In both cases the dominant harmonics are the odd harmonics 150 Hz, 250 Hz, 350 Hz and so on, which decay progressively in magnitude with increasing frequency. The even harmonic frequencies can be ignored. This is typical of a square wave frequency domain plot. The relative amplitude of the third harmonic for the voltage and current waveforms can be determined from the decibel equation where

$$dB = 20 \log_{10} \frac{V_2}{V_1}$$

The third harmonic for the voltage plot is 28 dB down on the fundamental so that

$$\frac{V_3}{V_f} = 4 \text{ per cent}$$

and in the case of the current

$$\frac{V_3}{V_f} = 0{,}6 \text{ per cent}$$

This is in agreement with the voltage and current traces shown in plates 1 and 2.

The linear decay of the odd harmonic frequencies (when plotting on a log scale) suggests that the harmonic amplitudes can be deduced from a measurement of the third harmonic only. However, in the harmonic measuring system which has been developed, the composite average of all the odd harmonics is measured since this simplifies the measurement equipment. This is adequate, since the major errors in the measurement are a result of the interaction between the phases and a high precision in the measurement equipment is not necessary.

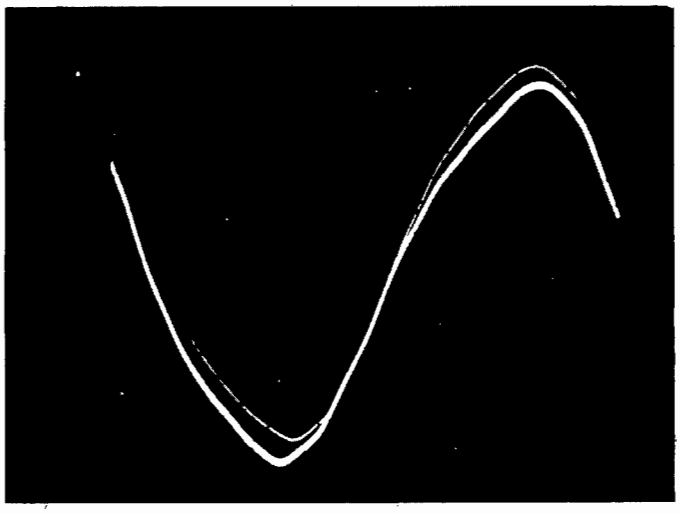

Plate 1. Typical voltage waveform

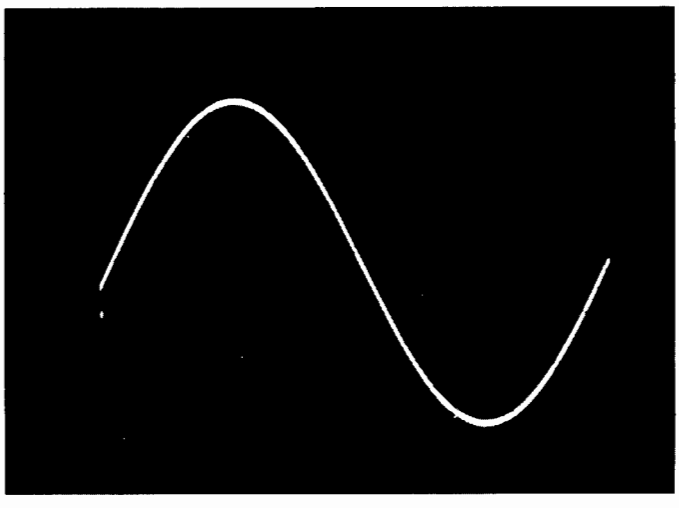

Plate 2. Typical current waveform

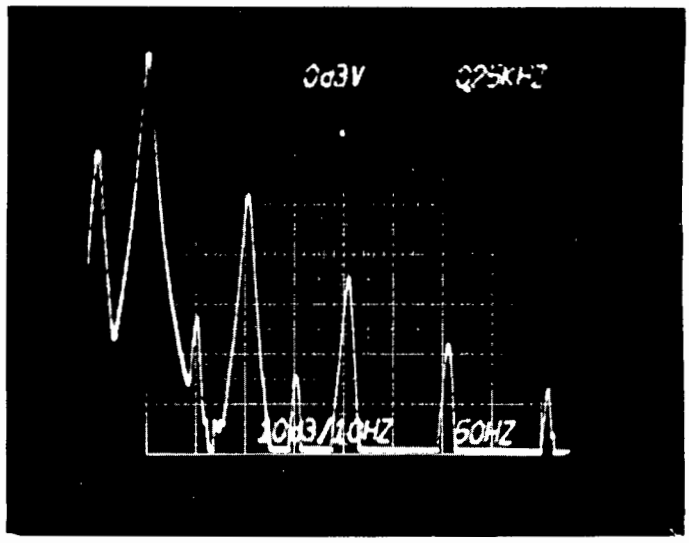

Plate 3. Frequency domain plot of a typical voltage waveform

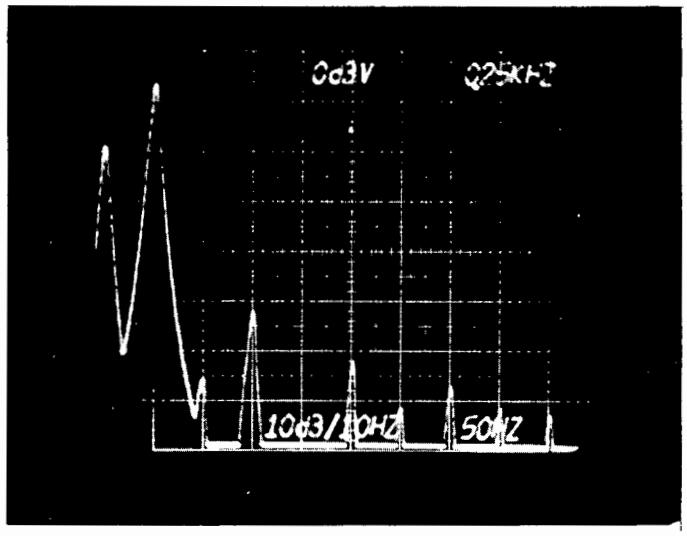

Plate 4. Frequency domain plot of a typical current waveform

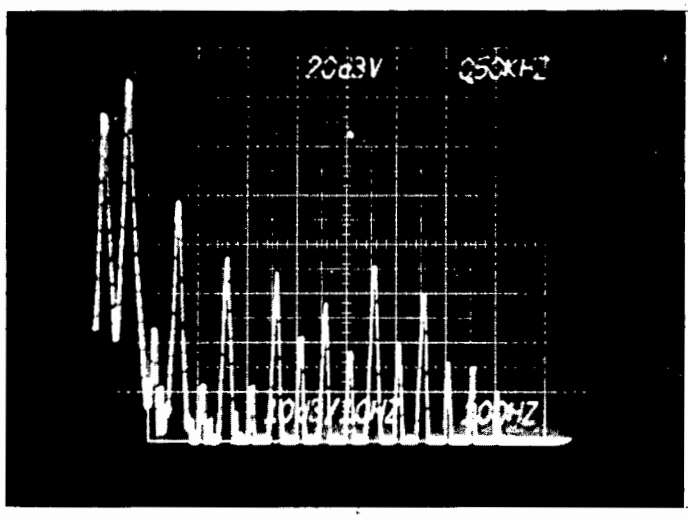

Plate 5. Frequency domain plot of voltage with compressed frequency scale

Any more complexity in the measuring system would only be justified if additional information could be obtained by measurement of a number of harmonics separately. Plate 5 shows that there could be some advantage in carrying out this exercise. The plate is a frequency domain plot of phase voltage, with the frequency scale compressed to 100 Hz per division, and shows the 11th and 13th harmonics much higher than they should be for the normal linear decay of the odd harmonics. This situation comes and goes in the operation of the furnace so that there is a possibility that a knowledge of its occurrence could be useful.

The relationship between arc factor as measured by the computer (harmonic voltage per phase divided by voltage per phase), and the amplitude of the third harmonic relative to the fundamental is shown plotted in Figure 7.4. This has been derived from a number of frequency domain plots of voltage which were taken at the same time as arc factor measurements. An arc factor of 1,0 (harmonic voltage of 170 with a phase voltage of 170) represents a typical arcing condition during tapping when the arcing is relatively high. Here the third harmonic amplitude is approximately 8,5 per cent of the fundamental. Assuming a phase voltage of 170 volts (peak) this represents an amplitude of 14,5 volts. From the arcing equation

$$V_a = \frac{4V_a}{\Pi} \sum_{n=o}^{\infty} \frac{\sin(2n+1)w(t-t_A)}{2n+1}$$

The amplitude of the third harmonic (n=1) is 14,5 volts so that

$$V_a = \frac{3 \times \Pi \times 14,5}{4}$$

$$= 34 \text{ volts}$$

The voltage of 170 volts (peak) has been chosen as it relates to the three-phase arcing conditions derived in section 5.6 where the line voltage was set at 300 volts (peak). This corresponds to a phase voltage of 173 volts (peak). The normal operating voltage of the furnace is 280 volts rms which is approximately 400 volts (peak) so that, for the furnace, the arc voltage Va,

for an arc factor of 1,0, would be about 45 volts. This derivation is only approximate; however, it does show the order of the arcing conditions in the furnace.

In addition to arcing, the level of the harmonics in the furnace phase voltages are also affected by saturation of the furnace transformers. This effect has not been examined in detail, however, the wide variations in harmonic voltages down to fairly low levels, which have been observed during approximately constant current conditions suggest that this effect is small.

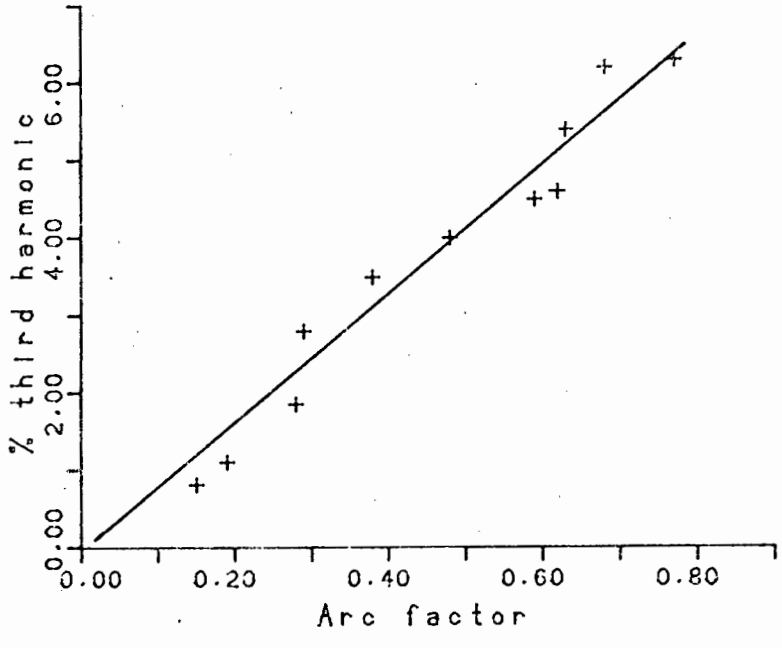

FIGURE 7.4 : PLOT OF AMPLITUDE OF THIRD HARMONIC AGAINST ARC FACTOR

8. ELECTRICAL MEASUREMENTS AND ELECTRODE LENGTH

The measurement of the length of the electrodes in a submerged-arc furnace is an important requirement since these measurements provide the basis for maintaining the reaction zones under each electrode at their optimum positions. However, there are no reliable methods available for directly measuring the length of the electrodes continuously, and only indirect techniques backed up by periodic direct measurements, based on the technique discussed in section 4.4, have been used up till now. The electrodes form part of the current loops in the furnace circuit, and since the reactances in the circuit are related to the dimensions of the current loops, there is a possibility that reactance measurements could be used to determine electrode lengths. The relationships between electrode lengths and reactances have been examined on a model of the furnace and the results are discussed in Chapter 6. It was found that under the ideal conditions of the furnace model a relationship between electrode lengths and star reactances could be established.

8.1 Variation in Star Reactances in an Operating Furnace

The star reactances in an operating furnace undergo cyclic variations as metal and slag build up in the furnace and are periodically tapped out resulting in changes in the current paths in the furnace. This was shown in Figure 7.3 for electrode 1. This electrode exhibits the most consistent cyclic nature as it is closest to the tap holes and its molten bath is always drained during tapping. The reactances of the back two electrodes do not always show a cyclic nature as the baths under these electrodes sometimes form separate dams which drain into the bath under electrode 1 at varying rates. In addition the nature of the electrode 2 bath (dead phase) is different from the electrode 3 bath (live phase) which tends to drain more easily into the electrode 1 bath. These conditions can be deduced from observations of the changes in the phase reactances and electrode hoist positions. In contrast to the fairly well defined cyclic variations of electrode 1 reactance and hoist position over a tap, the other two electrodes usually exhibit more frequent

smaller reactance changes. This can be attributed to repeated collapsing and forming of the dams under these electrodes. The back two electrodes also sometimes go through periods when there are very little reactance and hoist position variations even during tapping.

Variations in arcing also affect the phase reactances, particularly under high arcing conditions. In Figure 5.18 the reactance effect was shown to be appreciable for an arc voltage above 40 volts (for line voltage of 300 volts peak) which represents an arc factor of about 1,0. This is a moderate arcing condition which occurs in the furnace during tapping, particularly if an electrode is short or there is a deficiency of coke around an electrode. This means that reactance corrections for changing arcing conditions are important when the arcing in the furnace is high. However, it is more important to be able to correct the phase reactances for changes resulting from varying bath conditions under each electrode. It is possible to correct reactance variations resulting from arcing by using harmonic voltage measurements (the interaction effects between phases reduce the accuracy of the corrections), but there is no reliable measurement available which can even approximately describe the bath conditions under each electrode. Curr[27] has had some success in relating bath conditions (metal build up under each electrode) to heat flow measurements in the floor of the furnace under each electrode. However, these measurements only give positive results some of the time.

8.2 Relationship between electrode lengths and secondary electrical Measurements

The variation of the furnace bath conditions under each electrode over time means that reactances alone cannot be used for predicting the lengths of the electrodes. This has led to an investigation into the relationships between other electrical variables and electrode lengths. During this investigation, at a time when the author was engaged in trying to develop a fundamental relationship between the secondary electrical variables and

electrode lengths, Barcza[4] was examining the relationships between electrode lengths and all available measurements using stepwise linear regression techniques[30]. On the suggestion of the author it was decided to try a combination of reactance and arc factor measurements for developing a model to predict electrode lengths. This has subsequently proved to be a good model which has been used successfully to predict the lengths of the electrodes over an extended period of time. The initial investigation was done during a period of fairly stable resistance operation. However, subsequent operation has necessitated the inclusion of phase resistances in the model. The data for the models are summarized in Tables 8.1, 8.2 and 8.3 together with the results of regression analysis. The data are also plotted in Figure 8.1, 8.2 and 8.3 for each electrode.

In Figure 8.1 the most obvious observation is that both the arc factor and reactance are high when the electrode length is low. This also applies to the arc factors and reactances for electrodes 2 and 3 in Figures 8.2 and 8.3. In fact, in all three cases the arc factors are negatively correlated with the electrode lengths to quite a large degree. This can also be seen from the correlation matrix values in Tables 8.1, 8.2 and 8.3. In the case for electrodes 1 and 2 the reactances are correlated with the arc factors, particularly for electrode 1, however, the correlation is quite low for electrode 3 (0,425). The good negative correlations between arc factors and electrode lengths provide the basis for the accuracy of the models summarized in the tables. The best results are for electrode 3 where the maximum error is 13 cms which is much better than the worst error of 25 cm for electrode 2. However, if one considers that the accuracy of the direct measurements used for comparison are $\pm$ 15 cms, then the results of the models are quite satisfactory. Also, the electrode length accuracy requirements for maintaining good furnace operation are not high. One really only wants to know when an electrode is getting too short or too long without having to resort to the technique of burning down the burden and observing the length of the electrodes.

This results in a loss in production and stresses the roof refractory lining. The models have certainly been successful in achieving this goal as the furnace has been run successfully for a number of months without having to carry out any direct measurements.

	ARC FACTOR	RESISTANCE	REACTANCE
ARC FACTOR	1,0		
RESISTANCE	- 0,266	1,0	
REACTANCE	0,947	- 0,682	1,0
ELEC.LENGTH	- 0,791	0,176	- 0,729

CORRELATION MATRIX

DATE	ARC FACTOR	RESISTANCE mΩ	REACTANCE mΩ	ELECTRODE LENGTH m	PREDICTED ELECTRODE LENGTH m	ERROR m
14/3	0,479	1,29	0,718	3,35	3,32	0,03
21/3	0,69	1,185	0,756	3,2	3,21	-0,01
28/3	0,863	1,316	0,856	3,0	3,13	-0,13
3/4	1,105	1,436	0,945	2,96	3,0	-0,04
12/4	1,127	1,37	0,931	3,0	2,99	0,01
18/4	0,815	1,417	0,847	3,29	3,15	0,14
10/5	0,473	1,566	0,705	3,22	3,27	-0,05
18/5	0,547	1,442	0,74	3,46	3,26	0,20
24/5	0,614	1,428	0,747	3,2	3,22	-0,02
30/5	0,410	1,594	0,777	3,3	3,35	-0,05
19/7	0,279	1,402	0,607	3,3	3,37	-0,07

Length = -0,69 * arc factor - 0,159 * resistance + 0,627 * reactance +3,4

TABLE 8.1 : Electrode length prediction based on electrical measurements (Electrode 1)

	ARC FACTOR	RESISTANCE	REACTANCE
ARC FACTOR	1,0		
RESISTANCE	0,907	1,0	
REACTANCE	0,823	0,811	1,0
ELEC.LENGTH	-0,919	-0,813	-0,703

CORRELATION MATRIX

DATE	ARC FACTOR	RESISTANCE mΩ	REACTANCE mΩ	ELECTRODE LENGTH m	PREDICTED ELECTRODE LENGTH m	ERROR m
14/3	2,321	1,787	0,993	2,15	2,2	-0,05
21/3	2,279	1,953	1,033	2,35	2,27	0,08
28/3	1,496	1,544	0,927	2,8	2,79	0,01
3/4	0,791	0,783	0,842	3,2	3,23	-0,03
12/4	1,381	1,341	0,883	2,65	2,84	-0,19
18/4	1,439	1,475	1,013	2,85	2,88	-0,03
10/5	1,153	1,205	0,788	2,69	2,94	-0,25
18/5	1,272	1,183	0,832	3,02	2,87	0,15
24/5	1,104	1,239	0,857	3,05	3,02	0,03
30/5	1,246	1,127	0,823	3,1	2,89	0,21
19/7	0,82	1,264	0,794	3,3	3,21	0,09

Length = -0,779 * arc factor + 0,672 * resistance + 0,625 * reactance
+ 3,27

TABLE 8.2 : Electrode length based on electrical measurements (Electrode 2)

	ARC FACTOR	RESISTANCE	REACTANCE
ARC FACTOR	1,0		
RESISTANCE	0,722	1,0	
REACTANCE	0,425	0,506	1,0
ELEC. LENGTH	-0,874	-0,926	-0,569

CORRELATION MATRIX

DATE	ARC FACTOR	RESISTANCE mΩ	REACTANCE mΩ	ELECTRODE LENGTH m	PREDICTED ELECTRODE LENGTH m	ERROR m
14/3	1,494	1,912	1,17	2,4	2,36	0,04
21/3	1,019	1,326	0,688	3,0	3,03	-0,03
28/3	1,165	1,738	0,790	2,7	2,68	0,02
3/4	1,195	1,486	0,693	2,77	2,85	-0,08
12/4	1,423	1,387	0,712	2,8	2,82	-0,02
18/4	1,234	1,957	0,951	2,45	2,48	-0,03
10/5	0,857	1,148	1,062	3,06	3,14	-0,08
18/5	1,018	1,288	0,79	3,16	3,03	0,13
24/5	0,625	1,255	0,707	3,2	3,24	-0,04
30/5	0,708	1,217	0,723	3,35	3,22	0,13
29/7	0,446	1,195	0,683	3,32	3,35	-0,03

Length = -0,415 * arc factor -0,647 * resistance - 0,198 * reactance
+ 4,45

TABLE 8.3 : Electrode length based on electrical measurements (Electrode 3)

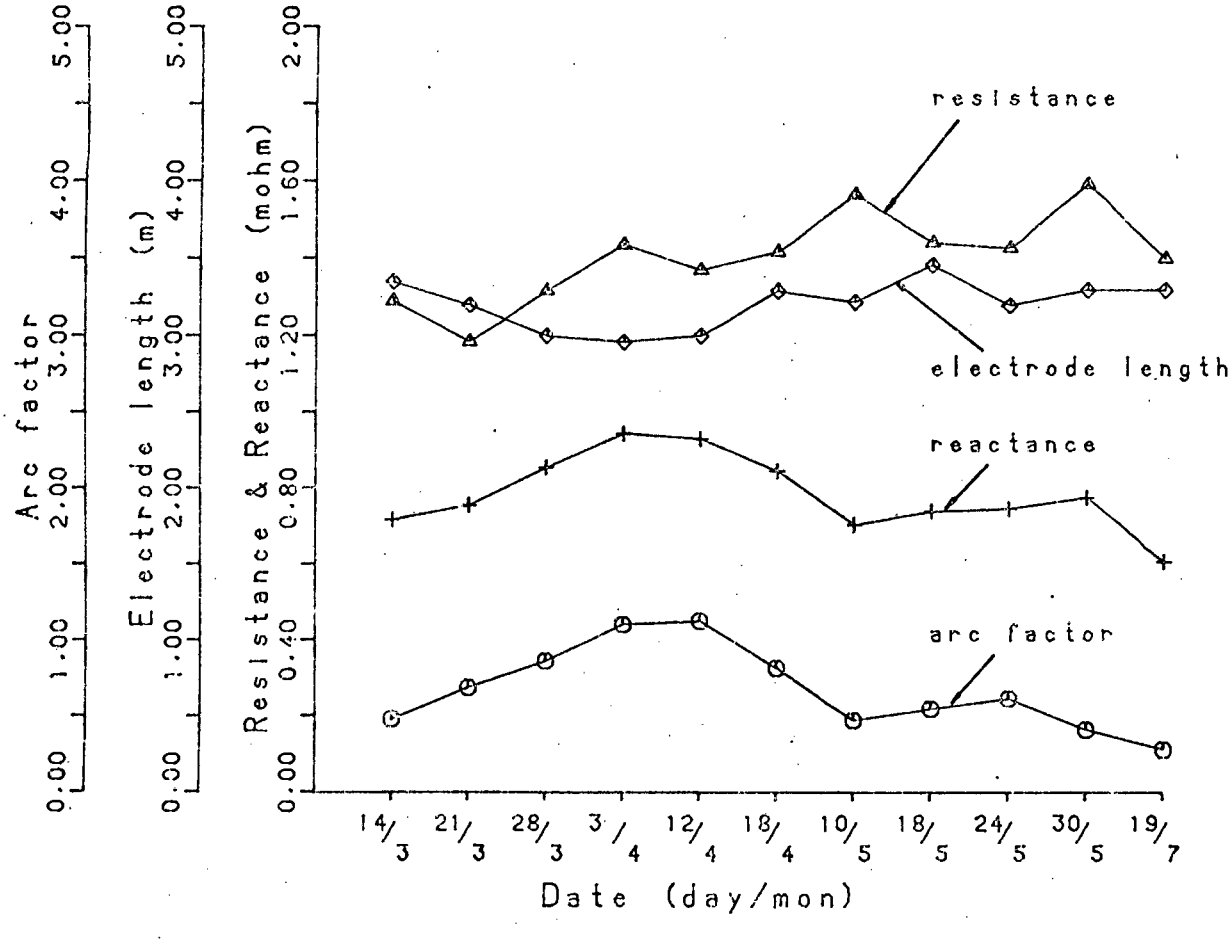

FIGURE 8.1 : PLOT OF ELECTRICAL VARIABLES FOR DATES WHEN ELECTRODE LENGTHS WERE MEASURED (Electrode 1)

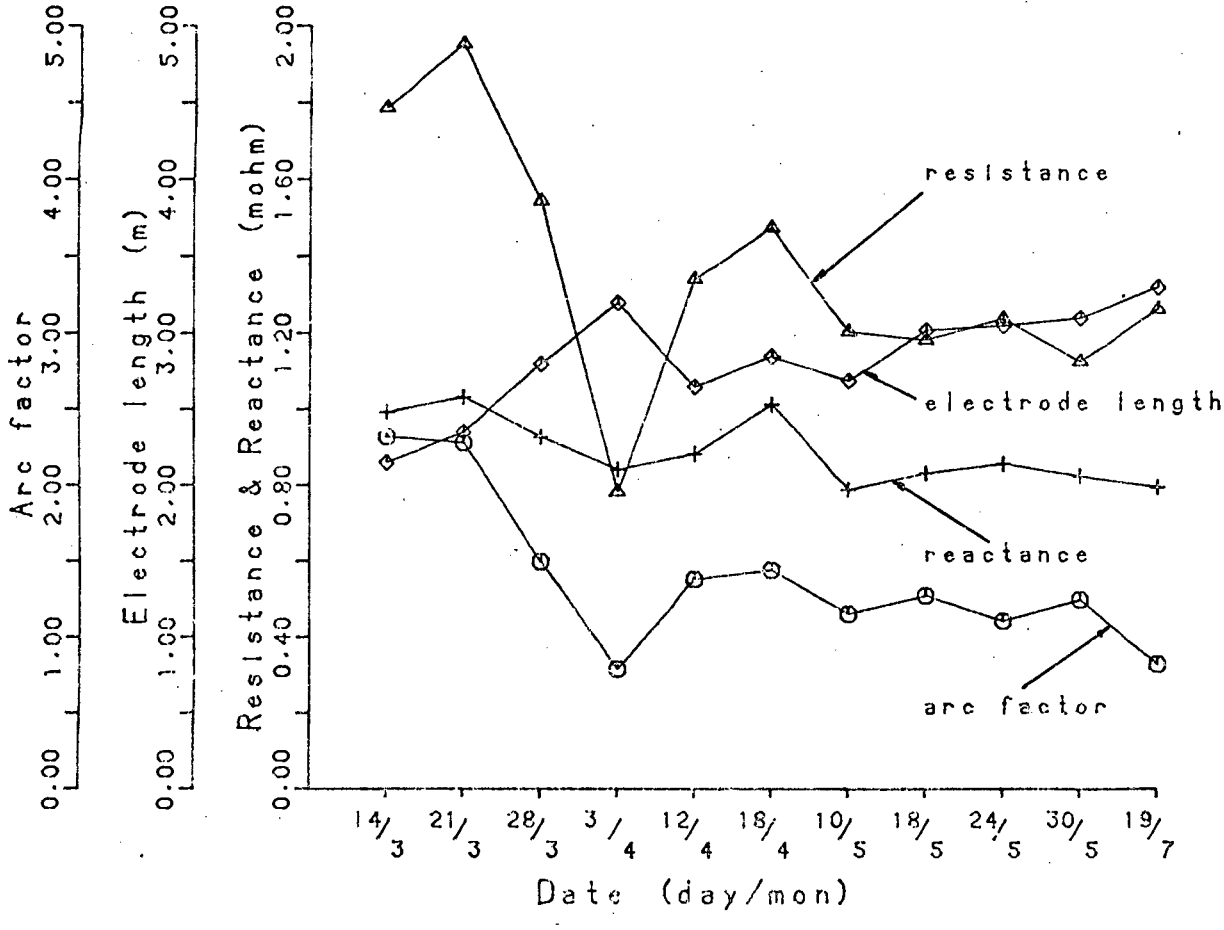

FIGURE 8.2 : PLOT OF ELECTRICAL VARIABLES FOR DATES WHEN ELECTRODE LENGTHS WERE MEASURED (Electrode 2)

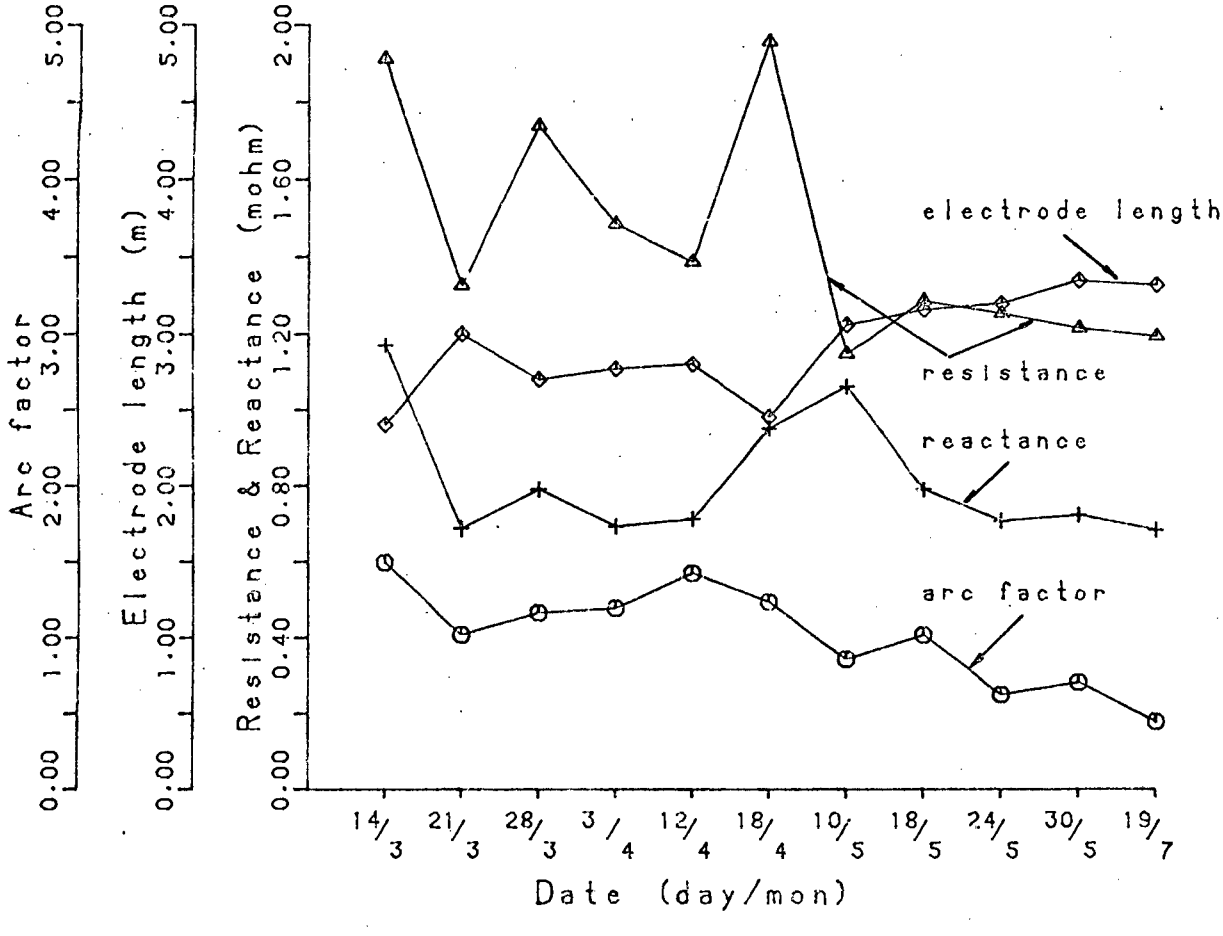

FIGURE 8.3 : PLOT OF ELECTRICAL VARIABLES ON DATES WHEN ELECTRODE LENGTHS WERE MEASURED (Electrode 3)

9. CONCLUSION

The development of the strategy for operation of the electrical circuit of submerged-arc furnaces has, until recently, been fairly stagnant owing to the ease of operation of small furnaces. The electrical circuit of these furnaces can be controlled satisfactorily using current control and the major effort in the operation concerns the regulation of the metallurgical processes. The instrumentation on small furnaces is very simple and usually consists of an energy meter on the high voltage supply and voltmeters and ammeters for the monitoring of the electrical circuit. There are no phase power measurements so that the phase resistances and reactances are not monitored. The furnaces were built when there was little concern over pollution and they are constructed with the top of the furnace open. The open-top allows the operator to observe the operation fairly closely and perform adjustments based on experience. The open top also allows the raw-material burden to be rabbled (raw material is pushed up against the electrodes to compensate for the higher rate of throughput of raw material around the electrodes) which ensures that the surface of the burden is even.

The operating costs of small furnaces, relative to production, are high compared to larger furnaces and this has led to the construction of progressively larger furnaces. With increasing size of furnace, many factors in the operation change. The increased rate of throughput of raw material results in the necessity for tighter control. The erosion of the electrodes is more rapid so that the monitoring of the lengths of the electrodes is more difficult. The furnaces usually have closed tops so as to reduce the amount of gas to be cleaned. This means that it is no longer possible to observe the burden and the raw material feeders have to be very carefully positioned to ensure an even flow of raw materials.

Large furnaces have a higher reactance than smaller furnaces. This is a major problem in the control of the electrical circuit. The high reactance causes a large amount of interaction between the phases in the circuit and

this results in current control being unsatisfactory. On small furnaces the distribution of power is moderately balanced even for relatively unbalanced currents. This is not the case on large furnaces where an imbalance in the currents results in large imbalances in the distribution of power. However, although this is a problem in itself, it is made more serious by the fact that the power imbalance is not related to the magnitude of the currents, so that measurements of the currents alone cannot be used for control. This means that it is necessary to control the circuit by measurements which do not suffer from the interaction problems. Measurements of phase resistances, being directly related to the power and to the conditions which occur below each electrode, can be used to control the electrical circuit. Unfortunately the measurement of these variables based on standard techniques is inaccurate as a result of induced errors in the measurement of secondary electrode-to-bath voltages.

This problem has become acute on a number of large furnaces which have been constructed in South Africa recently. These furnaces include the facility for automatic resistance control. However, this is based on inaccurate measurements of the electrode-to-bath voltages so that it cannot be used. The problem could be solved by the provision of an accurate system for the measurement of the electrode-to-bath voltages. However, although such a system has been developed by the author, it suffers from a disadvantage that measurement connections have to be made in the hot, harsh environment of the furnace and these leads are burnt away periodically and have to be replaced. It is also necessary to have reliable connections to the bath of the furnace and this is not always possible. As a result of these problems the author and Barker developed a measurement technique for the computation of the phase resistances based on primary measurements which are reliable. The technique takes advantage of the fact that the relationship between the phase reactances is fairly constant and can be assumed to be constant. The measurement method has been used as the basis for the development of a resistance controller which

has operated very successfully on a furnace and has solved the problems due to the interaction effects. The accuracy of the indirect measurements has been checked using the new measurement system and found to be reliable enough for control. Further resistance controllers are currently being installed on other furnaces.

The system which has been developed to provide accurate measurements of the electrode-to-bath voltages, although not used for direct control, has been used for modelling the electrical circuit and for control of other aspects of the furnace operation. A knowledge of the lengths of the electrodes is a very important parameter in the operation. The most widely used method for determining the lengths involves the periodic carrying out of direct length measurements and the modification of these lengths based on a prediction of the rate of electrode erosion. The phase power measurements provided by the standard arrangement are inaccurate and cannot be used for erosion rate predictions. Before an accurate measurement was available, the phase power distribution was inferred from the rate of throughput of raw materials around each electrode. The installation of the new measurement system included measurements of the degree of arcing under each electrode. The use of arcing measurements, together with the accurate phase power measurements, for electrode erosion predictions resulted in a large improvement in the accuracy. However, it was subsequently found by Barcza that the electrical variables provided by the new system could be used to develop empirical models for the direct prediction of the lengths of the electrodes. The models, being empirical, are still based on the direct length measurements. However, once the constants for these models have been established, the frequency of the direct measurements can be reduced considerably.

An analysis of arcing in a furnace has shown that an appreciable amount of arcing occurs below each electrode particularly during tapping. The development of measurements of the arcing conditions associated with each electrode has

provided a new measurement which has proved to be very useful in the operation of the furnace. A theoretical analysis of arcing in a three-phase circuit has shown that the level of arcing in each phase can be determined from measurements of the harmonics in the electrode-to-bath voltage waveforms. It has also been shown that it is important to take voltage measurements as close to the arcs as is possible, i.e. at the electrodes close to the contact shoes.

With the availability of reliable phase resistance and arcing measurements, it is possible to observe the mechanism of electrical conduction under the electrodes. Using the new measurement system, Rennie has studied the changes in resistances and arcing during peturbations of the electrodes. This has resulted in the development of new models which describe the height of each electrode tip above the metal bath and the resistivity of the conduction regions below each electrode. These are important parameters in the operation of furnaces and previously had to be guessed at.

The new secondary measurement system relies on reliable neutral connections at symmetrical positions in the lining of the furnace and, until recently, these have not been available. A neutral connection design has been established by the author and this design is currently being used for the installation of neutrals on other furnaces so that the new measurement system can be applied to these furnaces.

The analysis of the electrical circuit of a submerged-arc furnace has resulted in a large improvement in the measurement, control and understanding of the electrical aspects of the furnace operation. This analysis has been part of an extensive research effort to improve the operation of a large ferrochromium furnace and the overall effort has resulted in a considerable improvement in the production of the furnace. It has also resulted in South Africa becoming a leader in ferroalloy furnace technology. The analysis of the electrical circuit has contributed towards this success. Any further investigations into the electrical circuit would involve the investigation of arcing conditions in more detail. However, this will not be easy as the arcing models are complex and it will be difficult to establish the validity of these models on the furnace.

LIST OF PRINCIPAL SYMBOLS

U_{12}, U_{23}, U_{31}	delta voltages
U_{10}, U_{20}, U_{30}	line-to-neutral voltages
V_{12}, V_{23}, V_{31}	star line-to-line voltages
I_R , I_S , I_T	delta currents
I_1 , I_2 , I_3	star currents
Va_1, Va_2, Va_3	arc voltages
R_1 , R_2 , R_3	star resistances
L_1 , L_2 , L_3	star inductances
X_1 , X_2 , X_3	star reactances
Z_R , Z_S , Z_T	delta impedances
Z_1 , Z_2 , Z_3	star impedances
Z_{TR}, Z_{TS}, Z_{TT}	transformer impedances
Z_{BR}, Z_{BS}, Z_{BT}	busbar impedances
Z_{FR1},Z_{FR2},Z_{FS2},Z_{FS3},Z_{FT3},Z_{FT1}	flexibles impedances
P	total real power
Q	total reactive power
S	total apparent power
D	electrode diameter

LIST OF FIGURES

LIST OF TABLES

REFERENCES

1. ANDREAE, F.V. "Design and control of Ferroalloy furnaces". A.I.E.E. Transactions, vol. 69, 1950, pp. 557-562.

2. ANDERSEN, Hans Chs. "Some significant metallurgical aspects of the smelting of pig iron in electric furnaces". The Canadian Mining and Metallurgical Bulletin, Jul. 1963, pp. 509-516.

3. ASEA. "Seminar on Electrical Equipment for Reduction Furnaces". Johannesburg, 9 to 10 Jun., 1977.

4. BARCZA, N.A. National Institute for Metallurgy, Randburg. Private Communication.

5. BARKER, I.J. "An electrode controller for submerged-arc furnaces". 3rd IFAC Symposium on Automation in Mining, Mineral and Metal Processing". Montreal, 18 to 20 Aug., 1980.

6. BARKER, I.J. "Arcing in the electrical circuit of a submerged-arc furnace". Electrowärme Int., (to be published, Mar. 1980).

7. BARKER, I.J., and STEWART, A.B. "Inductive reactance and the operation of submerged-arc furnaces". Journal of S.A. Inst. of Mining and Metallurgy, (to be published, vol. 80, no. 3, Mar. 1980).

8. BLOCH, G. National Institute for Metallurgy, Randburg. Private communication.

9. BÖCKMAN, O.C. "Arrangement for measuring the crater voltages in a three phase electric furnace with electrodes arranged in delta". Norwegian patent no. 3919/71, 22nd Oct., 1971.

10. BÖCKMAN, O.C., and OLSEN, L. "Skin and proximity effects in electrodes of large smelting furnaces". 6th Int. congress on Electro-heat, Brighton, May 1968, paper no. 127.

11. BOWMAN, B., JORDAN, G.R., and FITZGERALD, F. "The physics of high circuit arcs". Journal of the Iron and Steel Inst., Jun. 1969, pp. 798-805.

12. BRETTHAUER, K., and TIMM, K. "A contribution to the theory of three phase arc furnaces". Electrowärme Int., vol. 28, 1970, pp. 115-120. (In German.)

13. BRETTHAUER, K., and TIMM, K. "The measurement of the electrical variables on the secondary side of three-phase furnaces". Electrowärme Int., vol. 29, no. 7, 1971, pp. 381-387. (In German.)

14. BRETTHAUER, K., and TIMM, K. "Effects of unbalance on the wear of arc furnaces and how they are measured". U.I.E., vol. 7, 1972. (In German.)

15. BRETTHAUER, K. "Optimization of arc furnaces for steel production". Electrowärme Int., vol. 34, Feb. 1976, pp. 21-25. (In German.)

16. BRETTHAUER, K., and FARSCHTSCHI, A.A. "Circuit course and voltage course in alternating current circuits with electric arcs". Archiv fur Electrotechnik, vol. 57, 1975, pp. 145-152. (In German.)

17. BRETTHAUER, K., and FARSCHTSCHI, A.A. "Problems with magnetic fields in the high-current carrying conductors of electric arc furnaces". Electrowärme Int., vol. 32, Feb. 1974, pp. 33-37. (In German.)

18. BRETTHAUER, K., and FARSCHTSCHI, A.A. "Symmetrization of electrical parameters of arc furnaces". Electrowärme Int. vol. 34, 1976, B5, pp. 245-251. (In German.)

19. BRETTHAUER, K., and FARSCHTSCHI, A.A. "Calculation of currents in three-phase circuits of arc furnaces". Archiv fur Electrotecknik, vol. 58, 1976, pp. 111-115. (In German.)

20. BRETTHAUER, K., FARSCHTSCHI, A.A., and TIMM, K. "Measurement of the electrical dimensions of arcs in electric steel furnaces". Electrowärme Int., vol. 33, 1975, pp. 221-225. (In German.)

21. BRETTHAUER, K., FARSCHTSCHI, A.A., and TIMM, K. "Investigation into asymmetry and measuring errors with a UHP electric arc furnace". Stahl u Eisen, vol. 93, no. 17, 1973, pp. 761-765. (In German.)

22. BROWNE, T.E. "The electric arc as a circuit element". Electrochemical Society Journal, vol. 102, 1955, pp. 27-37.

23. CAVIGLI, M.D. "Trends in the technology of self-baking electrodes". 36th Electric furnace conference proceedings, Dec 5 to 8, Toronto, 1978.

24. CHANNON, W.P. et al. "The mode of current transfer between electrode and slag in the submerged-arc furnace". Journal of S.A. Inst. of Mining and Metallurgy, vol. 75, no. 1, 1974, pp. 4-7.

25. CLAUSERT, H. "Lead systems of three-phase furnaces and their equivalent circuit diagrams". Electrowärme Int., vol. 33, 1975, pp. 232-233. (In German)

26. COOK, W.G. "Trends and developments in electric arc furnace transformers". Journal of Metals, Mar. 1966, pp. 345-352.

27. CURR, T. National Institute for Metallurgy. Randburg. Private communication.

28. DEN OUDEN, G. "The electric arc". Phillips welding reporter, vol. 1, 1971.

29. DOWNING, J.H., and URBAN, L. "Electrical conduction in submerged-arc furnaces". Journal of Metals, Mar. 1966, pp. 337-344.

30. DRAPER, N.R., and SMITH, H. "Applied regression analysis". New York, Wiley, 1966.

31. DUNSKI, C.V. "The distribution of current in the electrodes of a three-phase arc furnace under equilibrium and non-equilibrium conditions". Electrowärme, vol. 20, no. 10, Oct. 1962, pp. 503-511. (In French.)

32. ELYUTIN, V.P., et al. "Production of ferroalloys" Electrometallurgy 2nd edition, Jerusalem, 1957.

33. ENOMOTO, RYO. "Arc characteristics in a silicon furnace". Ferroalloys, vol. 24, no. 1. 1975, pp. 61-69. (In Japanese.)

34. GEIGEL, M.J. "Determination of electrode position and its significance". Electric furnace conference proceedings, 1959, pp. 430-434.

35. GRAY, G.T. "The design and implementation of a microcomputer system for control of a submerged arc furnace". 6th IFAC/IFIP conference on digital computer applications to process control, Düsseldorf, Oct. 14 to 17, 1980.

36. JORDAN, G.R. "Electrode erosion in electric arc furnaces - the controlling parameters". Ironmaking and steelmaking, no. 4, 1978, pp. 177-183.

37. JORDAN, G.R., BOWMAN, B., and WAKELAM, D. "Electrical and photographic measurements of high-power arcs." J. Phys. D: Appl. Phys., 1970, vol. 3., pp. 1089-1099.

38. KASPER, VON R., and JAHN, H.H. "A refined equivalent circuit diagram of a three-phase a.c. arc furnace". Electrowärme Int., vol. 36, no. 1, Feb. 1978, pp. 26-29. (In German.)

39. KELLY, W.M. "Design and construction of the submerged-arc furnace". Carbon and graphite news, vol. 5, no. 1, 1958.

40. KÖHLE, S. "Relationships between the inductances of the secondary systems of arc furnaces". Electrowärme Int., vol. 36, no. 6, Dec. 1978, pp. 314-320. (In German.)

41. KUHLMANN, A.M. "Electrode penetration in submerged-arc furnaces". Electric furnace conference proceedings, 1959, pp. 438-442.

42. LANGMAN, R.D. "Energy rate input control of arc furnaces". Journal of the Iron and Steel Institute, vol. 204, Dec. 1966, pp. 1194-1199.

43. LINDGVIST, C. "ASEA furnace transformers". Seminar on Electrical Equipment for reduction furnaces, Johannesburg, 9 to 10 Jun., 1977.

44. MADDEVER, W.T., and SEGSWORTH, R.S. "The influence of gas injection arc stabilization and electrode consumption in electrode furnaces". Canadian Metallurgical quarterly, vol. 15, no. 1, 1976, pp. 49-52.

45. MEREDITH, W.R., et al. "Determination and control of electrode penetration". Electric furnace conference proceedings, 1959, pp. 435-437.

46. MONTGOMERY, R.W., DENBY, M., and HOWES, B.D. "The dissipation of energy from a high current arc in a steelmaking environment". IEE conference publications, no. 143, pp. 16-19.

47. MOSTOWSKI, J.H. "Selecting electrical parameters for large arc furnaces". Electric furnace conference proceedings, 1969, pp. 183-188.

48. MULLER, M.B. "Scaling-up of submerged-arc furnaces by criteria evaluated from water model studies of pilot smelting craters". Scandinavian Journal of Metallurgy, vol. 4, pp. 161-169.

49. NAUDE, D.E. National Institute for Metallurgy, Randburg. Private communication.

50. OLSEN, L., ARNESEN, A.G., BENCZE, I., and INNVAER, R. "Temperature distribution in Söderberg electrodes". U.I.E., vol. 7, 1972, no. 405.

51. OTANI, Y., SAITO, M., USUI, K., and CHINO, N. "The inner structure of the submerged-arc furnace". 6th int. congress on electroheat, Brighton, 1968, no. 112.

52. PERSSON, J.A. "The significance of electrode-to-hearth voltage in electric smelting furnaces". Electric furnace conference proceedings, 1970, vol. 28, pp. 168-169.

53. REDDY, A.K.N. "The theory and design of electric smelting furnaces". J. of electrochemical society, India, vol. 22, no. 4, 1973, pp. 275-289.

54. RENNIE, M.S. "Computer-aided operation of a furnace for the production of ferrochromium". National Institute for Metallurgy, Randburg, Report no. 1990, Nov. 1978.

55. RENNIE, M.S. "The application of on-line data and the development of models relating to the production of charge chrome". Electric furnace conference proceedings, Detroit, 4 to 6th Dec., 1979.

56. ROBIETTE, A.G.E. "Electric smelting processes". Griffin, London, 1973.

57. SCHWABE, W.E. "Fundamentals of heat distribution and refractory wear in electric steel furnaces". Iron and steel engineer, Dec. 1961, pp. 104-112.

58. SCHWABE, W.E. "The electric arc in melting furnaces". American Foundrymen's association convention, Cleveland, 1958, pp. 571-577.

59. SKREIEN, N. "Method for determination of operating conditions by metallurgical processes in electrical electrode furnaces". Norwegian patent no. 3606/72, 9th Oct., 1972.

60. SÖDERBERG, C.W. "Söderberg self-baking continuous electrodes". Chemical and Metallurgical Engineering, vol. 26, no. 25, 1922, pp. 1178-1182.

61. SOMMER, G., BENCZE, I., MARTIN, P., RENNIE, M., and STEWART, A.B. "The computer control of a ferrochromium furnace". National Institute for Metallurgy, Report no. 1676, 1st Nov., 1974.

62. SOMMER, G., BARCZA, N.A., BARKER, I.J., GRAY, G.T., RENNIE, M.S., POTGIETER, J.H., and STEWART, A.B. "The cancer project : A summary of the computer-aided operation of a 48 MVA ferrochromium furnace". National Institute for Metallurgy, Report no. 2032, 28th Nov., 1979.

63. STEPANYANTS, S.L. et al. "Investigation of the thermal schedule of self-sintering electrodes of electric ferro-alloy furnaces with the aim of automating the process". Stal, vol. 8, 1977, pp. 714-717. (In Russian.)

64. STEWART, A.B. "An analysis of the electrical circuit of a submerged-arc furnace". Electric furnace conference proceedings, Detroit, 4 to 6th Dec., 1979.

65. STEWART, A.B., and BARKER, I.J. "The control of electrical arc furnaces" S.A. Patent no. 77/3923.

66. STEWART, A.B., and BARKER, I.J. "A solution to the measurement and interaction effects in the control of submerged arc furnaces". INFACON 80, Lausanne.

67. STEWART, A.B., and MARTIN, P.D. "The implementation of data logging and raw material feed control on a submerged-arc furnace". Proc. 2nd IFAC Symp. on Automation in Mining, Mineral and Metal Processing, 1976, pp. 583-588.

68. STRÖM, N. "Electrical equipment for electric smelting furnaces". Seminar on electrical equipment for reduction furnaces, Johannesburg, 9 to 10 Jun. 1977.

69. SUNDBERG, Y. "The power circuit of arc furnaces". Electrowärme Int. vol. 30, no. 2, Apr. 1972, pp. 93-99.

70. TIMM, K. "Contribution to the symmetrisation of three-phase furnaces". Elektronische Zeitschrift, vol. 94, no. 4, 1973, pp. 204-208. (In German.)

71. TOBEY, G.E., et al. "Operational amplifiers - Design and application" McGraw-Hill. (1971).

72. URQUHART, R.C. et al. "The dissipation of electrical power in the burden of a submerged-arc furnace". Electric furnace conference proceedings, 1973, pp. 73-78.

73. URQUHART, R.C. "The role of the coke bed in the electric-furnace production of ferro-alloys". Electric furnace conference proceedings, 1978, pp. 79-84.

74. VOLBERT, G., and FRANK, K.D. "The metallurgy of ferroalloys". Springer, Berlin, 1972.

75. WILLAND, K. "Measurement of the resistance of ferrochromium furnace charges". National Institute for Metallurgy, Report No. 1698, 29th Apr., 1975.

76. WILLAND, K., TAYLOR, J.F., and STEWART, A.B. "An examination of the suitability of various reducing agents for the production of ferrochromium". National Institute for Metallurgy, Report No. 1708, 27th Feb., 1975.

77. YAMAGISHI, K., et al. "A comprehensive analysis of a furnace interior for high-carbon ferrochromium". INFACON 74 proceedings. Edited by H. Glen, Apr. 1974, pp. 143-148.

LIST OF APPENDICES

A P P E N D I X A

MUTUAL AND SELF INDUCTANCE RELATIONSHIPS IN THE SECONDARY CIRCUIT OF ARC FURNACES

The measurement of the electrode-to-bath voltages in the secondary circuit of a furnace involves the addition of a measurement lead to the secondary equivalent circuit. It was shown in Section 4.1.3 that the measurement of the electrode-to-bath voltages (including a measuring lead) can be resolved into terms which are based on the mutual inductances between the measuring leads and the secondary current loops. Rewriting equations 4.6:

$$\begin{aligned} U_{1M} &= I_1(R_1 + jwL_1) + I_1\, jwL_{3M,12} - I_3\, jwL_{1M,23} \\ U_{2M} &= I_2(R_2 + jwL_2) + I_2\, jwL_{1M,23} - I_1\, jwL_{2M,31} \\ U_{3M} &= I_3(R_3 + jwL_3) + I_3\, jwL_{2M,31} - I_2\, jwL_{3M,12} \end{aligned} \qquad \text{(A1)}$$

The mutual inductances are connected with each other by the relationship:

$$L_{3M,12} + L_{1M,23} + L_{2M,31} = 0 \qquad \text{(A2)}$$

so that

$$\begin{aligned} U_{1M} &= U_{10} + U_{0M} \\ U_{2M} &= U_{20} + U_{0M} \\ U_{3M} &= U_{30} + U_{0M} \end{aligned} \qquad \text{(A3)}$$

Köhle[40] has shown that the mutual inductances are related to the self inductances by the relationship:

$$\begin{aligned} L_{3M,12} &= \tfrac{1}{2}(L_2 - L_1) + \tfrac{1}{2}(L_{1M} - L_{2M}) \\ L_{1M,23} &= \tfrac{1}{2}(L_3 - L_2) + \tfrac{1}{2}(L_{2M} - L_{3M}) \\ L_{2M,31} &= \tfrac{1}{2}(L_1 - L_3) + \tfrac{1}{2}(L_{3M} - L_{1M}) \end{aligned} \qquad \text{(A4)}$$

This is an important relationship which is worth examining in more detail. As a starting point it is necessary to look at the inductance relationships in a four-conductor system shown below, where the lower ends are joined together and

the upper ends lie as close to each other as is desired. This approximates to the secondary lead arrangement in a furnace.

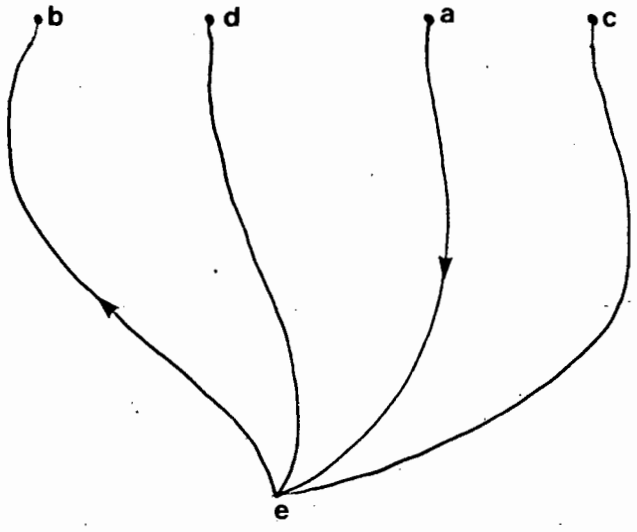

A current flowing in loop ab.will generate a voltage in cd given by

$$e_{cd} = L_{cd,ab} \frac{di}{dt} \qquad (A5)$$

The current in ab can be replaced by equal currents flowing in loops ac, cd and db so that

$$e_{cd} = (L_{cd,ac} + L_{cd,cd} + L_{cd,db}) \frac{di}{dt} \qquad (A6)$$

$L_{cd,cd}$ is the self inductance $L_{cd} = L_{dc}$ of the loop cd.

Using equation 3.4 and combining A5 and A6

$$L_{cd,ab} = L_{cd} - L_{cd,ca} - L_{dc,db} \qquad (A7)$$

Considering the current in loop ab generating a voltage in loop ac

$$e_{ac} = L_{ac,ab} \frac{di}{dt} \qquad (A8)$$

The current in loop ab can be replaced by equal currents in loops ac and cb so that

$$e_{ac} = (L_{ac,ac} + L_{ac,cb}) \frac{di}{dt} \qquad (A9)$$

Using equation 3.4 again and considering that $L_{ac,ac} = L_{ac} = L_{ca}$

$$L_{ac,ab} + L_{cb,ca} = L_{ca} \qquad \text{(A10)}$$

The relationship between the mutual inductances and the self inductance in loop bc can be determined by considering the voltage induced in loop bc by a current in loop ba

$$e_{bc} = L_{bc,ba} \frac{di}{dt} \qquad \text{(A11)}$$

Replacing the current in loop ba by currents in loops bc and ca

$$e_{bc} = (L_{bc,bc} + L_{bc,ca}) \frac{di}{dt} \qquad \text{(A12)}$$

so that

$$L_{ba,bc} + L_{cb,ca} = L_{bc} \qquad \text{(A13)}$$

Finally considering the voltage induced in loop ab as a result of a current in loop ac

$$L_{ac,ab} + L_{ba,bc} = L_{ab} \qquad \text{(A14)}$$

Combining equations A10, A13 and A14 into matrix notation

$$\begin{vmatrix} 1 & 1 & 0 \\ 0 & 1 & 1 \\ 1 & 0 & 1 \end{vmatrix} \cdot \begin{vmatrix} L_{ac,ab} \\ L_{ba,bc} \\ L_{cb,ca} \end{vmatrix} = \begin{vmatrix} L_{ab} \\ L_{bc} \\ L_{ca} \end{vmatrix} \qquad \text{(A15)}$$

Inverting the matrix

$$\begin{vmatrix} L_{ac,ab} \\ L_{ba,bc} \\ L_{cb,ca} \end{vmatrix} = \frac{1}{2} \begin{vmatrix} 1 & -1 & 1 \\ 1 & 1 & -1 \\ -1 & 1 & 1 \end{vmatrix} \cdot \begin{vmatrix} L_{ab} \\ L_{bc} \\ L_{ca} \end{vmatrix} \qquad \text{(A16)}$$

This gives the relationship between the mutual inductances and self inductances in a three-conductor system.

In individual notation the first term in the matrix equation is

$$L_{ac,ab} = \tfrac{1}{2}(L_{ab} - L_{bc} + L_{ca}) \qquad \text{(A17)}$$

The mutual inductance between two loops of a three conductor system can be expressed as 'half the sum of the self inductances of the two loops being considered minus half the self inductance of the loop which does not include the common conductor of the two loops'. In the above example the two loops are ac and ab and a is the common conductor so that the remaining loop is bc ($L_{ac} = L_{ca}$).

Applying this rule to the three conductor systems acd and bcd

$$\begin{aligned} L_{cd,ca} &= \tfrac{1}{2}(L_{cd} + L_{ca} - L_{da}) \\ L_{dc,db} &= \tfrac{1}{2}(L_{dc} + L_{db} - L_{cb}) \end{aligned} \qquad \text{(A18)}$$

Substituting equations A18 back into A7 gives the relationship between the mutual and self inductances in a four conductor system

$$L_{cd,ab} = \tfrac{1}{2}(L_{da} + L_{cb} - L_{ca} - L_{db}) \qquad \text{(A19)}$$

The equation for the mutual inductance $L_{ad,bc}$ can be determined by considering the voltage induced in loop ad as a result of a current flowing in loop bc

$$e_{ad} = L_{ad,bc} \frac{di}{dt} \qquad \text{(A20)}$$

If the current in loop bc is replaced by equal currents in loops ba, ad and dc

$$e_{ad} = (L_{ad,ba} + L_{ad,ad} + L_{ad,dc}) \frac{di}{dt} \qquad \text{(A21)}$$

and $L_{ad,bc} = L_{ad} - L_{da,dc} - L_{ad,ab}$ (A22)

Using the three conductor system rule

$$\begin{aligned} L_{da,dc} &= \tfrac{1}{2}(L_{da} + L_{dc} - L_{ac}) \\ L_{ad,ab} &= \tfrac{1}{2}(L_{ad} + L_{ab} - L_{db}) \end{aligned} \qquad \text{(A23)}$$

so that

$$L_{ad,bc} = \tfrac{1}{2}(L_{ac} + L_{db} - L_{dc} - L_{ab}) \qquad \text{(A24)}$$

Similarly

$$L_{bd,ca} = \tfrac{1}{2}(L_{ab} + L_{cd} - L_{bc} - L_{da}) \qquad \text{(A25)}$$

If a, b and c are replaced by 1, 2 and 3 and d is replaced by m, then equations A16, A19 A24 andA25 can be combined together in matrix notation as:

$$\begin{vmatrix} L_{13,12} \\ L_{21,23} \\ L_{32,31} \\ L_{3M,12} \\ L_{1M,23} \\ L_{2M,31} \end{vmatrix} = \tfrac{1}{2} \begin{vmatrix} 1 & -1 & 1 & 0 & 0 & 0 \\ 1 & 1 & -1 & 0 & 0 & 0 \\ -1 & 1 & 1 & 0 & 0 & 0 \\ 0 & 1 & -1 & 1 & -1 & 0 \\ -1 & 0 & 1 & 0 & 1 & -1 \\ 1 & -1 & 0 & -1 & 0 & 1 \end{vmatrix} \cdot \begin{vmatrix} L_{12} \\ L_{23} \\ L_{31} \\ L_{1M} \\ L_{2M} \\ L_{3M} \end{vmatrix} \qquad \text{(A26)}$$

The above matrix is singular so that it cannot be inverted as it stands, however, if the self inductances ΔL_{1M} and ΔL_{2M} are used where

$$\begin{aligned} \Delta L_{1M} &= L_{1M} - L_{2M} \\ \Delta L_{2M} &= L_{2M} - L_{3M} \\ \Delta L_{3M} &= L_{3M} - L_{1M} = -(\Delta L_{1M} + \Delta L_{2M}) \end{aligned} \qquad \text{(A27)}$$

then A_{26} can be rewritten as

$$\begin{vmatrix} L_{13,12} \\ L_{21,23} \\ L_{32,31} \\ L_{3M,12} \\ L_{1M,23} \\ L_{2M,31} \end{vmatrix} = \tfrac{1}{2} \begin{vmatrix} 1 & -1 & 1 & 0 & 0 \\ 1 & 1 & -1 & 0 & 0 \\ -1 & 1 & 1 & 0 & 0 \\ 0 & 1 & -1 & 1 & 0 \\ -1 & 0 & 1 & 0 & 1 \\ 1 & -1 & 0 & -1 & -1 \end{vmatrix} \cdot \begin{vmatrix} L_{12} \\ L_{23} \\ L_{31} \\ \Delta L_{1M} \\ \Delta L_{2M} \end{vmatrix} \qquad \text{(A28)}$$

This can be split into

$$\begin{vmatrix} L_{13,12} \\ L_{21,23} \\ L_{32,31} \end{vmatrix} = \tfrac{1}{2} \begin{vmatrix} 1 & -1 & 1 \\ 1 & 1 & -1 \\ -1 & 1 & 1 \end{vmatrix} \cdot \begin{vmatrix} L_{12} \\ L_{23} \\ L_{31} \end{vmatrix} \qquad \text{(A29)}$$

$$\underline{m}_{11} = \underline{A}_{11} \cdot \underline{x}_1$$

and

$$\begin{vmatrix} L_{3M,12} \\ L_{1M,23} \\ L_{2M,31} \end{vmatrix} = \tfrac{1}{2} \begin{vmatrix} 0 & 1 & -1 \\ -1 & 0 & 1 \\ 1 & -1 & 0 \end{vmatrix} \cdot \begin{vmatrix} L_{12} \\ L_{23} \\ L_{31} \end{vmatrix} + \tfrac{1}{2} \begin{vmatrix} 1 & 0 \\ 0 & 1 \\ -1 & -1 \end{vmatrix} \cdot \begin{vmatrix} \Delta L_{1M} \\ \Delta L_{2M} \end{vmatrix} \qquad \text{(A30)}$$

$$\underline{m}_{12} = \underline{A}_{21} \cdot \underline{x}_1 + \underline{A}_{22} \cdot \underline{x}_2$$

$$\underline{x}_1 = \underline{A}_{11}^{-1} \cdot \underline{m}_{11} \qquad \text{(A31)}$$

so that

$$\underline{m}_{12} = \underline{A}_{21} \cdot \underline{A}_{11}^{-1} \cdot \underline{m}_{11} + \underline{A}_{22} \cdot \underline{x}_2 \qquad \text{(A32)}$$

and

$$\begin{vmatrix} \underline{x}_1 \\ \underline{x}_2 \end{vmatrix} = \begin{vmatrix} \underline{A}_{11}^{-1} & \underline{o} \\ -(\underline{A}'_{22} \cdot \underline{A}_{22})^{-1} \cdot \underline{A}'_{22} \cdot \underline{A}_{21} \cdot \underline{A}_{11}^{-1} & (\underline{A}'_{22} \cdot \underline{A}_{22})^{-1} \cdot \underline{A}'_{22} \end{vmatrix} \cdot \begin{vmatrix} \underline{m}_{11} \\ \underline{m}_{12} \end{vmatrix} \qquad \text{(A33)}$$

Returning to the expanded notation after solving the partial matrices above gives

$$\begin{vmatrix} L_{12} \\ L_{23} \\ L_{31} \\ \\ \Delta L_{1M} \\ \Delta L_{2M} \end{vmatrix} = \frac{1}{3} \begin{vmatrix} 3 & 3 & 0 & 0 & 0 & 0 \\ 0 & 3 & 3 & 0 & 0 & 0 \\ 3 & 0 & 3 & 0 & 0 & 0 \\ & & & & & \\ 3 & -3 & 0 & 4 & -2 & -2 \\ 0 & 3 & -3 & -2 & 4 & -2 \end{vmatrix} \cdot \begin{vmatrix} L_{13,12} \\ L_{21,23} \\ L_{32,31} \\ L_{3M,12} \\ L_{1M,23} \\ L_{2M,31} \end{vmatrix} \qquad \text{(A34)}$$

This gives the relationship between the self-inductances and mutual inductances in a furnace. If the first part of equation A34, viz:

$$\begin{vmatrix} L_{12} \\ L_{23} \\ L_{31} \end{vmatrix} = \begin{vmatrix} 1 & 1 & 0 \\ 0 & 1 & 1 \\ 1 & 0 & 1 \end{vmatrix} \cdot \begin{vmatrix} L_{13,12} \\ L_{21,23} \\ L_{32,31} \end{vmatrix} \qquad \text{(A35)}$$

is substituted back into equation A_{30}, this gives

$$\begin{vmatrix} L_{3M,12} \\ L_{1M,23} \\ L_{2M,31} \end{vmatrix} = \tfrac{1}{2} \begin{vmatrix} 0 & 1 & -1 \\ -1 & 0 & 1 \\ 1 & -1 & 0 \end{vmatrix} \cdot \begin{vmatrix} 1 & 1 & 0 \\ 0 & 1 & 1 \\ 1 & 0 & 1 \end{vmatrix} \cdot \begin{vmatrix} L_{13,12} \\ L_{21,23} \\ L_{32,31} \end{vmatrix} + \tfrac{1}{2} \begin{vmatrix} 1 & 0 \\ 0 & 1 \\ -1 & -1 \end{vmatrix} \cdot \begin{vmatrix} \Delta L_{1M} \\ \Delta L_{2M} \end{vmatrix} \qquad \text{(A36)}$$

$$= \tfrac{1}{2} \begin{vmatrix} -1 & 1 & 0 \\ 0 & -1 & 1 \\ 1 & 0 & -1 \end{vmatrix} \cdot \begin{vmatrix} L_{13,12} \\ L_{21,23} \\ L_{32,31} \end{vmatrix} + \tfrac{1}{2} \begin{vmatrix} 1 & -1 & 0 \\ 0 & 1 & -1 \\ -1 & 0 & 1 \end{vmatrix} \cdot \begin{vmatrix} L_{1M} \\ L_{2M} \\ L_{3M} \end{vmatrix} \qquad \text{(A37)}$$

However, in section 31 it was shown that

$$L_1 = L_{13,12}$$
$$L_2 = L_{21,23}$$
$$L_3 = L_{32,31} \qquad \text{(Equation 3.9)}$$

Where L_1, L_2, L_3 are the uncoupled fictitious inductances of the star equivalent circuit.

Therefore,

$$L_{3M,12} = \tfrac{1}{2}(L_2 - L_1) + \tfrac{1}{2}(L_{1M} - L_{2M})$$
$$L_{1M,23} = \tfrac{1}{2}(L_3 - L_2) + \tfrac{1}{2}(L_{2M} - L_{3M})$$
$$L_{2M,31} = \tfrac{1}{2}(L_1 - L_3) + \tfrac{1}{2}(L_{3M} - L_{1M}) \qquad \text{(A38)}$$

This is the same as equation A4.

A P P E N D I X B

INSTALLATION AND WIRING OF NEW MEASUREMENT SYSTEM

As discussed in Section 4.1.3 an arrangement for measurement of the electrode-to-bath voltages has been developed which results in a reduction in measurement errors. This is shown in Figure 4.5. Each phase voltage is measured by a connection to the electrode and to a neutral placed in the carbon lining under the electrode. A wire is brought up the side of the furnace from the neutral connection to a position close to the electrode. The measurement leads from the neutral and electrode connections are then taken by a multicore, twisted cable to the furnace control room. The details of the wiring arrangement for each electrode are shown in Figure B1.

The electrode voltage lead is connected by a clamping arrangement to one of the water-coolled bustubes situated around the electrode. This connection is below the smoke hood of the furnace and is in a very hot, harsh environment. As a result, all permanent cabling is situated in the cooler region above the smoke hood and a multistrand steel and copper cable wrapped in asbestos tape is connected between the bus-tube clamp and a connection box in the smoke hood. The connections for the flexible cable are arranged so that the cable can be replaced fairly quickly and easily if it is burnt away.

The neutral connections in the furnace lining are constructed from 316 stainless steel. The construction details of the neutrals which are installed in the 48 MVA ferrochromium furnace are shown in Figure B2(a). In more recent installations the construction arrangement shown in Figure B2(b) has been used. The latter arrangement has a better chance of lasting the life of the furnace lining since there are six separate connections to the carbon lining. The connections between the neutrals and junction boxes in the furnace shell consist of stainless steel bands (strapping) which are rivetted to the neutrals and connected through the refractory brick to insulated bolts in the furnace floor.

After six months of operation on the 48MVA ferrochromium furnace, the neutral connection under electrode 1 was lost. Fortunately, a spare neutral connection situated in the centre of the furnace lining between the three electrodes was available. This neutral was then used for all three phase voltage measurements. Kohle's theory (see Appendix A) shows that the errors in the measurement of electrode-to-bath voltages will be low if the self inductances of the loops formed by the measurement leads and the electrodes are the same for each phase. With a separate neutral connection under each electrode, the measurement loops for each phase are fairly independent of the position of the floating neutral in the furnace. However, with a centrally placed neutral connection the measurement loops are more sensitive to changes in the position of the neutral in the furnace. Therefore, the modification of the wiring to use the central neutral resulted in a reduction in the accuracy of the measurement system.

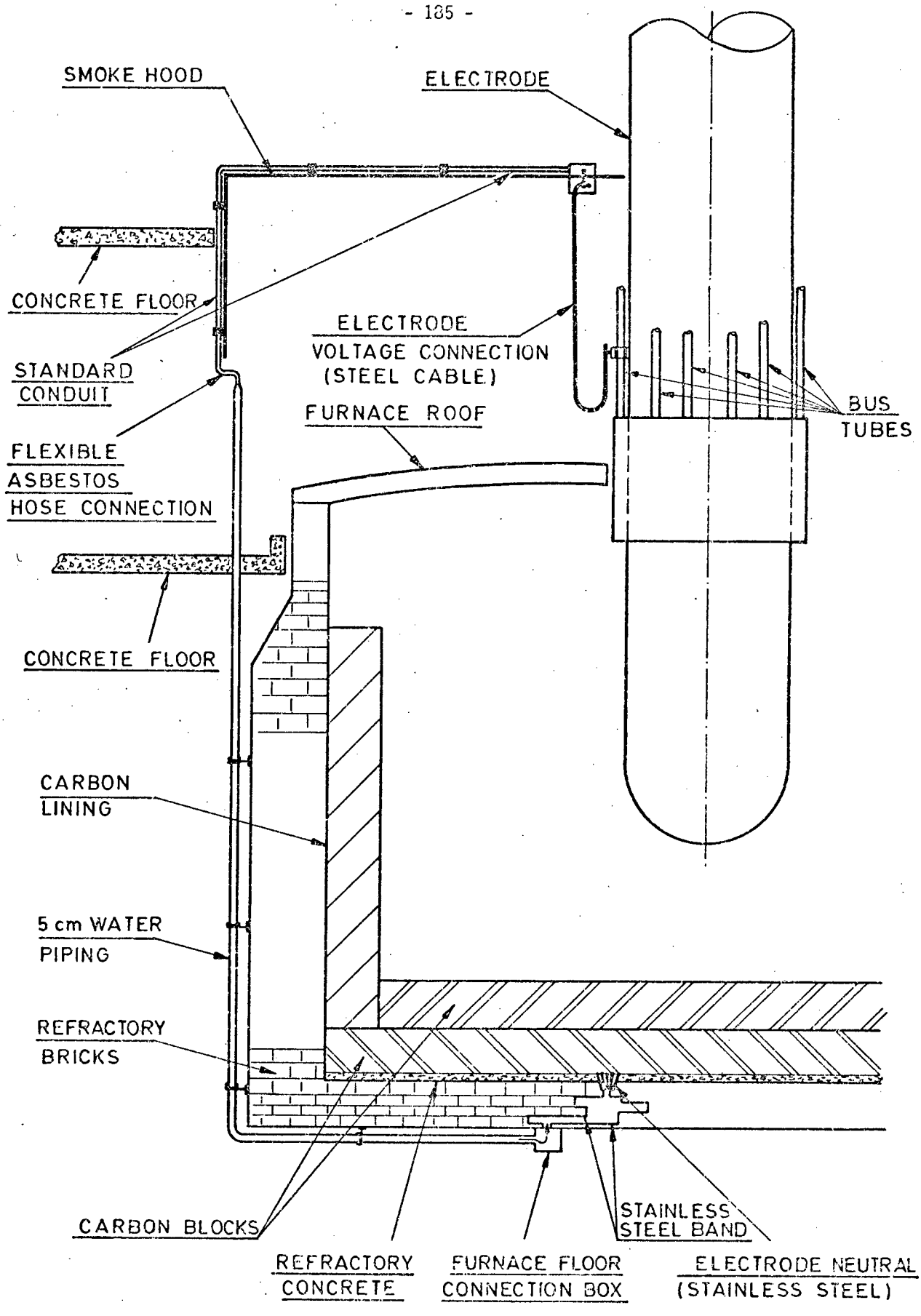

FIGURE B1 : ELECTRODE VOLTAGE AND NEUTRAL CONNECTION ON FURNACE.

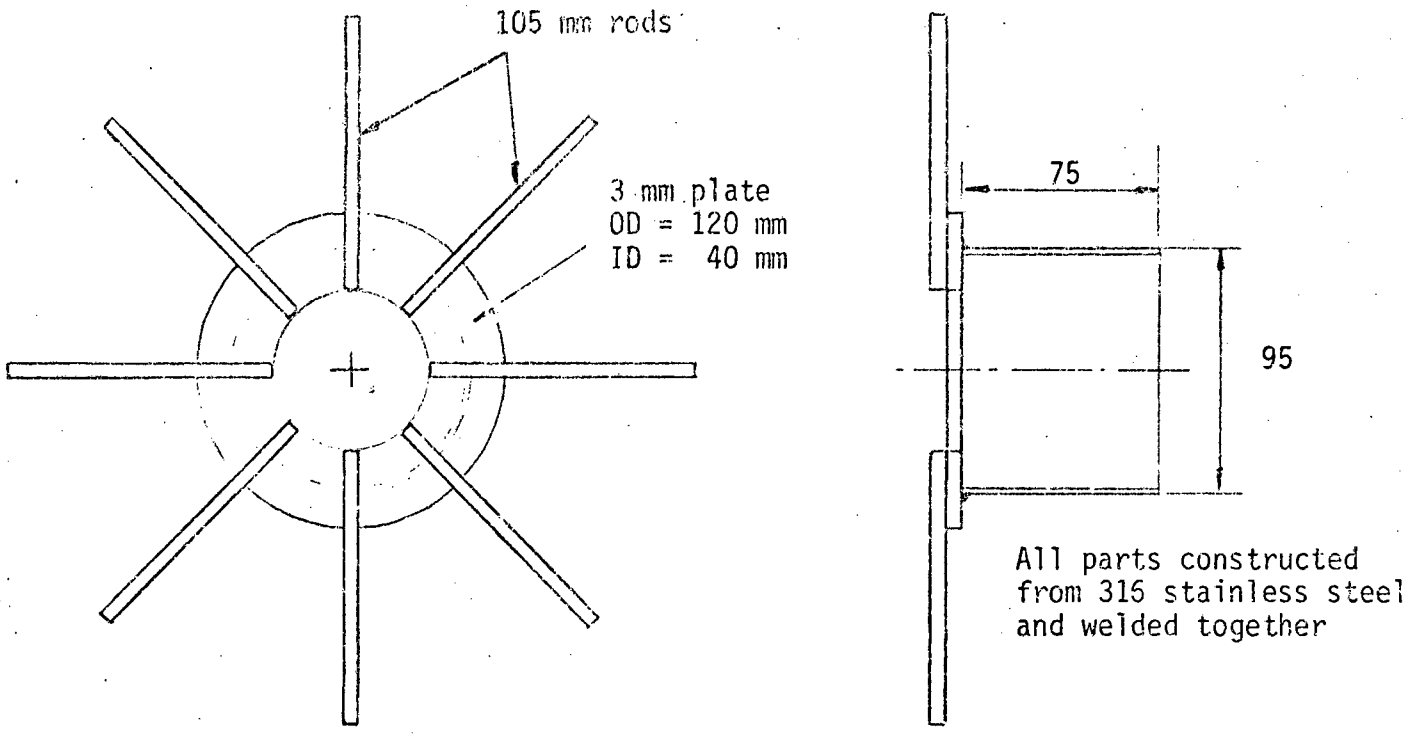

(a) Neutral construction (Mark 1)

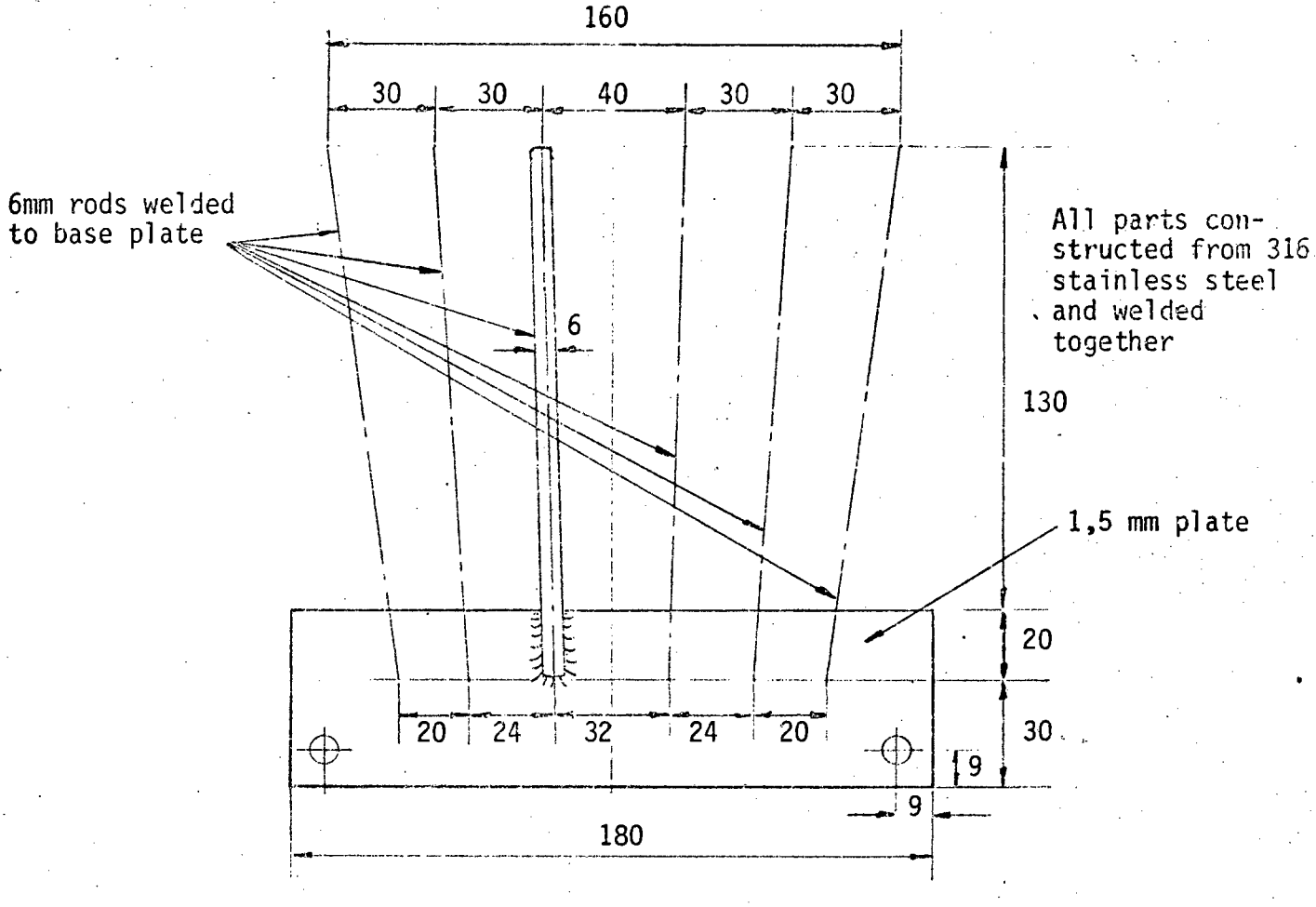

(b) Neutral construction (Mark 2)

FIGURE B2 : CONSTRUCTION OF NEUTRALS.

A P P E N D I X C

DERIVATION OF DATA FOR TABLE 4.3

Table 4.3 gives a comparison of the operating characteristics of a number of furnaces of different sizes where the data for 3 of the furnaces are taken from actual operating furnaces and the rest of the data are derived using formulae from Kelly[39] and Andraae[1] for deriving furnace operating characteristics. The data for the 3 furnaces are summarized in Table C1. The data for the other furnaces in Table 4.3 are based on the choice of electrode diameters which fill in the gaps between the known data. The currents are then derived using Kelly's formula

$$\text{electrode current density (amps/in}^2) = \frac{250}{\sqrt{D}} \qquad \text{(C1)}$$

where D is the electrode diameter in inches. The electrode current is given by electrode current = current density $*$ $\frac{\pi D^2}{4}$.

Kelly's formula represents the higher limit of electrode operating current and the operating currents of the 3 furnaces in Table C1 have been designed on the conservative side so that Kelly's constant of 250 has to be replaced by 225 (current set approximately at 90% of Kelly's limit). The operating currents for all the electrode diameters can thus be determined using the formula

$$\text{electrode current (kA)} = \frac{225*\pi}{4} * D^{1,5} \qquad \text{(C2)}$$

The resistances can be determined using Andraae's formula where

$$R\pi D = \text{const.} \quad (R = \text{resistance, } D = \text{diameter}) \qquad \text{(C3)}$$

If R is in milliohms and D in cms then the constant for the three known furnaces is approximately 640. Thus the resistances can be determined using the equation

$$\text{resistance (m}\Omega) = \frac{640}{\pi D} \qquad \text{(C4)}$$

where D = electrode diameter (cms)

There is no definite formula for determining the reactances of various sizes of furnace, however, a plot of the three known reactances against electrode diameter gives a fairly good straight line as shown in Figure C1. The unknown reactances have been derived from this graph. With the reactances, resistances and currents the remaining data in Table 4,3 can be derived using standard electrical circuit formulae.

Phase impedance, $Z = \sqrt{R^2 + X^2}$ (C5)

line voltage, $V_L = \sqrt{3} \cdot I \cdot Z$ (C6)

real power, $P = 3 \cdot I^2 \cdot R$ (C7)

reactive power, $Q = 3 \cdot I^2 \cdot X$ (C8)

apparent power, $S = \sqrt{P^2 + Q^2}$ (C9)

Trans-former rating MVA	Electrode diameter (cms)	Electrode current (nominal) kA	Resist-ance mΩ	Reactance mΩ	Operating Voltage (line) Volts
9	85	35	2,4	0,5	145
16	110	50	1,85	0,68	172
48	170	100	1,2	1,1	275

TABLE C1 : Operating characteristics of typical furnaces producing charged chrome

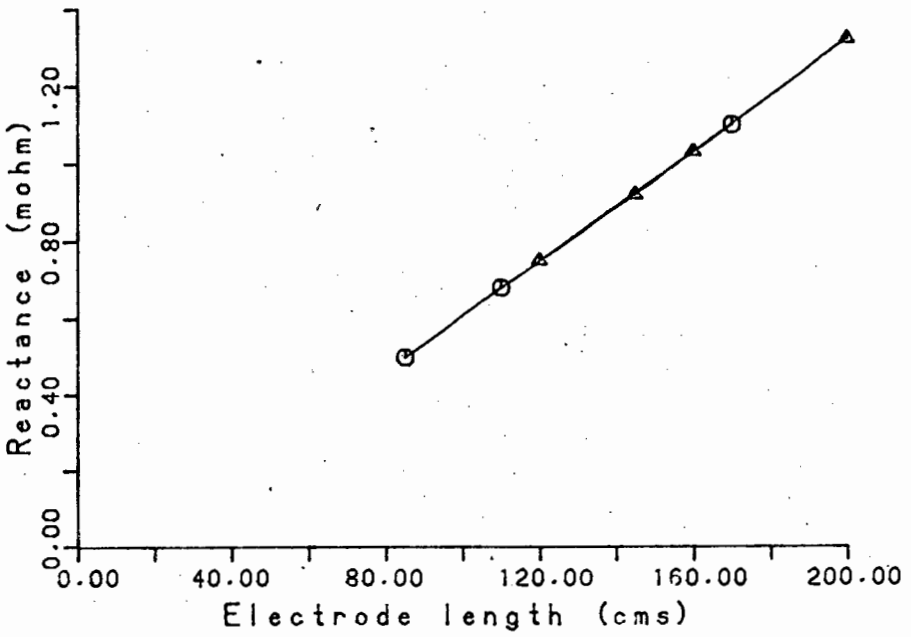

FIGURE C1 : PLOT OF ELECTRODE LENGTHS AGAINST FURNACE REACTANCE

APPENDIX D

SINGLE-PHASE CIRCUIT WITH ARCING

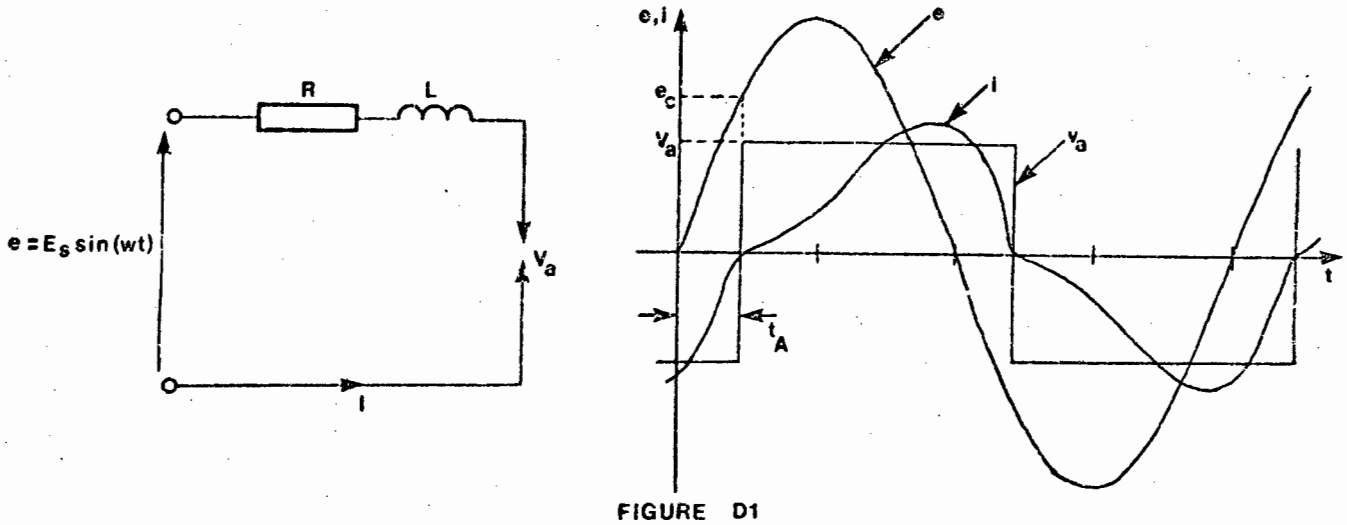

FIGURE D1

The single-phase circuit with arcing can be considered as being represented by three elements; a resistance R, a reactance L, and an arc V_a. These are driven by a purely sinusoidal source voltage e and the arc is represented by a square wave in phase with the current waveform with peak voltage equal to the arc striking voltage V_a. The resulting waveforms are shown above. The inductance in the circuit causes the current waveform to lag the voltage waveform by a time t_A so that when the current waveform passes through zero the voltage waveform is at a point where the voltage is equal to e_c. If this voltage is greater than the striking voltage of the arc V_a, the arc will restrike immediately at $t = t_A$ resulting in a continuous current waveform. Alternatively, if V_a is greater than e_c no current will flow until there is sufficient voltage available to restrike the arc. These two modes of arcing are usually described as non-extinction and extinction operation respectively. In the operation of large submerged-arc furnaces the inductances in the circuit are relatively high and with the arc striking voltages usually encountered, there is no extinction of the arcs. The analysis that follows will, therefore only consider the continuous or non-extinction arc operation.

The arc voltage waveform can be described mathematically by a constant voltage, V_a, whose sign is dependent on the sign of the current waveform, so that the differential equation for the circuit is:

$$L\frac{di}{dt} + iR + V_a(\text{sign } i) = E_s \sin wt \qquad D1$$

which can be rearranged as

$$\frac{di}{dt} + \frac{R}{L} i = \frac{1}{L}\left[E_s \sin wt - V_a (\text{sign } i)\right] \qquad D2$$

This is an equation of the form

$$\frac{dy}{dx} + Py = Q \qquad D3$$

where P and Q are functions of x and can be solved using the integrating factor $\rho = e^{\int P dx}$ with a solution of the form

$$\rho y = \int \rho Q dx + C \qquad D4$$

Applying this to D2 gives

$$e^{\frac{Rt}{L}} . i = \int \frac{e^{\frac{Rt}{L}}}{L} . E_s . \sin wt . dt - \int \frac{e^{\frac{Rt}{L}}}{L} . V_a(\text{sign } i) . dt + C \qquad D5$$

From standard integration tables

$$\int e^{ax} \sin bx \, dx = \frac{e^{ax}(a \sin bx - b \cos bx)}{a^2 + b^2} + C \qquad D6$$

Applying this to the first term of D5

$$\int \frac{e^{\frac{Rt}{L}}}{L} . E_s . \sin wt . dt = \frac{E_s}{L} . e^{\frac{Rt}{L}} . \frac{(\frac{R}{L} \sin wt - w \cos wt)}{(\frac{R}{L})^2 + w^2} \qquad D7$$

$$= E_s . e^{\frac{Rt}{L}} . \frac{R \sin wt - wL \cos wt}{R^2 + (wL)^2} + C \qquad D8$$

Introducing $Z^2 = R^2 + (wL)^2$ and $\tan \Theta = \frac{wL}{R}$

$$= \frac{E_s}{Z} . e^{\frac{Rt}{L}} . \sin (wt - \Theta) + C \qquad D9$$

Considering the second term of D5

$$\int \frac{e^{\frac{Rt}{L}}}{L} . V_a(\text{sign } i)\, dt = \frac{1}{R} . \frac{e^{\frac{Rt}{L}}}{L} . V_a(\text{sign } i) + C \qquad D10$$

$$= \frac{e^{\frac{Rt}{L}}}{R} \cdot V_a(\text{sign } i) + C \qquad \text{D11}$$

Substituting D9 and D11 back into D5

$$i = \frac{E_s}{z} \cdot \sin(wt-\theta) - \frac{V_a}{R}(\text{sign } i) + Ce^{-\frac{R_t}{L}} \qquad \text{D12}$$

The boundary conditions for the integration are:

$i = 0$ at $t = t_A$ and $t = t_A + \frac{\Pi}{w}$ for the positive current half cycle and:

$i = 0$ at $t = t_A + \frac{\Pi}{w}$ and $t = t_A + \frac{2\Pi}{w}$ for the negative current half cycle.

Considering the positive half cycle

$$C = \frac{2.E_s}{Z} \cdot \sin(wt_A - \theta) \cdot \frac{e^{\frac{Rt_A}{L}}}{\left(e^{\frac{-R\Pi}{X}} - 1\right)} \qquad \text{D13}$$

and

$$\sin(wt_A - \theta) = \frac{V_a Z}{E_s . R} \cdot \frac{(e^{\frac{-R\Pi}{X}} - 1)}{\left(e^{\frac{-R\Pi}{X}} + 1\right)} \qquad \text{D14}$$

where $X = wL$

Therefore

$$i = \frac{E_s}{Z} \cdot \sin(wt-\Theta) - \frac{V_a}{R} + \frac{2.E_s.\sin(wt_A-\Theta)}{Z} \cdot \frac{e^{\frac{R}{L}(t_A-t)}}{\left(e^{\frac{-R\Pi}{X}} - 1\right)} \qquad \text{D15}$$

For the negative half cycle

$$C = -\frac{2.E_s}{Z} \cdot \sin(wt_A - \theta) \cdot \frac{e^{\frac{Rt_A}{L}}}{e^{\frac{-R\Pi}{X}}\left(e^{\frac{-R\Pi}{X}} - 1\right)} \qquad \text{D16}$$

The average current for a half cycle can be determined from

$$i_{av} = \frac{w}{\Pi}\int_{t_A}^{t_A+\frac{\Pi}{w}} i.dt \qquad D17$$

so that

$$i_{av} = \frac{w}{\Pi}\left\{\left[\frac{-E_s\cos(wt-\theta)}{wZ} - \frac{V_a t}{R} - 2E_s.\sin(wt_A-\theta).\frac{L}{R}.e^{\frac{R}{L}(t_A-t)}\right]_{t_A}^{t_A+\frac{\Pi}{w}}\right\} \qquad D18$$

$$= \frac{2E_s}{\Pi R}\left[\frac{R.\cos(wt_A-\theta) - wL\sin(wt_A-\theta)}{Z}\right] - \frac{V_a}{R} \qquad D19$$

$$= \frac{2E_s\cos wt_A}{\Pi R} - \frac{V_a}{R} \qquad D20$$

The arc power is simply the product of the average current and the arc voltage, so that

$$P_{arc} = \frac{2.E_s.V_a.\cos wt_A}{\Pi R} - \frac{V_a^2}{R} \qquad D21$$

SINGLE-PHASE CIRCUIT WITH ARCING AND NO RESISTANCE

The special hypothetical case of single-phase arcing with no resistance is useful to analyse since the equations are much simpler than for the case where resistance is present in the circuit. The equation for the current can be derived very easily from D1 by ignoring the resistance term. However, as an exercise in comparison, the equations derived above will be used as a starting point. From D14

$$\sin(wt_A-\theta) = \frac{V_a Z}{E_s.R}.\frac{\left(e^{\frac{-R\Pi}{x}}-1\right)}{\left(e^{\frac{-R\Pi}{x}}+1\right)}$$

For small y, e^{y} approaches 1 + y

so that as R → 0 $\quad e^{\frac{-R\Pi}{X}}+1$ approaches $\frac{R\Pi}{X}$

and $\quad e^{\frac{-R\Pi}{X}}+1$ approaches 2

Using this

$$\sin(wt_A-\theta) = \frac{V_a.Z}{E_s.R} \cdot - \frac{R\Pi}{X} \cdot \frac{1}{2} \quad \text{for small R}$$

Also for small R, Z approaches X

and tan θ approaches infinity so that $\theta = \frac{\Pi}{2}$

Therefore at the limit where R = 0

$$\sin\left(wt_A - \frac{\Pi}{2}\right) = \frac{V_a\Pi}{2E_s}$$

$$\cos wt_A = \frac{V_a\Pi}{2E_s} \qquad \text{D22}$$

The equation for the current can be derived from D15 where

$$i = \frac{E_s}{Z} \cdot \sin(wt-\theta) - \frac{V_a}{R} + \frac{Z.E_s \sin(wt_A-\theta)}{Z} \cdot \frac{e^{\frac{R}{L}(t_A-t)}}{\left(e^{\frac{-R\Pi}{X}}-1\right)} \qquad \text{D23}$$

Using D14 rearranged in terms of $\frac{V_a}{R}$

$$i = \frac{E_s}{Z}\sin(wt-\theta) - \frac{E_s.\sin(wt_A-\theta)}{Z.\left(e^{\frac{-R\Pi}{X}}-1\right)} \cdot \left[e^{\frac{-R\Pi}{X}} + 1 - 2e^{\frac{R}{L}(t_A-t)}\right] \qquad \text{D24}$$

for R → 0 $\quad \theta \to \frac{\Pi}{2}$, $\quad z \to X$, $\quad e^{\frac{-R\Pi}{X}} \to 1 - \frac{R\Pi}{X}$

and $e^{\frac{R}{L}(t_A-t)} \to 1 + \frac{R}{L}(t_A-t)$

so that

$$i = -\frac{E_s \cos wt}{X} + \frac{E_s \cos wt_A}{X \cdot (\frac{-R\Pi}{X})} \cdot \left\{ 2 - \frac{R\Pi}{X} - 2\left[1 + \frac{R}{L}(t_A - t)\right] \right\} \qquad D25$$

and using D22

$$i = -\frac{E_s \cos wt}{X} + \frac{V_a}{L}(t_A - t) + \frac{V_a \Pi}{2X} \qquad D26$$

FREQUENCY DOMAIN ANALYSIS OF SINGLE-PHASE CIRCUIT WITH ARCING

The arc voltage waveform can be described mathematically in the frequency domain as a Fourier series of the form

$$v_a = \frac{4V_a}{\Pi} \sum_{n=o}^{\infty} \frac{\sin\left[(2n+1)w(t-t_A)\right]}{2n+1} \qquad D27$$

Rewriting D1 gives

$$L\frac{di}{dt} + iR + \frac{4V_a}{\Pi} \sum_{n=o}^{\infty} \frac{\sin\left[(2n+1)w(t-t_A)\right]}{2n+1} = E_s \sin wt \qquad D28$$

Applying the same integration technique as before

$$i.e^{\frac{Rt}{L}} = \int \frac{e^{\frac{Rt}{L}}}{L} \cdot E_s . \sin wt . dt - \int \frac{e^{\frac{Rt}{L}}}{L} \cdot \frac{4V_a}{\Pi} \sum_{n=o}^{\infty} \frac{\sin\left[(2n+1)w(t-t_A)\right]}{2n+1} . dt + C$$

D29

Considering the second term of D29 and using D6

$$= \frac{4V_a}{\Pi} \cdot e^{\frac{Rt}{L}} \cdot \frac{1}{L} \sum_{n=o}^{\infty} \cdot \frac{1}{2n+1} \cdot \frac{\{\frac{R}{L}\sin\left[(2n+1)w(t-t_A)\right]\} - (2n+1)w \cos\left[(2n+1)w(t-t_A)\right]}{(\frac{R}{L})^2 + \left[(2n+1)w\right]^2} + C$$

D30

Introducing $Z_n^2 = R^2 + \left[(2n+1)wL\right]^2$ and $\tan\theta_n = \frac{(2n+1)wL}{R}$

$$= \frac{4V_a}{\Pi} \cdot e^{\frac{Rt}{L}} \cdot \sum_{n=o}^{\infty} \frac{\left[\sin (2n+1)w(t-t_A) - \theta_n\right]}{(2n+1) \cdot Zn} + C \qquad D31$$

The first term of D29 is given by D8 so that

$$i = \frac{E_s}{Z}\sin(wt-\theta) - \frac{4V_a}{\Pi}\sum_{n=o}^{\infty}\frac{\sin\left[(2n+1)w(t-t_A)-\theta_n\right]}{(2n+1).Z_n} + Ce^{\frac{-Rt}{L}} \qquad D32$$

The constant C will be zero under steady state conditions. The value of t_A can be determined by noting that $i = 0$ at $t = t_A$ so that

$$0 = \frac{E_s}{Z}.\sin(wt_A-\theta) - \frac{4V_a}{\Pi}\sum_{n=o}^{\infty}\frac{\sin(-\theta_n)}{(2n+1).Zn} \qquad D33$$

$$\sin(wt_A-\theta) = \frac{-4V_a.Z}{\Pi E_s}.\sum_{n=o}^{\infty}\frac{wL}{Z_n^2} \qquad D34$$

For the special case where $R=0$, $Z=X$, $\theta = \frac{\Pi}{2}$, $Z_n=(2n+1)X$, $\theta_n = \frac{\Pi}{2}$

and

$$i = -\frac{E_s}{x}\cos wt + \frac{4V_a}{\Pi X}\sum_{n=o}^{\infty}\cos\frac{\left[(2n+1)w(t-t_A)\right]}{(2n+1)^2} \qquad D35$$

APPENDIX E

KASPER AND JAHN'S EQUIVALENT CIRCUIT WITH ARCING

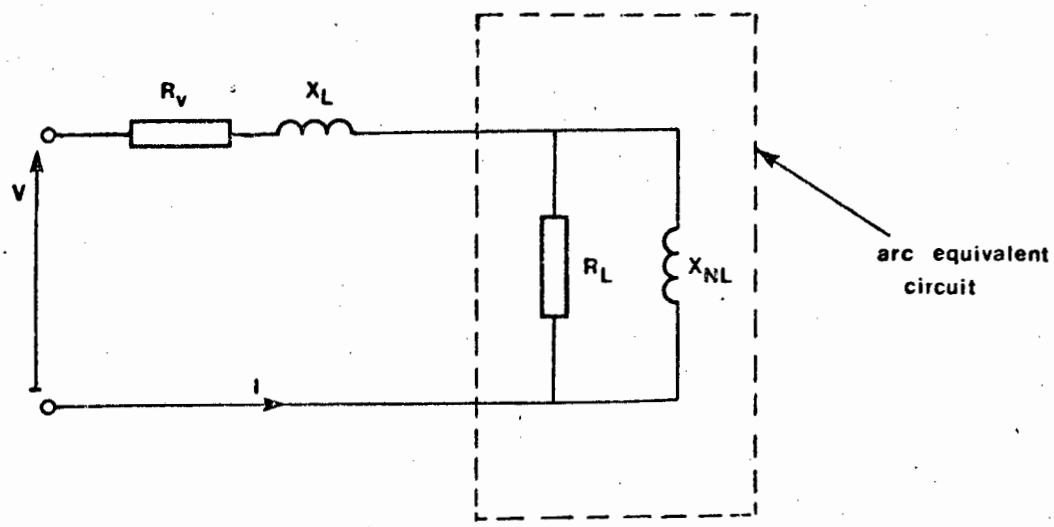

Kasper and Jahn's equivalent circuit for an arc consists of a resistance and reactance in parallel as shown above. The impedance of the arc circuit is given by:

$$Z_{arc} = \frac{X_{NL}^2 . R_L}{R_L^2 + X_{NL}^2} + j\left(\frac{X_{NL} . R_L^2}{R_L^2 + X_{NL}^2}\right)$$

Combining this with R_V and X_L gives the total circuit impedance as

$$Z_T = \left(R_V + \frac{X_{NL}^2 . R_L}{R_L^2 + X_{NL}^2}\right) + j\left(X_L + \frac{X_{NL} R_L^2}{R_L^2 + X_{NL}^2}\right) \qquad E2$$

From this

$$\text{current, } I = \frac{V}{Z_T} \qquad E3$$

$$\text{real power, } P = I^2\left(R_V + \frac{X_{NL}^2 . R_L}{R_L^2 + X_{NL}^2}\right) \qquad E4$$

$$\text{Apparent power, } S = V.I \qquad E5$$

$$\text{reactive power, } Q = \sqrt{S^2 - P^2} \qquad E6$$

The power circle diagram is determined by varying R_L between zero and a large value and plotting P against Q for each value of R_L. The value of X_{NL} can be determined from the equation

$$X_{NL} = \frac{\sigma}{1-\sigma} \cdot X_L \qquad E7$$

where σ represents the type of arcing present. If the arc is assumed to be a square wave, then

$$\sigma = \frac{8}{\pi 2} = 0,8119$$

for single-phase arcing. For this case

$$X_{NL} = 4,28\ X_L$$

A P P E N D I X F

BARKER'S ARCING EQUATION

Barker's arcing equation is the same as the power operating characteristic of a furnace with the exception that a constant k is introduced which describes the type of arcing waveform assumed. The equation is

$$P = k\, X_L . I_{rms} \sqrt{I_{max}^2 - I_{rms}^2} \qquad F1$$

The power circle diagram can be determined for a range of currents if the source voltage, V (rms), circuit reactance X_L and constant k are known, since

$$I_{max} = \frac{V_{rms}}{X_L}$$

apparent power, $S = V_{rms} \cdot I_{rms}$

reactive power, $Q = \sqrt{S^2 - P^2}$

The constant k is the same as Kasper and Jahn's constant σ and $k = \frac{8}{\pi^2}$ for single-phase operation.

THEORETICAL BASIS FOR BARKER'S EQUATION

The arc power in a single-phase circuit can be derived from the average of the product of the arc voltage, V_a and the arc current, i, so that

$$P_{arc} = \frac{w}{\pi} \int_{t_A}^{t_A + \frac{\pi}{w}} v_a . i \, dt \qquad F2$$

The derivation of the arc power that follows will be based on the equations for single-phase circuit arcing with no resistance as this simplifies the analysis

From D27

$$v_a = \frac{4V_a}{\pi} \sum_{n=o}^{\infty} \frac{\sin (2n+1)w(t-t_A)}{2n+1}$$

and from D35

$$i = \frac{-E_s \cos wt}{X} + \frac{4V_a}{\pi X} \sum_{n=o}^{\infty} \frac{\cos\left[(2n+1)w(t-t_A)\right]}{(2n+1)^2}$$

Considering the 50 Hz component

$$i_{50} = \frac{-E_s \cos wt}{X} + \frac{4V_a}{\pi X} \cdot \cos w\,(t-t_A) \qquad F3$$

This can be converted to terms of sin $w(t-t_A)$ and cos $w(t-t_A)$ by replacing wt by $wt_A + w(t-t_A)$

$$i_{50} = \frac{-E_s}{X} \cos\left[wt_A + w(t-t_A)\right] + \frac{4V_a}{\pi X} \cos w(t-t_A) \qquad F4$$

$$= \frac{\frac{4V_a}{\pi} - E_s \cos wt_A}{X} \cdot \cos w(t-t_A) + \frac{E_s}{X} \sin wt_A . \sin w(t-t_A) \qquad F5$$

$$= A \cos w(t-t_A) + B \sin w(t-t_A) \qquad F6$$

This gives the 50 Hz arc power as

$$P_{50} = \frac{w}{\pi} \int_{t_A}^{t_A+\frac{\pi}{w}} \left[A \cos w(t-t_A) + B \sin w(t-t_A)\right] . \frac{4V_a}{\pi} \sin w(t-t_A).dt \qquad F7$$

Now

$$\int_o^{\frac{\pi}{w}} \sin wt.\cos wt\, dt = o \quad \text{and} \quad \int_o^{\frac{\pi}{w}} \sin^2 wt\, dt = \frac{\pi}{2w} \qquad F8$$

so that

$$P_{50} = \frac{w}{\pi} \frac{E_s}{X} \sin w\, t_A \cdot \frac{4V_a}{\pi} \cdot \frac{\pi}{2w} \qquad F9$$

Considering the higher harmonics

$$i_n = \frac{4V_a}{\pi X} \sum_{n=o}^{\infty} \frac{\cos\left[(2n+1)w(t-t_A)\right]}{(2n+1)^2} \qquad F10$$

$$v_n = \frac{4V_a}{\Pi} \sum_{n=o}^{\infty} \sin \frac{\sin \left[(2n+1)w(t-t_A)\right]}{(2n+1)} \qquad \text{F11}$$

$$P_n = \frac{w}{\Pi} \int_{t_A}^{t_A+\frac{\Pi}{w}} \text{constant X (product of a sin and cos term)} dt. \qquad \text{F12}$$

$$= 0$$

so that total arc power is

$$P_{arc} = \frac{2 V_a E_s \sin wt_A}{\Pi X} \qquad \text{F13}$$

This equation can be converted to the form

$$P = k X_L I_{rms} \sqrt{I_{max}^2 - I_{rms}^2}$$

if I_{rms} is the rms value of the current which contributes towards the arc power, i.e., the component which is in phase with the arc voltage

$$I_{\text{in phase}} = \frac{E_s}{X} \sin wt_A \sin w(t-t_A) \qquad \text{F14}$$

Computing the rms value

$$I_{\text{in phase (rms)}} = \frac{E_s}{2.X} \sin wt_A \qquad \text{F15}$$

From D22

$$V_a = \frac{2E_s \cos wt_A}{\Pi}$$

so that from F13

$$P_{arc} = \frac{2E_s \cos wt_A}{\Pi} \cdot \frac{2.E_s \sin wt_A}{\Pi X} \qquad \text{F16}$$

$$= \cos wt_A \cdot \frac{2E_s}{\Pi} \cdot \frac{2}{\Pi} \cdot \sqrt{2} \cdot I_{\text{in phase (rms)}} \qquad \text{F17}$$

$$= \sqrt{1-\sin^2 wt_A} \cdot \frac{8}{\Pi^2} \cdot \frac{E_s}{\sqrt{2}} \cdot I_{\text{in phase (rms)}} \qquad \text{F18}$$

$$= \sqrt{\left(\frac{E_s}{\sqrt{2}\,X}\right)^2 - \left(\frac{E_s}{\sqrt{2}\,X}\right)^2 \cdot \sin^2 wt_A} \cdot \frac{\sqrt{2}\,X}{E_s} \cdot \frac{8}{\pi^2} \cdot \frac{E_s}{\sqrt{2}} \cdot I_{\text{in phase (rms)}} \quad \text{(F19)}$$

$$= \frac{8}{\pi^2} \cdot X \cdot I_{\text{in phase (rms)}} \sqrt{I_{max}^2 - I_{\text{in phase (rms)}}^2} \quad \text{(F20)}$$

which is the same as F1. This results in a power characteristic which does not agree with the true power operating characteristic over the entire range, however, it does agree sufficiently over the operating region of interest.

REACTANCES IN A SINGLE-PHASE CIRCUIT USING BARKER'S EQUATION

Barker's equation can be used to convert the total reactance in a single-phase circuit with arcing to the reactance dependent on the furnace geometry and an arc reactance. Barker's equation gives

$$P = k X_L . I \sqrt{I_{max}^2 - I^2} \qquad I_{max} = \frac{V}{X_L}$$

Comparing this with an equivalent circuit containing resistance and reactance only

$$P = X_L\, I \sqrt{I'^2_{max} - I^2} \qquad I'_{max} = \frac{V}{X}$$

Equating these two equations

$$k^2 x_L^2 I^2(I_{max}^2 - I^2) = X^2 I^2(I'^2_{max} - I^2) \quad \text{F21}$$

$$V^2(k^2-1) = I^2(k^2 X_L^2 - X^2)$$

$$= I^2 k^2(X_L^2 - X^2) + X^2(k^2-1) \quad \text{F22}$$

Now $\frac{V}{I} = Z = \sqrt{R^2 + X^2}$

so that $(R^2 + X^2)(k^2-1) = k^2(X_L^2 - X^2) + X^2(k^2-1)$ F23

$$R^2(k^2-1) = k^2(X_L^2 - X^2)$$

$$X^2 = X_L^2 + \left(\frac{1-k^2}{k^2}\right).R^2 \quad \text{F24}$$

This provides a means for determining the inductive reactance X_L by measuring R and X if k is known

A P P E N D I X G :

THREE-PHASE CIRCUIT WITH ARCING

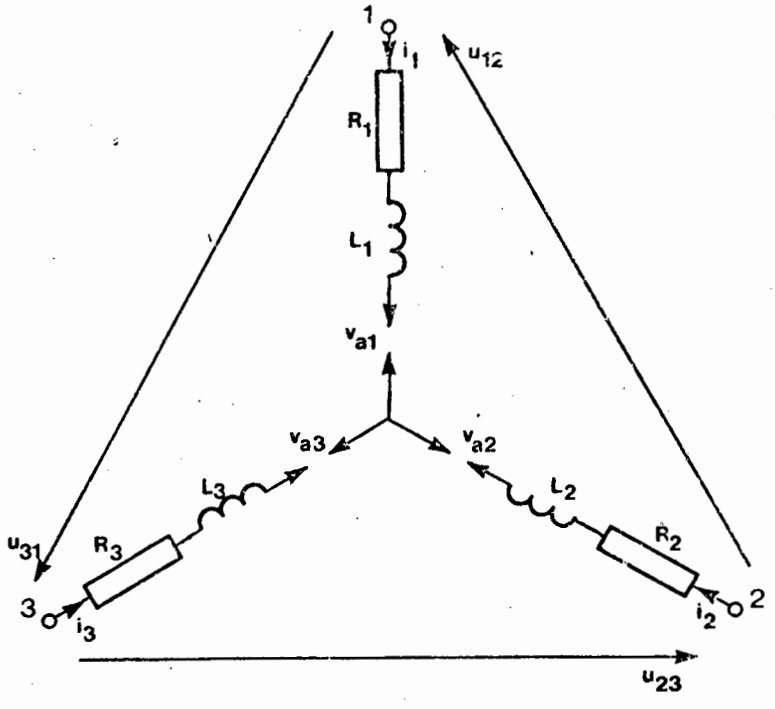

The equivalent circuit for a three-phase star circuit which includes arcing is shown above. Each phase consists of a resistance, an inductance, and an arc. The voltage sources u_{12}, u_{23} and u_{31} are assumed to be displaced α electrical degress in time and the sources are assumed to have negligible source impedances (i.e., an 'infinite bus' provides power to the furnace). The angle α is usually assumed to be equal to 120^{o}. Applying Kirchoff's laws the circuit equations can be written as

$$L_1 \frac{di_1}{dt} + i_1 R_1 + va_1 - L_2 \frac{di_2}{dt} + i_2 R_2 + va_2 = u_{12} \qquad G1$$

$$L_2 \frac{di_2}{dt} + i_2 R_2 + va_2 - L_3 \frac{di_3}{dt} + i_3 R_3 + va_3 = u_{23} \qquad G2$$

$$i_1 + i_2 + i_3 = 0 \qquad G3$$

Choosing u_{12} as the reference phasor the line voltages are

$$\begin{aligned} u_{12} &= U_{12} \sin wt \\ u_{23} &= U_{23} \sin (wt - \alpha) \\ u_{31} &= u_{12} + u_{23} \end{aligned} \qquad G4$$

Differentiating G3 gives

$$\frac{di_3}{dt} = -\frac{di_1}{dt} - \frac{di_2}{dt} \qquad \text{G5}$$

Substituting G3 and G5 back in G2 gives the set of equations

$$(L_1 \frac{di_1}{dt} + i_1R_1) - (L_2 \frac{di_2}{dt} + i_2R_2) = u_{12} - v_{a_1} + v_{a_2}$$

$$(L_3 \frac{di_1}{dt} + i_1R_3) + [(L_2+L_3)\frac{di_2}{dt} + (R_2+R_3)i_2] = u_{23} - v_{a_2} + v_{a_3} \qquad \text{G6}$$

The solution of these equations in this form is complex. They can, however, be simplified by assuming that the resistances R_1, R_2 and R_3 and the inductances L_1, L_2 and L_3 are each equal. This is a reasonable assumption since in this analysis we are interested in looking at the effects of arcing on the circuit, and allowing for variations in the individual resistances and reactances introduces unnecessary extra variables. Using these assumptions the equations simplify to

$$(L \frac{di_1}{dt} + i_1R) - (L \frac{di_2}{dt} + i_2R) = u_{12} - v_{a_1} + v_{a_2} \qquad \text{G7}$$

$$(L \frac{di_1}{dt} + i_1R) + 2\,(L \frac{di_2}{dt} + i_2R) = u_{23} - v_{a_2} + v_{a_3} \qquad \text{G8}$$

Multiplying G7 by 2 and adding

$$(L \frac{di_1}{dt} + i_1R) = \frac{1}{3}\,[2u_{12} + u_{23} - 2va_1 + v_{a_2} + v_{a_3}] \qquad \text{G9}$$

Subtracting G7 from G8

$$(L \frac{di_2}{dt} + i_2R) = \frac{1}{3}\,[-u_{12} + u_{23} + v_{a_1} - 2v_{a_2} + v_{a_3}] \qquad \text{G10}$$

These equations are similar in form to the single phase equations and can be solved in the same way, so that

$$e^{\frac{Rt}{L}} \cdot i_1 = \frac{1}{3L} \int e^{\frac{Rt}{L}} (2u_{12} + u_{23} - 2v_{a_1} + v_{a_2} + v_{a_3})dt$$

$$e^{\frac{Rt}{L}} \cdot i_2 = \frac{1}{3L} \int e^{\frac{Rt}{L}} (-u_{12} + u_{23} + v_{a_1} - 2v_{a_2} + v_{a_3})dt \qquad \text{G11}$$

Introducing $Z^2 = R^2 + (wL)^2$ and $\tan \theta = \frac{wL}{R}$, the line voltage terms in G11 yield solutions which are similar to the single-phase case (see D9).

$$\frac{1}{3L} \int e^{\frac{Rt}{L}} (2u_{12} + u_{23}) = \frac{e^{\frac{Rt}{L}}}{Z} [2U_{12} \sin(wt-\theta) + U_{23} \sin (wt-\alpha-\theta)] + C \qquad \text{G12}$$

$$\frac{1}{3L} \int e^{\frac{Rt}{L}} (-u_{12} + u_{23}) = \frac{e^{\frac{Rt}{L}}}{Z} [-U_{12} \sin(wt-\theta) + U_{23} \sin (wt-\alpha-\theta)] + C \qquad \text{G13}$$

Considering now the arc voltages these can be represented by the Fourier series where t_1, t_2 and t_3 are the zero crossing times for each arc voltage.

$$v_{a_1} = \frac{4V_{a_1}}{\Pi} \sum_{n=\sigma}^{\infty} \frac{\sin[(2n+1)w(t-t_1)]}{2n+1} + C \qquad \text{G15}$$

$$v_{a_2} = \frac{4V_{a_2}}{\Pi} \sum_{n=o}^{\infty} \frac{\sin[(2n+1)w(t-t_2)]}{2n+1} \qquad \text{C14}$$

$$v_{a_3} = \frac{4V_{a_3}}{\Pi} \sum_{n=o}^{\infty} \frac{\sin[(2n+1)w(t-t_3)]}{2n+1}$$

Once again the single-phase case is similar and considering the v_{a_1} term (see D31)

$$= \frac{1}{3L} \int e^{\frac{Rt}{L}} \cdot \frac{4V_{a_1}}{\Pi} \sum_{n=o}^{\infty} \frac{\sin[(2n+1)w(t-t_1)].dt}{2n+1}$$

$$= e^{\frac{Rt}{L}} \cdot \frac{4V_{a_1}}{\Pi} \sum_{n=o}^{\infty} \frac{\sin[(2n+1)w(t-t_1) - \theta_n]}{(2n+1)Z_n} + C \qquad \text{G15}$$

where $Z_n^2 = R^2 + [(2n+1)wL]^2$

and $\tan \theta_n = \frac{(2n+1)wL}{R}$

The integration of the other arcing terms is similar.

The final solution is therefore

$$i_1 = \frac{1}{3}\left\{\frac{1}{Z}\left[2U_{12}\sin(wt-\theta) + U_{23}\sin(wt-\alpha-\theta)\right] - \frac{8V_{a_1}}{\Pi}\sum_{n=o}^{\infty}\frac{\sin\left[(2n+1)w(t-t_1)-\theta_n\right]}{(2n+1)Z_n} + \right.$$

$$\left.\frac{4V_{a_2}}{\Pi}\sum_{n=o}^{\infty}\frac{\sin\left[(2n+1)w(t-t_2)-\theta_n\right]}{(2n+1)Z_n} + \frac{4V_{a_3}}{\Pi}\sum_{n=o}^{\infty}\frac{\sin\left[(2n+1)w(t-t_3)-\theta_n\right]}{(2n+1)Z_n}\right\} + C_1 e^{\frac{-Rt}{L}}$$

$$i_2 = \frac{1}{3}\left\{\frac{1}{Z}\left[-U_{12}\sin(wt-\theta)+U_{23}\sin(wt-\alpha-\theta)\right] + \frac{4V_{a_1}}{\Pi}\sum_{n=o}^{\infty}\frac{\sin\left[(2n+1)w(t-t_1)-\theta_n\right]}{(2n+1)Z_n} - \right.$$

$$\left.\frac{8Va_2}{\Pi}\sum_{n=o}^{\infty}\frac{\sin\left[(2n+1)w(t-t_2) - \theta_n\right]}{(2n+1)\,Z_n} + \frac{4Va_3}{\Pi}\sum_{n=o}^{\infty}\frac{\sin\left[(2n+1)w(t-t_3)-\theta_n\right]}{(2n+1)Z_n}\right\} + C_2 e^{\frac{-Rt}{L}}$$

$$i_3 = -i_1 - i_2 \qquad \text{G16}$$

For steady-state conditions C_1 and C_2 are zero.

The equations G16 are still not in a form where they can be used, since the zero crossing times t_1, t_2 and t_3 are unknown. The solution of these times based on the initial conditions is not an easy task since each equation contains all three time terms buried in summed sin terms so that it is not possible to solve for each term separately. The equations can, however, be solved fairly easily for the arc voltages if the zero crossing times are known. An iterative solution is thus possible.

Before continuing it is necessary to simplify the notation of the equations as they are cumbersome. The arcing summation terms including the $\frac{4}{\Pi}$ will be denoted by S_1, S_2 and S_3 respectively and the non arcing terms by A_1 and A_2 so that

$$i_1 = \frac{1}{3}[A_1 - 2Va_1.S_1 + Va_2.S_2 + Va_3.S_3]$$

$$i_2 = \frac{1}{3}[A_2 + Va_1.S_1 - 2Va_2.S_2 + Va_3.S_3] \qquad G17$$

$$i_3 = \frac{1}{3}[(A_1 + A_2) - Va_1.S_1 - Va_2.S_2 + 2Va_3.S_3]$$

The boundary conditions are that

$$i_1 = 0 \text{ at } t = t_1$$
$$i_2 = 0 \text{ at } t = t_2$$
$$i_3 = 0 \text{ at } t = t_3$$

and

$$\begin{aligned} -2Va_1.S_1 + Va_2S_2 + Va_3S_3 &= -A_1 \text{ at } t = t_1 \\ Va_1.S_1 - 2Va_2S_2 + Va_3.S_3 &= -A_2 \text{ at } t = t_2 \\ Va_1.S_1 + Va_2.S_2 - 2Va_3.S_3 &= A_1+A_2 \text{ at } t = t_3 \end{aligned} \qquad G18$$

With assumed values of t_1,t_2 and t_3 the equations above are fairly simple to solve. The starting point of the iterative solution is determined by computing the zero crossing times for the special case where $Va_1 = Va_2 = Va_3 = V$ so that

$$t_3 - \frac{4\Pi}{3w} = t_2 - \frac{2\Pi}{3w} = t_1$$

The value of V is determined from the average of the three required arc voltages

$$V = \frac{Va_1 + Va_2 + Va_3}{3}$$

COMPUTER PROGRAMME TO SOLVE THREE-PHASE CIRCUIT WITH ARCING

The solution of the equations for a three-phase circuit with arcing requires the use of a computer to perform the many calculations in a reasonable amount of time. The programme which has been developed is of sufficient complexity to require some explanation.

The operations which are performed are summarized in flowchart form in Figure G2. The programme is divided into four subroutines - data input, zero crossing angle determination, main calculation and data output. The inputs for the programme are:

(i) line voltages - it is usually assumed that all three line voltages are equal so that $U_{12} = U_{23} = U_{31} = U$ and $\alpha = \frac{2\pi}{3}$ radians;

(ii) resistance, R and reactance, X (wL) - in this derivation $R_1 = R_2 = R_3 = R$ and $X_1 = X_2 = X_3 = X$;

(iii) arc voltages Va_1, Va_2 and Va_3;

(iv) number of harmonic terms, n_{max} (set to 30);

(v) maximum permissable arc voltage error for the zero crossing angle determination, V_{err} (set to 0,1 volts).

The flowchart for the zero crossing angles determination is shown in Figure G3. The stability of the iteration is based on the observation that a change in a zero crossing angle effects the arc voltage in that phase more than for the other phases. This is shown in Figure G1 where the changes in arc voltages are plotted against a variation in phase one zero-crossing angle. The iteration starting point is at a balanced arc voltage point set by the average of the required arc voltages. Each iteration cycle involves the determination of the phase with the maximum difference between the calculated arc voltage and the required arc voltage.

The zero crossing angle for this phase is then adjusted by an amount which is proportional to the magnitude of the voltage difference. The proportionality constant is set by the slope of the phase 1 curve shown in Figure G1. This iteration technique has proved to be adequately stable even for widely imbalanced arc voltages and the convergence speed is acceptable (typically 20 iterations).

Once the zero crossing angles have been determined the rest of the calculations are fairly straightforward using the equations. The waveforms are determined by calculating the voltages and currents over a full cycle with t incremented from 0 to 1,0 in 100 increments of 0,01. The rms voltages and currents are determined by computing the sums of the squares of the voltages and currents for each increment and computing the square roots of the averages of the sums. The powers are computed as the averages of the products of voltages and currents over the cycle.

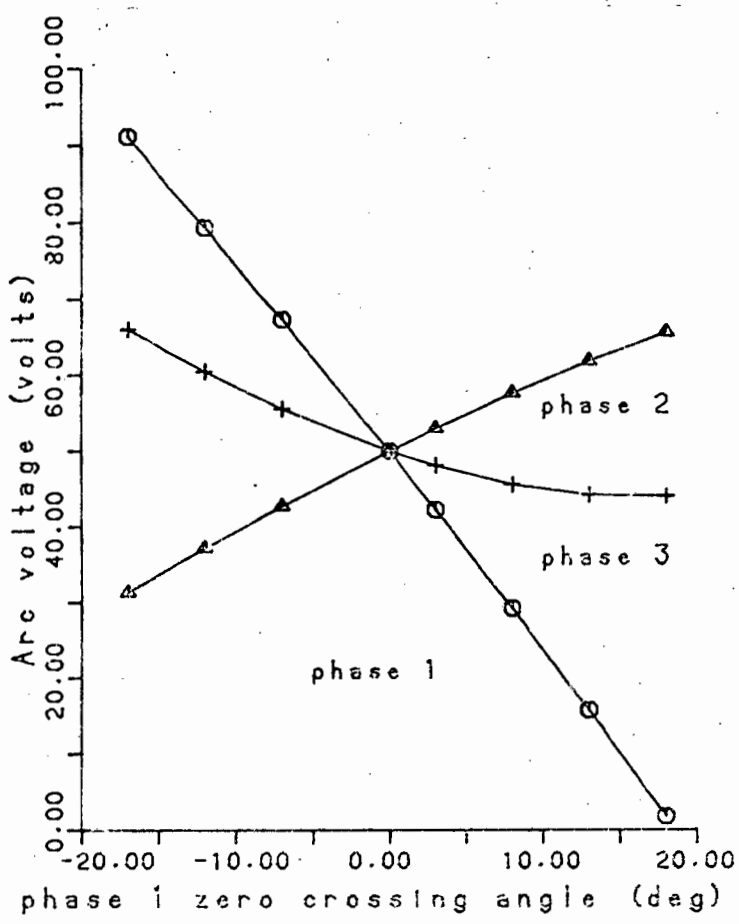

FIGURE G1 : VARIATION OF ARC VOLTAGES WITH CHANGES IN PHASE 1 ZERO CROSSING TIME

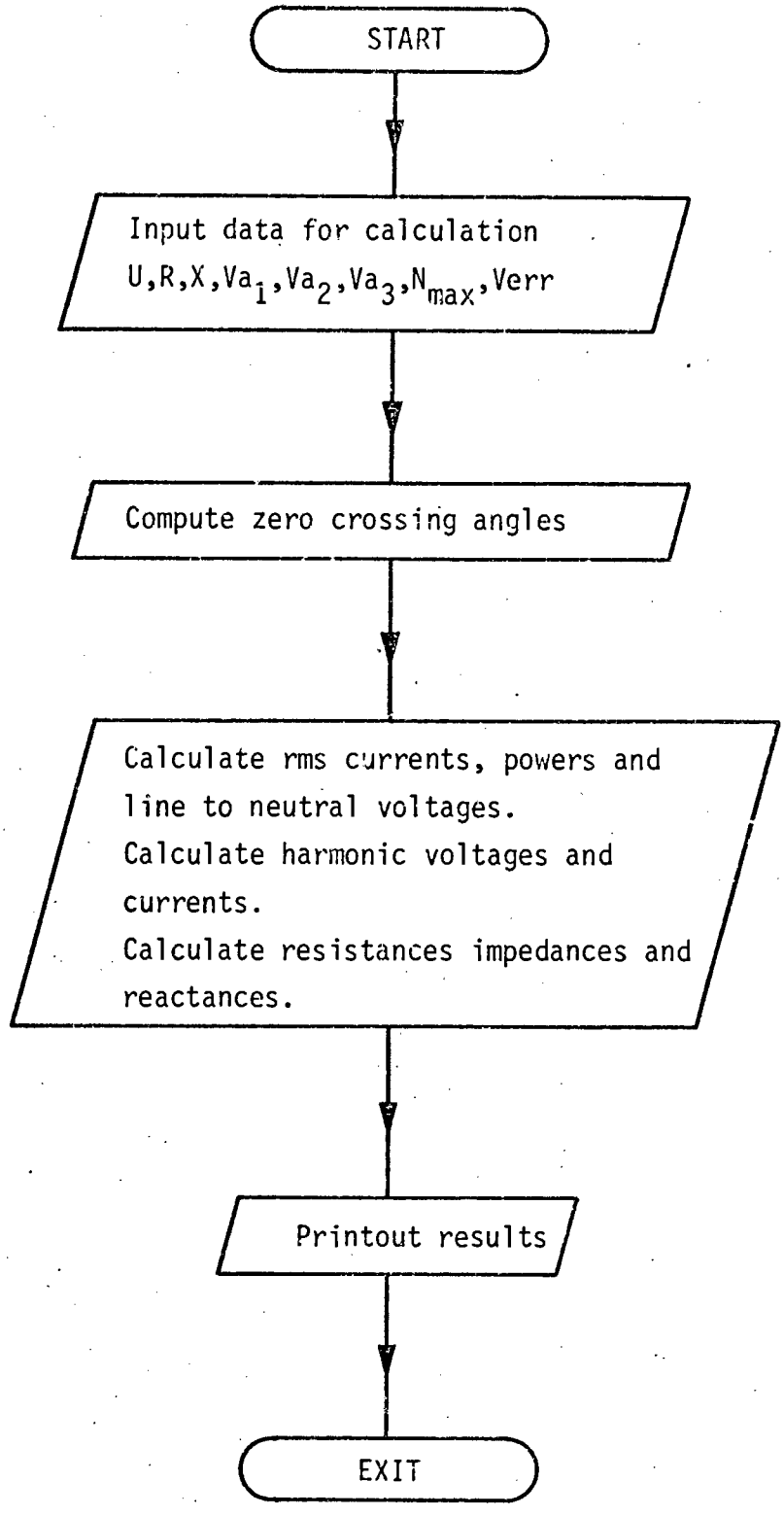

FIGURE G2 : Flowchart of programme to solve three-phase circuit with arcing

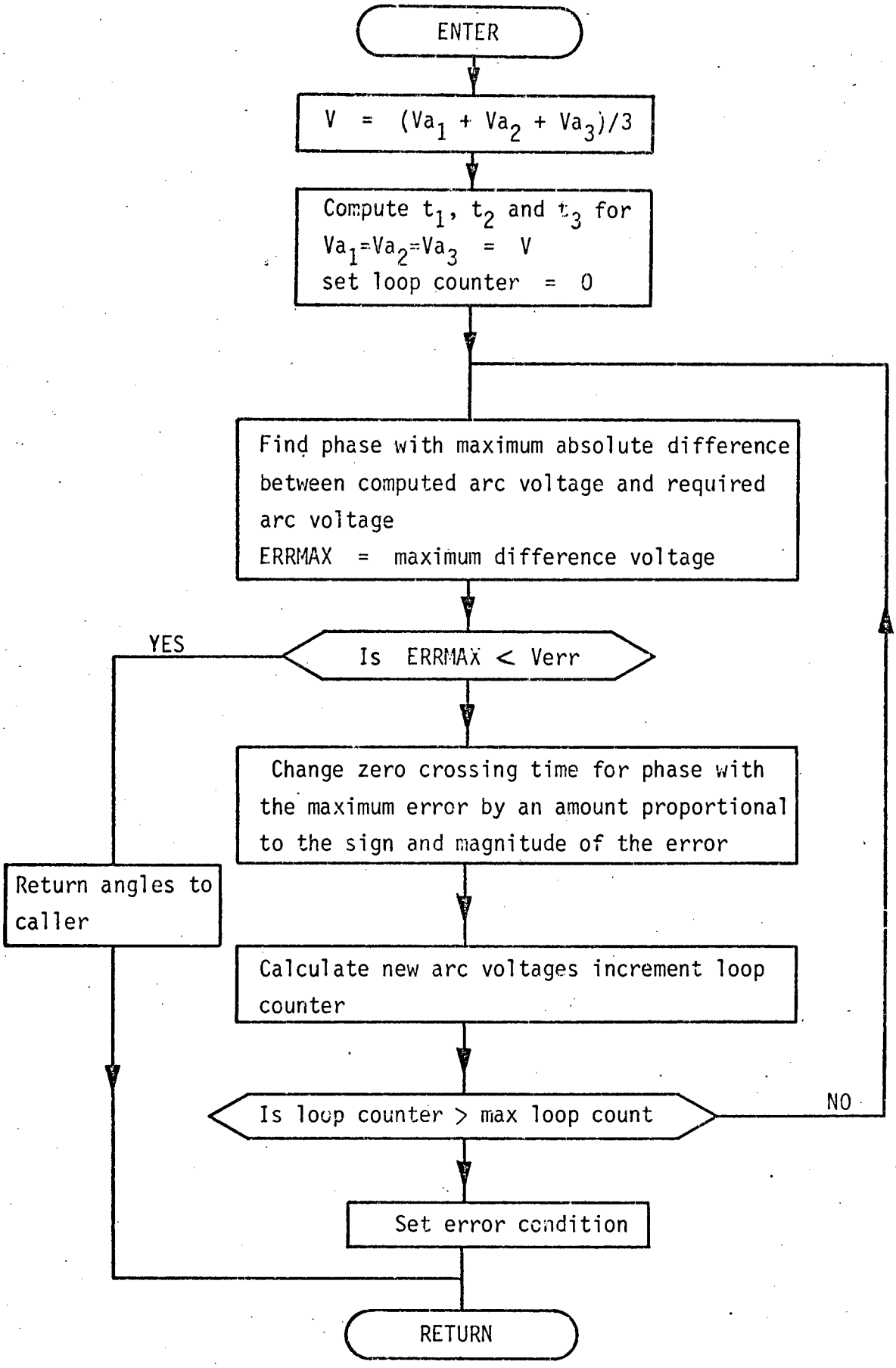

FIGURE G3 : Flowchart of zero crossing angle iteration subroutine

APPENDIX H

COMPARISON OF DIFFERENCE IN POWER EFFICIENCY BETWEEN SINGLE- AND THREE-PHASE ARCING

The difference in power efficiency between single- and three-phase arcing was shown in Figure 5.14 (Chapter 5.6). The reason for this can be qualitatively shown by considering the three-phase arcing equations described in terms of the neutral shift voltage u_o as:

$$L\frac{di_1}{dt} + i_1R = u_1 - Va_1 - u_o$$

$$L\frac{di_2}{dt} + i_2R = u_2 - Va_2 - u_o \qquad \text{H1}$$

$$L\frac{di_3}{dt} + i_3R = u_3 - Va_3 - u_o$$

where u_1, u_2 and u_3 are the phase to supply neutral voltages.

Adding the equations:

$$L\left(\frac{di_1}{dt} + \frac{di_2}{dt} + \frac{di_3}{dt}\right) + R(i_1 + i_2 + i_3) = (u_1 + u_2 + u_3) - \Sigma V_a - 3u_o$$

If the supply voltages are assumed balanced which is the usual case then

$$u_o = -\frac{1}{3}\Sigma V_a$$

Considering phase one, Va_1 and u_o combine together to give the staircase waveform shown in Figure H1. This waveform is more closely sinusoidal than the arc voltage alone which accounts for the difference in power efficiencies between single-phase and three-phase arcing. This effect can also be seen as 'bumps' in the current waveforms of Figure 5.19.

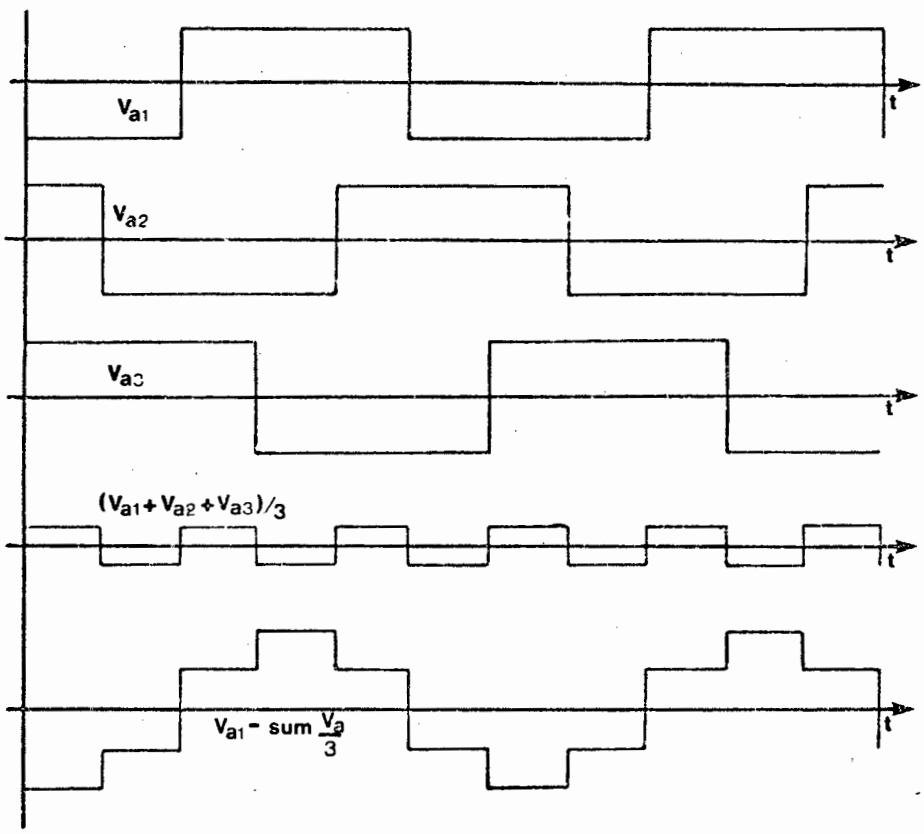

FIGURE H1

APPENDIX I :

SECONDARY ELECTRICAL MEASUREMENT SYSTEM USED ON 48 MVA FERROCHROME FURNACE

After the rebuild of the 48 MVA ferrochrome furnace in April 1977, the furnace was equipped with neutrals under each electrode and also in the centre of the furnace and voltage connections to each electrode. Secondary electrode current signals were available from primary current transformers connected through tap changing current transformers to give inferred secondary current signals (Figure 4.1). It was decided to build a new measuring system for these signals so as to be able to compare them with the old arrangement. In addition a fundamental frequency measuring system was built which could be compared with the rms measuring system, so as to be able to compare the two measuring techniques.

The electrical circuit for one phase can be solved completely if the voltage, current and power for that phase are known, thus rms and 50 Hz transducers providing these three signals were constructed for each phase.

Input Transformers

The voltage and current signals were all isolated using potential and current transformers for rejection of common mode voltages and protection of the transducer circuitry. The potential transformers transformed the electrode to bath voltages down to a level compatible with the analogue circuitry and included various tappings (0-200,250,300,350,400V to 9V), while the current transformers were simply isolation transformers with a turns ration of 1 amp/ 1 amp. A constantan wire of 0,5 Ω resistance was used on the output of each current transformer to provide a voltage signal.

Rms Watt, Amp, Volt Transducers

The circuit diagram of the transducers for rms voltage, current and real power is shown in Figure I1. The rms conversion of the voltage and current is achieved using Burr Brown 4341 rms to DC converters and the real power is

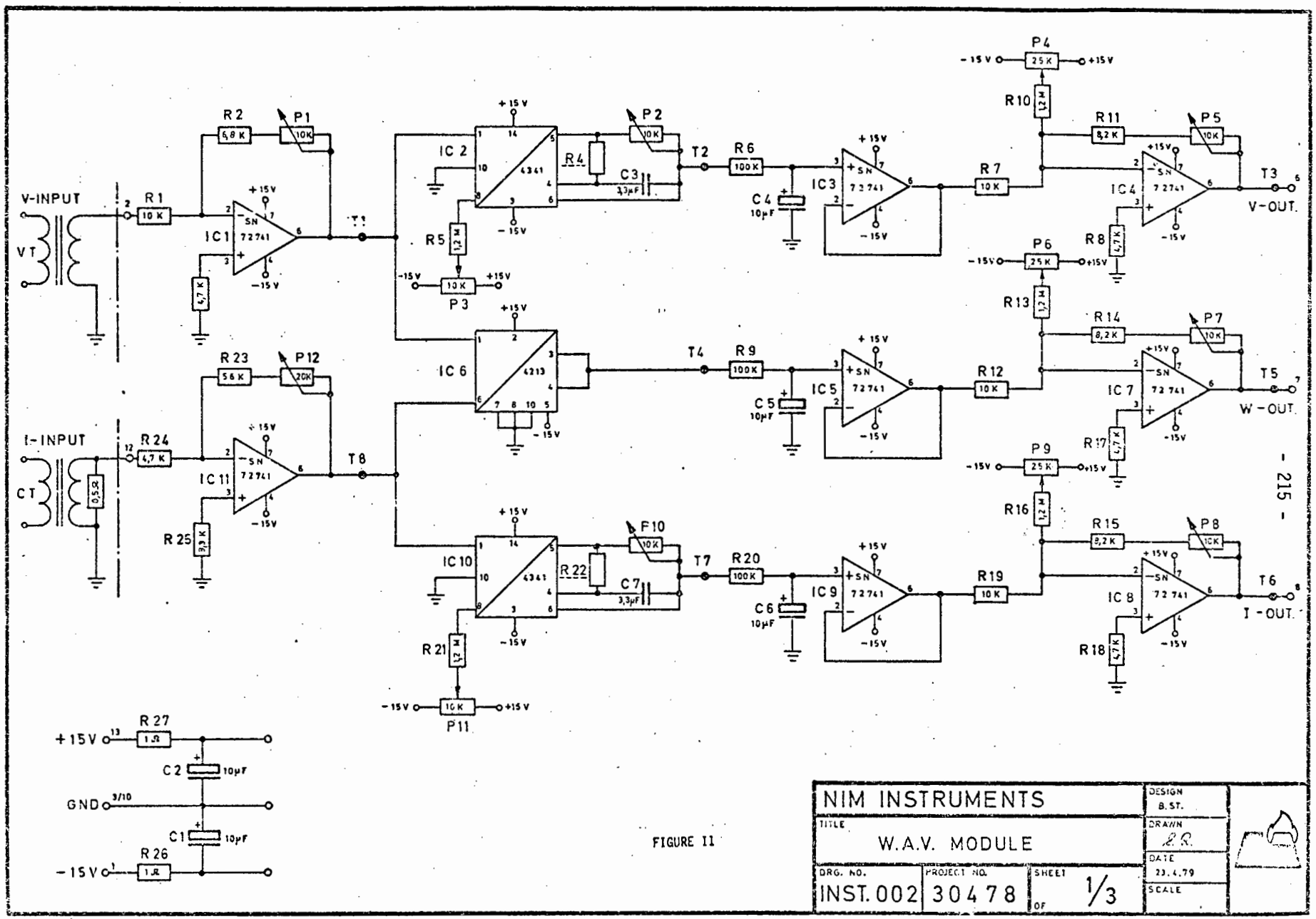

FIGURE II

NIM INSTRUMENTS			DESIGN B.ST.
TITLE: W.A.V. MODULE			DRAWN L.S.
DRG. NO. INST. 002	PROJECT NO. 30478	SHEET 1/3	DATE 23.4.79
			SCALE

obtained by averaging the instantaneous product of the voltage and current signals using a Burr Brown 4213 analogue multiplier. The rest of the circuitry is fairly straight forward and includes, a protection and signal condition stage for each input, and a low-pass filter and a variable gain and d.c. offset stage for each output.

The operational amplifiers used are 741's as there is no requirement for high input impedances. The low-pass filter time constant is set at 1 second. If this needs to be increased the 741's in the low pass filter stage could be replaced by TL081's or CA3140's which would allow the 100 k resistors to be replaced by much higher values without introducing errors.

50 Hz Watt, Amp, Volt Transducer

The measurement of 50 Hz voltage, current and real power is achieved by filtering the voltage and current signals with 3-stage low-pass filters and then computing voltages and currents using full-wave rectifier and low-pass filter stages, and real power using a multiplier and a low-pass filter stage. The circuit diagram for the transducer is shown in Figure I2. After an input protection and signal conditioning stage the voltage and current signals are each passed through the low pass filter stages with the cut-off frequency set at 90 Hz. The filters are Butterworth filters designed using standard techniques[71] and had an overall gain of 1 000 at 50 Hz and 0,05 at 150 Hz. The 150 Hz harmonic is the most dominant harmonic and its amplitude is approximately 10 per cent of the fundamental frequency amplitude which means that after filtering its amplitude will be less than 1/200th of the fundamental frequency amplitude. The filters were very carefully matched so as to avoid any differences in phase shifts across the stages which would alter the power measurement. This was a fairly simple task as all it meant was that the corresponding resistors and capacitors in each stage had to be matched, i.e., R4 = R25, C1 = C11 and so on. It was also necessary to make sure that

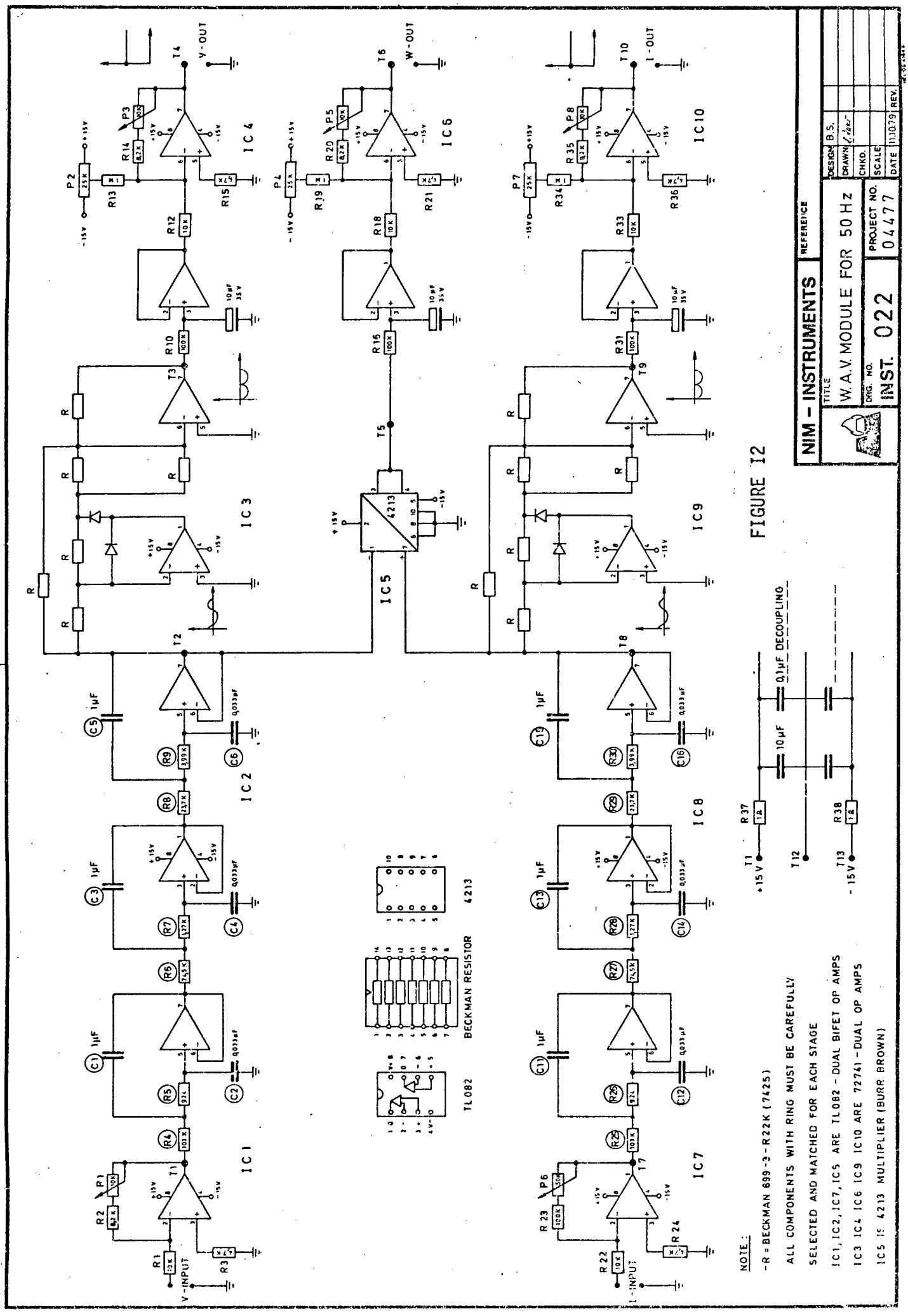
NIM – INSTRUMENTS
REFERENCE
TITLE
W.A.V. MODULE FOR 50 Hz
DRG. NO.
INST. 022
PROJECT NO.
04477
DESIGN B.S.
DRAWN
CHKD.
SCALE
DATE 11.10.79
REV.
V - OUT
W - OUT
I - OUT
V - INPUT
W - INPUT
I - INPUT
IC 1
IC 2
IC 3
IC 4
IC 5
IC 6
IC 7
IC 8
IC 9
IC 10
4213
TL082
BECKMAN RESISTOR
0.1µF DECOUPLING
10 µF
+15 V
- 15 V
NOTE :
-R = BECKMAN 699 -3 - R22K (7425)
ALL COMPONENTS WITH RING MUST BE CAREFULLY SELECTED AND MATCHED FOR EACH STAGE
IC1, IC2, IC7, IC8 ARE TL082 - DUAL BIFET OP AMPS
IC3 IC4 IC6 IC9 IC10 ARE 72741 - DUAL OP AMPS
IC5 IS 4213 MULTIPLIER (BURR BROWN)

FIGURE 12

all resistors and capacitors were within 1 per cent tolerance otherwise the filter would not have a standard attenuation response. The effectiveness of the filter matching was tested by making the gain of the current input stage the same as the gain of the voltage stage, and then feeding a signal generator output to both voltage and current inputs and checking the differences between the outputs at T2 and T8 with a dual trace oscilloscope. No discernible difference in both amplitude and phase shift could be detected for a frequency range from 10 Hz to 150 Hz. All operational amplifiers used were dual bifets (TL082's) which were necessary because of the high resistance values used in the filter stages.

Calibration

All calibration was carried out using a Yokogawa digital a.c. power meter. This is an rms measuring instrument with an accuracy of 0,1 per cent of full scale for all the ranges. It can measure single phase or 3-phase power (two wattmeter method) and rms voltages and currents. The currents and voltages for the calibration were provided by a 220 V a.c. supply driving a variable resistance load circuit. Fixed inductances were also used to test accuracy with non-unity power factor loads. The 220 V supply was taken from a 100 KVA 3-phase transformer connected to a 6,6kV bus with no other loads on it, which provided a relatively pure sinusoidal waveform. The Yokogawa meter was interfaced to the computer system so that calibration could be carried out semi-automatically. This was carried out on a number of occasions and the long-term accuracy of the transducers was found to be better than 1 per cent.

APPENDIX J

HARMONIC MEASUREMENTS

Arcing is a non-linear effect which causes the voltage and current waveforms in the furnace to be distorted from their standard sinusoidal form. These distorted waveforms can be resolved by Fourier's theorem into summations of a fundamental frequency term and harmonics (multiple frequencies of the fundamental). Fairly sophisticated techniques have been developed for analysing non-linear periodic waveforms (e.g., Fast Fourier Transform). However, these have not been used in this investigation owing to their complexity and difficulty of implementation. Alternatively a number of critical harmonic frequencies could be measured using bandpass analogue filtering techniques. However, this was also felt to be too complex, particularly since apart from the third harmonic, it was not known what harmonics were important. Bandpass filters are also difficult to use owing to their high changes in gain for small frequency changes (the use of N-path filters[49] would solve this problem). It was decided therefore that, rather than spend a lot of time developing sophisticated equipment, it would be better to implement the simplest solution which would give a measure of the level of arcing in each phase.

The system that was used consisted of a multiple stage high-pass filter used to remove the fundamental frequency, followed by a rectify and average stage to give a composite measure of the level of the harmonics. The high-pass filter was relatively simple to set up since the only critical factors were that the attenuation at 50 Hz must be high and the filter must have a moderately flat gain response over the pass band for frequencies of 150 Hz and higher. A five-stage Butterworth filter was selected with a cut-off frequency of 100 Hz which gave a gain of 0,001 at 50 Hz and 1,000 at 150 Hz.

The voltage waveforms on the furnace contain typically 10 per cent (in amplitude relative to the fundamental) 150 Hz harmonic with the higher harmonics being less than this. Considering the fundamental equal to 100 volts and the 150 Hz harmonic, equal to 10 volts, the fundamental frequency would be attenuated to 1 per cent (0,1 volts) of the 150 Hz harmonic. This is acceptable.

The circuit diagram for the harmonic transducer is shown in Figure J1. It contains similar input and output stages as the WAV transducers. The components for the filter stages were selected by, firstly matching the required number of capacitors to better than 1 per cent tolerance but not necessarily exactly equal to 0,22 F, then calculating the resistances required for the matched capacitance values. The resistances were then selected based on a 1 per cent tolerance limit.

The use of a full-wave rectifier to provide a composite signal of the harmonics is reasonable since the only dominant harmonics are odd harmonics. Any even harmonics present would not be measured by rectifying and averaging the filtered signal, however, it was assumed that these harmonics would not occur to any large extent. Even harmonics would only be generated if the arc exhibits widely different properties for the half cycles when the electrode is the anode and the cathode, and examination of the furnace waveforms showed no evidence of this.

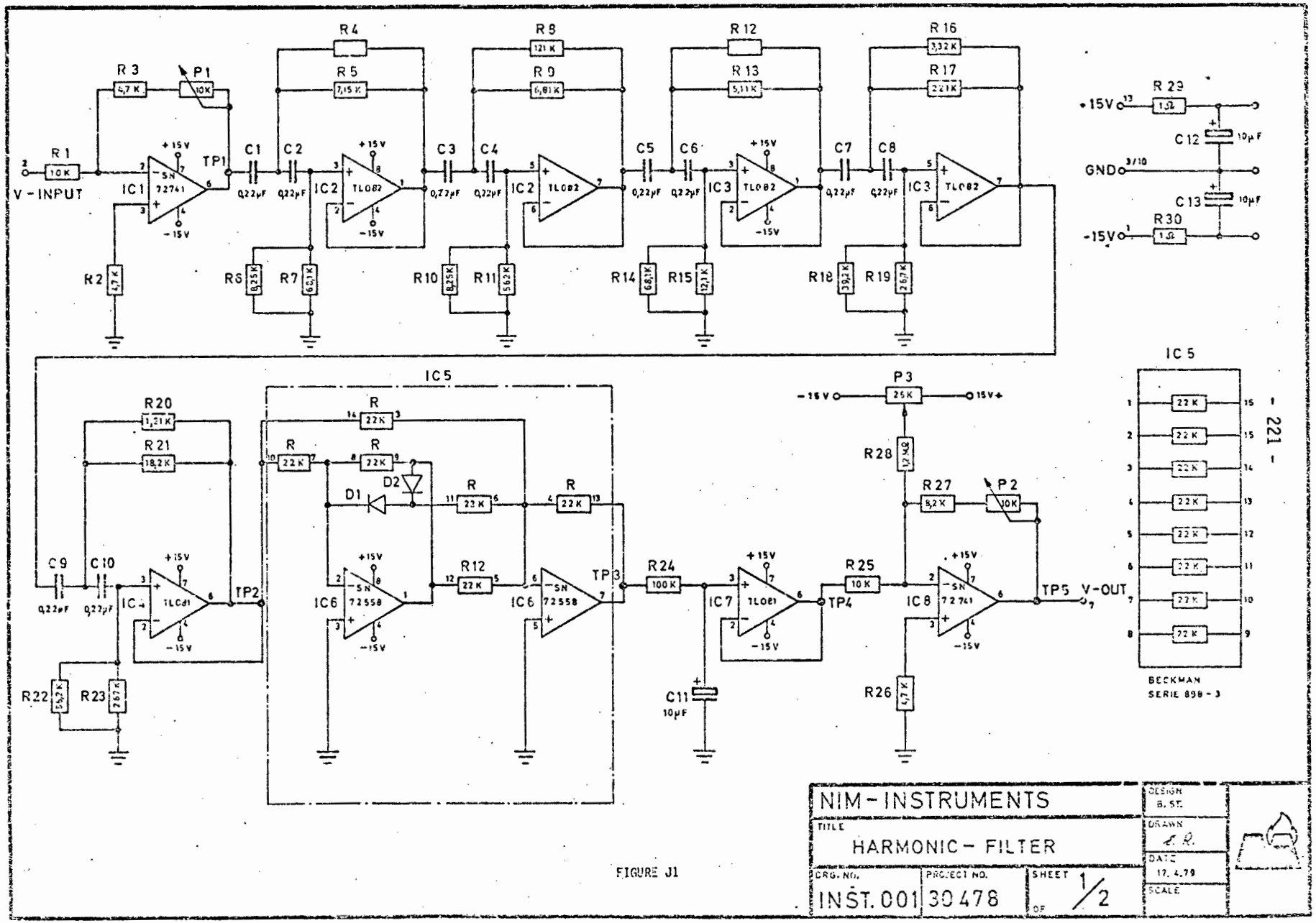

FIGURE J1

NIM-INSTRUMENTS			DESIGN B. ST.
TITLE: HARMONIC-FILTER			DRAWN A. R.
			DATE 17. 4. 79
ORG. NO. INST. 001	PROJECT NO. 30478	SHEET 1/2 OF	SCALE